Chemistry Dissertations                                              Department of Chemistry

8-12-2014

# Cleavage of Lipids and DNA by Metal Ions and Complexes

Dominique Williams

Recommended Citation

CLEAVAGE OF LIPIDS AND DNA BY METAL IONS AND COMPLEXES

by

DOMINIQUE EBONY WILLIAMS

Under the Direction of Dr. Kathryn B. Grant

ABSTRACT

Metal ions and complexes utilized as cleavage agents have influenced many synthetic approaches of scientists to assist in the cleavage and transformation of biomolecules. These metal-based synthetic cleavage agents have potential applications in biotechnology or as molecular therapeutic agents.  Herein, we have examined Ce(IV) metal ion and complexes as acidic hydrolytic agents in lipid hydrolysis reactions (Chapter 2 and 3), and a copper(II) complex that photo-oxidizes DNA upon exposure to ultraviolet light (Chapter 4).  In Chapter 2 we examined the hydrolysis of sphingomyelin vesicles by $Ce(NH_4)_2(NO_3)_6$ (Ce(IV)) and compared the results to twelve d- and f-block metal salts, hydrolysis of mixed lipid vesicles and mixed micelles of sphingomyelin by Ce(IV), and hydrolysis of phosphatidylcholine vesicles by Ce(IV), using either MALDI-TOF mass spectrometry or colorimetric assays.  In Chapter 3, we described the study of a Ce(IV) complex based on 1,3-bis[tris(hydroxymethyl)methylamino]propane as a

potential acidic hydrolytic agent of phospholipids using colorimetric assays and NMR

spectroscopy.  The hydrolytic agent provided markedly enhance hydrolysis at lysosomal pH (~

4.8), but suppress hydrolysis when pH was raised to near-neutral pH (~ 7.2).  This was due to the

pK$_a$ values of the donor atoms of the ligand, in which the metal's electrophilicity was reduced to

a greater extent at ~ pH 7.2 compared to ~ pH 4.8. Chapter 4 describes the synthesis and study of

a Cu(II) complex based on a hexaazatriphenylene derivative for photo-assisted cleavage of

double-helical DNA.  Scavenger and chemical assays suggested the formation of DNA damaging

reactive oxygen species, hydroxyl and superoxide radicals, and hydrogen peroxide, in the

photocleavage reactions.  Thermal denaturation and UV-vis absorption studies suggested that the

Cu(II) complex binds in a non-intercalative fashion to duplex DNA.

INDEX WORDS: Hydrolysis, Cerium(IV), Phospholipid, DNA, Photocleavage, External
        binding, Copper(II)/I redox, Hydroxyl radical

CLEAVAGE OF LIPIDS AND DNA BY METAL IONS AND COMPLEXES

by

DOMINIQUE EBONY WILLIAMS

A Dissertation Submitted in Partial Fulfillment of the Requirements for the Degree of

Doctor of Philosophy

in the College of Arts and Sciences

Georgia State University

2014

CLEAVAGE OF LIPIDS AND DNA BY METAL IONS AND COMPLEXES

by

DOMINIQUE EBONY WILLIAMS

| | |
|---|---|
| Committee Chair: | Kathryn B. Grant |
| Committee: | Dabney Dixon |
| | Gangli Wang |

Electronic Version Approved:

Office of Graduate Studies

College of Arts and Sciences

Georgia State University

August 2014

## DEDICATION

My Mother and Father, Jovita and Stephen R. Williams.

# ACKNOWLEDGMENTS

Overall, this process has been a gratifying and rewarding experience. Georgia State University and the Department of Chemistry have provided me vital training to succeed as a chemist. I am excited about my future and development into a chemist to assist my goals to better society, mentor, and inspire the future generation of scientists. If it was not for the persistence and support of my Mother and Father and many mentors and opportunities, I would not be obtaining a Ph.D. in Chemistry!

I want to acknowledge my Mother and Father who both instilled in me as a young child the importance of an education. They, along with my family members, friends, and younger sister Shardae, have been supportive and loving throughout this entire journey.

I want to thank all my elementary school teachers at Dumfries Elementary. The impact you all had on my life as a little girl will never be forgotten and I still remember each of your faces. You all taught me at a young age the value of hard work and determination, and I thank you for your dedication and commitment to teaching. I want to thank my high school chemistry teacher at Forest Park Senior High School in Woodbridge, VA for efficiently preparing me for college level chemistry. My mentor and teacher Dr. Crawley at Virginia Commonwealth University, thank you for all your time and advice to join a doctorate program.

This dissertation would not have been possible without the help and guidance of my Advisor, Dr. Kathryn Grant. Thanks for accepting me into your lab, and your patience, Girl Scout cookies, support, and guidance during these five years. Dr. Dixon and Dr. Gangli Wang, all your help have been invaluable. I appreciate your time and commitment as members of my dissertation committee.

# TABLE OF CONTENTS

## LIST OF TABLES

## LIST OF FIGURES

# CHAPTER 1

# INTRODUCTION

## 1.1. Prelude

There have been tremendous efforts to simulate the wonders of nature, such as the intricate functions of natural enzymes. Enzymes have roles in relatively all biological functions and the sustentation of life. The chemistry of enzymes involves electrostatic, nucleophilic, and metal ion catalysis. Furthermore, optimal activity, employment of metal cofactors, flexibility and self-organization of the functional groups are substantial properties inherent in natural enzymes.[1] However, these physical and chemical properties of enzymes are difficult to mimic in synthetic, non-enzymatic catalytic systems.

Great effort has been made toward the engineering of small-molecule, metal-based synthetic hydrolytic agents to simulate the intricate functions of natural hydrolases. The utilization of metal ions and complexes as synthetic mimics is advantageous because most active sites of hydrolases contain two or more metal ions. Due to strong Lewis acidity of lanthanide metal centers, they have been employed as robust hydrolytic agents for the cleavage of macromolecules, such as phospholipids and nucleic acids. Herein, in the introduction of my research I will discuss the structures and mechanisms of natural phosphodiesterases, and lanthanide metal ions and complexes utilized as hydrolytic agents. Subsequently, I will discuss my challenging and gratifying journey toward constructing a biomimetic model of acidic phospholipase based on cerium(IV) and my brief efforts to study a synthetic, metal-based photonuclease.

## 1.2. Inspired Inquiry into Natural Phosphodiesterases

Living organisms employ enzymes to accelerate reactions necessary for the sustentation of life. There are enzymes responsible for selective binding to corresponding substrates and acceleration of the rate of the hydrolytic breakdown of cellular macromolecules into their monomeric building blocks. These enzymes are known as hydrolases, and many of the active site of these enzymes utilize two or more metal ions located 3 - 5 Å apart from each other.[2] The roles of the metal ions are to bind and activate the substrate, and for some, to activate the nucleophile in enzymatic reactions. Typical metal centers of hydrolases are $Zn^{2+}$, $Mg^{2+}$, $Ni^{2+}$, $Mn^{2+}$, and $Fe^{2+}$.[2] In most of this dissertation, I will focus on hydrolases known as phosphodiesterases that are responsible for the hydrolytic cleavage of phosphate ester bonds of macromolecules.



| Alkaline phosphatase | Phospholipase C | P1 nuclease |
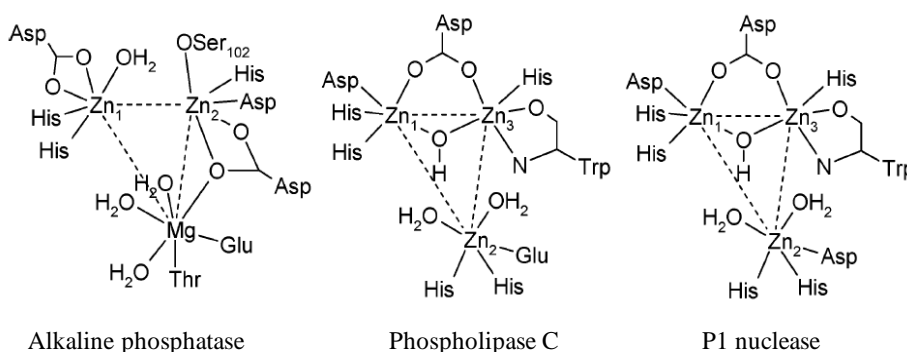
**Figure 1.1** Structures of the trinuclear active site of three phosphodiesterases.[2]

Figure 1.1 shows three common trinuclear phosphodiesterases, alkaline phosphatase, phospholipase C, and P1 nuclease. Alkaline phosphatase is responsible for the non-specific cleavage of the phosphate monoester bonds of macromolecules, such as nucleic acids and phosphorylated proteins, and is capable of performing enzymatic reactions under both acidic and alkaline conditions.[2] The active site of this enzyme contains two zinc metal ions and one magnesium metal ion. The $Mg^{2+}$ is not involved in catalysis, but serves an ancillary role in the

enzymatic reaction.[2] In the absence of $Mg^{2+}$, alkaline phosphatase exists as an inactive symmetric dimer, but in the presence of $Mg^{2+}$, alkaline phosphatase exists as an active unsymmetric dimer.[2] The two $Zn^{2+}$ metal ions have a major role in catalysis and are responsible for binding and activating the substrate, and activating a serine nucleophile.[2] The Lewis acidity of the $Zn^{2+}$ ions assists in the deprotonation of the hydroxyl group of serine, by decreasing the $pK_a$ of serine hydroxyl group from 13.60 to 5.5, to furnish an alkoxide nucleophile.[2,3]

To catalyze the hydrolytic cleavage of nucleic acids and phospholipids, nature utilizes nucleases and phospholipases, respectively. Nucleases have significant roles in nucleic acid metabolism, the replication and repair of DNA, and gene expression.[4] Phospholipases have essential roles in phospholipid metabolism and the signal transduction pathway.[5] Phospholipase C and P1 nuclease are trinuclear zinc enzymes with similar active sites (Figure 1.1) and reaction mechanisms. Dissimilarity between these two enzymes is their substrates, single-stranded DNA and RNA are P1 nuclease substrates and phospholipids are substrates of phospholipase C. An additional difference is a glutamate is replaced with an aspartate residue in P1 nuclease compared to phospholipase C.[2] Even though these enzymes have different substrates, they have very similar reaction mechanisms. Since most of my research has been dedicated toward the search for a phospholipid hydrolytic cleavage agent, I will focus solely on phospholipases in this introductory segment.
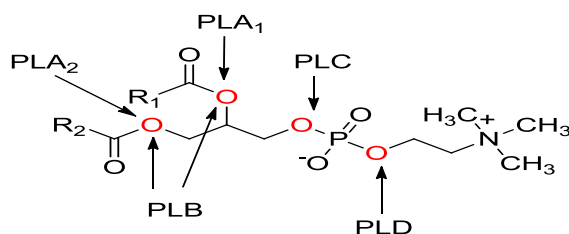


**Figure 1.2.** Phospholipases specificity to phosphatidylcholine ($R_1$ and $R_2$ represents long chain fatty acids).

Phospholipases catalyze the hydrolytic cleavage of specific phospholipid bonds. Figure 1.2 shows phospholipase specificity for the phosphoglyceride phosphatidylcholine. Phospholipases $A_1$ and $A_2$ produce fatty acid and lysophosphatidylcholine by the hydrolysis of the acyl ester bond of at either the sn-1 or sn-2 position. The role of phospholipase B is to hydrolyze both acyl ester bonds of phospholipids. Phospholipase C hydrolyzes the phosphate ester on the side of the glycerol unit of the phospholipid to produce 1,2- diacylglycerol and phosphocholine. Alternatively, phospholipase D hydrolyzes the phosphate ester bond on the polar head group side to produce phosphatidic acid and choline.[6]

Major characteristics of lipids are their hydrophilic (head group) and hydrophobic (backbone) moieties which provide the lipid with an amphiphilic-type character. There are two main groups of phospholipids, phosphoglycerides and sphingolipids.
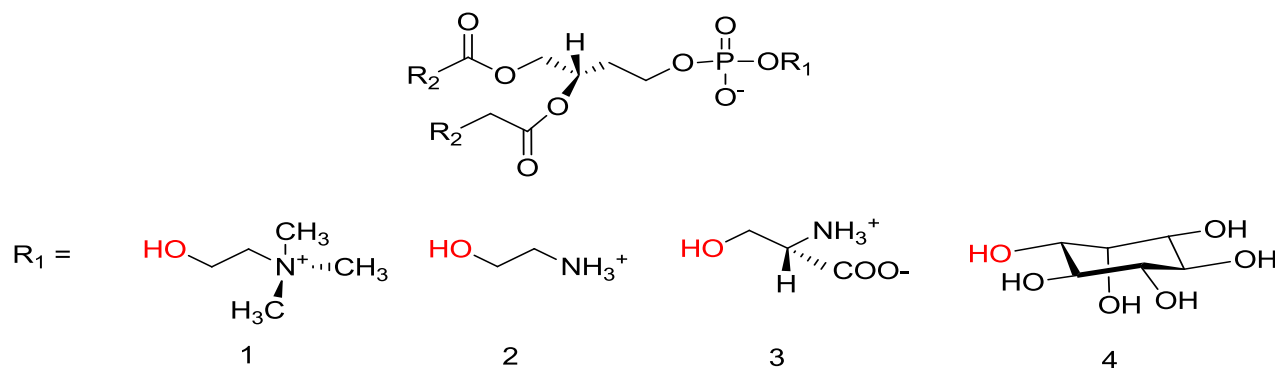


**Figure 1.3.** Phosphoglycerides (top) contain a glycerol backbone, two fatty acid chains ($R_2$), and a phosphorylated alcohol. The alcohols ($R_1$) present in phosphoglycerides are choline (**1**), ethanolamine (**2**), serine (**3**), and inositol (**4**).

Phosphoglycerides contain a glycerol backbone with two fatty acid chains (hydrophobic moiety) and a phosphorylated alcohol (hydrophilic moiety). The four common phosphoglycerides (Figure 1.3) are phosphatidylcholine, phosphatidylethanolamine, phosphatidylserine, and

phosphatidylinositol that include the polar head groups, choline (**1**), ethanolamine (**2**), serine (**3**), and inositol (**4**), respectively.
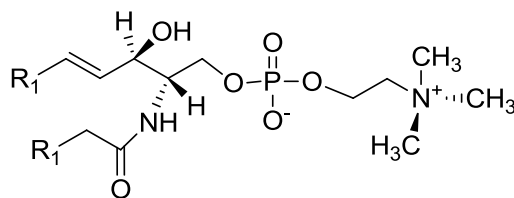


**Figure 1.4.** The structure of the sphingolipid sphingomyelin. $R_1$ represents long chain fatty acid hydrocarbons of variable lengths.

The two major lipids that make up 50 % of the lipids in the membrane bilayer of eukaryotic cells are the phosphoglyceride phosphatidylcholine and sphingolipid sphingomyelin (Figure 1.4).[7] Phosphatidylcholine and sphingomyelin contain the same phosphocholine polar head group, but have different backbones.  In contrast to phosphoglycerides, sphingomyelin contains a sphingosine backbone made up of an amino alcohol with unsaturated hydrocarbon chains.[4]

Phospholipases C and D, and sphingomyelinase are considered phosphodiesterases which hydrolytically cleave the phosphate ester bonds of phospholipids.  Their hydrolysis products include diacylglycerol and phosphatidic acid from the degradation of phosphoglycerides by phospholipase C and phospholipase D, and ceramide from the degradation of sphingomyelin by sphingomyelinase.  As a messenger in signal transduction, diacylglycerol activates protein kinase C, a membrane-bound protein involved in cell growth, by increasing the affinity of the enzyme for calcium ions.[2,8]  Phosphatidic acid plays a role as a lipid second messenger and is a major intermediate in the synthesis of phosphoglycerides and triacylglycerols.[4]  Ceramide acts as a signaling molecule and mediator of cell differentiation.[4,9,10]

Phosphatidylcholine-preferring phospholipase C isolated from *Bacillus cereus* has been studied extensively.  Phospholipase C catalyzes the cleavage of the phosphate ester bond of phosphatidylcholine to produce diacylglycerol and phosphocholine.   This enzyme requires

divalent cations and has optimum activity at neutral pH.[2,11] The active site (Figure 1.1) contains

a trinuclear zinc center coordinated to an aspartate, five histidines, a glutamate, and a

tryptophan.[2,8]
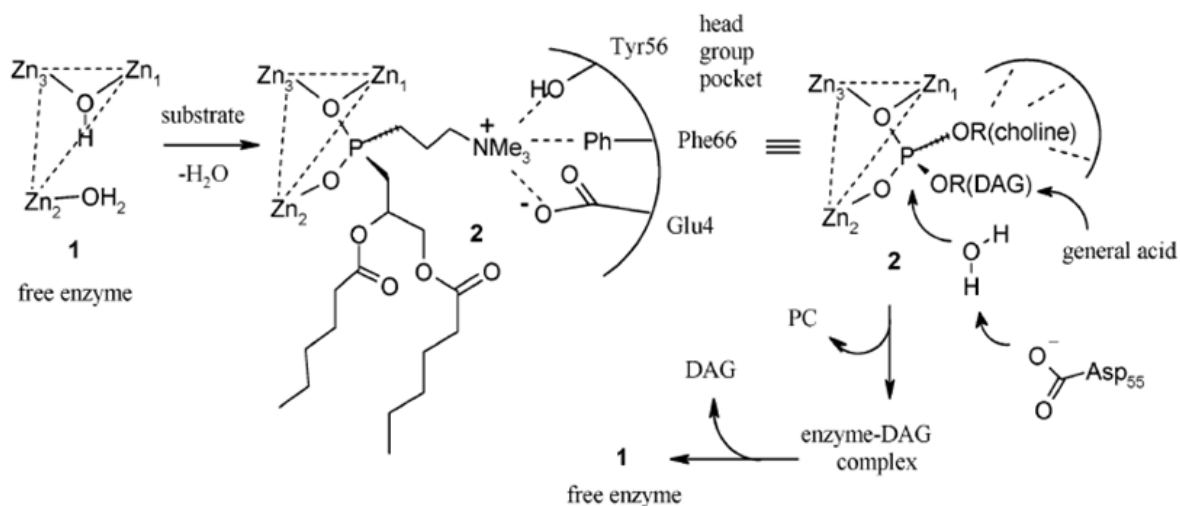


**Figure 1.5.** General mechanism of phosphatidylcholine-preferring phospholipase C.[2]

The choline of the substrate binds to a glutamate, tyrosine, and phenylalanine residues of the

enzyme, and these three residues create substrate specificity (Figure 1.5).[2] The $Zn_1$ and $Zn_3$

metal ions are bridged by an aspartate residue and an oxygen species (Figure 1.1).[2,8] The

mechanism of this reaction (Figure 1.5) starts with the formation of an enzyme-substrate

complex by the substrate displacing the bridging –OH between $Zn_1$ and $Zn_3$. In addition,

displacement of the free water ($OH_2$) on $Zn_2$ occurs. The nucleophile is a water molecule that is

deprotonated by a general base, aspartate residue. The roles of the zinc ions are to activate the

substrate by neutralization of the negatively charged oxygens on the phosphate group, and

stabilization of the trigonal bipyramidal transition state formed by the hydroxide anion attack on

the phosphorous center of the substrate. The collapse of the transition state leads to the two

products diacylglycerol and phosphocholine.[2]

Phospholipase D is located in the plasma membrane and is responsible for the cleavage of the phosphate ester bond on the side of the polar head group of glycerophospholipids to produce the second messenger phosphatidic acid and an alcohol. *Streptomyces* phospholipase D, which includes an α-β-α-β-α sandwich structure, belongs to the phospholipase D superfamily.[12] All enzymes from this family, including mammalian and bacterial, contain one or two copies of the conserved HxKxxxxD (HKD) (x = any amino acid) motif.[12] *Streptomyces* phospholipase D contains two motifs, one located in the N- and C-terminal regions of the enzyme. The residue His170 (N-terminal HKD motif) acts as a nucleophile in the hydrolysis reaction, and His 448 (C-terminal HKD motif) supports the formation of a substrate-enzyme complex and acts as a general acid in hydrolysis. There are two aspartate residues in the active site that interact with His448 and His170 by hydrogen bonding and ion-pair interactions.[12]
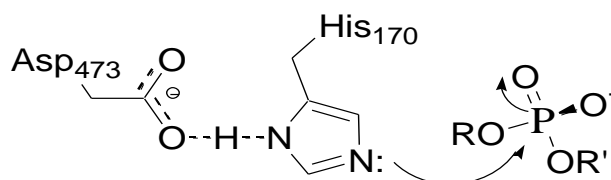


**Figure 1.6.** First step of lipid hydrolysis by phospholipase D starts with a histidine (**His₁₇₀**) residue located in the N-terminal HKD motif acting as a nucleophile by attacking the phosphorus atom of the substrate. **R** = diacylglycerol and **R'** = polar head group.[12]

The first step of the conversion of phospholipid to phosphatidic acid and an alcohol by phospholipase D, starts with the nucleophilic attack of the lipid's phosphorus atom by the nitrogen atom of the imidazole ring of His170.[12] The alcohol released from the substrate is protonated by His448.[12] The phosphatidyl-histidine intermediate thus formed is attacked by an activated water molecule.[12] Phosphatidic acid is then released from the enzyme.[12]

Unlike *Bacillus cereus* phospholipase C, lysosomal phospholipase C does not require metal cations for activity and has optimum activity at a pH of 4.4.[11] Lysosomal phospholipase C

has not been studied as extensively as *B. cereus* phospholipase C, and no molecular mechanism has been proposed for the enzyme. Similar to lysosomal phospholipase C, lysosomal phospholipase $A_2$, which hydrolyzes the fatty acyl ester bond of phospholipids, does not need metal ions for activity and has optimal activity at lysosomal pH (~ 4.8). However, in contrast to lysosomal phospholipase C, this enzyme has been studied extensively. This enzyme is a 45 kDa water-soluble glycoprotein containing a single peptide chain.[13] The amino acid residues Ser198, Asp360, and His392 belong to the catalytic triad of the enzyme. Serine198 is part of a strand-turn-helix that forms an acyl intermediate, thus to act as a nucleophile in the hydrolysis reaction.[13] In addition, lysosomal phospholipase $A_2$ contains four cysteine residues which are responsible for maintaining the tertiary structure of the enzyme's catalytic triad.[13]

## 1.3. The Superiority of Ce(IV)-mediated Hydrolysis of Macromolecules

Great effort has been made toward the engineering of small-molecule, metal based synthetic hydrolytic agents to simulate the intricate functions of natural hydrolases. The utilization of metals in these synthetic mimics is advantageous because most hydrolase's active sites contain two or more metal ions. Lanthanide metal ions and complexes utilized as hydrolytic catalysts have influenced many synthetic approaches of scientists to assist the hydrolysis of biomolecules. A reason lanthanides show great promise as synthetic hydrolytic agents is they are hard acids that interact preferably with hard bases ($PO_4^{3-}$ group of the phosphate ester linkage).[14] Yet, one lanthanide, cerium(IV) [Ce(IV)] has caught the attention of many scientists due to high electrophilicity, the ability to promote hydrolysis at low and high pH values, high coordination number (up to 12), high charge density, and fast ligand exchange rates.[14-17] Cerium(IV) metal ions and complexes have assisted in the hydrolysis of not only phosphate ester bonds, but also amides, carbon esters, and organophosphorus compounds.
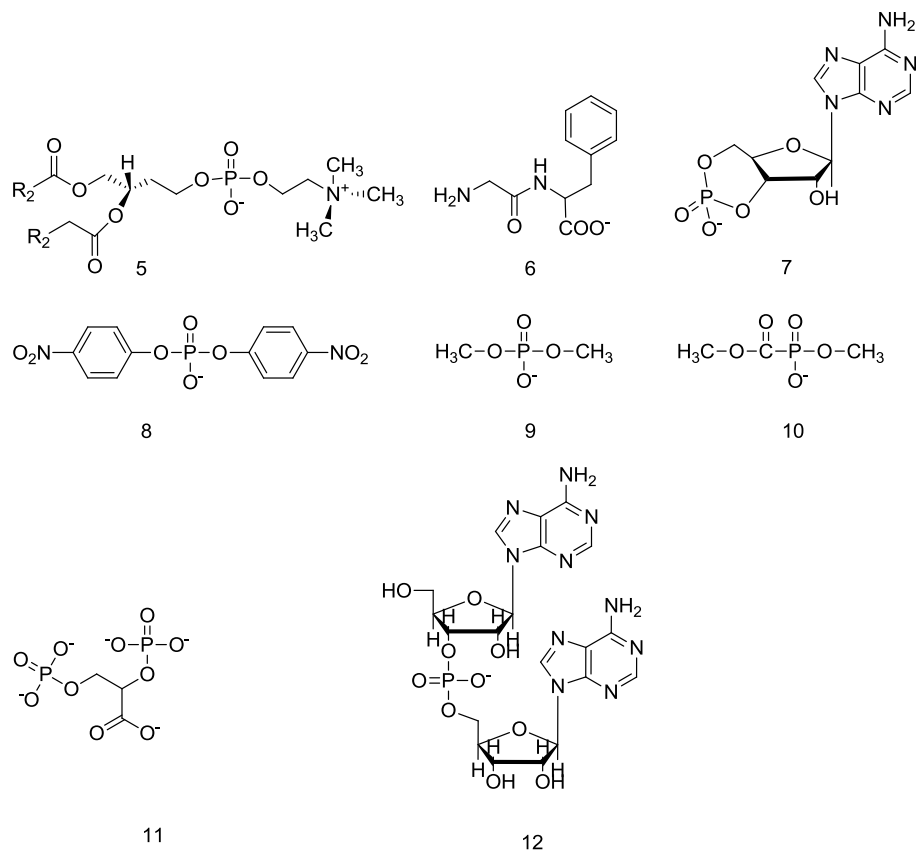
**Figure 1.7.** Ce(IV)-assisted hydrolysis of the substrates phosphatidylcholine **(5)**, a dipeptide (Gly-Phe) **(6)**, adenosine 3',5'-cyclic monophosphate (cAMP) **(7)**, bis(4-nitrophenyl) phosphate (BNPP) **(8)**, dimethyl phosphate (DMP) **(9)**, dimethyl phosphonoformate (DMPF) **(10)**, 2,3-bisphosphoglycerate (BPG) **(11)**, and adenylyl (3'-5') adenosine (ApA) **(12)**.

Compounds (Figure 1.7 and Table 1.1) hydrolyzed by Ce(IV) are phospholipids **(5)**,[14,18,19] peptides **(6)**,[20] activated **(8)** and inactivated **(9, 10)** synthetic phosphate ester-containing derivatives,[15,16,21-26] nucleic acids **(7, 12)**,[24,27-32] antiviral phosphonoformates **(10)**,[33] and 2,3-bisphosphoglycerate **(11)**.[34]

**Table 1.1.** Ce(IV)-assisted hydrolysis of macromolecules and other phosphate ester-containing compounds.

| Substrate[a] | Concentrations | | Temp | pH | Rate or yield (%) | Ref. |
|---|---|---|---|---|---|---|
| | Substrate | Ce(IV) | | | | |
| PC (**5**) | 2 mM | 10 mM | 37 °C | 4.8 | 21 % (20 h) | 19 |
| Gly-Phe (**6**) | 10 mM | 10 mM | 50 °C | 7.0 | $9.7 \times 10^{-5}$ s$^{-1}$ | 20 |
| cAMP (**7**) | ---[b] | 10 mM | 30 °C | 7.0 | $1.0 \times 10^{-1}$ s$^{-1}$ | 32 |
| BNPP (**8**) | 0.05 mM | 1 mM | 37 °C | 3.5 | $80 \times 10^{-3}$ s$^{-1}$ | 35 |
| DMP (**9**) | 1 mM | 10 mM | 60 °C | 1.8 | $5.3 \times 10^{-4}$ s$^{-1}$ | 36 |
| DMPF (**10**) | 10 mM | 25 mM | 25 °C | 1.9 | $5.2 \times 10^{-4}$ s$^{-1}$ | 33 |
| BPG (**11**) | 0.1 mM | 9.8 mM | 37 °C | 7.4 | 83 % (5 h) | 34 |

[a]PC = phosphatidylcholine, Gly- Phe = glycine and phenylalanine dipeptide, cAMP = adenosine 3',5'-cyclic monophosphate, BNPP = bis(4-nitrophenyl) phosphate, DMP = dimethyl phosphate, DMPF = dimethyl phosphonoformate, and BPG = 2,3-bisphosphoglycerate
[b]Paper does not give substrate concentration
(**n**) are correlated to structures shown in Figure 1.7

In search of an acidic hydrolytic agent, Kassai et al. reported twelve metal ion salts-assisting the hydrolytic cleavage of the phosphate ester bonds of L-α-phosphatidylcholine (PC) (**5**, Figure 1.7) at lysosomal pH (pH 4.8) and cytosolic pH (pH 7.2).[19] Out of twelve lanthanide and transition metal salts tested, the tetravalent metal ions Ce(IV), Zr(IV), and Hf(IV) produced the most inorganic phosphate from PC after a 20 h reaction at 60 °C and ~ pH 4.8. Most importantly, the study demonstrated that Ce(IV) was superior compared to the other tetravalent metal ions, in terms of metal-assisted inorganic phosphate production from PC in the order of

Ce(IV) >>> Zr(IV) > Hf(IV).   Additionally, Ce(IV) was found to produce substantially more PC phosphate ester bond cleavage at acidic pH (~ 4.8) compared to neutral pH (~ 7.2), whereas the metal ions Pd(II), Yb(III), Eu(III), and La(III) preferentially hydrolyzed PC at neutral pH compared to lysosomal pH (~ 4.8).  Notably, high levels of hydrolysis by Ce(IV) was still observed when the temperature was decreased to core body temperature, 37 °C (Table 1.1).[19] The reason for superior levels of hydrolysis at mildly acidic pH values compared to the other metal ions, Ce(IV) is a stronger Lewis acid and more capable of forming catalytically active metal bound hydroxide nucleophiles at mildly acidic pH.[19]  The reasoning underlying low hydrolysis at neutral pH compared to mildly acidic pH was suggested to be due to the formation and precipitation of less active, lower net positive charge Ce(IV) hydroxo species with reduced Lewis acidity.

Takarada et al. explored twenty-three metal ions (lanthanide, alkaline-earth, and transition metals) as potential synthetic peptidases to hydrolyze the amide bonds of the dipeptide Gly-Phe (**6**, Figure 1.7) at 80 °C and pH 7.[20]  Similar to phosphatidylcholine hydrolysis, Ce(IV), Zr(IV), and Hf(IV) enhanced the hydrolytic amide bond cleavage of the dipeptide the most, generating hydrolysis yields of ~ 90 %, ~ 25 %, and ~ 19 %, respectively.[20]  Not only was Ce(IV) superior over the other metal ions, but it selectively promoted the hydrolysis of Gly-Phe over cyclization.  In contrast, Zr(IV), Hf(IV), and the other metal ions afforded similar hydrolysis and cyclization rates under the same reaction conditions.  Notwithstanding, Ce(IV) promoted enhance levels of amide cleavage under relatively milder conditions (pH 7.0 and 50 °C) (Table 1.1), and was capable of hydrolyzing tripeptides and tetrapeptides.  An explanation for Ce(IV) superiority in metal-assisted amide bond hydrolysis of peptides is its strong Lewis acidity which lowered the $pK_a$ of the N-terminal amino group from 8.08 to 6.23.[20]
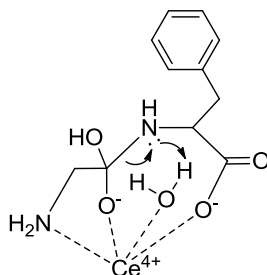
**Figure 1.8.** Tetrahedral intermediate in the Ce(IV)-mediated hydrolysis of the dipeptide Gly-Phe.[20]

This allows the Ce(IV) metal ion to coordinate to the amino group at pH 7.0 which directs

coordination to the carbonyl oxygen to form a stable five-membered ring.[20] There is additional

metal coordination to the carboxylate at the C-terminus of the peptide.[20] Due to complex

formation, the substrate's amide bond is efficiently activated by Ce(IV) and the electrophilicity

of the carbonyl carbon is increased, which leads to nucleophilic attack by a hydroxide ion and

the formation a tetrahedral intermediate (Figure 1.8). The collapse of the intermediate will then

lead to the respective amino acid products.[20] Takarada et al. also noted slower hydrolysis of

peptides containing metal-coordinating side chains, such as in Gly-Asp, compared to peptides

without.[20] They postulated that the Lewis acidity of Ce(IV) decreased due to the additional

coordination to the extra carboxylate group from the side chain of aspartate. This resulted in less

efficient substrate activation.[20] The group also noted that the tri- and tetra-peptides presented

similar hydrolysis rates compared to the dipeptides, and were preferentially cleaved at the N-

terminal amide bond due to the formation of a stable five-membered ring between the amino and

carbonyl carbon of the substrate.[20]

There are many examples of Ce(IV) displaying superiority over other metal ions toward

the hydrolysis of the phosphate ester bonds of nucleic acids. An example is Ce(IV)-assisted

hydrolysis of cyclic adenosine 3',5'-monophosphate (cAMP) (**7**, Figure 1.7, Table 1.1) for which

cleavage at the 5'-O-P end of the substrate is preferred.[32] Cleavage was $10^4$-fold faster compared

to the trivalent form of cerium [Ce(III)] and $10^{13}$-fold faster compared to cAMP hydrolysis in the absence of any catalyst (pH 7.0 and 30 °C).[32] The pseudo-first-order rate constant for Ce(IV)-assisted hydrolysis was 6.1 min$^{-1}$ with a half-life of 7 s. Additionally, Ce(IV) provided relatively constant hydrolytic cleavage rates from pH 2 to pH 8. Sumaoka et al. attributed the superior levels of hydrolysis over a wide pH range to the existence of metal-bound hydroxide species at low and high pH values compared to the other metal ions tested in this study.[32]

In another example, Moss et al. investigated Ce(IV)-, Zr(IV)-, and Hf(IV)-assisted hydrolysis of the DNA model substrate bis(4-nitrophenyl) phosphate (BNPP) (**8**, Figure 1.7, Table 1.1) in homogeneous acidic aqueous solutions (~ pH 3.5 and 37 °C).[35] Similarly, Ce(IV) provided 10-fold and 27-fold faster phosphate ester bond cleavage compared to Zr(IV) and Hf(IV), respectively.[35] The prowess of Ce(IV) also led Moss et al. to study Ce(IV)-assisted hydrolysis of another DNA model substrate, dimethyl phosphate (DMP) (**9**, Figure 1.7, Table 1.1), in acidic homogeneous aqueous solutions (pH 1.8 and 60 °C).[36] Compared to the half-life of DMP at pH 7 and 60 °C without catalyst, Ce(IV) produced a 2 x $10^{8}$-fold rate enhancement and reduced the half-life of DMP to 22 min.[36]

The above findings also led Moss et al. to turn their attention to Ce(IV)-assisted hydrolysis of the carbon ester- and phosphate ester-containing substrate phosphonoformate diester (**10**, Figure 1.7, Table 1.1), a potential antiviral agent.[33] Enhanced hydrolytic cleavage of dimethyl phosphonoformate (DMPF) by acidic homogeneous solutions of Ce(IV) in $D_2O$ at pD 1.9 was followed by $^1H$- and $^{13}C$-NMR spectroscopy.
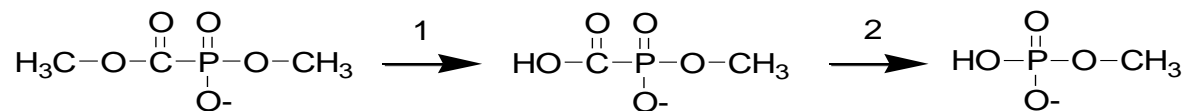
**Figure 1.9.** Scheme of Ce(IV)-assisted hydrolysis of DMPF.

Their findings show Ce(IV)-assisted hydrolysis of DMPF to be selective, and kinetically

preferred, toward the cleavage of the carbon ester (C-O) bond of DMPF (step 1, Figure 1.9).

Subsequently, the metal assisted decarboxylation of the cleaved product provided methyl

phosphate (step 2, Figure 1.9).  Ce(IV)-assisted hydrolysis of DMPF was compared  to other

tetravalent metal ions (Zr(IV), Hf(IV), and Th(IV)) at pD values between 1.7 – 3.1.[33]  The group

discovered a strong correlation between the metal ions speciation in aqueous solution and the

regioselective cleavage of either the phosphate ester (P-O) bond or the carbon ester (C-O) bond

of DMPF.
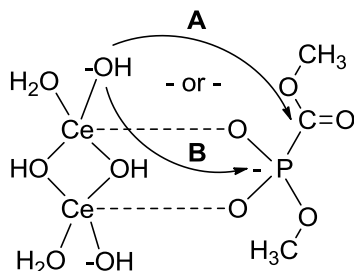


**Figure 1.10.**  Two possible DMPF cleavage mechanisms: Attack of the carbon ester to form a five-membered ring **(A)** or attack of the phosphate ester to form a four-membered ring **(B)**.[33]

The interactions between dinuclear Ce(IV) hydroxo species present in acidic aqueous

solutions and DMPF afforded a kinetically preferred transition state, after the metal bound

hydroxide anion nucleophile attacked the carbon atom of the C-O bond to form, a five-

membered ring (**A**, Figure 1.10).[33]  If the hydroxide anion attacked the phosphorus atom of the

P-O bond a less stable transition state, a four-membered ring, would have formed (**B**, Figure

1.10).[33] Similar selectivity was shown for Th(IV), for which monomeric and dimeric hydroxo species dominated in the acidic solution. However, Th(IV) did not have the ability to promote decarboxylation of the cleaved DMPF to produce a final methyl phosphate product (step 2, Figure 1.9 ). Unlike Ce(IV) and Th(IV), Zr(IV) and Hf(IV) exist as tetrameric and octameric hydroxo species and selectively cleaved the P-O bond of phosphonoformate in acidic solutions.[33]

The allosteric effector 2,3-bisphosphoglycerate (BPG) (**11**, Figure 1.7, Table 1.1) was also reacted with Ce(IV) metal ions.[34] BPG plays a biological role in the regulation of hemoglobin binding affinity toward oxygen. Zhu et al. tested seventeen metal ions toward the hydrolysis of BPG by monitoring product production with $^{31}$P-NMR spectroscopy and a molybdenum blue phosphate assay.[34] The seventeen metals tested included all the trivalent lanthanides and Ce(IV). Again, Ce(IV) cleaved BPG more compared to the other metals tested. The higher product production by Ce(IV) was postulated to be due to enhance substrate activation. Cerium(IV) activated BPG by binding to and then neutralizing the negatively charged oxygens of the phosphate group. This step activates the substrate toward nucleophilic attack by a metal bound hydroxide ion. Additionally, with this particular substrate, hydrolysis occurred preferentially at the 2' phosphate ester bond because of the additional interactions between the carboxylate of the substrate and the metal ion.

In my review of the literature, I have described Ce(IV) superiority as a catalyst for enhanced hydrolysis of certain phosphate ester and amide containing substrates. However, there is one instance where Ce(IV) was relatively mediocre in the enhancement of phosphate ester bond hydrolysis. This occurred in the case of the hydrolysis of adenylyl (3'-5') adenosine, a diribonucleotide (ApA or RNA) (**12**, Figure 1.7).[17,37] Even though all lanthanide metals tested showed some hydrolytic activity toward ApA, Ce(IV) did not lead in the hydrolysis ranking.

The lanthanide(III) (Ln(III)) metal ions $Tm^{3+}$, $Yb^{3+}$, and $Lu^{3+}$ enhanced the hydrolysis of APA at pH 7.2 and 30 °C more than Ce(IV). For example, $Lu^{3+}$ provided ~ 11 fold faster hydrolysis compared to Ce(IV) which provided a rate constant of 1.8 x $10^{-2}$ $min^{-1}$.[37]



**(1)**          **(2)**
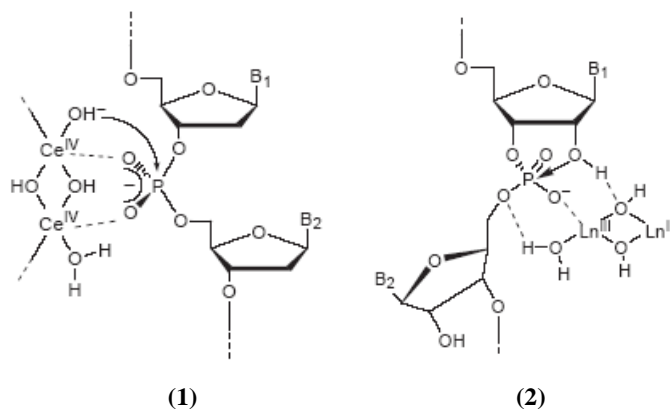
**Figure 1.11.** Proposed mechanisms of cerium(IV)-assisted hydrolysis of DNA **(1)** vs. lanthanide(III)-assisted hydrolysis of RNA **(2)**.[17]

In order to account for this finding, Komiyama et al. took an in-depth look into the mechanisms of enhanced DNA and RNA hydrolysis by lanthanide metal ions.[17] While metal-assisted hydrolysis of DNA entails the metal-bound hydroxide anion, for RNA the 2'-OH belonging to the ribose acts as a nucleophile in the hydrolysis reaction (Figure 1.11).[17] The second step was the same for both substrates and entailed the metal ion acting as an acid catalyst by the removal of the 5'-OH from the 2' phosphate ester end of the substrate.[17] The second step is rate-limiting for both RNA and DNA. However, the differences exhibited in the first step attribute to the contrast in rankings of metal ions toward enhance b cleavage of DNA vs. RNA. While the high charged density and strong Lewis acidity of Ce(IV) promoted higher levels of DNA hydrolysis, the larger radii lanthanides ($Tm^{3+}$, $Yb^{3+}$, and $Lu^{3+}$) promoted higher levels of RNA cleavage. For RNA hydrolysis, the first step is intramolecular attack by the 2'-OH of the substrate, in which it is not as essential for substrate activation and stabilization of the

intermediate compared to DNA hydrolysis by metal ions. However, the second step in RNA hydrolysis is more effectively carried out by the Ln(III) metal ions which display metal-bound water $pK_a$ values in the range of $8 - 9$ compared to $\sim -1$ value of Ce(IV)-bound water. The Ln(III) metal ions are therefore better acid catalysts than Ce(IV) in releasing the 5'-OH of the RNA substrate.[17]

## 1.4. Insight into Cerium and Metal Enhanced Hydrolysis Reactions

With an atomic number of 58 in the periodic table, the lanthanide cerium is one out of the fifteen rare earth elements. Cerium is ranked 25th in abundance out of all the elements and 65 ppm can be found in the earth's crust.[38] Cerium is unique compared to the other lanthanide metals. Not only does the element exist in a stable +3 oxidation state, but it has a +4 oxidation state. The other lanthanides exist only in a stable +3 oxidation state with the exception of europium, can exist in stable +3 and +2 oxidation states. The cerium +3 oxidation state has an electronic configuration of [Xe] $4f^1$, and +4 oxidation state has one less electron and displays xenon's noble gas electronic configuration [Xe] $4f^0$. Cerium was discovered in 1804 by a Swedish geologist, Wilhelm Hisinger, and by Swedish and German chemists, Jöns Jacob Berzelius and Martin Klaproth.[38] Cerium was named after an asteroid that was named after the Roman Goddess of agriculture, Ceres.[38]

The versatility of cerium has allowed the metal to be employed in a plethora of materials and synthetic techniques. In the mid-1800's, 65 mg three times per day of cerium(III) nitrate were prescribed to female patients to rid them of morning sickness.[38] It was also prescribed to alleviate unrelated stomach pain and gastrointestinal problems.[38] Cerium(III) oxalate was prescribed to relieve seasickness and coughing associated with tuberculosis.[38] Today, cerium is scarcely used in the preceding medical applications, but is utilized in topical creams to treat full

thickness burns in South America and Europe. The metal has found a niche in synthetic organic and inorganic chemistries and in material science. For example, cerium in the form of $Ce(IV)O_2$ can be found in many optical devices and is used in catalytic converters to assist in cleaning vehicle exhaust. Additionally, cerium's unique redox chemistry, in which the metal interconverts between its stable +3 and +4 oxidation states, has led to the development of cerium complexes as one-electron oxidizing agents. Thus, Ce(IV) has been utilized by synthetic organic chemists to assist in carbon-carbon and carbon-heteroatom bond formation, and as an oxidation catalyst to convert alcohols to corresponding ketones and aldehydes with high yields and short reaction times.[39,40]

Ce(IV) is commercially available as cerium ammonium nitrate $[Ce(NH_4)_2(NO_3)_6]$, cerium ammonium sulfate $[Ce(NH_4)_4(SO_4)_4]$, cerium dioxide $(CeO_2)$, cerium hydroxide $[Ce(OH)_4]$, and cerium sulfate $[Ce(SO_4)_2]$. The Ce(IV) metal ion salt $Ce(NH_4)_2(NO_3)_6$ is most commonly used in hydrolytic cleavage reactions.
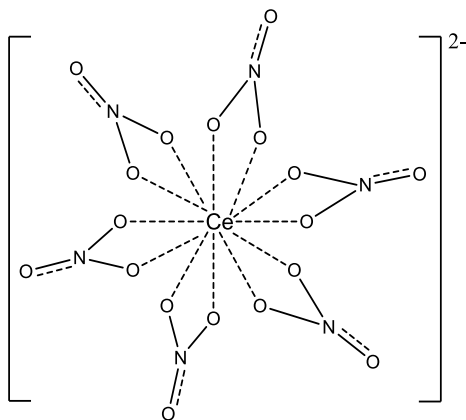


**Figure 1.12.** Structure of hexanitratocerate.

X-ray diffraction data of $Ce(NH_4)_2(NO_3)_6$ revealed hexanitratocerate anions, $[Ce(NO_3)_6]^{2-}$ (Figure 1.12), which are neutralized by the two ammonium cations.[41,42] The bidentate

coordination by each of the six $NO_3^-$ anions presents a total Ce(IV) coordination number of twelve and an icosahedral geometry. Both $Ce(SO_4)_2$ and $Ce(NH_4)_4(SO_4)_4$ have been used for assisted hydrolysis of 2,3-bisphosphoglycerate and dipeptides, respectively.[20,34] However, when compared to $Ce(NH_4)_2(NO_3)_6$, $Ce(SO_4)_2$ and $Ce(NH_4)_4(SO_4)_4$ provided lower hydrolysis yields. Two reasons have been postulated for this difference. The higher stability constant of Ce(IV) sulfate may suppress the formation of Ce(IV) hydroxo species, and therefore, hydroxide nucleophiles needed for hydrolysis are less likely to form.[34] The second reason is that the sulfate anions are shown to act as competitive inhibitors in the hydrolysis reactions by binding to the metal ion and thus reducing substrate-metal interactions. The other Ce(IV) precursors, $CeO_2$ and $Ce(OH)_4$ are not suitable for hydrolysis reactions because they are insoluble in water.[20]

Many questions arise pertaining to Ce(IV) superiority over other metal ions in enhancing phosphate ester and amide bond hydrolysis. The first question that needs to be answered is: what are the properties that distinguish Ce(IV) from other metal ions, in particular trivalent lanthanide and tetravalent metals, for the enhancement of hydrolytic cleavage reactions? The three main answers are: Ce(IV) displays high Lewis acidity, has a stable trivalent state, and favors high coordination numbers.

### 1.4.1. Lewis acidity: substrate activation and formation of active polynuclear metal hydroxo species

Enhancement of phosphate ester and amide bonds hydrolysis by Ce(IV) is mainly due to the high Lewis acidity of the metal ion. The metal ion has a high Lewis acidity because of its high charge density, presenting a +4 charge and a 0.97 Å ionic radius.[20,43]
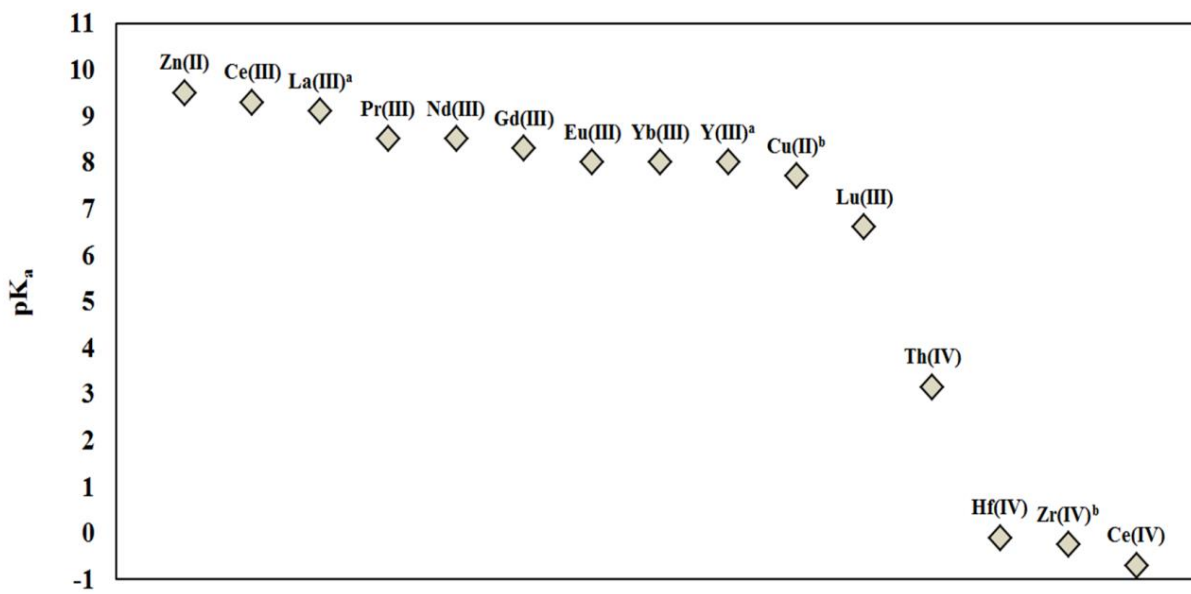
**Figure 1.13.** pK$_a$ values for water bound metal ions in aqueous solutions. pK$_a$ values taken from ref. 46. [a]Determined in aqueous solutions with ionic strength greater than 0. [b]Median number from a range of pK$_a$ values.

This substantial quality of Ce(IV) is illustrated by Figure 1.13, which displays the pK$_a$ values of water bound to Ce(IV) and other metal ions. Previous studies have shown Ce(IV) to be superior over the Ln(III) metal ions in the hydrolytic cleavage of substrates with Ce(IV) followed by Zr(IV) and Hf(IV) promoting the most hydrolytic cleavage.[19,20,35] This trend correlates to the pK$_a$ values of the metal-bound water, -0.7, -0.3, and -0.1 assigned to Ce(IV), Zr(IV), and Hf(IV), respectively.[44] The trivalent lanthanide metal ions displayed pK$_a$ values in the range of ~ 8 − 9. The metal ions common in natural hydrolase enzymes, Mg(II) and Zn(II), displayed pK$_a$ values of 11.4 and 9.5, respectively. Trivalent lanthanide metal ions are typically inactive in acidic solution because of the requirement for basic conditions to generate an active hydroxide nucleophile. Thus, in acidic solution Ln(III) metal ions have primarily water molecules bound. Alternatively, the low pK$_a$ of Ce(IV) bound water promotes hydrolysis at low and high pH values, since there is always an active hydroxide nucleophile even under very acidic solutions.

Cerium(IV) is capable of forming high concentrations of active mononuclear and polynuclear hydroxo species in solution at low and high pH values. Before I go in-depth into the aqueous solution chemistry of Ce(IV), I will present a short lesson on the formation of metal hydroxo species in solution.

$$M^{n+} + H_2O \rightarrow M(OH)^{(n-1)+} + H_3O^+ \quad \textbf{(1.1)}$$

The coordination of a water molecule to a metal ion ($M^{n+}$) will lead to the deprotonation of the water molecule to produce a metal bound hydroxide [metal hydroxo species, $M(OH)^{(n-1)+}$] and a hydronium ion (Equation 1.1).[45] The greater the charge density of the metal ion, the more susceptible the water molecule is to deprotonation.[45] The formation of polynuclear species in aqueous solution is commonly seen for trivalent and tetravalent metal ions at applicable pH ranges.[44]

$$2M(OH)^{2+} \rightarrow M_2(OH)_2^{4+} \quad \textbf{(1.2)}$$

Equation 1.2 shows the condensation of two mononuclear metal hydroxo species ($M(OH)^{2+}$) into one polynuclear metal hydroxo species ($M_2(OH)_2^{4+}$).[44] The metal ions are held together by hydroxo bridges .[44] This tetracationic binuclear species is common for Ln(III) metal ions at the appropriate, typically basic pH.

$$Ce(IV) + H_2O \rightleftharpoons [Ce(OH)]^{3+} + H^+ \qquad \log K = 1.1 \qquad \textbf{(1.3)}$$

$$Ce(IV) + 2H_2O \rightleftharpoons [Ce(OH)_2]^{2+} + 2H^+ \qquad \log K = 0.3 \qquad \textbf{(1.4)}$$

$$2Ce(IV) + 2H_2O \rightleftharpoons [Ce_2(OH)_2]^{6+} + 2H^+ \qquad \log K = 3.6 \qquad \textbf{(1.5)}$$

$$2Ce(IV) + 3H_2O \rightleftharpoons [Ce_2(OH)_3]^{5+} + 3H^+ \qquad \log K = 4.1 \qquad \textbf{(1.6)}$$

$$2Ce(IV) + 4H_2O \rightleftharpoons [Ce_2(OH)_4]^{4+} + 4H^+ \qquad \log K = 3.5 \qquad \textbf{(1.7)}$$

$$6Ce(IV) + 12H_2O \rightleftharpoons [Ce_6(OH)_{12}]^{12+} + 12H^+ \quad \log K = 15.4 \qquad \textbf{(1.8)}$$
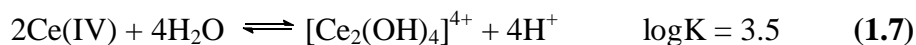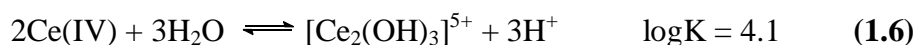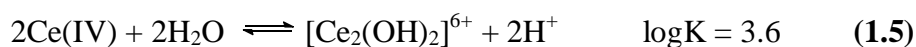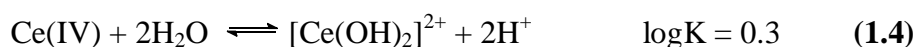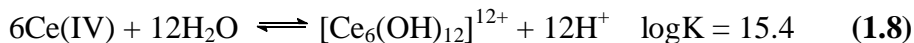
The aqueous solution chemistry of the Ce(IV) metal ion was studied in acidic solutions containing 3 M NaClO$_4$. Six equilibria were then formulated (Equations 1.3 – 1.8).[46] Mononuclear, Ce(OH)$^{3+}$ and Ce(OH)$_2{}^{2+}$, and polynuclear, Ce$_2$(OH)$_2{}^{6+}$, Ce$_2$(OH)$_3{}^{5+}$, Ce$_2$(OH)$_4{}^{4+}$, and Ce$_6$(OH)$_{12}{}^{12+}$, hydroxo species were present in the acidic perchlorate solution of Ce(IV). Komiyama et al. identified polynuclear Ce$_2$(OH)$_4{}^{4+}$ as the catalytically active species for the hydrolysis of cAMP (**7**, Figure 1.7) and dinucleoside monophosphate thymidylyl (3'-5') thymidine in homogeneous acidic solutions (less than pH 2.5; 1 mM Ce(IV)).[17] In the same solution, the mononuclear species Ce(OH)$_2{}^{2+}$ is present at even higher concentrations. However, this species was less involved in the hydrolysis reaction.[17] Additionally, Komiyama et al. suggested that the same polynuclear Ce$_2$(OH)$_4{}^{4+}$ was involved in DNA hydrolysis by heterogeneous solutions of insoluble Ce(IV) hydroxo gels under neutral conditions, since hydrolysis rates were similar when compared to homogeneous acidic solutions of Ce(IV). The tendency of Ce(IV) metal ions to form binuclear species at low and high pH provides more efficient substrate activation compared to mononuclear species. Thus, two metal ions each binding to a negatively charged phosphate oxygen atom enhance the electrophilicity of the phosphorus atom (activation of the substrate) of the phosphate linkage more compared to one metal ion.[17]
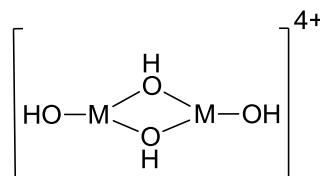


**Figure 1.14.** Structure of the tetracationic binuclear Ce(IV) hydroxo complex Ce$_2$(OH)$_4{}^{4+}$, the active species for hydrolysis of cAMP and thymidylyl (3'-5') thymidine.[17]

The tetracationic binuclear Ce(IV) hydroxo complex $Ce_2(OH)_4^{4+}$ has two hydroxo-bridges (Figure 1.14). The higher the pH, the more Ce(IV) is prone to the formation of insoluble polynuclear hydroxo clusters. For this reason, there have been limited studies on the catalytic active species of Ce(IV) toward the hydrolysis of substrates in aqueous neutral solution because of precipitation of this metal ion as Ce(IV) hydroxo clusters at pH values greater than 4.[16] However, in homogeneous solutions aided by excess imidazole buffer under near-neutral conditions (pH 6 - 8) and Ce(IV) concentration of ~ 0.1 mM, Maldonado and Yatsimirsky found the monocationic binuclear Ce(IV) hydroxo species $Ce_2(OH)_7^+$ to be present in solution.[16] Possible complex formation between the metal ion and buffer prevented the formation of insoluble Ce(IV) hydroxo clusters, making it possible for speciation to be studied by potentiometric titration method.

### 1.4.2. Stable trivalent state allows for stronger substrate activation

The high Lewis acidity of Ce(IV) provides more favorable conditions for substrate activation compared to other metals. However, the most distinguishable quality of the metal ion in assisting hydrolysis is the stability of the metal's trivalent state, which contributes to the electron accepting ability of Ce(IV) in substrate activation. This notable feature of Ce(IV) was established in a series of spectroscopy studies conducted by Shigekawa et al.[47,48] Core level spectroscopies, such as photoelectron spectroscopy or x-ray absorption near edge structure (XANES), can provide details of the local electronic structure around an atomic site to offer insight into bonding interactions. First, monitoring the binding energy by photoelectron spectroscopy of phosphorus $2p$ orbital's core level spectra of a DNA model substrate, diphenyl phosphate (DPP) (**9**, Figure 1.7), showed higher binding energy when coordinated to Ce(IV) metal ion compared to other metals.[47] The higher binding energy displayed by the DPP-Ce(IV)

complex suggested that the metal ion withdraws electrons from the phosphodiester bond more compared to the other metal ions tested (La(III), Eu(III), and Lu(III)). Further studies by XANES showed that upon complex formation, Ce(IV), which has an electronic configuration of [Xe] $4f^0$, displayed $0.67 - 0.69f$ electrons when coordinated to DPP.[48] Thus, Ce(IV) partially withdraws an electron from the phosphate linkage into its $4f$ orbital. Ce(III) metal ion was also tested and showed no electronic transfer from DPP.[48] These spectroscopy studies suggest that Ce(IV) binds to DPP by slight covalent interactions by withdrawing electrons from the phosphate residue of the substrate. The main reason for this notable quality that distinguishes Ce(IV) from Ln(III) and other tetravalent metal ions is the metal's stable trivalent state which allows this partial electron transfer to occur. Whereas, the tetravalent metal ions $Zr^{4+}$ and $Hf^{4+}$, and most Ln(III) metals do not have stable trivalent and divalent states, respectively. Thus, these metal ions can only interact with the substrate electrostatically. This explains why $Zr^{4+}$ and $Hf^{4+}$, as Ce(IV), decrease the $pK_a$ of water to a value less than 1, but assisted hydrolysis of phosphatidylcholine 20 fold less,[19] peptides $\sim 4 - 5$ fold less,[20] and BNPP $10 - 27$ fold slower[35] compared to Ce(IV). In summary, Ce(IV) stable trivalent state allows for a partial electron withdrawal from the substrate, and consequently, allows efficient substrate activation by enhancing the electrophilicity of the phosphorus atom.

### 1.4.3. High coordination number: nucleophiles and acid/base catalysis

Ln(III) metal ions typically have a coordination number of 8 - 9, but Ce(IV) is known to have coordination numbers up to 12. This provides Ce(IV) with a higher probability for a coordinated water to act as a nucleophile for the cleavage of the substrate, even when the metal ion is complexed to a ligand and/or substrate.[20] Even better, there is a higher chance for a coordinated water to be present for acid/base catalysis to assist in the hydrolysis reaction.[17] In

summary, superior Ce(IV)-assisted hydrolysis is mainly due to the high Lewis acidity, electron withdrawing ability provided by its stable trivalent state, and high coordination numbers, which leads to other advantages, such as providing hydrolysis at low and high pH, acid/base catalysis, and substrate activation.

**1.5. The Mechanism and Limitations of Cerium(IV)-assisted Hydrolysis**
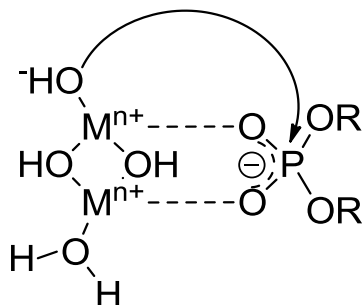


**Figure 1.15.** Mechanism of Ce(IV)-assisted hydrolysis of phosphate ester bonds.

A general mechanism for Ce(IV)-assisted hydrolysis of phosphate ester bonds is shown in Figure 1.15.[17] The first step entails the cationic binuclear Ce(IV) hydroxo species functioning as a strong Lewis acid and forming a complex with the substrate. Thus, both Ce(IV) metal ions coordinate to one of the free oxygen atoms of the phosphate ester linkage of the substrate.[17] This step neutralizes the negatively charged oxygen, and enhances the electrophilicity of the phosphorus to activate the substrate toward nucleophilic attack. The second step involves the nucleophilic attack of the activated phosphorus center by one of the unbridged hydroxyls coordinated to one of the Ce(IV) metal ions.[17] Nevertheless, in this step the cationic binuclear Ce(IV) metal center is responsible for stabilization of the transition state which then collapses to provide products. Additionally, there is the possibility that in preparation for nucleophilic attack of the phosphorus center a water bound to Ce(IV) may assist in the hydrolysis by acting as an acid catalyst.[17]

The Ce(IV) metal ion has shown itself to be a superior agent in enhancing hydrolysis reactions. However, Ce(IV) can present certain limitations. Aqueous solutions of Ce(IV) are susceptible to the formation of insoluble polynuclear hydroxo clusters as the pH increases above 4.[16] However, these reaction conditions are not practical for broader applications.[16] One way to escape these confinements is to perform hydrolysis in acidic homogeneous aqueous solution, less than pH 4. However, the former approach is not practical for biological applications. A more practical and advantageous way to eliminate some of the confinements of working with Ce(IV) is through the formation of a complex with a ligand that help control metal speciation in aqueous solutions.

## 1.6. Ligands Can Tune, Provide Selectivity, and Enhance Phosphate Ester Bond Hydrolysis by Ce(IV)

Complex formation between the Ce(IV) metal ion and a ligand can, in theory, eliminate certain confinements and improve the catalytic stability of the metal ion in aqueous solution. The ligand can prevent precipitation of the metal ion at pH values greater than 4 while providing hydrolytic active Ce(IV) species with a definite composition.[16] Additionally, ligands can enhance and tune hydrolysis, and provide selectivity for the hydrolysis process. As an example, Branum et al. designed a selective DNA hydrolase mimic.[28] Ce(IV) in the presence of two mole equivalents of the polyaminocarboxylate derivative ligand HXTA (**12**, Figure 1.16) facilitated double-stranded hydrolysis of supercoiled plasmid DNA (produced 63 % nicked and 20 % linear after 12 h at 37 °C) and preferentially cleaved at the 3'- phosphate end of the DNA restriction fragments phosphate ester linkage at pH 8 and 37 °C.[28]

**12**          **13**          **14**
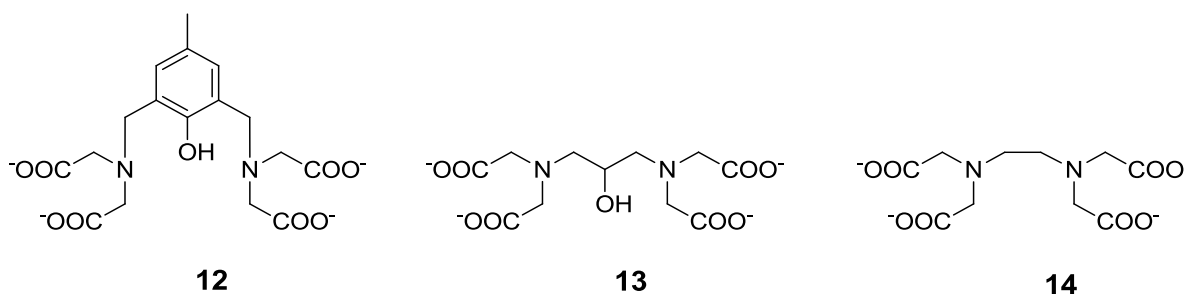
**Figure 1.16.** Structures of polyaminocarboxylate ligands utilized in Ce(IV)-assisted hydrolysis of DNA. 5-methyl-2-hydroxy-1,3-xylene-α,α-diamine-*N,N,N',N'*-tetraacetic acid (HXTA) (**12**), 1,3-diamino-2-hydroxypropane-*N,N,N',N'*-tetraacetic acid (HPTA) (**13**), and ethylenediaminetetraacetic acid (EDTA) (**14**).

The ligand HXTA contains four carboxylate groups and a central phenol moiety to afford a phenoxo-bridged dicerium complex comprised of two 6-membered chelate rings and four 5-membered chelate rings. The ligand was a key contributor to the regioselective cleavage of the DNA restriction fragments. The other significant role of the ligand was to facilitate double-stranded hydrolysis of supercoiled plasmid to produce linear DNA. This was attributed to the formation of the dicerium complex, which provided more efficient Lewis activation of both strands of DNA.[28] DNA hydrolysis by Ce(IV) and HXTA was then compared to polycarboxylate ligands capable of forming mononuclear and binuclear Ce(IV) complexes, and Ce(IV) in the absence of ligand.[27] The ligand HPTA (**13**, Figure 1.16) was also capable of forming binuclear complexes with Ce(IV) by the coordination of two metal ions to the alkoxo bridge of the ligand. This produced 33 % linear DNA product from supercoiled plasmid DNA after 3 h at pH 8 and 55 °C.[49] Interestingly, the 1:1 complex (Ce:HPTA) and Ce(IV) in the absence of ligand did not cleave supercoiled plasmid DNA under the same reaction conditions. Additionally, EDTA (**14**, Figure 1.16), which forms mononuclear complexes with Ce(IV), provided only 2 % linear DNA from supercoiled plasmid DNA after 3 h at pH 8 and 55 °C.[27] In summary, the results of Branum et al. suggested that the ligands HPTA and HXTA directed the

formation of a binuclear Ce(IV) metal ion center, which provided efficient Lewis activation of the substrate. The complexes mimicked natural DNA hydrolases by preferentially cleaving the 3'-phosphate end of DNA restriction fragments and by providing linear DNA products from supercoiled DNA.

An exceptional example of a Ce(IV) complex used as a hydrolytic catalyst is a two-step site selective DNA hydrolysis method called ARCUT which utilizes the ligand EDTA.[30,50] The first step employs a double-duplex invasion strategy[51] which entails selective activation of the target DNA cleavage site by the addition of two pseudo-complementary oligonucleotide strands to duplex DNA. Therefore, the addition of the two strands creates "hot spots", transforming the double-stranded target DNA into single-stranded DNA. The second step involves the addition of a homogeneous solution containing one mol equivalent of Ce(IV) and EDTA, which selectively cleaves single-stranded DNA over double-stranded DNA under physiological conditions (pH 7 and 37 °C).[30] The group also noted that Ce(IV) in the absence of EDTA formed heterogeneous solutions containing Ce(IV) hydroxide gels, and the process lost its selectivity and randomly cleaved single- and double-stranded DNA at relatively the same rate. The ARCUT method was also successful in site-selective cleavage of human genomic DNA.[52]

| **Table 1.2.** Ce(IV)-assisted hydrolysis of BNPP by Ce(IV) complexes | | | | |
|---|---|---|---|---|
| Ligand (Ce(IV): Ligand) | $T$ (° C) | pH | $k_2$ ($M^{-1}$ $s^{-1}$)[a] | References |
| HXTA (2:1) | 37 | 8.0 | 0.1 | 28 |
| Palmitate in micelle solution (2:1) | 37 | 7.0 | 13 | 21 |
| Ce-MPGN (4:1) | 25 | 7.0 | 0.3 | 15 |
| EDDA bridged by two β-CD (1:1) | 25 | 7.0 | 2.3 | 25 |
| Phen bridged by two β-CD (1:1) | 35 | 7.0 | $2.3 \times 10^2$ | 26 |
| [a] Values taken from reference 26 | | | | |

Bracken et al. studied BNPP (**8**, Figure 1.7) hydrolysis by Ce(IV) complexes in micellar

solutions.[21]  Brij medium provided the micelles and along with the ligands in Figure 1.17 (**15 -**

**17**) were able to provide stable homogeneous aqueous solutions of Ce(IV) at pH values greater

than 5.



**15**  **16**  **17**
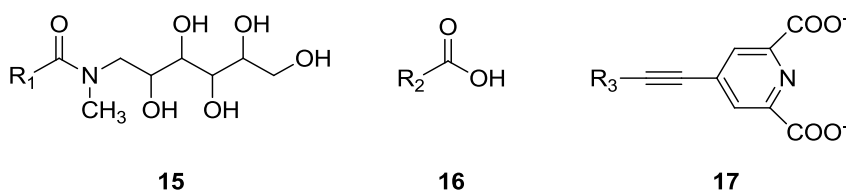
**Figure 1.17.** Structures of ligands utilized for Ce(IV)-assisted hydrolysis of BNPP.  The ligands are n-octanoyl-N-methyl-D-glucamine (**15**), palmitate (**16**), and 4-(1-hexadecynyl)-2,6-pyridinedicarboxylate (**17**). $R_1 = n\text{-}C_7H_{15}$, $R_2 = n\text{-}C_{15}H_{31}$, and $R_3 = n\text{-}C_{14}H_{29}$.

The ligands (**15 - 17**, Figure 1.17) mediated Ce(IV)-assisted hydrolysis of BNPP at high rates

over a broad pH range.  In addition, Ce(IV)-enhanced hydrolysis was controlled as a function of

pH by the donor atoms of the ligands.[21]  At a metal to ligand ratio of 1:1, Ce(IV) and **15** (Figure

1.17) enhanced hydrolysis of BNPP at similar rates compared to Ce(IV) in the absence of ligand

at pH 4.0 and 5.0.[21]  Hydrolysis by Ce(IV) in the absence of ligand could not be tested at pH

values greater than 5 because of metal ion precipitation.  Alternatively, 1:1 and 2:1 metal to

ligand ratios of Ce(IV) and **15** allowed Branum et al. to study the rate of BNPP hydrolysis up to

pH values of 9.0 and 11.0, respectively.  The rate of BNPP by the Ce(IV) complex decreased as

pH increased at both ligand to metal ratios.  Ce(IV) in the presence of **16** (Figure 1.17) reduced

hydrolysis compared to Ce(IV) in the absence of ligand at pH 4.0.  However, as pH increased to

7, the rate of hydrolysis in the presence of **16** was increased to $2.6 \times 10^{-2}$ $s^{-1}$ (Table 1.2, 2:1

Ce(IV) to **16**), which in this study was the highest hydrolysis rate compared to the other

complexes and Ce(IV) in the absence of ligand.[21]  The ligand **17** (Figure 1.17), which is capable

of forming two 5-membered chelate rings by the bidentate carboxylates, increased Ce(IV)

hydrolysis as a function of pH at metal to ligand ratios of 1:1 (pH 7.0 – 12) and 2:1 (pH 9.0 –

11).[21]

Bonomi et al. were interested in the design of a synthetic catalyst to mimic a natural

enzyme. Towards this end, they investigated a multivalent synthetic catalyst with flexible and

self-organized metal chelating thiolate groups on the surface of gold nanoparticles (Ce(IV)-

MPGN) (Figure 1.18).[15]
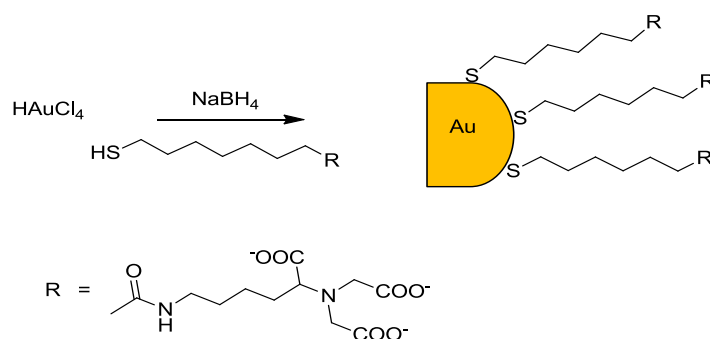


**Figure 1.18.** Synthesis and design of monolayer protected gold nanoparticles (MPGNs)
decorated with thiolate ligands containing polycarboxylate groups.

Remarkable hydrolytic activity towards the cleavage of BNPP was exhibited by Ce(IV)

coordinated to the tridentate carboxylates of the thiolated ligands on gold nanoparticles. In the

absence of a catalyst, BNPP has a hydrolytic half-life of 2000 years at pH 7 and 25 °C.

However, the catalyst (Ce(IV)-MPGN) gave a 2.5 million-fold rate enhancement in BNPP

hydrolysis ($4.5 \times 10^{-5}\,s^{-1}$) at pH 7 and 25 ° C (Table 1.2). There was no detected BNPP

hydrolysis by Ce(IV) in the presence of the polycarboxylate ligand (**R**, Figure 1.18) under the

same reaction conditions.[15]

Other groups researched ligands (**18** and **19**, Figure 1.19) bridged by β-cyclodextrin

derivatives that provided neutral homogeneous aqueous solutions and enhanced substrate binding

between Ce(IV) and BNPP.[25,26]
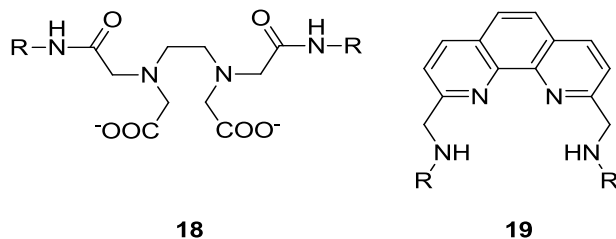
**Figure 1.19.** β-cyclodextrin derivatives (**R**) bridged by ethylenediamine-*N,N'*-diacetic acid (EDDA) derivative (**18**) and phenanthroline derivative (phen) (**19**).

One hydrolytic agent was constructed from β-cyclodextrin (7- membered sugar ring) dimers bridged by an ethylenediamine-*N,N'*-diacetic acid (EDDA) linker (**18**, Figure 1.19).[25] The β-cyclodextrin provided hydrophobic interactions and improved binding affinity to the substrate, and contributed to a 520 fold increase in the rate of BNPP hydrolysis.[25] EDDA was responsible for complex formation with Ce(IV) metal ion through its bidentate carboxylate groups. To improve hydrolysis rates, Zhao et al. switched to a N-donor phenanthroline derivative (phen) to bridge the β-cyclodextrin dimers (**19**, Figure 1.19).[26] The tetradentate ligand coordinates Ce(IV) to form three 5-membered chelate rings. This hydrolytic agent provided a second-order rate constant of 2.3 x $10^2$ $M^{-1}s^{-1}$ for BNPP hydrolysis at pH 7.0 and 35 °C and increased BNPP hydrolysis ~ 100 fold compared to the Ce(IV) hydrolytic agent containing β-cyclodextrin dimers bridged by EDDA under the same reaction conditions (Table 1.2).[26] β-Cyclodextrin dimers bridged by Ce(IV) phen complex produced the fastest hydrolytic cleavage of BNPP compared to all other Ce(IV) complexes tested (Table 1.2).

**1.7. Potential Applications of Ce(IV) Metal Ion and Complexes as Phospholipase Mimics and as Therapeutic Agents to Alleviate Phospholipidosis**

The investigation of Ce(IV) metal ion and complexes as DNA hydrolase mimics has given rise to significant advances in our understanding of metal-assisted phosphate ester hydrolysis. Lipid hydrolysis by the metal ion has been studied scarcely.[18,19,53-56] Nevertheless,

lipids play essential roles in biological systems as energy-storage molecules and chemical messengers in cell signaling and regulation, and as major components of the biological membranes that surround cells and organelles.[4,9,10] Most vital functions of lipids are provided by the products produced from lipid degradation by phospholipid-specific hydrolases called phospholipases. Examples of lipid hydrolysis products are diacylglycerol (**23**, Figure 1.20) and phosphatidic acid (**22**, Figure 1.20) from the degradation of phosphoglycerides (Figure 1.3) by phospholipase C or phospholipase D, and ceramide from the degradation of sphingomyelin (Figure 1.4) by sphingomyelinase. These products from lipid degradation have vital biological roles, such as intermediates in lipid synthesis and secondary messengers in signal transduction.[4,9,10]

Our research group has shown that Ce(IV)-assisted hydrolysis provided enhance levels of hydrolytic cleavage of the phosphate ester bonds of the naturally occurring phospholipids, phosphatidylcholine and sphingomyelin.[19]
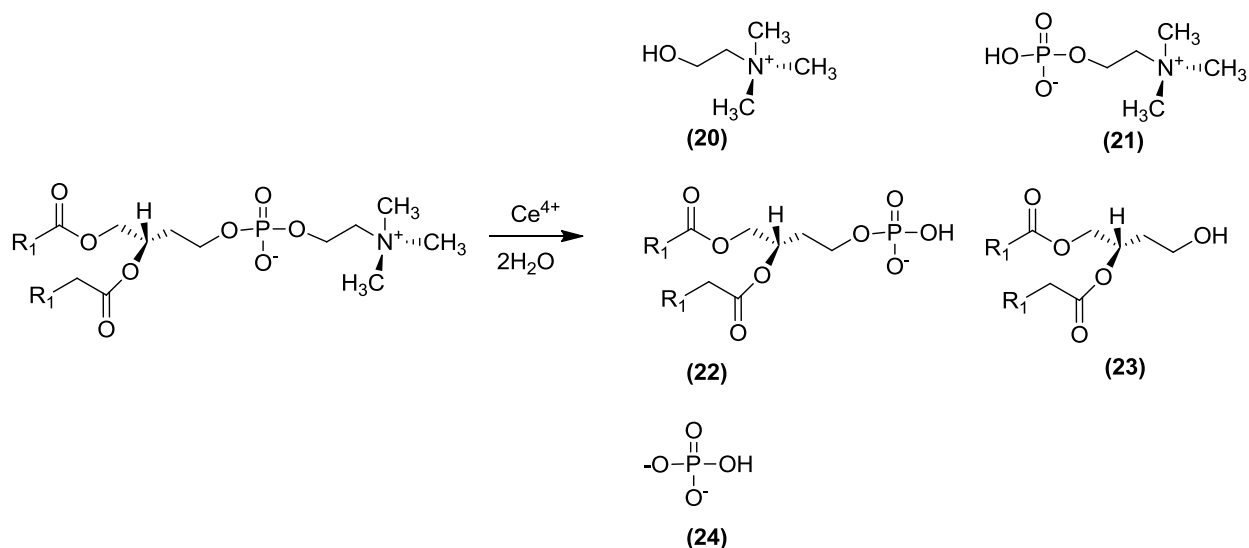


**Figure 1.20.** Ce(IV)-assisted hydrolysis of phosphatidycholine (PC) produced the products, choline (**20**), phosphocholine (**21**), phosphatidic acid (**22**), diacylglycerol (**23**), and phosphate (**24**). **R₁** represents long chain fatty acid hydrocarbons of variable lengths.

Employment of MALDI-TOF mass spectrometry to detect choline (**20**, Figure 1.20) and

phosphocholine (**21**), and colorimetric assays to quantitate inorganic phosphate (**24**) and choline,

Kassai et al. have shown phospholipase C and phospholipase D-type activity for Ce(IV)-assisted

hydrolysis of lipid vesicles of L-α-phosphatidylcholine (PC).[19] Additional products that may be

produced from the reaction are 1,2-diacylglycerol (**23**) and phosphatidic acid (**22**) (Figure 1.20).

Hydrolysis of PC by Ce(IV) generated ~ 12 % phosphate and ~ 31 % choline hydrolysis yields

after 20 h at 37 °C and ~ pH 7.2.[19] At slightly acidic conditions, ~ pH 4.8, hydrolysis yields of

phosphate and choline increased to 21 % and 43 %, respectively.[19] Thus, it would be reasonable

to employ Ce(IV) metal ions and complexes as lysosomal or cytoplasmic phospholipase mimics

to study signal transduction pathways, probes to study lipid model systems, or even as potential

therapeutic agents to reverse the build-up of phospholipids in acquired or genetic forms of

phospholipidosis.

Acquired and genetic forms of phospholipidosis are known as drug-induced

phospholipidosis and lysosomal storage disease, respectively. Both of these disorders result

from the impairment of phospholipid/lipid degradation, but the mechanisms and basis of the two

are different. Drug induced phospholipidosis is caused by cationic amphiphilic drugs (CADs).

CADs have similar structural features as phospholipids; the drugs contain hydrophobic and

hydrophilic moieties. In addition, CADs typically include a primary or substituted amine.[57]

Thus, these drugs can easily concentrate in the lysosome and act as competitive inhibitors of

phospholipases to reduce the degradation of phospholipids. Another way phopholipidosis could

be aided by CADs is by the formation of lipid-drug complexes which causes the phospholipid to

be less receptive to degradation.[57]
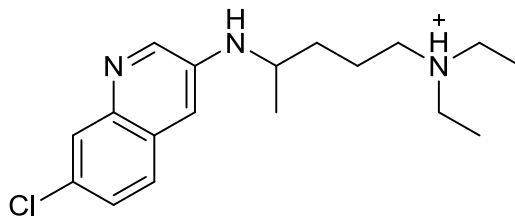
**Figure 1.21.** Cationic amphiphilic drug, chloroquine

An example, chloroquine (Figure 1.21) is an anti-rheumatic and antimalarial drug that inhibits

phospholipases A and C and bears a net positive charge at acidic pH.[57] Thus, this weakly basic

compound can enter, become ionized and trapped inside the lysosome.[57]

In lysosomal storage disorders (LSDs), phospholipidosis is caused by a defective enzyme

with reduced or eliminated activity, the result of mutation in a gene that codes for a specific

enzyme.[57] There are forty recognized LSDs. An example is Niemann-Pick Disease (NPD) types

A and B, which are the neurological and non-neurological forms of NPD, respectively. The

defective SMPD1 gene results in the production of inefficient and defective acid

sphingomyelinase that displays reduced activity which leads to the accumulation of the lipid

sphingomyelin in lysosomes.[58]

The impairment of phospholipid metabolism results in the accumulation of lipid

substrates inside lysosomes and lamellar bodies constructed from undegraded lipids.[57]

Lysosomes are cellular organelles that have an acidic pH (~ 4.8) environment, and are

responsible for intracellular digestion and recycle of macromolecules. Lamellar bodies are

intracellular concentric structures that have a mildly acidic environment similar to lysosomes,

but typically serve as storage vesicles and transporters of surfactant proteins in type II

pneumocytes.[57] The accumulation of phospholipids in lysosomes and lamellar bodies can have a

variety of negative consequences. Histopathological and histochemical changes occur that

adversely affect organs and tissues, such as the lung, brain, kidney, and cornea.[57] Additionally,

lipid accumulation could result in the lysosome rupture and leakage of acidic hydrolases into the cytoplasm.[57] The disrupted lipid metabolism in LSDs and drug-induced phospholipidosis can create respiratory infections which is a pulmonary complication developed from the accumulation of phospholipids in the lung.[59] Phosphatidylcholine constitutes to 70% of pulmonary surfactant and the accumulation of this phospholipid can reduce surface tension in the lung.[59]

Symptoms caused by drug-induced phospholipidosis can be reversed by stopping medication intake.[57] However, there is no cure for the recessive genetic LSDs. Current treatments for LSDs are lavaging (washing of the organs), bone marrow transplantation, splenectomy, and enzyme replacement therapy.[60,61] Enzyme replacement therapy is the most successful out of the four, however, not all defective enzymes have been pinpointed for every LSD.[60,61] Additionally, a person with LSD on enzyme replacement therapy can still experience the common complications caused by phospholipidosis.[60,61]

## 1.8. Conclusions

Ce(IV) increased hydrolysis yields of inorganic phosphate and choline from PC 1.8 and 1.4 fold, respectively, upon lowering the pH from ~ 7.2 to ~ 4.8. The metal ion released 21 % of phosphate and 43 % of choline from PC after 20 h at 37 °C and ~ pH 4.8. These results are significant in the search for a therapeutic agent that can alleviate the symptoms of phospholipidosis, in which phospholipids accumulates in the mildly acidic environment of the lysosome.[19] However, there are limitations to the hydrolytic efficiency of Ce(IV). Complexation of Ce(IV) to a ligand can prevent precipitation, create active species with definite compositions, tune hydrolysis, and create selectivity.[15,16] Taking clues from natural lysosomal phospholipases, an ideal Ce(IV) complex would be required to promote sufficient hydrolysis at

the acidic pH of the lysosome, but suppress hydrolysis significantly at cytosolic pH. Even though the single layer of the lysosome's membrane protects the cell from damage that could be caused by the Ce(IV) complexes, further protection would be provided by the pH dependency of the hydrolytic agent. Therefore, the goal of the research described in this dissertation is to construct a synthetic acidic hydrolytic agent. The studies reported here are directed toward designing Ce(IV) complexes that have acidic phospholipase-type activity (Chapter 3). In addition to this work, this dissertation describes experiments involving Ce(IV)-assisted hydrolysis of the sphingolipid sphingomyelin (Chapter 2) and a copper(II) hexaazatriphenylene complex that photo-oxidizes DNA upon exposure to ultraviolet light (Chapter 4).

## 1.9. References

(1) Fersht, A. *Structure and mechanism in protein science*; W. H. Freeman and Company: New York, 1999.

(2) Weston, J., Mode of action of bi- and trinuclear zinc hydrolases and their synthetic analogues. *Chem Rev* **2005,** *105*, 2151.

(3) Bruice, T. C.; Fife, T. H.; Bruno, J. J.; Brandon, N. E., Hydroxyl group catalysis. II. The reactivity of the hydroxyl group of serine. The nucleophilicity of alcohols and the ease of hydrolysis of their acetyl esters as related to their pKa. *Biochemistry* **1962,** *1*, 7.

(4) Stryer, L. *Biochemistry*; fourth ed.; W. H. Freeman and Company: New York, 1995.

(5) Mishra, C. N. *Nucleases: Molecular biology and application*; John Wiley & Sons, Inc.: Hoboken, 2002.

(6) Hawthorne, J., N.; Ansell, G, B.; Neuberger A; Van Deenen L, M. *Phospholipids*; Elsevier Biomedical: New York, 1982; Vol. 4.

(7)  Niemela, P.; Hyvonen, M. T.; Vattulainen, I., Structure and dynamics of sphingomyelin bilayer: Insight gained through systematic comparison to phosphatidylcholine. *Biophys J* **2004,** *87*, 2976.

(8)  Liao, R. Z.; Yu, J. G.; Himo, F., Phosphate mono- and diesterase activities of the trinuclear zinc enzyme nuclease P1-insights from quantum chemical calculations. *Inorg Chem* **2010,** *49*, 6883.

(9)  Dennis, A. E. R., G. S.; Billah, M. M.; Hannun, A. Y., Role of phospholipases in generating lipid messengers in signal transduction. *FASEB J* **1991,** *5*, 2068.

(10)  Hannun, A. Y. B., M. R., Functions of sphingolipids and sphingolipid breakdown products in cellular regulation. *Science* **1989,** *243*, 500.

(11)  Matsuzawa, Y. H., K. K., Properties of phospholipase C isolated from rat liver lysosomes. *J Biol Chem* **1980**, 646.

(12)  Uesugi, Y.; Hatanaka, T., Phospholipase D mechanism using Streptomyces PLD. *Biochim Biophys Acta, Mol Cell Biol Lipids* **2009,** *1791*, 962.

(13)  Hiraoka, M.; Abe, A.; Shayman, J. A., Structure and function of lysosomal phospholipase A(2): identification of the catalytic triad and the role of cysteine residues. *J Lipid Res* **2005,** *46*, 2441.

(14)  Grant, K. B.; Kassai, M., Major advances in the hydrolysis of peptides and proteins by metal ions and complexes. *Curr Org Chem* **2006,** *10*, 1035.

(15)  Bonomi, R.; Scrimin, P.; Mancin, F., Phosphate diesters cleavage mediated by Ce(IV) complexes self-assembled on gold nanoparticles. *Org Biomol Chem* **2010,** *8*, 2622.

(16)  Maldonado, A. L.; Yatsimirsky, A. K., Kinetics of phosphodiester cleavage by differently generated cerium(IV) hydroxo species in neutral solutions. *Org Biomol Chem* **2005,** *3*, 2859.

(17) Komiyama, M.; Takeda, N.; Shigekawa, H., Hydrolysis of DNA and RNA by lanthanide ions: mechanistic studies leading to new applications. *Chem Commun* **1999**, 1443.

(18) Cepeda, S. S.; Williams, D. E.; Grant, K. B., Evaluating metal ion salts as acid hydrolase mimics: metal-assisted hydrolysis of phospholipids at lysosomal pH. *Biometals* **2012,** *25*, 1207.

(19) Kassai, M.; Teopipithaporn, R.; Grant, K. B., Hydrolysis of phosphatidylcholine by cerium(IV) releases significant amounts of choline and inorganic phosphate at lysosomal pH. *J Inorg Biochem* **2011,** *105*, 215.

(20) Takarada, T.; Yashiro, M.; Komiyama, M., Catalytic hydrolysis of peptides by cerium(IV). *Chem-Eur J* **2000,** *6*, 3906.

(21) Bracken, K.; Moss, R. A.; Ragunathan, K. G., Remarkably rapid cleavage of a model phosphodiester by complexed ceric ions in aqueous micellar solutions. *J Am Chem Soc* **1997,** *119*, 9323.

(22) Matsumiya, H.; Nakamura, H.; Hiraide, M., Phosphoester hydrolysis by cerium(IV)-thiacalix[4]arene complexes and its application to immunoassay. *Anal Bioanal Chem* **2009,** *394*, 1471.

(23) Moss, R. A.; Morales-Rojas, H., Loci of ceric cation mediated hydrolyses of dimethyl phosphate and methyl methylphosphonate. *Org Lett* **1999,** *1*, 1791.

(24) Sirish, M.; Franklin, S. J., Hydrolytically active Eu(III) and Ce(IV) EF-hand peptides. *J Inorg Biochem* **2002,** *91*, 253.

(25) Yan, J. M.; Atsumi, M.; Yuan, D. Q.; Fujita, K., (Ethylenediaminetetraacetic acid)cerium(IV) [Ce-IV(EDTA)] complexes with dual hydrophobic binding sites as highly efficient catalysts for the hydrolysis of phosphodiesters. *Helv Chim Acta* **2002,** *85*, 1496.

(26) Zhao, M.; Zhao, C.; Jiang, X. Q.; Ji, L. N.; Mao, Z. W., Rapid hydrolysis of phosphate ester promoted by Ce(IV) conjugating with a beta-cyclodextrin monomer and dimer. *Dalton T* **2012,** *41*, 4469.

(27) Branum, M. E.; Que, L., Double-strand DNA hydrolysis by dilanthanide complexes. *J Biol Inorg Chem* **1999,** *4*, 593.

(28) Branum, M. E.; Tipton, A. K.; Zhu, S. R.; Que, L., Double-strand hydrolysis of plasmid DNA by dicerium complexes at 37 degrees C. *J Am Chem Soc* **2001,** *123*, 1898.

(29) Katada, H.; Seino, H.; Mizobe, Y.; Sumaoka, J.; Komiyama, M., Crystal structure of Ce(IV)/dipicolinate complex as catalyst for DNA hydrolysis. *J Biol Inorg Chem* **2008,** *13*, 249.

(30) Kitamura, Y.; Komiyama, M., Preferential hydrolysis of gap and bulge sites in DNA by Ce(IV)/EDTA complex. *Nucleic Acids Res* **2002,** *30*.

(31) Cullis, P. M.; Snip, E., Stereochemical course of cerium(IV)-catalyzed hydrolysis of cyclic nucleotides. *J Am Chem Soc* **1999,** *121*, 6125.

(32) Sumaoka, J.; Miyama, S.; Komiyama, M., Enormous acceleration by cerium(Iv) for the hydrolysis of nucleoside 3',5'-cyclic monophosphates at pH 7. *J Chem Soc Chem Comm* **1994**, 1755.

(33) Moss, R. A.; Morales-Rojas, H.; Vijayaraghavan, S.; Tian, J. Z., Metal-cation-mediated hydrolysis of phosphonoformate diesters: Chemoselectivity and catalysis. *J Am Chem Soc* **2004,** *126*, 10923.

(34) Zhu, B.; Xue, D. P.; Wang, K., Lanthanide ions promote the hydrolysis of 2,3-bisphosphoglycerate. *Biometals* **2004,** *17*, 423.

(35) Moss, R. A.; Zhang, J.; Ragunathan, K. G., Zirconium and hafnium cations rapidly cleave model phosphodiesters in acidic aqueous solutions. *Tetrahedron Lett* **1998,** *39*, 1529.

(36) Moss, R. A.; Ragunathan, K. G., Remarkable acceleration of dimethyl phosphate hydrolysis by ceric cations. *Chem Commun* **1998**, 1871.

(37) Matsumura, K.; Komiyama, M., Enormously fast RNA hydrolysis by lanthanide(III) ions under physiological conditions: eminent candidates for novel tools of biotechnology. *J. Biochem* **1997,** *122*, 387.

(38) Emsley, J. *An A-Z guide to the elements: Nature's building block*; Oxford University Press: New York, 2001.

(39) Nair, V.; Deepthi, A., Cerium(IV) ammonium nitrate-A versatile single-electron oxidant. *Chem Rev* **2007,** *107*, 1862.

(40) Sridharan, V.; Menendez, J. C., Cerium(IV) ammonium nitrate as a catalyst in organic synthesis. *Chem Rev* **2010,** *110*, 3805.

(41) Beineke, A. T. D., J., The crystal structure of ceric ammonium nitrate. *Inorg Chem* **1968,** *7*, 715.

(42) Larsen, D. R. B., H. G., The structure of ammonium hexanitratocerate(IV) in solution. *J Phys Chem* **1964,** *68*, 3060.

(43) Shannon, R. D., Revised effective ionic radii and systematic studies of interatomic distances in halides and chalcogenides. *Acta Crystallogr, Sect A* **1976,** *A32*, 751.

(44) Burgess, J. *Metal ions in solution*; John Wiley & Sons: New York, 1978.

(45) Burgess, J. *Ions in solution: basic principles of chemical interactions*; Horwood Publishing: Chichester, 1999.

(46) Baes, F. C.; Mesmer, R. E. *The hydrolysis of cations*; John Wiley & Sons, Inc.: New York, 1976.

(47)  Shigekawa, H.; Ikawa, H.; Yoshizaki, R.; Iijima, Y.; Sumaoka, J.; Komiyama, M., Core level photoelectron spectroscopy on the lanthanide-induced hydrolysis of DNA. *Appl. Phys. Lett.* **1996,** *68*, 1433.

(48)  Shigekawa, H.; Ishida, M.; Miyake, K.; Shioda, R.; Iijima, Y.; Imai, T.; Takahashi, H.; Sumaoka, J.; Komiyama, M., Extended x-ray absorption fine structure study on the cerium(IV)-induced DNA hydrolysis: Implication to the roles of 4f orbitals in the catalysis. *Appl Phys Lett* **1999,** *74*, 460.

(49)  Branum, M. E.; Que, L., Jr., Double-strand DNA hydrolysis by dilanthanide complexes. *JBIC, J. Biol. Inorg. Chem.* **1999,** *4*, 593.

(50)  Miyajima, Y.; Ishizuka, T.; Yamamoto, Y.; Sumaoka, J.; Komiyama, M., Origin of high fidelity in target-sequence recognition by PNA-Ce(IV)/EDTA combinations as site-selective DNA cutters. *J Am Chem Soc* **2009,** *131*, 2657.

(51)  Nielsen, P. E.; Egholm, M.; Berg, R. H.; Buchardt, O., Sequence-selective recognition of DNA by strand displacement with a thymine-substituted polyamide. *Science* **1991,** *254*, 1497.

(52)  Ito, K.; Katada, H.; Shigi, N.; Komiyama, M., Site-selective scission of human genome by artificial restriction DNA cutter. *Chem Commun* **2009**, 6542.

(53)  Matsumura, K.; Komiyama, M., Hydrolysis of phosphatidylinositol by rare-earth-metal ion as a phospholipase-C mimic. *J Inorg Biochem* **1994,** *55*, 153.

(54)  Liu, H. X.; Hu, J.; Liu, X. T.; Li, R. C.; Wang, K., Effects of lanthanide ions on hydrolysis of phosphatidylinositol in human erythrocyte membranes. *Chinese Sci Bull* **2001,** *46*, 401.

(55)  Scrimin, P.; Caruso, S.; Paggiarin, N.; Tecilla, P., Ln(III)-catalyzed cleavage of phosphate-functionalized synthetic lipids: Real time monitoring of vesicle decapsulation. *Langmuir* **2000,** *16*, 203.

(56) Moss, R. A.; Park, B. D.; Scrimin, P.; Ghirlanda, G., Lanthanide cleavage of phosphodiester liposomes. *J Chem Soc Chem Comm* **1995**, 1627.

(57) Anderson, N.; Borlak, J., Drug-induced phospholipidosis. *FEBS Lett* **2006,** *580*, 5533.

(58) Schuchman, E. H., The pathogenesis and treatment of acid sphingomyelinase-deficient Niemann-Pick disease. *J Inherit Metab Dis* **2007,** *30*, 654.

(59) Buccoliero, R.; Palmeri, S.; Ciarleglio, G.; Collodoro, A.; De Santi, M. M.; Federico, A., Increased lung surfactant phosphatidylcholine in patients affected by lysosomal storage diseases. *J Inherit Metab Dis* **2007,** *30*, 983.

(60) Futerman, A. H.; van Meer, G., The cell biology of lysosomal storage disorders. *Nat Rev Mol Cell Bio* **2004,** *5*, 554.

(61) Vellodi, A., Lysosomal storage disorders. *Brit J Haematol* **2005,** *128*, 413.

**CHAPTER 2**

**EVALUATING METAL ION SALTS AS ACID HYDROLASE MIMICS: METAL-**

**ASSISTED HYDROLYSIS OF PHOSPHOLIPIDS AT LYSOSOMAL PH**

**2.1. Abstract**

Niemann-Pick disease and drug-induced phospholipidosis are lysosomal storage disorders in which there is an excessive accumulation of sphingomyelin in cellular lysosomes. Here we have explored the possibility of developing metal-based therapeutic agents to reverse phospholipid build-up through phosphate ester bond hydrolysis at lysosomal pH (~ 4.8). Towards this end, we have utilized a malachite green/molybdate-based colorimetric assay to quantitate the inorganic phosphate released upon the hydrolysis of sphingomyelin by twelve d- and f-block metal ion salts. In reactions conducted at 60 ºC, the yields produced by the cerium(IV) complex $Ce(NH_4)_2(NO_3)_6$ were superior. An Amplex® Red-based colorimetric assay and mass spectrometry were then employed to detect choline. The data consistently showed that Ce(IV) hydrolyzed sphingomyelin more efficiently at lysosomal pH: *i.e.*, yields of choline and phosphate were 54 ± 4% and 22 ± 5% at ~ pH 4.8, compared to 8 ± 1% and 5 ± 2% at ~ pH 7.2. Hydrolysis at 60 ºC could be significantly increased by converting sphingomyelin vesicles to mixed lipid vesicles and mixed micelles of Triton X-100. We then utilized cerium(IV) to cleave sphingomyelin at 37 ºC (no Triton X-100). Although choline and phosphate levels were relatively low, hydrolysis continued to be considerably more efficient at lysosomal pH. A

comparison to phosphatidylcholine was then made. While the yields of choline and phosphate produced by phosphatylcholine were higher, the ratio of ~ pH 4.8 hydrolysis to ~ pH 7.2 hydrolysis was usually more favorable for sphingomyelin (37 ℃ and 60 ℃).

## 2.2. Introduction

An acid hydrolase is a lysosomal enzyme that is responsible for the hydrolytic breakdown of macromolecules into their original, monomeric building blocks. Enzymatic activity is optimal at lysosomal pH (~ pH 4.8) and significantly lower in the cell cytoplasm (~ pH 7.2). When a particular acid hydrolase is impaired, pathogenic levels of the corresponding macromolecular substrate build-up in lysosomes, causing lysosomal storage disease. Examples include Niemann-Pick disease (NPD) types A and B (Schuchman and Desnick 2008) and drug-induced phospholipidosis (Hruban 1984; Reasor 1989; Reasor and Kacew 2001; Anderson and Borlak 2006). In these disorders, serious respiratory complications can be brought on by the occurrence of high levels of the phosphoglyceride phosphatidylcholine (PC; **1** in Figure. 2.1) in the lysosomes of pulmonary cells (Hruban 1984; Reasor et al. 1988; Padmavathy et al. 1993; Gonzalez-Rothi et al. 1995; Ikegami et al. 2003; Buccoliero et al. 2004; Buccoliero et al. 2007). Additional clinical symptoms can arise from the accumulation of the sphingolipid sphingomyelin (SM; **2** in Figure. 2.1) in the cellular lysosomes of multiple organ systems (Reasor et al. 1988; Padmavathy et al. 1993; Schuchman and Desnick 2008).
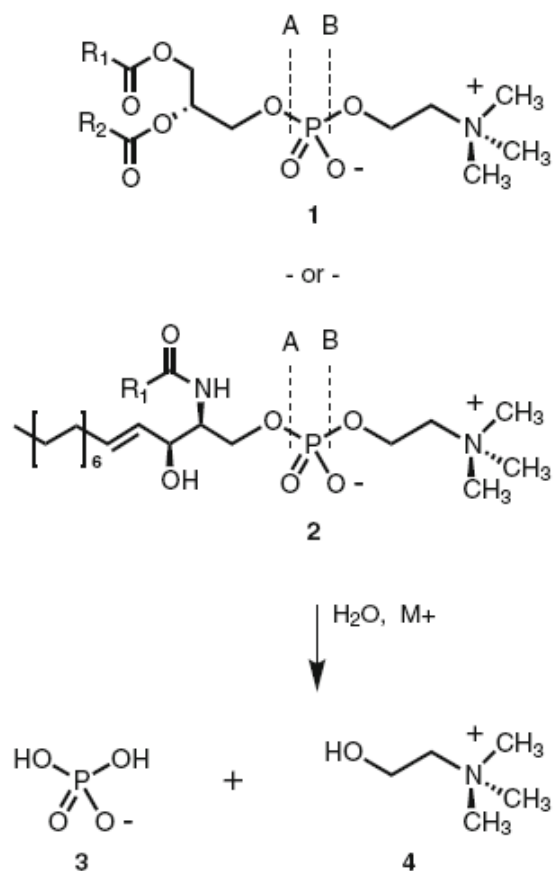
**Figure 2.1** Metal-assisted hydrolysis of phosphatidylcholine **(1)** or of sphingomyelin **(2)** at phosphate ester bonds A and B releases inorganic phosphate **(3)** and choline **(4)**. M+ = metal ion; $R_1$ and $R_2$ = long chain fatty acid hydrocarbons of variable length.

Drug-induced phospholipidosis is an acquired disorder in which the administration of cationic, amphiphilic medications (*e.g.,* the antiarrhythmic drug amiodarone, the antidepressant fluoxetine, and the aminoglycoside antibiotic gentamicin) reduce the activity of the lysosomal acid phopholipases A1, A2, and/or C (Hruban 1984; Reasor et al. 1988; Reasor 1989; Padmavathy et al. 1993; Gonzalez-Rothi et al. 1995; Reasor and Kacew 2001; Anderson and Borlak 2006; Buccoliero et al. 2007). In addition to pulmonary complications, clinical manifestations sometimes include inflammation, fibrosis, and/or nephrotoxicity.

In the inherited, metabolic lysosomal storage disorder Niemann-Pick disease, autosomal recessive mutations in the gene coding for acid sphingomyelinase (ASM) (Schuchman and Desnick 2008) lead to a total or partial loss of enzyme activity. ASM is a phosphodiesterase whose normal role is to hydrolyze the phosphate ester bond on the ceramide side of the phosphorous atom in sphingomyelin. Thus, there is an extensive accumulation of sphingomyelin in the lysosomes of multiple organ systems, with lysosomes of phagocytic cells of the monocyte-macrophage system (*e.g.*, bone marrow, lymph nodes and spleen) containing the most lipid. Although ASM displays low levels of phoshodiesterase activity against PC (Freeman et al. 1985), there is no generally accepted explanation linking the genetically compromised lysosomal acid hydrolase to the build-up of phosphatidylcholine that occurs in pulmonary lysosomes (Schuchman and Desnick 2008). In the severe infantile form of Niemann-Pick disease (Type A), acid sphingomyelinase activity is less than 5% of normal. As a result of the lysosomal accumulation of phospholipid, afflicted patients present with hepatosplenomegaly, compromised pulmonary function, and rapid neurodegeneration that leads to death by age two or three (Schuchman and Desnick 2008). While the symptoms of drug-induced phospholipidosis are reversed by the termination of drug therapy (Reasor and Kacew 2001), there is no cure for Niemann-Pick disease (Schuchman and Desnick 2008).

One approach to decreasing phospholipid accumulation in lysosomal storage disease is to assist the impaired lysosomal enzyme with the hydrolysis of phospholipid phosphate ester bonds. Thus, in ASM knockout mice, enzyme replacement therapy involving intravenous administration of recombinant human ASM has been shown to reduce lipid storage in reticuloendothelial organs such as the liver, spleen, and to a lesser extend, the lung (Schuchman and Desnick 2008). Due in part to its large size, ASM is unable to cross the blood-brain barrier, and as a result, neurological

symptoms are not improved. ERT is further limited by the need to generate large amounts of fully glycosylated enzyme (Schuchman, 2007). In order to achieve more widespread distribution of therapeutic agent, new treatment approaches relying on small-molecules can be considered.

The pH of the interior of lysosomes is approximately 4.8, and is thus considerably more acidic than the surrounding cytoplasm (~ pH 7.2). In order to avoid the hydrolysis of normal phospholipids outside of the lysosome, it would therefore be ideal for a small-molecule, hydrolytic agent to have optimal activity at ~ pH 4.8, with considerably less reactivity at pH 7.2. Towards this end, our research group is exploring the use of metal ions and complexes as pH dependant, acid hydrolase mimics. In a previous report, we utilized metal ion salts of Ce(IV), Zr(IV), Hf(IV), Co(II), Cu(II), Eu(III), La(III), Ni(II), Pd(II), Y(III), Yb(III), and Zn(II) in an attempt to hydrolyze the phosphoglyceride phosphatidylcholine (**1**) (Kassai et al. 2011). Colorimetric assays were used to quantitate inorganic phosphate (**3**) and choline (**4**) produced by metal-assisted hydrolysis of phosphatidylcholine phosphate ester bonds. This work showed that cerium(IV) gave rise to considerably more phospholipid hydrolysis than the eleven other metal ion salts, with high levels of cleavage at lysosomal pH (~ 4.8) compared to ~ pH 7.2. In the present report, the twelve metal ion salts were used to target the phosphate ester bonds of the sphingolipid sphingomyelin (**2**). In hydrolysis reactions run at 60 °C and 37 °C, a systematic comparison to phosphatidylcholine was then carried out. Consistent with the phosphatidylcholine data, cerium(IV) was found to generate superior levels of sphingomyelin hydrolysis. While the cleavage of phosphatidylcholine proceeded in higher yields, the ratio of ~ pH 4.8 hydrolysis to ~ pH 7.2 hydrolysis was usually greater in the sphingomyelin reactions. To the best of our knowledge, the present work represents the first example of a research study that has reported on successful, metal-assisted cleavage of a naturally occurring sphingolipid.

## 2.3. Experimental

### 2.3.1. Materials and methods

All chemicals were of the highest available purity and were utilized without further purification. De-ionized, distilled water (ddH$_2$O) was used in the preparation of aqueous reactions and buffers. Sphingomyelin (Brain, Porcine; catalog number 860062P, MW = 760.22 gmol$^{-1}$) and L-α-phosphatidylcholine (Egg, Chicken; catalog number 840051P, MW = 760.19 gmol$^{-1}$) were purchased from Avanti Polar Lipids, USA. The metal ion salts Ce(NH$_4$)$_2$(NO$_3$)$_6$, ZrCl$_4$, HfCl$_4$, CoCl$_2$·H$_2$O, CuCl$_2$·2H$_2$O, EuCl$_3$·6H$_2$O, LaCl$_3$·H$_2$O, NiCl$_2$·6H$_2$O, K$_2$PdCl$_4$, YCl$_3$·6H$_2$O, YbCl$_3$·6H$_2$O, and ZnCl$_2$ were acquired from The Aldrich Chemical Company (purity > 99%). Piperazine and Triton X-100 and were from Fluka (Sigma-Aldrich, USA). QuantiChrom™ Assay and Malachite Green Phosphate Assay Kits (catalog numbers DIPI-500 and POMG-25H, respectively) were purchased from BioAssay Systems, USA. An Amplex® Red Sphingomyelinase Assay Kit (catalog number A12220) was from Invitrogen, USA. Choline chloride, tris(hydroxymethyl)aminomethane (Tris) and 4-(2-hydroxyethyl)piperazine-1-ethanesulfonic acid (HEPES) were obtained from Sigma-Aldrich.

### 2.3.2. Preparation of micelles and lipid vesicles

Porcine brain sphingomyelin was added to a round-bottomed flask and was dissolved in 1 mL of chloroform. The chloroform was evaporated to dryness *in vacuo* overnight. In order to form lipid vesicles, a 120 mM solution of the phospholipid was prepared by adding pre-heated ddH$_2$O (55 °C). The solution was sonicated for 20 min at 55 °C, a temperature above the gel-to-fluid transition temperature ($T_m$) range displayed by naturally occurring sphingomyelins (30-45 °C; Bar et al. 1997). Triton X-100 (10% in water (w/v), 0.16 M) was added to the sphingomyelin solution and was reacted for 30 min at room temperature to change the phospholipid vesicles (0

mM Triton X-100, final concentration) into mixed lipid vesicles (11.4 mM Triton X-100, final concentration), and mixed micelles (43.3 mM Triton X-100, final concentration) (Alonso et al. 1981). The Triton X-100:sphingomyelin molar mixing ratios of these solutions equaled 0.0 (0 mM:120 mM); 0.10 (11.4 mM:111.5 mM); and 0.79 (43.3 mM:55.1 mM). The conversion of the SM vesicles to mixed vesicles and mixed micelles of Triton X-100 was confirmed by recording turbidity measurements (Alonso et al. 1981; Figure 2.S1 in Electronic supplementary material). Micelles and lipid vesicles of L-α-phosphatidylcholine were prepared as previously described (Kassai et al. 2011).

### 2.3.3. Lipid hydrolysis

A 1:1 (v/v) ratio of a 100 mM aqueous solution of metal ion salt, ($Ce(NH_4)_2(NO_3)_6$, $ZrCl_4$, $HfCl_4$, $CoCl_2 \cdot H_2O$, $CuCl_2 \cdot 2H_2O$, $EuCl_3 \cdot 6H_2O$, $LaCl_3 \cdot H_2O$, $NiCl_2 \cdot 6H_2O$, $K_2PdCl_4$, $YCl_3 \cdot 6H_2O$, $YbCl_3 \cdot 6H_2O$, or $ZnCl_2$) was combined with an buffer solution (200 mM aqueous piperazine or HEPES) to prepare a series of metal/buffer cocktails. By adding HCl and/or 50% NaOH (w/v) solutions, the piperazine and HEPES cocktails were adjusted to final pH values of ~ 5.2 and 7.2, respectively. Two hundred microliters of each cocktail were then transferred to a volume of lipid solution, either 17 μL of the 0 mM Triton X-100 solution, 18.3 μL of the 11.4 mM Triton X-100 solution, or 37 μL of the 43.3 mM Triton X-100 solution. After being brought to a final volume 1000 μL with $ddH_2O$, individual reactions contained 2 mM of sphingomyelin or of phosphatidylcholine, 0 mM, 0.2 mM or 1.6 mM Triton X-100, 10 mM metal ion salt, and 20 mM of piperazine ~pH 4.8 or of HEPES ~pH 7.2. The resulting solutions were allowed to react at 37 °C or 60 °C for 0 h and 20 h time intervals. In negative control reactions, metal ion salt solutions were replaced by equivalent volumes of $ddH_2O$. Average reaction pH values were calculated using pre- and post-reaction pH measurements.

### *2.3.4. Colorimetric detection of inorganic phosphate*

A malachite green/molybdate-based colorimetric assay kit (BioAssay Systems) was used to detect inorganic phosphate released upon metal-assisted hydrolysis of sphingomyelin and phosphatidylcholine (Cogan et al. 1999). Depending on the metal ion salt employed, an aliquot of the hydrolysis reaction was diluted from 6.7 to 173.7 fold with $ddH_2O$. A total of 167 μL to 300 μL of the resulting aqueous solution was further diluted to a final volume of 500 μL with malachite green/molybdate reagent and reacted at rt for 30 min. The absorbance of the colorimetric product thus obtained was then measured at 620 nm in a UV-1601 Shimadzu spectrophotometer against a $ddH_2O$ blank. In order to correct for the presence of background levels of inorganic phosphate, the absorbance recorded for the hydrolysis reaction at the $t = 0$ h time interval was subtracted from the corresponding absorbance recorded at the $t = 20$ h time interval. The same calculation was performed for the parallel, negative control reaction run in the absence of metal. The absorbance difference of the reaction run in the absence of metal was then subtracted from the absorbance difference of the reaction run in the presence of metal. For each set of reaction conditions tested, the absorbance difference values were determined over multiple trials. The concentration of inorganic phosphate was then quantitated using linear plots generated by treating inorganic phosphate standards with the malachite green/molybdate reagent (Figure. 2.S2 in Electronic supplementary material).

### *2.3.5. Colorimetric detection of choline*

Reagents obtained from an Amplex® Red Sphingomyelinase Assay Kit (Invitrogen) were used to detect free choline released upon metal-assisted hydrolysis of sphingomyelin and phosphatidylcholine (He et al. 2002). In a typical procedure, an Amplex® Red reaction cocktail was prepared by mixing 2850 μL of 1X Tris buffer, 40 μL of Amplex® Red, 30 μL of

horseradish peroxidase, 30 μL of choline oxidase with 60 μL of ddH$_2$O. Depending upon the original concentration of metal ion salt and on the reaction temperature, a total of 13 μL to 80 μL of the hydrolysis reaction was diluted to 1000 μL with ddH$_2$O.  Then, a total of 40 μL of the resulting solution was treated with 80 μL of the Amplex® Red cocktail and incubated for 55 min at 37 °C.  The reactions were further diluted 6.3 with ddH$_2$O. Free choline was then quantitated with the UV-1601 Shimadzu spectrophotometer by measuring absorbance at 570 nm against a ddH$_2$O blank. In order to account for background levels of free choline, the absorbance recorded for the hydrolysis reactions at the t = 0 h time interval was subtracted from the corresponding absorbance recorded at the t = 20 h time interval. Concentrations of free choline were then quantitated over multiple trials using linear plots generated by treating choline chloride standards with the Amplex® Red reagents (Figure 2.S3 in Electronic supplementary material).

### 2.3.6. MALDI-TOF mass spectrometry

A total of 2 mM of sphingomyelin (without Triton X-100, sonicated) was treated at 60 °C and ~ pH 4.8 (20 mM piperazine buffer) or ~ pH 7.2 (20 mM HEPES buffer) for 20 h in the absence or presence of 10 mM of Ce(NH$_4$)$_2$(NO$_3$)$_6$. Cerium(IV) hydrolysis reactions were then quenched by the addition of 1/5 volume of 0.5 M EDTA pH 8. Matrix-assisted laser desorption ionization time-of-flight (MALDI-TOF) mass spectra were recorded by the Georgia State University Mass Spectrometry Facility as follows. A total of 1 μL of lipid hydrolysis reaction was mixed with 10 μL of saturating amounts of 2,5-dihydroxybenzoic acid (DHB) matrix in 50% acetonitrile/50% ddH$_2$O water. One μL of the resulting solution was transferred to a MALDI-TOF plate and air-dried. Mass spectra were then recorded using a 4800 MALDI-TOF/TOF$^{TM}$ analyzer (Applied Biosystems, Foster City, CA) in a reflectron-positive mode with delayed extraction. Ionization was achieved with a Nd:YAG 355-nm over an average of 500 random

shots. The instrument's reflectron positive mode was calibrated using a 4700 Proteomics Analyzer calibration mixture (Applied Biosystems). Spectra were processed with Data Explore Software (Applied Biosystems).

## 2.4. Results and Discussion

### 2.4.1. Sphingomyelin hydrolysis by metal ion salts at 60 °C, colorimetric detection of inorganic phosphate

The goal of our first experiment was to quantitate the amounts of inorganic phosphate (**3**) released upon metal-assisted hydrolysis of the two phosphate ester bonds of the sphingolipid sphingomyelin (Bonds A and B in **2**, Figure 2.1). Small-molecule metal ion salts of Ce(IV), Zr(IV), Hf(IV), Co(II), Cu(II), Eu(III), La(III), Ni(II), Pd(II), Y(III), Yb(III), and Zn(II) were selected based on the ability of these metal centers to hydrolyze *p*-nitrophenol-activated and/or unactivated amide and/or phosphate ester linkages in biologically related molecules (Ghirlanda et al. 1993; Matsumura and Komiyama 1994; Moss et al. 1995; Scrimin et al. 1998; Moss and Jiang 2000; Scrimin et al. 2000; Takarada et al. 2000; Franklin 2001; Liu et al. 2001; Milovic and Kostic 2003; Suh 2003; Zhu et al. 2004; Grant and Kassai 2006; Kassai et al. 2011; Katada and Komiyama 2011). Our objective was to identify a metal ion salt with strong activity at lysosomal pH (~ 4.8) accompanied by appreciably less hydrolysis at cytoplasmic pH (~ 7.2). Lipid vesicles of porcine brain sphingomyelin were prepared by sonication. Treatment of the vesicles with the nonionic surfactant Triton X-100 at surfactant:sphingomyelin molar mixing ratios of 0.10 and 0.79 afforded sphingomyelin-surfactant mixed vesicles and mixed micelles, respectively (Alonso et al. 1981). The lipid solutions were then used to prepare individual reactions consisting of 2 mM of sphingomyelin, 20 mM piperazine buffer pH 4.8 or 20 mM HEPES buffer pH 7.2, and 10 mM of one of the twelve metal ion salts. Hydrolysis was allowed

to proceed at 60 °C for 20 h, after which inorganic phosphate was colorimetrically quantitated with the triarylmethane dye malachite green (Cogan et al. 1999).
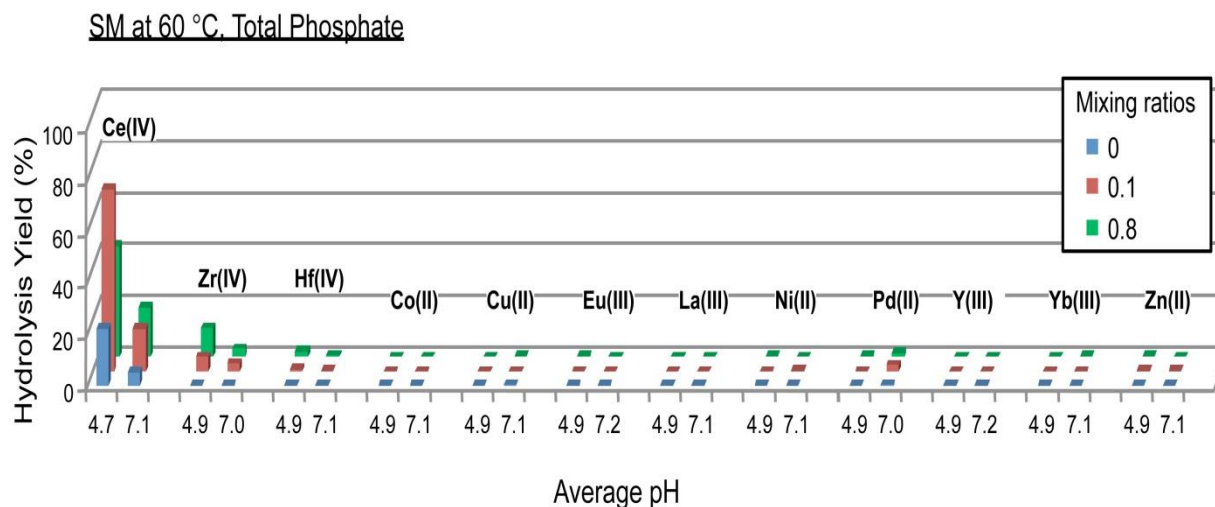


**Figure 2.2.** Averaged hydrolysis yields plotted as a function of Triton X-100:sphingomyelin (SM) molar mixing ratio and pH for malachite green detection of free phosphate released in hydrolysis reactions. A total of 2 mM of sphingomyelin was treated at 60 °C and ~ pH 4.8 (20 mM piperazine buffer) or at 60 °C and ~ pH 7.2 (20 mM HEPES buffer) for 20 h in the presence of 10 mM of $Ce(NH_4)_2(NO_3)_6$, $ZrCl_4$, $HfCl_4$, $CoCl_2 \cdot H_2O$, $CuCl_2 \cdot 2H_2O$, $EuCl_3 \cdot 6H_2O$, $LaCl_3 \cdot H_2O$, $NiCl_2 \cdot 6H_2O$, $K_2PdCl_4$, $YCl_3 \cdot 6H_2O$, $YbCl_3 \cdot 6H_2O$, or $ZnCl_2$.
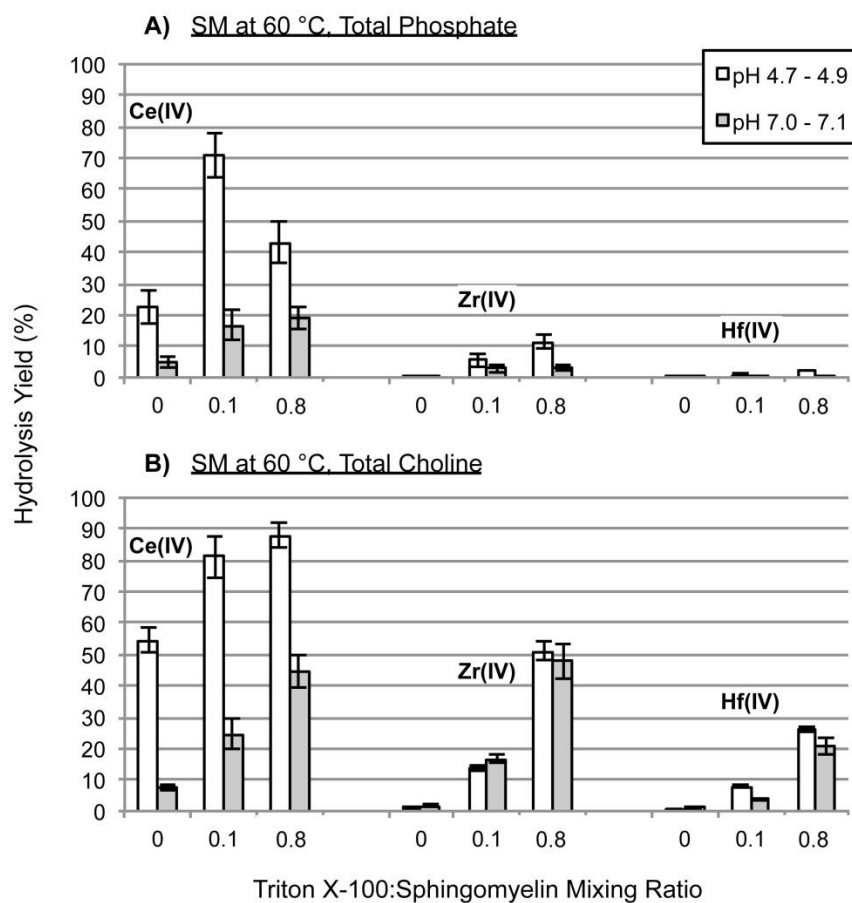
**Figure 2.3.** Averaged hydrolysis yields plotted as a function of Triton X-100: sphingomyelin (SM) molar mixing ratio and pH for **A)** malachite green detection of free phosphate (data taken from Fig. 1) and **B)** Amplex® Red detection of free choline. A total of 2 mM of sphingomyelin was treated at 60 °C and ~ pH 4.8 (20 mM piperazine buffer) or at 60 °C and ~ pH 7.2 (20 mM HEPES buffer) for 20 h in the presence of 10 mM of $Ce(NH_4)_2(NO_3)_6$, $ZrCl_4$, or $HfCl_4$. The number of trials: $\geq 6$ (**A**) and $> 3$ (**B**). Error bars represent standard deviation.

As shown in Figures 2.2 and 2.3A, four of the twelve metal centers (Ce(IV), Zr(IV), Hf(IV), Pd(II)) hydrolyzed sphingomyelin (**2**), to release detectable levels of inorganic phosphate (**3**). The identities of the four most reactive metals, as well as their ordering and pH preferences, were in agreement with our previous colorimetric study of the phosphoglyceride phosphatidylcholine (**1**) (Kassai et al. 2011). For both phospholipids, the levels of cleavage generated by Ce(IV) were overwhelmingly superior and relative activity was in the order Ce(IV) $>>>$ Zr(IV) $>$ Hf(IV) $\sim$ Pd(II) (Figures 2.2 and 2.3A; Kassai et al. 2011).

In our analyses of 12 metal ion salts, we found that the ability of a given metal ion to accelerate phospholipid hydrolysis could be correlated to the relative acidity of its metal-bound water (Figure 2.2; Kassai et al. 2011). The p$K_A$ value of water is lowered from 15.7 to −1.1 for Ce(IV); -0.3 for Zr(IV); 0.2 for Hf(IV) (Wulfsberg 1991); and 1.0 for Pd(II) (Burgess 1978). In the case of the inactive ions Co(II), Cu(II), Eu(III), La(III), Ni(II), Y(III), Yb(III), and Zn(II) (Figure 2.2), the p$K_A$s of metal-bound water range from 7.3 to 9.9 (Burgess 1978). Previously published NMR and Fourier transform (FT) Raman spectra show that Ln(III) metal cations coordinate to phospholipids such as sphingomyelin and phosphatidylcholine primarily at a free oxygen atom (Hauser et al. 1976) on the polar head group phosphate (Yuan et al. 1996a; Yuan et al. 1996b). Taken together with our data, the observations are consistent with a mechanism frequently described in the literature (Bracken et al. 1997; Moss and Jiang 2000; Kassai et al. 2011). To accelerate hydrolysis, cerium(IV) and other metal ions act as strong Lewis acids that bind to the negatively charged phosphate oxygen in the polar head group of the phospholipid (activating the phosphorous atom towards nucleophilic attack), while delivering a hydroxide nucleophile to the activated phosphate ester bond.

In general, the averaged levels of cleavage produced by metal ion centers Ce(IV), Zr(IV), and Hf(IV) were higher at lysosomal pH (~ 4.8) compared to cytoplasmic pH (~ pH 7.2) (Figures 2.2 and 2.3A). We concurrently observed moderate amounts of metal ion precipitation at ~ pH 4.8 accompanied by significantly more turbidity as pH values were increased to pH 7.2 (Kassai et al. 2011). These trends point to a possible relationship between metal ion speciation and phosphodiester hydrolysis yields. The effect is best understood in the case of cerium(IV). The aqueous chemistry of cerium(IV) is characterized by metal ion speciation that involves the formation of polynuclear Ce(IV)-hydroxo species, gels, and precipitates. At acidic pH values,

$Ce_4(OH)_{13}^{+3}$ has been shown to display high activity towards phosphodiester hydrolysis (Maldonado and Yatsimirsky 2005). However, as reaction pH is raised above ~ 4.0, catalytically active Ce(IV) hydroxide gels or precipitates begin to form and there is gradual speciation of $Ce_4(OH)_{13}^{+3}$ into $Ce_4(OH)_{14}^{+2}$ and $Ce_4(OH)_{15}^{+1}$. The lower net positive charges acquired by the Ce(IV) hydroxo species reduce their Lewis acid strength, accounting for the decline in the rate of phosphate ester hydrolysis that occurs at higher pH values (Bracken et al. 1997; Maldonado and Yatsimirsky 2005).

In the above reactions, the nonionic surfactant Triton X-100 was utilized in order to study the effects of lipid dynamics and structure on sphingomyelin cleavage yields. The data in Figures 2.2 and 2.3A show that the amounts of inorganic phosphate released by Ce(IV), Zr(IV), and Hf(IV) were usually increased upon the Triton X-100-induced transition of pure sphingomyelin vesicles (0.0 surfactant:sphingomyelin molar mixing ratio) to Triton X-100-sphingomyelin mixed vesicles (0.1 surfactant:sphingomyelin molar mixing ratio) and to mixed micelles (0.79 surfactant:sphingomyelin molar mixing ratio). These trends can be addressed as follows. Triton X-100 and other detergents are known to significantly increase the permeability of sonicated lipid vesicles to small-molecules (Alonso et al. 1981). At sub-micellar concentrations, Triton X-100 has been shown to reduce the gel-to-fluid transition temperature of PC bilayers, increasing their fluidity (Goñi et al. 1986). A second factor concerns the relative accessibility of scissile phosphate ester bonds. In micelles, all of the polar head groups of the constituent phospholipid are near the micellar surface. Alternatively, in lipid vesicles, approximately 40% to 50% of the polar head groups are on the inner leaflet of the bilayer, and are therefore less accessible to interaction with hydrolytic agent (Reid Kensil and Dennis 1981; Scrimin et al. 1998).

***2.4.2. Sphingomyelin hydrolysis by metal ion salts at 60 °C, detection of free choline by colorimetry and mass spectrometry***

In addition to inorganic phosphate (**3**), hydrolysis of the two phosphate ester bonds of sphingomyelin (Bonds A and B in **2**, Figure 2.1) should theoretically afford free choline (**4**). The dihydroxyphenoxazine dye Amplex® Red (Invitrogen) was therefore employed to detect the latter cleavage product. A total of 2 mM of sphingomyelin at surfactant:sphingomyelin molar mixing ratios of 0, 0.10, and 0.97 was reacted for 20 h at 60 °C with 10 mM of Ce(IV), Zr(IV), or Hf(IV) metal ion salt as previously described. The sphingomyelin hydrolysis reactions were then treated with choline oxidase and horseradish peroxidase, catalyzing the oxidation of the Amplex® Red dye to resorufin ($\lambda_{max}$ = 572 nm). Yields of free choline were then quantitated with a UV-visible spectrophotometer.

As shown in Figure 2.3B, the metal ion salts reacted with sphingomyelin in the general order Ce(IV) > Zr(IV) > Hf(IV), reflecting the increasing p$K_A$ values of metal-bound water (Ce(IV) < Zr(IV) < Hf(IV)). The amounts of free choline produced by cerium(IV) at lysosomal pH (~ 4.8) were significantly higher compared to reactions employing neutral media and/or the other metal ion salts (Zr(IV) and Hf(IV)). The choline data also helped to confirm that metal-assisted hydrolysis of Triton X-100-sphingomyelin mixed vesicles (0.1 surfactant:sphingomyelin molar mixing ratio) and mixed micelles (0.79 surfactant:sphingomyelin molar mixing ratio) proceeded more efficiently than hydrolysis of pure sphingomyelin vesicles. Finally, choline, which requires only one cleavage event (Bond B in **2**, Figure 2.1), was always produced in higher yields than inorganic phosphate, which requires cleavage of both sphingomyelin phosphate ester bonds (Figure 2.3).

**A)** SM at 60 °C, 10 mM Ce(IV), pH 4.8
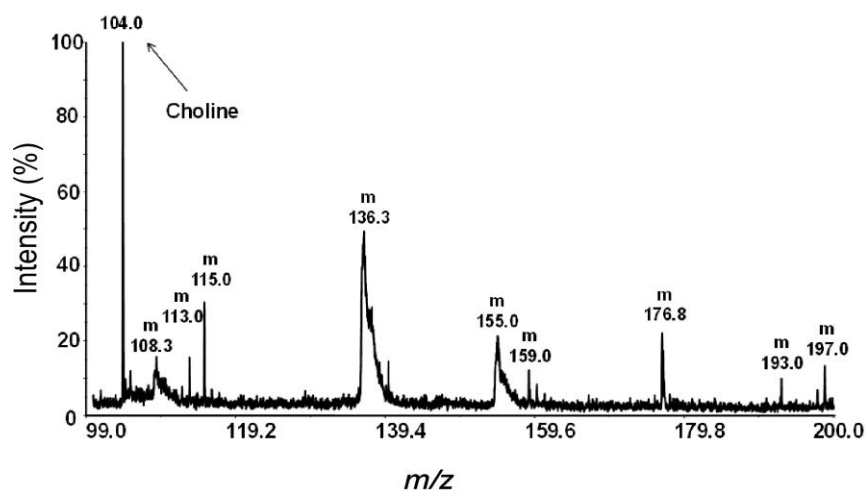


**B)** SM at 60 °C, 10 mM Ce(IV), pH 7.2
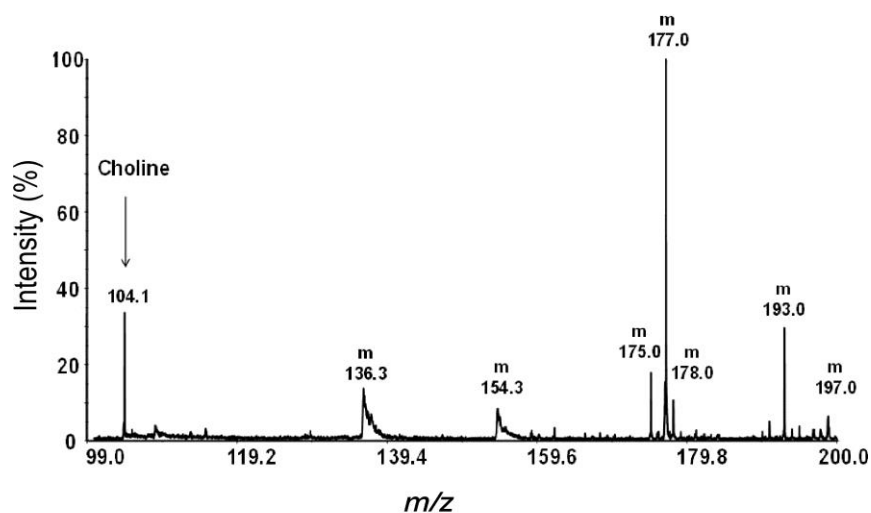


**Figure 2.4.** MALDI-TOF mass spectra of 2 mM of sphingomyelin (SM; no Triton X-100) treated at 60 °C for 20 h in the presence of 10 mM of $Ce(NH_4)_2(NO_3)_6$ and: **A)** ~ pH 4.8 (20 mM piperazine buffer) or **B)** ~ pH 7.2 (20 mM HEPES buffer). M = matrix

Matrix-assisted laser desorption ionization time-of-flight (MALDI-TOF) mass spectrometry was used to further examine sphingomyelin hydrolysis reactions with cerium(IV) metal ion salt (60 °C, 20 h, no Triton X-100; Figure 2.4). The MALDI-TOF mass spectra confirmed that free choline is a major product (choline $m/z$ = 104.0 to 104.1 obsd, 104.1 calcd

for $[C_5H_{14}N_1O_1]^{1+}$). Consistent with the colorimetric data (Figures 2.2 and 2.3), the choline peak in the pH 4.8 reaction (relative abundance 100%, Figure 2.4A) was more prominent than at pH 7.2 (relative abundance ~ 35%, Figure 2.4B). In parallel controls in which Ce(IV) was replaced by ddH$_2$O, the relative abundance of the choline peak was ~ 10% (Figures 2.S4B and 2.S4D in Electronic supplementary material).

### 2.4.3. *Hydrolysis of sphingomyelin and phosphatidylcholine by cerium(IV), a systematic comparison*

Under normal, physiological conditions, sphingomyelin and phosphatidylcholine constitute approximately 50% of the phospholipid content in the bilayer membranes of eukaryotic cells (Niemelä et al. 2004). Although SM and PC both contain phosphocholine as a polar head group, there are significant structural differences between the two phospholipids. In the sphingolipid sphingomyelin, the glycerol diester backbone of the phosphoglyceride phosphatidylcholine is replaced by a sphingosine unit that participates in extensive intramolecular and intermolecular hydrogen bonding (Chiu et al. 2003; Niemelä et al. 2004). A second distinguishing feature concerns the fatty acid units, with sphingomyelin being significantly more saturated than phosphatidylcholine. As a result, bilayers of SM and PC have different structural and dynamic properties. This encouraged us to carry out a more extensive comparison of the two lipids. In these experiments, hydrolysis reactions consisting of 2 mM of sphingomyelin or of phosphatidylcholine, 10 mM of Ce(NH$_4$)$_2$(NO$_3$)$_6$, and 20 mM of piperazine buffer pH 4.8 or of HEPES buffer pH 7.2 were allowed to sit at 60 ºC for 20 h (no Triton X-100). Because a therapeutic agent should also be active at normal, core body temperature, a second set of solutions was reacted at 37 ºC. The malachite green/molybdate- and Amplex® Red-based

assays were then used to detect and quantitate the average amounts of free phosphate (Figure

2.5) and free choline (Figure 2.6) released upon Ce(IV)-assisted hydrolysis.

**A)**   Lipid at 60 °C, Total Phosphate



**B)**   Lipid at 37 °C, Total Phosphate
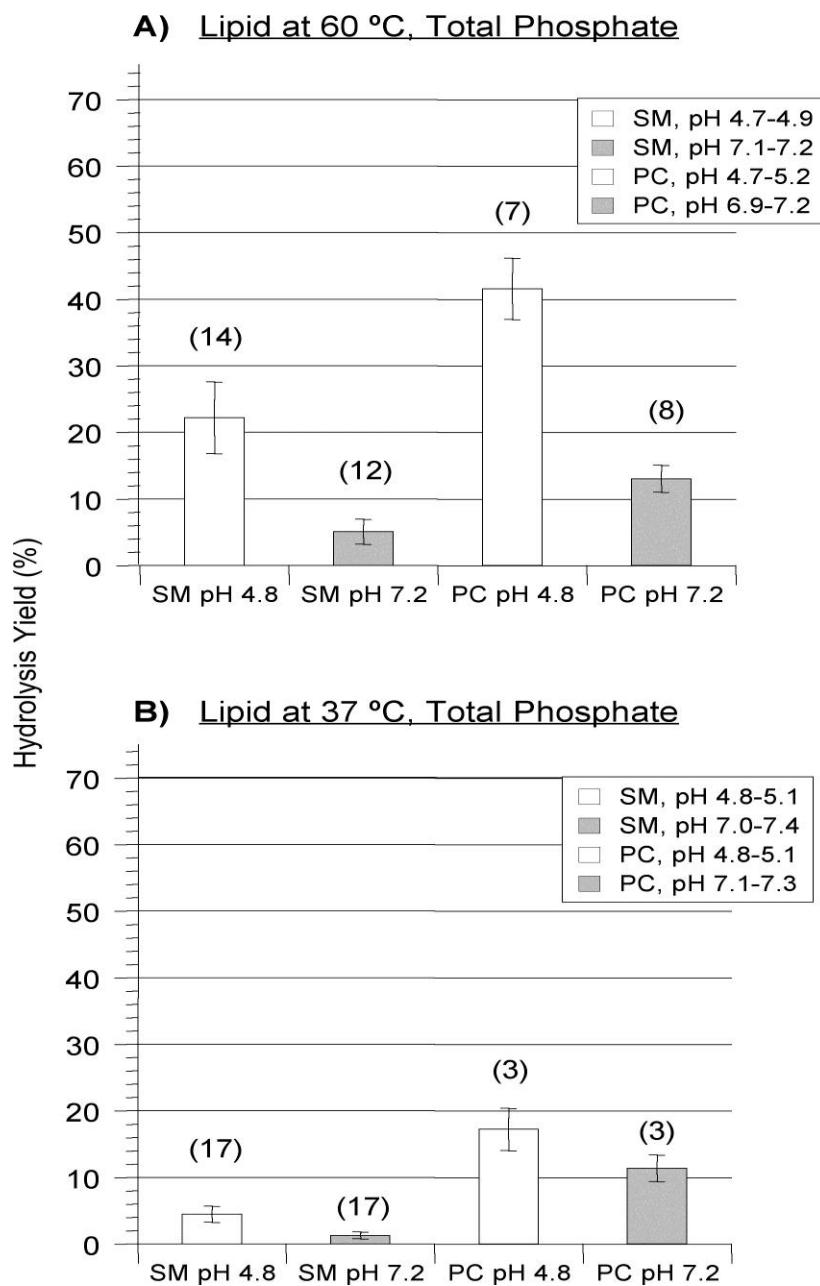


**Figure 2.5.** Averaged hydrolysis yields plotted as a function pH for malachite green detection of free phosphate. A total of 2 mM of sphingomyelin (SM) or 2 mM of phosphatidylcholine (PC) was treated for 20 h at **A)** 60 °C or at **B**) 37 °C. Reactions were run in the presence of 10 mM of Ce(NH$_4$)$_2$(NO$_3$)$_6$ and 20 mM piperazine buffer  (~ pH 4.8)  or 20 mM HEPES buffer (~ pH 7.2). The number of trials (**n**) appears in parenthesis. Error bars represent standard deviation. The 60 °C PC data (**a**) have been reported previously (Fig. 3 in Kassai et al., 2011).
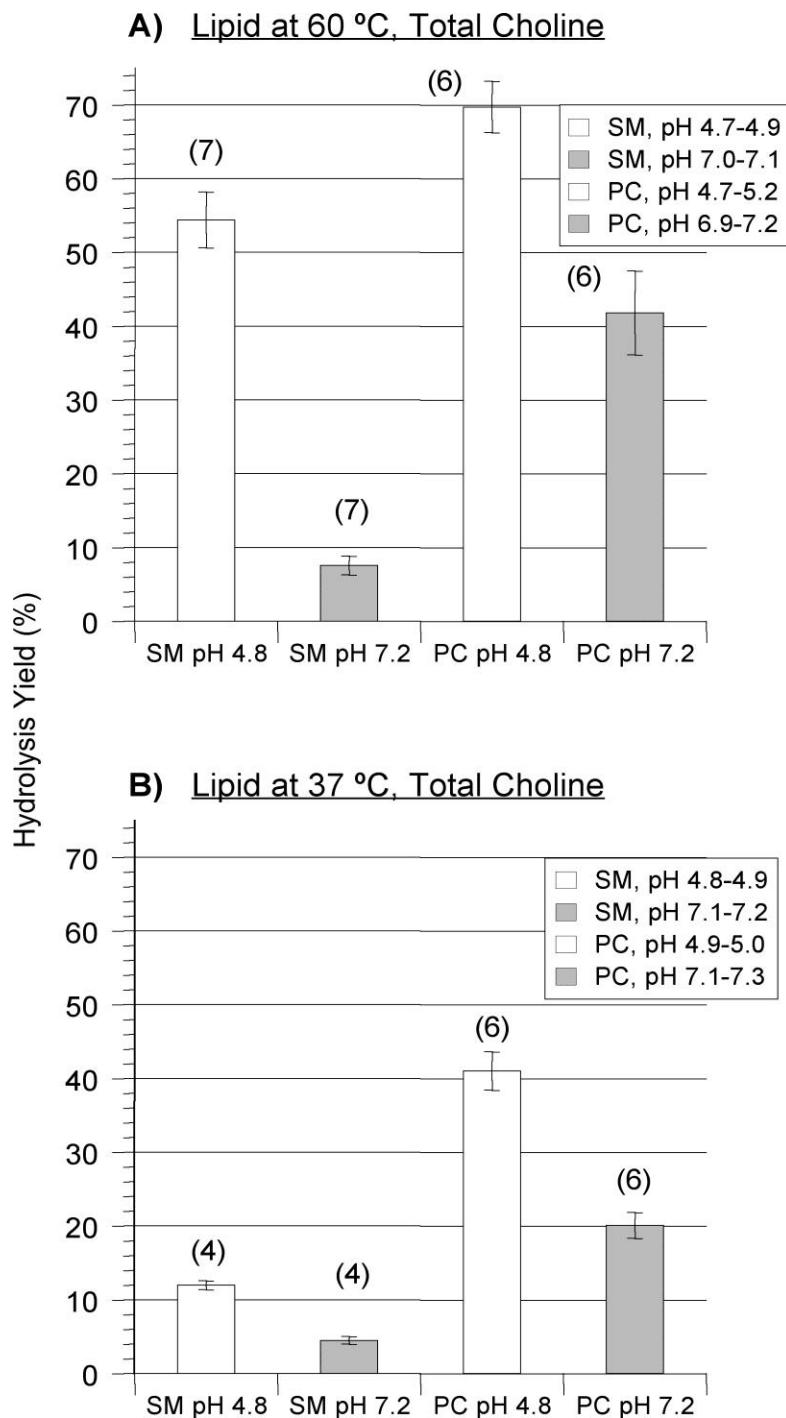
**Figure 2.6.** Averaged hydrolysis yields plotted as a function pH for Amplex® Red detection of free choline. A total of 2 mM of sphingomyelin (SM) or 2 mM of phosphatidylcholine (PC) was treated for 20 h at **A)** 60 °C or at **B)** 37 °C. Reactions were run in the presence of 10 mM of $Ce(NH_4)_2(NO_3)_6$ and 20 mM piperazine buffer (~ pH 4.8) or 20 mM HEPES buffer (~ pH 7.2). The number of trials (**n**) appears in parenthesis. Error bars represent standard deviation. The 60 °C PC data used to prepare Figs. 5A and 6A have been reported previously (Kassai et al., 2011).

The 60 ºC and 37 ºC data shown in Figures 2.5 and 2.6 display trends consistent with our initial colorimetric experiments (Figures 2.2 and 2.3; Kassai et al. 2011). Cerium(IV) hydrolyzed pure lipid vesicles of sphingomyelin and phosphatidylcholine more efficiently at mildly acidic pH compared to near-neutral values, with the amounts of choline being significantly higher or equivalent to free phosphate. A new finding concerned the relative susceptibilities of the two phospholipids towards hydrolysis. Under all of the reaction conditions tested, phosphatidylcholine generated more choline and phosphate than sphingomyelin. Treatment of phosphatidylcholine with Ce(IV) at 60 ºC and ~ pH 4.8 accordingly released choline and inorganic phosphate in $70 \pm 4\%$ and $42 \pm 5\%$ yields (Figures 2.5A and 2.6A), values that are 1.3 and 5.5 fold higher than SM hydrolysis yields at ~ pH 4.8. When the reaction temperature was lowered from 60 ºC to 37 ºC, measurable hydrolytic activity was still observed (Figures 2.5B and 2.6B). In the phosphatidylcholine reactions, the amounts of choline and inorganic phosphate were $41 \pm 3\%$ and $17 \pm 3\%$, yields that were 3.4 and 3.8 fold higher than SM hydrolysis at the same pH. In parallel controls in which the metal solutions were replaced with equivalent volumes of ddH$_2$O, levels of choline and inorganic phosphate were considerably lower (Figure 2.S5 in Electronic supplementary material; Kassai et al. 2011).

A number of factors are likely to contribute to the relative susceptibilities of sphingomyelin and phosphatidylcholine towards metal-assisted hydrolysis. Published NMR and FT Raman structural data show that the polar head groups of SM and PC are approximately parallel with respect to the bilayer surface due to the gauche conformation of the choline O-C-C-N+ backbone. The head group of PC lies almost exactly along the surface. In the case of SM, however, intramolecular hydrogen bonding between the OH group of sphingosine and the phosphate ester oxygen on the ceramide side of phosphorous causes the polar head group to tilt

15 degrees towards the interior of the bilayer (Niemelä et al. 2004). The interaction between the phosphate oxygen and the sphingosine hydroxyl reduces the binding of Ca(II) to sphingomyelin relative to phosphatidylcholine (Shah and Schulman 1966). The hydrogen bond also decreases the ability of SM to hydrogen bond to water, lowering the overall hydration state of the polar region of SM (Schmidt et al. 1997; Chiu et al. 2003; Niemelä et al. 2004). Interestingly, the enzymatic activity of the acid hydrolase phospholipase $A_2$ has been correlated to levels of phospholipid bilayer hydration (Oliver et al. 1995). Because water is also required in metal-assisted hydrolysis reactions, the reduced levels of sphingomyelin hydration that arise from intramolecular hydrogen bonding could explain why this phospholipid less susceptible to cerium(IV) hydrolysis than phosphatidylcholine.

A second explanation takes into account the effects of membrane fluidity on hydrolysis yields. The fatty acid chains of the sphingomyelin and phosphatidylcholine preparations used in this study have an average of 0.2 and 1.28 double bonds per molecule, respectively. The higher fatty acid saturation state of SM coupled with extensive intramolecular and intermolecular hydrogen bonding afforded by the NH and OH groups of sphingosine result in significant differences in the dynamic properties of SM and PC bilayers (Niemelä et al. 2004). For example, sphingomyelin membranes have reduced fluidity, with suppressed lateral and rotational diffusion rates (Niemelä et al. 2004) and average gel-to-fluid transition temperatures (~ 37 ℃; Bar et al. 1997) that are significantly higher than phosphatidylcholine. Ruiz-Argüello et al. (2002) have demonstrated that the rate of acid sphingomyelinase hydrolysis can be enhanced by using phosphoglycerides to increase the fluidity of SM bilayers. The authors proposed that higher rates of sphingomyelin diffusion increased the probability of an interaction between the enzyme and substrate. Similarly, in our Ce(IV) reactions with SM (Figures 2.2 and 2.3) and PC (Kassai et al.

2011), hydrolysis yields were substantially increased upon the addition of sub-micellar concentrations of Triton X-100, a non-ionic surfactant that increases the fluidity of PC bilayers (Goñi et al. 1986). Taken together, the above information suggests that the differences in membrane dynamics exhibited by sphingomyelin and phosphatidylcholine have an influence on Ce(IV) hydrolysis levels. When using Ln(III) cations to cleave unilamellar vesicles of a *p*-nitrophenol-activated anionic lipid, Moss and co-workers observed that cleavage yields could be increased by the high transverse diffusion (flip-flop) rates occurring above the $T_m$ of the lipid vesicles (Scrimin et al. 1998). In contrast to anionic and other charged lipids that promote flip-flop by repelling one another electrostatically, the translocation of PC, SM, and other neutral, zwitterionic phospholipids across the bilayer is extremely slow, even at temperatures above the $T_m$ (Moss 1994; Contreras et al. 2010). Furthermore, hydrolysis of phosphate ester bonds of SM and PC would yield ceramide and diacylglycerol, respectively (bonds A and B; Figure 2.1). Ceramide increases the flip-flop rates of other lipids in the bilayer, but diacylglycerol has no effect (Contreras et al. 2010). While it is possible that accelerated lateral diffusion makes a significant contribution to the relatively high levels of phosphatidylcholine hydrolysis produced by Ce(IV), it is less likely that transverse diffusion of PC from the inner to the outer membrane leaflet plays an major role.
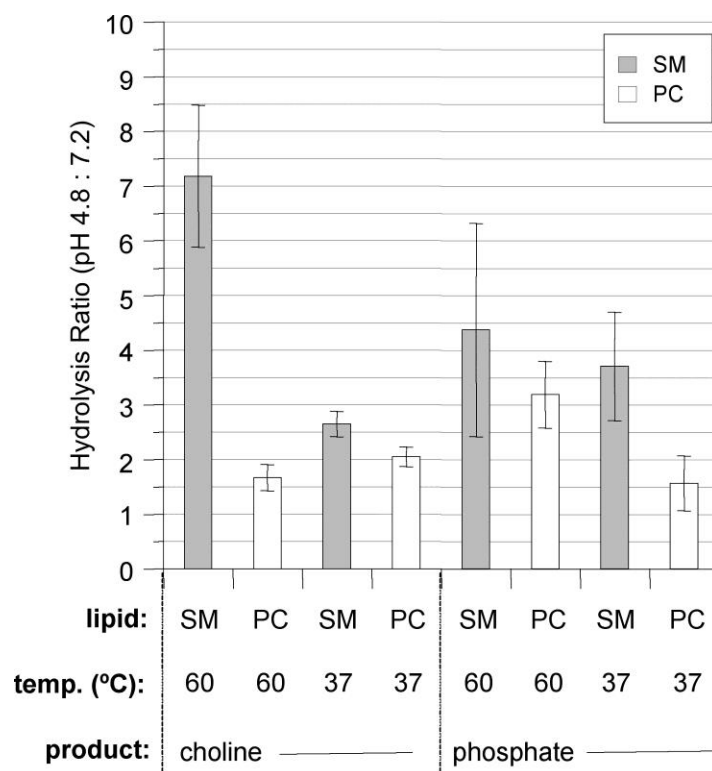
**Figure 2.7.** Ratio of averaged hydrolysis yields at ~ pH 4.8 to averaged hydrolysis yields at ~ pH 7.2 for 2 mM of sphingomyelin (SM) or 2 mM of phosphatidylcholine (PC) treated with 10 mM of $Ce(NH_4)_2(NO_3)_6$. The averaged hydrolysis yields used to calculate the ratios and the number of trials (n) are in Figs. 5 and 6. Error bars represent standard deviation.

In Figures 2.5 and 2.6, we have established that cleavage of phosphatidylcholine proceeds in higher yield than sphingomyelin. In order to be effective in the treatment of lysosomal storage disease, a small-molecule, hydrolytic agent should display optimal levels of activity at lysosomal pH (~ 4.8) accompanied by low amounts of cleavage under near-neutral conditions. This prompted us to compare the differential levels of phospholipid hydrolysis produced by $Ce(NH_4)_2(NO_3)_6$ at the two pH values. In Figure 2.7 are hydrolysis ratios calculated using the data from Figures 2.5 and 2.6. Thus, for sphingomyelin and phosphatidylcholine reactions at 60 °C and 37 °C, yields of inorganic phosphate and choline hydrolysis at ~ pH 4.8 have been divided by corresponding yields at ~ pH 7.2 (Figure 2.7). A high ratio is desirable, because it indicates that phospholipid cleavage at ~ pH 7.2 is suppressed with respect to cleavage

at ~ pH 4.8. All of the ratios in Figure 2.7 are above 1, indicating that cerium(IV) hydrolyzes lipid vesicles of sphingomyelin and phosphatidylcholine more efficiently at lysosomal pH. Interestingly, under any given set of reaction conditions, the averaged sphingomyelin ratios of ~ pH 4.8 hydrolysis to ~ pH 7.2 hydrolysis are usually greater (Figure 2.7). The causes underlying the latter phenomenon have yet to be determined and continue as a subject of research in our laboratory. Factors such as phospholipid bilayer hydration, cation binding, and gel-to-fluid transition temperature are sensitive to changes in pH (Hauser and Phillips 1979; Chemin et al. 2008) and, in theory, can play a role. However, sphingomyelin and phosphatidylcholine are predominately zwitterionic over a wide pH range (~ pH 3 to pH 13), with minimal protonation of the phosphate ester oxygen. (In PC monolayers, only 2.6% of the phospholipid molecules are protonated at pH 2.5 (Moncelli et al. 1994).) As a result, binding of Ln(III) cations to PC is independent of pH between pH 3.0 and pH 10.0 (Hauser and Phillips 1979), the hydration of SM is unaffected from pH 3.0 to pH 7.0 (Chemin et al. 2008), and the gel-to-fluid transition temperature of PC is constant from ~ pH 4.5 to pH 7.0 (Furuike et al. 1999). It is therefore conceivable that many of the physical parameters pertinent to SM and PC bilayers remain relatively constant over the ~ 4.8 to ~ 7.2 pH range employed in our study.

## 2.5. Summary and Discussion, Concluding Remarks

There has been considerable interest in using metal ions and complexes as tools to effect the reversible, hydrolytic cleavage of biological molecules under non-denaturing conditions of temperature and pH (Takarada et al. 2000; Franklin 2001; Milovic and Kostic 2003; Suh 2003; Grant and Kassai 2006; Liu and Wang 2009; Kassai et al. 2011; Katada and Komiyama 2011). The overwhelming majority of the studies in this area have focused on the hydrolysis of the phosphodiester bonds of nucleic acids and the amide bonds in peptides and proteins.

Alternatively, there are only a few published examples of metal-assisted lipid hydrolysis. In these experiments, rare earth or transition metal ions or complexes were utilized to cleave unactivated, phosphate ester bonds of the naturally occurring phosphoglycerides phosphatidylcholine (Kassai et al. 2011) and phosphatidylinositol (Matsumura and Komiyama 1994; Liu et al. 2001) and the *p*-nitrophenol activated phosphate ester and ester bonds of synthetic lipid analogs (Ghirlanda et al. 1993; Moss et al. 1995; Scrimin et al. 1998; Moss and Jiang 2000; Scrimin et al. 2000). Herein we have employed simple metal ion salts in an attempt to hydrolyze the phosphate ester bonds of the sphingolipid sphingomyelin (**2** in Figure 2.1). In support of previous studies on peptide amide and phosphate ester bond hydrolysis (Takarada et al. 2002; Zhu et al. 2004; Kassai et al. 2011), cleavage of sphingomyelin by cerium(IV) was found to be overwhelmingly superior to other metal ion centers (Figures 2.2 and 2.3). A comparison to phosphatidylcholine was then made (Figures 2.5 and 2.6). For both lipids, considerably higher levels of phosphate ester bond hydrolysis occurred at lysosomal pH (~ 4.8) compared to near neutral, cytoplasmic pH (~ 7.2). At pH ~ 4.8, treatment of PC with $Ce(NH_4)_2(NO_3)_6$ at 60 ℃ released choline and inorganic phosphate in 70 ± 4% and 42 ± 5% yields (Figures 2.5A and 2.6A), values 1.3 and 5.5 fold higher than SM. Addition of the solubilizing agent Triton X-100 to sphingomyelin and phosphatidylcholine vesicles significantly increased the efficiency of Ce(IV)-assisted hydrolysis (Figures 2.2 and 2.3). At 37 ℃, yields of choline and inorganic phosphate were 41 ± 3% and 17 ± 3% and 3.4 and 3.8 fold higher compared SM hydrolysis yields at the same pH (Figures 2.5B and 2.6B). While phosphatidylcholine was more susceptible to hydrolysis by Ce(IV), the ratio of pH 4.8 hydrolysis to 7.2 hydrolysis was usually more favorable in the case of sphingomyelin (Figure 2.7).

Several factors can account for the hydrolytic activity of cerium(IV). By virtue of its high charge density, Ce(IV) is a strong Lewis acid (Bracken et al. 1997; Maldonado and Yatsimirsky 2005). As a result, cerium(IV) has high affinity for the oxygen atoms in amide, ester, and phosphate ester bonds. Furthermore, lanthanide ions form complexes with high coordination numbers and rapid ligand exchange rates compatible with catalytic turnover (Franklin 2001). As we have mentioned, Ce(IV) lowers the p$K_A$ value of water from 15.7 to -1.1 (Wulfsberg 1991), and is therefore expected to be capable of generating hydrolytically active hydroxide nucleophiles under mildly acidic to neutral conditions. As reaction pH is raised above ~ 4.0, the lower net positive charges acquired by Ce(IV) hydroxo species reduce their Lewis acid strength, accounting for the decline in the rate of phosphate ester hydrolysis that occurs at higher pH values (Maldonado and Yatsimirsky 2005).

Cerium(IV) is capable of enhancing phosphate ester bond hydrolysis at lysosomal pH with low concurrent hydrolysis under near neutral conditions. This is consistent with a small-molecule approach to treating Niemann-Pick and other lysosomal storage diseases. In principal, the pathogenic lysosomal build-up of sphingomyelin and phosphatidylcholine could be reversed with minimal damage to the rest of the cell. Interestingly, the administration of Ce(III) and Ce(IV) oxides and salts to Winstar rats causes cerium ions to selectively localize in the lysosomes of multiple organ systems (Berry 1996; Berry et al. 1997; Manoubi et al. 1998). Similar to other lanthanides, cerium displays low to moderate cellular toxicity and has existing therapeutic applications. Examples have included cerium(III) nitrate, an active component of commercially topical creams used to treat full-thickness burns, and the anti-emetic agent cerium(III) oxalate (Fricker 2006). Indeed, complexes based on cerium(IV) may one day be useful as therapeutic agents to treat the symptoms that arise from phospholipid build-up in

lysosomal storage disease. Towards this end, our current research is focused on identifying coordinating ligands that optimize Ce(IV) speciation and phospholipid hydrolysis yields. We are also evaluating hydrolytically inert liposomes as drug transport vehicles to enhance bilayer permeability and increase the selective delivery of cerium(IV) to lysosomes (Bareford and Swaan 2007).

## 2.6. References

(1) Alonso A, Villena A, Goñi FM (1981) Lysis and reassembly of sonicated lecithin vesicles in the presence of Triton X-100. FEBS Lett 123:200-204

(2) Anderson N, Borlak J (2006) Drug-induced phospholipidosis. FEBS Lett 580:5533-5540

(3) Bar LK, Barenholz Y, Thompson TE (1997) Effect of sphingomyelin composition on the phase structure of phosphatidylcholine-sphingomyelin bilayers. Biochemistry 36:2507-2516

(4) Bareford LM, Swaan PW (2007) Endocytic mechanisms for targeted drug delivery. Adv Drug Deliv Rev 59:748-758

(5) Berry JP (1996) The role of lysosomes in the selective concentration of mineral elements. A microanalytical study. Cell Mol Biol (1996) 42:395-411

(6) Berry JP, Zhang L, Galle P, Ansoborlo E, Hengé-Napoli MH, Donnadieu-Claraz M (1997) Role of alveolar macrophage lysosomes in metal detoxification. Microsc Res Tech 36: 313-323

(7) Bracken K, Moss RA, Ragunathan KG (1997) Remarkably rapid cleavage of a model phosphodiester by complexed ceric ions in aqueous micellar solutions. J Am Chem Soc 119:9323–9324

(8) Buccoliero R, Ginzburg L, Futerman AH (2004) Elevation of lung surfactant phosphatidylcholine in mouse models of Sandhoff and of Niemann-Pick A disease. J Inherit Metab Dis 27:641-648

(9) Buccoliero R, Palmeri S, Ciarleglio G, Collodoro A, De Santi MM, Federico A (2007) Increased lung surfactant phosphatidylcholine in patients affected by lysosomal storage disease. J Inherit Metab Dis 30:983-985

(10) Burgess J (1978) In: Metal ions in solution, Halsted Press, New York, pp 263-267

(11) Chemin C, Bourgaux C, Péan JM, Pabst G, Wüthrich P, Couvreur P, Ollivon M (2008) Consequences of ions and pH on the supramolecular organization of sphingomyelin and sphingomyelin/cholesterol bilayers. Chem Phys Lipids 153:119–129

(12) Chiu SW, Vasudevan S, Jakobsson E, Jay Mashl R, Larry Scott H (2003) Structure of sphingomyelin bilayers: a simulation study. Biophys J 85:3624-3635

(13) Cogan EB, Birrell GB, Griffith OH (1999) A robotics-based automated assay for inorganic and organic phosphates. Anal Biochem 271:29-35

(14) Contreras FX, Sánchez-Magraner L, Alonso A, Goñi FM (2010) Transbilayer (flip-flop) lipid motion and lipid scrambling in membranes. FEBS Lett 584:1779-1786

(15) Franklin SJ (2001) Lanthanide-mediated DNA hydrolysis. Curr Opin Chem Biol 5:201-208

(16) Freeman SJ, Shankaran P, Wolfe LS, Callahan JW (1985) Phosphatidylcholine and 4-methylumbelliferyl phosphorylcholine hydrolysis by purified placental sphingomyelinase. Can J Biochem Cell Biol 63:272-277

(17) Fricker SP (2006) The therapeutic applications of lanthanides. Chem Soc Rev 35:524-533

(18) Furuike S, Levadny VG, Li SJ, Yamazaki M (1999) Low pH induces an interdigitated gel to bilayer gel phase transition in dihexadecylphosphatidylcholine membrane. Biophys J 77:2015-2023

(19) Ghirlanda G, Scrimin P, Tecilla P, Tonellato U (1993) A hydrolytic reporter of copper(II) availability in artificial liposomes. J Org Chem 58:3025-3029

(20) Goñi FM, Urbaneja MA, Arrondo JL, Alonso A, Durrani AA, Chapman D (1986) The interaction of phosphatidylcholine bilayers with Triton X-100. Eur J Biochem 160:659-65

(21) Gonzalez-Rothi RJ, Zander DS, Ros PR (1995) Fluoxetine hydrochloride (Prozac)-induced pulmonary disease. Chest 107:1763-1765

(22) Grant KB, Kassai M (2006) Major advances in the hydrolysis of peptides and proteins by metal ions and complexes. Curr Org Chem 10:1035-1049

(23) Hauser H, Phillips MC (1979) Interactions of the polar groups of phospholipid bilayer membranes. Prog Surface Membrane Sci 13: 297-413

(24) Hauser H, Phillips MC, Levine BA, Williams RJP (1976) Conformation of the lecithin polar group in charged vesicles. Nature 261: 390-394

(25) He X, Chen F, McGovern MM, Schuchman EH (2002) A fluorescence-based, high-throughput sphingomyelin assay for the analysis of Niemann-Pick disease and other disorders of sphingomyelin metabolism. Anal Biochem 306:115-123

(26) Hruban Z (1984) Pulmonary and generalized  lysosomal  storage induced by amphiphilic drugs. Environ Health Perspect 55:53-76

(27) Ikegami M, Dhami R, Schuchman EH (2003) Alveolar lipoproteinosis in an acid sphingomyelinase-deficient mouse model of Niemann-Pick disease. Am J Physiol Lung Cell Mol Physiol 284: L518-L525

(28) Kassai M, Teopipithaporn R, Grant KB (2011) Hydrolysis of phosphatidylcholine by cerium(IV) releases significant amounts of choline and inorganic phosphate at lysosomal pH. J Inorg Biochem 105:215-223

(29) Katada H, Komiyama, M (2011) Artificial restriction DNA cutters to promote homologous recombination in human cells. Curr Gene Ther 1:38-45

(30) Liu H, Hu J, Liu X, Li R, Wang K (2001) Effects of lanthanide ions on hydrolysis of phosphatidylinositol in human erythrocyte membranes. Chinese Sci Bull 46:401-403

(31) Maldonado AL, Yatsimirsky AK (2005) Kinetics of phosphodiester cleavage by differently generated cerium(IV) hydroxo species in neutral solutions. Org Biomol Chem 3:2859-2867

(32) Manoubi L, Hocine N, Jaafoura H, El Hili A, Galle P (1998) Subcellular localization of cerium in intestinal mucosa, liver, kidney, suprarenal and testicle glands after cerium administration in the rat. J Trace Microprobe Tech 16:209-219

(33) Matsumura K, Komiyama M (1994) Hydrolysis of phosphatidylinositol by rare earth metal ion as a phospholipase C mimic. J Inorg Biochem 55:153-156

(34) Milovic NM, Kostic NM (2003) Palladium(II) complex as a sequence-specific peptidase: hydrolytic cleavage under mild conditions of X-Pro peptide bonds in X-Pro-Met and X-Pro-His segments. J Am Chem Soc 12:781-788

(35) Moncelli MR, Becucci L, Guidelli R (1994) The intrinsic pKa values for phosphatidylcholine, phosphatidylethanolamine, and phosphatidylserine in monolayers deposited on mercury electrodes. Biophys J 66:1969-1980

(36) Moss RA (1994) Dynamics of lipids in synthetic membranes. Pure Appl Chem 66:851-858

(37) Moss RA, Jiang W (2000) Lanthanide-mediated cleavages of micellar phosphodiesters. Langmuir 16:49-51

(38) Moss RA, Park BD, Scrimin P, Ghirlanda G (1995) Lanthanide cleavage of phosphodiester liposomes. J Chem Soc Chem Commun 1627-1628

(39) Niemelä P, Hyvonen MT, Vattulainen I (2004) Structure and dynamics of sphingomyelin bilayer: insight gained through systematic comparison to phosphatidylcholine. Biophys J 87:2976-2989

(40) Oliver AE, Fisk E, Crowe LM, de Araujo PS, Crowe JH (1995) Phospholipase A2 activity in dehydrated systems: effect of the physical state of the substrate. Biochim Biophys Acta 1267:92-100

(41) Padmavathy B, Devaraj H, Devaraj N (1993) Amiodarone-induced changes in surfactant phospholipids of rat lung. N-S Arch Pharmacol 347:421-424

(42) Reasor MJ (1989) A review of the biology and toxicologic implications of the induction of lysosomal lamellar bodies by drugs. Toxicol Appl Pharmacol 97:47–56

(43) Reasor MJ, Kacew S (2001) Drug-induced phospholipidosis: are there functional consequences? Exp Biol Med 226:825-830

(44) Reasor MJ, Ogle CL, Walker ER, Kacew S (1988) Amiodarone-induced phospholipidosis in rat alveolar macrophages. Am Rev Respir Dis 137:510-518

(45) Reid Kensil C, Dennis EA (1981) Alkaline hydrolysis of phospholipids in model membranes and the dependence on their state of aggregation. Biochemistry 20:6079-6085

(46) Ruiz-Argüello MB, Veiga MP, Arrondo JL, Goñi FM, Alonso A (2002) Sphingomyelinase cleavage of sphingomyelin in pure and mixed lipid membranes. Influence of the physical state of the sphingolipid. Chem Phys Lipids 114:11-20

(47) Schmidt CF, Barenholz Y, Thompson TE (1977) A nuclear magnetic resonance study of sphingomyelin in bilayer systems. Biochemistry 16:2649–2656

(48) Schuchman EH (2007) The pathogenesis and treatment of acid sphingomyelinase-deficient Niemann-Pick disease. J Inherit Metab Dis 30:654-663

(49) Schuchman EH, Desnick RJ (2008) In: Rosenberg RN, DiMauro S, Paulson HL, Ptácek L, Nestler EJ (eds) The molecular and genetic basis of neurologic and psychiatric disease, 4th edn. Lippincott Williams & Wilkins, Philadelphia, pp 215-220

(50) Scrimin P, Caruso S, Paggiarin N, Tecilla P (2000) Ln(III)-catalyzed cleavage of phosphate-functionalized synthetic lipids: real time monitoring of vesicle decapsulation. Langmuir 16:203-209

(51) Scrimin P, Tecilla P, Moss RA, Bracken K (1998) Control of permeation of lanthanide ions across phosphate-functionalized liposomal membranes. J Am Chem Soc 12:1179-1985

(52) Shah DO, Schulman JH (1967) Interaction of calcium ions with lecithin and sphingomyelin monolayers. Lipids 2:21-27

(53) Suh J (2003) Synthetic artificial peptidases and nucleases using macromolecular catalytic systems. Acc Chem Res 36:562-570

(54) Takarada T, Yashiro M, Komiyama M (2000) Catalytic hydrolysis of peptides by cerium(IV) Chem Eur J 6:3906-3913

(55) Wulfsberg G (1991) In: Principles of descriptive inorganic chemistry, University Science Books, Mill Valley, California, p 25

(56) Yuan CB, Zhao DQ, Zhao B, Ni J (1996a) NMR and FT-Raman studies on the interaction of lanthanide ions with sphingomyelin bilayers. Spectro Lett 29:841-849

(57) Yuan CB, Zhao DQ, Zhao B, Wu Y, Liu J, Ni J (1996b) 2D NMR and FT-Raman spectroscopic studies on the interaction of lanthanide ions and Ln-DTPA with phospholipid bilayers. Langmuir 12:5375-5378

(58) Zhu B, Xue D, Wang K (2004) Lanthanide ions promote the hydrolysis of 2,3

bisphosphoglycerate. BioMetals 17:423-433

## 2.7. Supporting Information

### *2.7.1. Turbidity measurements to monitor the conversion of lipid vesicles to micelles.*
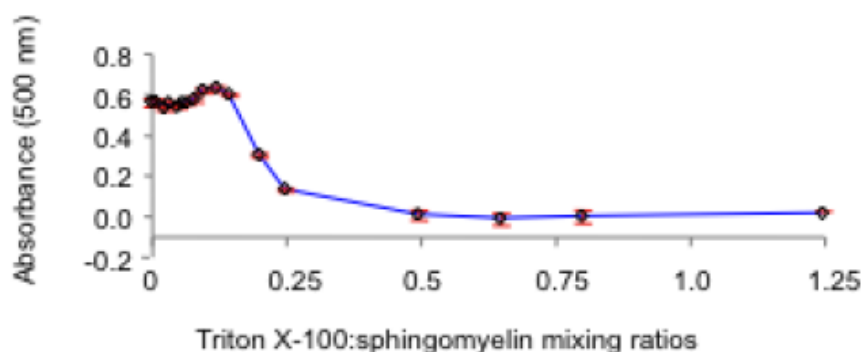


**Figure. 2.S1.** Absorbance at 500 nm plotted as a function of Triton X-100:sphingomyelin molar mixing ratio. Error bars indicate standard deviation.

Lipid vesicles of porcine brain sphingomyelin were prepared in pre-heated ddH₂O as described in the main manuscript (120 mM sphingomyelin, final concentration). In order to promote the conversion of the lipid vesicles to lipid vesicles and then to micelles [1, 2], increasing volumes of a 50 mM solution of the single-chain, nonionic surfactant Triton X-100 were combined with a fixed volume of the lipid vesicle preparation. The Triton X-100:sphingomyelin molar mixing ratios of the resulting series of solutions ranged from 0 to 1.25. Following a 30 min equilibration period at room temperature, piperazine buffer was added. The solutions were then diluted to 1000 mL with ddH₂O (2 mM sphingomyelin, 20 mM piperazine, final concentrations) and equilibrated at room temperature for 1 h. A turbidity profile was then generated by using a UV-1601 Shimadzu spectrophotometer to read for absorbance at 500 nm against a water blank. As shown in Figure 2.S1, the increase in absorption between molar mixing ratios of 0.0 and 0.12 points to the reorganization of sphingomyelin phospholipid vesicles (molar

mixing ratio of 0.0) into larger, mixed lipid vesicles of Triton X-100 and sphingomyelin [1, 3]. The subsequent decrease in absorption between molar mixing ratios of 0.12 and 0.65 indicates a gradual conversion of the mixed lipid vesicles to optically transparent mixed micelles (molar mixing ratios of 0.65, 0.80, and 1.25) [1, 3, 4].

### 2.7.2. Inorganic phosphate standard curves

The yields of free phosphate produced by metal-assisted hydrolysis of sphingomyelin and phosphatidylcholine were determined using inorganic phosphate standards containing 1.5 mM of a metal ion salt, 3.0 mM of buffer (HEPES or piperazine), and from 0 to 11 μM of inorganic phosphate. A total of 400 μL of each standard solution was reacted with 100 μL of the malachite green/molybdate reagent and read for absorbance at 620 nm as described in the main manuscript. The concentration of inorganic phosphate was then determined from the slope of the resulting linear plot (Figire 2.S2). The y intercept of each plot was set equal to zero to correct for background levels of inorganic phosphate. Percent hydrolysis yields were calculated using the formula: (calculated concentration of inorganic phosphate / 2.0 mM theoretical concentration of inorganic phosphate) x 100.
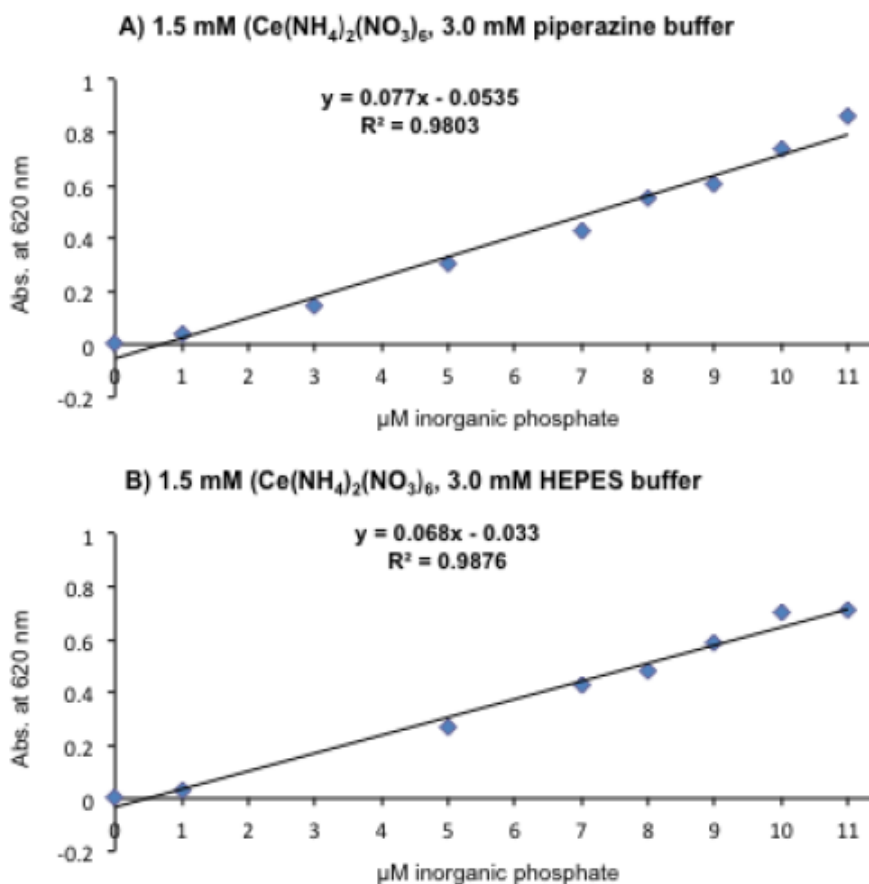
**Figure 2.S2.** Representative standard curves used for the determination of free phosphate in sphingomyelin and phosphatidylcholine hydrolysis reactions. Standard solutions contained: 1.5 mM of $Ce(NH_4)_2(NO_3)_6$, 0 to 11 µM of inorganic phosphate and: **A)** 3.0 mM of piperazine or **B)** 3.0 mM of HEPES buffer.

### 2.7.3. Choline standard curves

The yields of free choline produced by metal-assisted hydrolysis of sphingomyelin and phosphatidylcholine were determined using choline chloride standards containing 0.5 mM of a metal ion salt, 1.0 mM of buffer (HEPES or piperazine), and 0 to 0.07 mM of choline chloride. A total of 40 µL of each standard solution was reacted with 80 µL of the Amplex® Red cocktail and read for absorbance at 570 nm as described in the main manuscript. The concentration of free choline was then determined from the slope of the resulting linear titration curve (Figure

2.S3). Percent hydrolysis yields were calculated using the formula: (calculated concentration of

choline / 2.0 mM theoretical concentration of choline)*100.



**A) 0.5 mM (Ce(NH$_4$)$_2$(NO$_3$)$_6$, 1.0 mM piperazine buffer**

$y = 3.0555x + 0.0076$
$R^2 = 0.9908$

Abs. at 570 nm / mM choline chloride

**B) 0.5 mM (Ce(NH$_4$)$_2$(NO$_3$)$_6$, 1.0 mM HEPES buffer**

$y = 3.1996x + 0.0093$
$R^2 = 0.9946$

Abs. at 570 nm / mM choline chloride
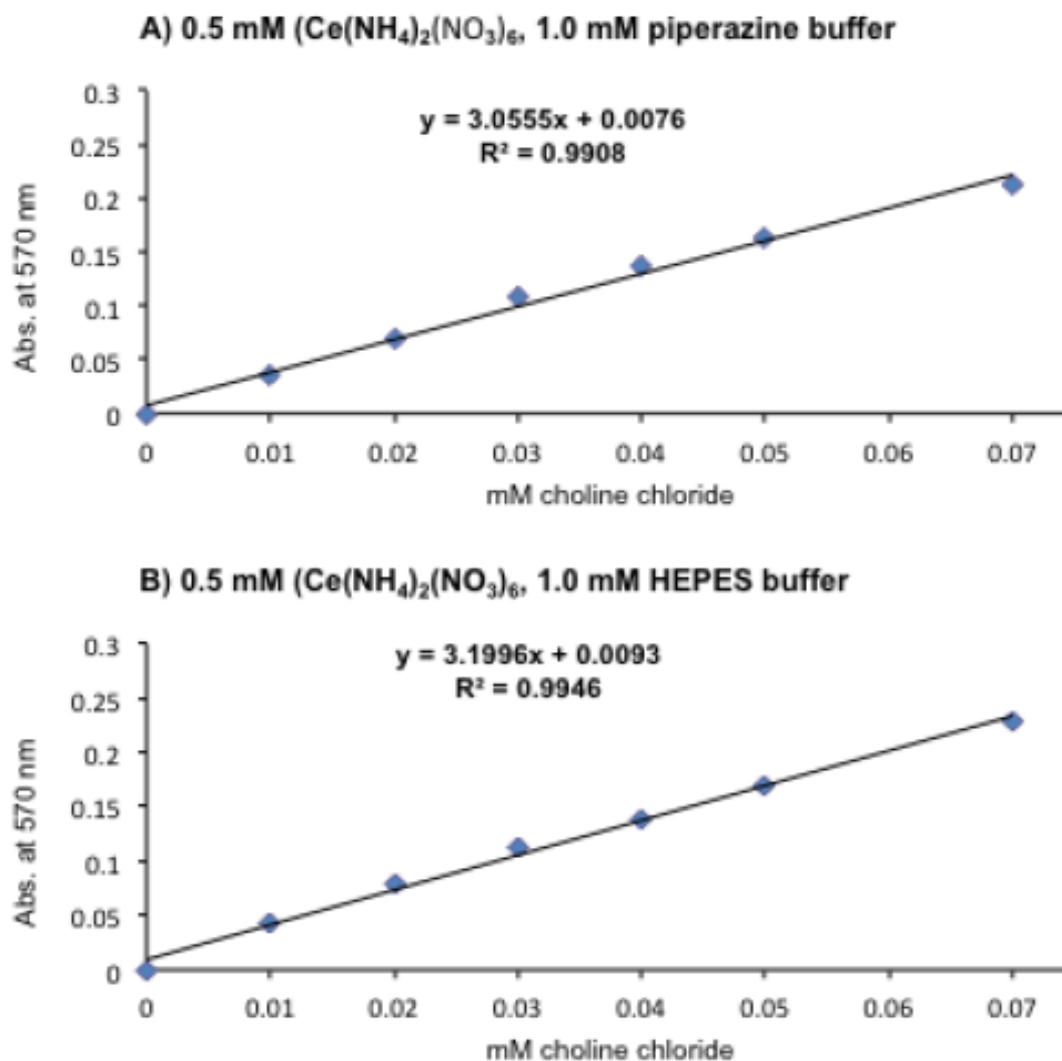
**Figure 2.S3.** Representative standard curves used for the determination of choline in sphingomyelin and phosphatidylcholine hydrolysis reactions. Standard solutions contained: 0.5 mM of Ce(NH$_4$)$_2$(NO$_3$)$_6$, 0 to 0.05 mM of choline and: **A)** 1.0 mM of piperazine or **B)** 1.0 mM of HEPES buffer.

### 2.7.4. MALDI-TOF mass spectrometry
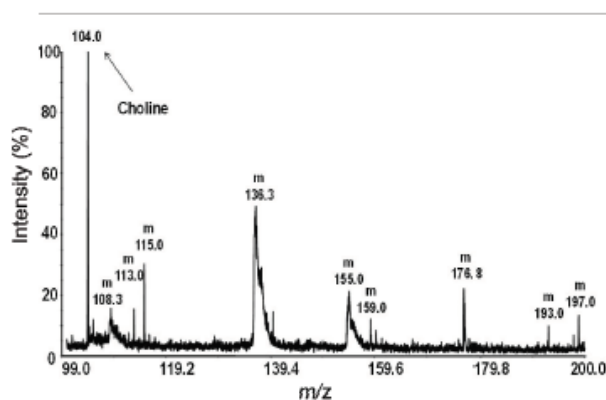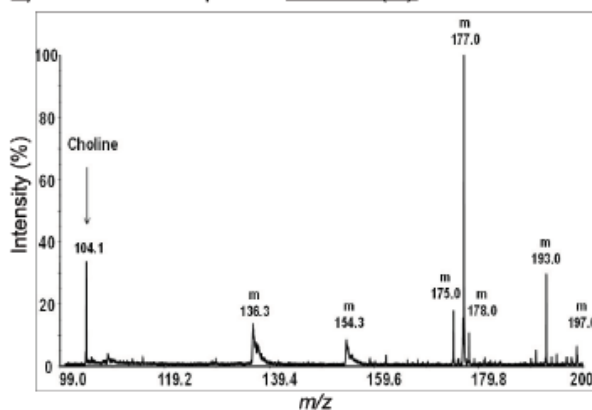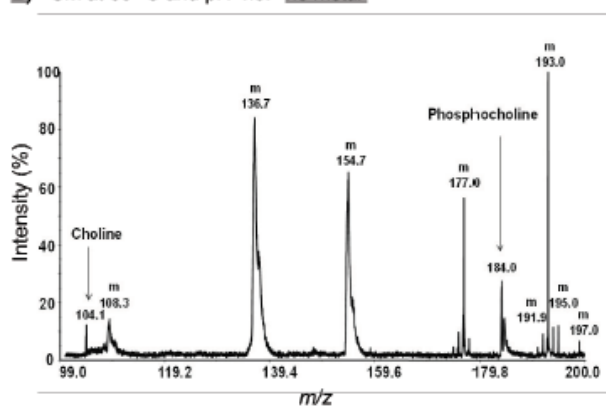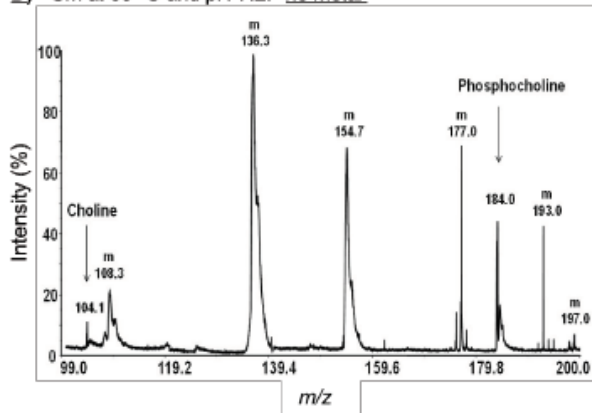


**Figure 2.S4** MALDI-TOF mass spectra of 2 mM of sphingomyelin (SM; no Triton X-100) treated for 20 h at 60 °C and: ~ pH 4.8 (20 mM piperazine buffer) in the presence (**A**) and absence (**B**) of 10 mM of Ce(NH$_4$)$_2$(NO$_3$)$_6$ or ~ pH 7.2 (20 mM HEPES buffer) in the presence (**C**) and absence (**D**) of 10 mM of Ce(NH$_4$)$_2$(NO$_3$)$_6$. M = matrix.

The following Matrix-assisted laser desorption ionization time-of-flight (MALDI-TOF) mass spectra are of sphingomyelin hydrolysis reactions (60 °C, 20 h, no Triton X-100; Figure 2.S4). The data were acquired as described in the main manuscript. In the presence of 10 mM of cerium(IV) metal ion salt, the MALDI-TOF spectra show a strong free choline peak (choline $m/z$ = 104.0 to 104.1 obsd, 104.1 calcd for [C$_5$H$_{14}$N$_1$O$_1$]$^{1+}$) in the pH 4.8 reaction (relative abundance 100%, Figure 2.S4A) and an intermediate peak in the pH 7.2 reaction (relative abundance ~

35%, Figure 2.S4C). In parallel no metal control reactions, the relative abundance of the choline peak is ~ 10% (Figures 2.S4B and 2.S4D). Accordingly, very little free choline and inorganic phosphate were detected when the control reactions were treated with the Amplex® Red and malachite green/molybdate reagents, respectively (Figure 2.S5A). At $m/z$ = 184.0 in the no metal control mass spectra (Figures 2.S4B and 2.S4D), there is a small to intermediate peak corresponding to phosphocholine (calcd for $[C_5H_{15}N_1O_4P_1]^{1+}$ 184.1), indicating that heat treatment (60 °C, no metal) may promote background hydrolysis of phosphate ester Bond A of sphingomyelin (Figure. 2.1).

## 2.7.5. Hydrolysis yields in control reactions run in the absence of metal ion salts



A) SM at 60 °C, Total Phosphate and Choline

Legend:
- phosphate, pH 4.8
- phosphate, pH 7.1-7.2
- choline, pH 4.8
- choline, pH 7.1-7.2

B) Lipid at 37 °C, Total Phosphate

Legend:
- SM, pH 4.7-4.8
- SM, pH 7.1-7.2
- PC, pH 4.9
- PC, pH 7.0

C) Lipid at 37 °C, Total Choline

Legend:
- SM, pH 4.8
- SM, pH 7.0
- PC, pH 4.7-4.8
- PC, pH 7.0
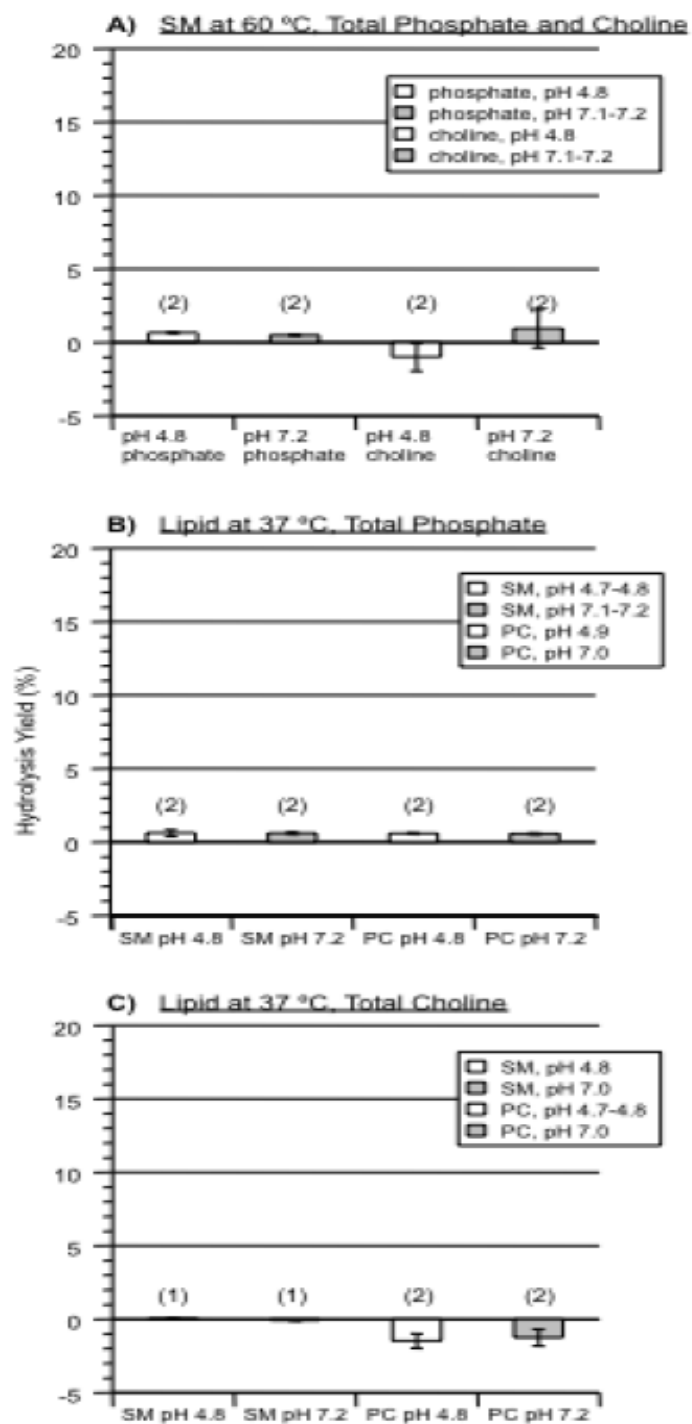
**Figure 2.S5.** Averaged yields plotted as a function of pH for background hydrolysis of sphingomyelin (SM) and of phosphatidylcholine (PC) in the absence of metal. Malachite green/molybdate detection of free phosphate and Amplex® Red detection of free choline for: **<u>A</u>)** SM at 60 °C; **<u>B</u>) & <u>C</u>)** SM and PC at 37 °C. A total of 2 mM of lipid (no Triton X-100) was treated for 20 h in 20 mM piperazine buffer pH 4.8 or in 20 mM HEPES buffer pH 7.2. The number of trials (**n**) appears in parenthesis. Error bars indicate standard deviation.

The following hydrolysis reactions are negative controls in which metal solutions were replaced with equivalent volumes of ddH$_2$O. A total of 2 mM of sphingomyelin or of phosphatidylcholine was treated for 20 h at: (i) 60 °C or at 37 °C and ~ pH 4.8 (20 mM piperazine buffer), and at (ii) 60 °C or at 37 °C and ~ pH 7.0 (20 mM HEPES buffer). Free inorganic phosphate and free choline were detected using the malachite green/molybdate- and Amplex® Red-based colorimetric assays described in the main manuscript. As shown in Figure 2.S5, the amounts of choline and inorganic phosphate generated in the no metal control reactions are less than ~ 2% to 3% in total yield.

### 2.7.6. References

(1) A. Alonso, A. Villena, F.M. Goñi, "Lysis and reassembly of sonicated lecithin vesicles in the presence of Triton X-100." FEBS Lett. 123 (1981) 200-204.

(2) R.A. Salkar, D. Mukesh, S.D. Samant, C. Manohar, "Mechanism of micelle to vesicle transition in cationic-anionic surfactant mixtures" Langmuir 14 (1998) 3778–3782.

(3) M.A. Urbaneja, F.M. Goñi, A. Alonso, "Structural changes induced by Triton X-100 on sonicated phosphatidylcholine liposomes." Eur. J. Biochem. 173 (1988) 585-588.

(4) O. López, A. de la Maza, L. Coderch, C. López-Iglesias, E. Wehrli, J.L. Parra, "Direct formation of mixed micelles in the solubilization of phospholipid liposomes by Triton X-100." FEBS Lett. 426 (1998) 314-318.

# CHAPTER 3

## AN ACIDIC HYDROLYTIC AGENT: EFFICIENT HYDROLYSIS OF

## PHOSPHATIDYLCHOLINE BY A CERIUM(IV) COMPLEX AT LYSOSMAL PH

### 3.1. Abstract

We investigated a total of seven ligands to control and tune hydrolysis of liposomes of phosphatidylcholine (PC) by cerium(IV) metal ion. Phosphate ester bond hydrolysis by Ce(IV) at ~ pH 4.8 displayed a trend of increasing phosphate production going from acidic to more basic ligands. This trend was correlated to the electrophilicity of the metal ion being less affected by the basic ligands compared to the acidic ligands. To maximize phosphate ester bond hydrolysis of PC at 37 °C, a $Ce(NH_4)_2(NO_3)_6$ concentration profile was conducted and displayed optimal levels of hydrolysis at metal salt concentration of 1.75 mM compared to concentrations lower than 0.75 mM and higher than 3.00 mM. Complexes of 1,3-bis[tris(hydroxymethyl)methylamino]propane (BTP) and $Ce(NH_4)_2(NO_3)_6$ provided enhanced levels of hydrolysis at lysosomal pH (~ 4.8) and reduced levels of hydrolysis at near-neutral pH (~ 7.2). $^1$H-NMR spectroscopy studies of Ce(IV)-induced chemical shift changes on the methylene protons of BTP as a function of pD showed BTP coordinated to Ce(IV) and not coordinated to Ce(IV) at ~ pD 7.6 and ~ pD 5.1, respectively. Comparison of lipid hydrolysis reactions to $pK_a$ values of BTP and NMR studies suggested that the ligand have little effect on the electrophilicity of the metal ion which assisted 42 %, 54 %, and 67 % inorganic phosphate from 35 μM PC (37°C and 20 h) at 1:2, 5:1, and 4:1 Ce(IV) to BTP ratios at ~ pH 4.8. When reaction pH was increased to ~ 7.2, complex formation was apparent between the complexes, and the pH 4.8 to 7.2 phosphate ester bond hydrolysis ratio increased from 2.1 to 9.6 for the 5:1 Ce(IV) to BTP complex compared to Ce(IV)-enhance hydrolysis in the absence of ligand.

**3.2 Introduction**

Small-molecule, metal based synthetic hydrolytic agents have potential applications in biotechnology or as molecular therapeutic agents. The lanthanide cerium(IV) has caught the attention of many scientists due to the high electrophilicity, formation of active polynuclear hydroxo species in aqueous solution, the ability to promote hydrolysis at low and high pH, high coordination number (up to 12), high charge density, and fast ligand exchange rates.[1-7] Ce(IV) metal ion and complexes have assisted the hydrolysis of not only phosphate ester bonds, but also amides, and organophosphorus compounds. Some compounds hydrolyzed by Ce(IV) are peptides,[8] DNA,[9-13] cyclic nucleotides,[14-15] activated and inactivated synthetic phosphate ester-containing derivatives,[1, 3, 13, 16-20] antiviral phosphonoformates,[21] the allosteric effector 2,3-bisphosphoglycerate,[22] and phospholipids.[2, 6] The hydrolytic ability of Ce(IV) is attributed to the electron-withdrawing ability of the ion which contributes to enhanced substrate activation.[4] Not only can Ce(IV) enhance the electrophilicity of phosphate ester bonds, the metal ion transforms water into a potent nucleophile. Ce(IV)-bound water has a $pK_a$ of $\sim$ - 0.7 (a $pK_a$ range of $\sim$ 8 - 9 is known for $H_2O$-Ln(III) ions).[23] The high coordination numbers of Ce(IV) provide a higher probability for a coordinated water molecule to act as a nucleophile toward hydrolytic cleavage of phosphate ester and amide bonds.[8]

Complex formation between Ce(IV) and a ligand can not only prevent precipitation of metal hydroxides at pH values greater than 4, but also provide active species with definite compositions, and in some cases, tune hydrolysis and create hydrolytic selectivity.[1, 8-10, 12, 16, 19-20, 24] There are numerous examples of hydrolytic cleavage by Ce(IV) complexes. Branum et al. demonstrated a selective DNA hydrolase mimic where a dicerium complex based on a polyaminocarboxylate ligand produced linear plasmid DNA and preferentially cleaved of DNA

restriction fragments at the 3'-O-P end.[10] Other investigators researched β-cyclodextrin ligands that provided neutral homogeneous aqueous solutions of Ce(IV) and enhanced binding affinity between Ce(IV) and the DNA model substrate bis(4-nitrophenyl) phosphate (BNPP).[19-20] As an additional example, Bracken et al. increased the stability, pH sensitivity, and cleavage selectivity for the hydrolysis of BNPP by Ce(IV) complexes in micellar solutions. Thus, the ligand extended hydrolytic cleavage of BNPP over a broader pH range while still maintaining high rates. Cerium(IV) hydrolytic activity was controlled as a function of pH by the donor atoms of the glucamine, palmitate, and pyridinedicarboxylate ligands utilized.[16] An additional example of Ce(IV) complexes used as hydrolytic agents is the site-selective DNA cleavage method of Komiyama et al.[12] In this approach, homogeneous solutions of 1 mole equivalents of Ce(IV) and EDTA selectively cleaved single-stranded DNA over double-stranded DNA under physiological conditions.[12] The group also noted that Ce(IV), in the absence of EDTA, formed insoluble hydroxide gels in solutions. The process then lost its selectivity and randomly cleaved single- and double-stranded DNA at relatively the same rates.[12]

The investigation of Ce(IV) metal ions and complexes as agents for DNA hydrolysis has been studied over the past two decades.[4, 9-15] In contrast, lanthanide metal-assisted hydrolysis of lipids has been studied rarely.[6-7, 25-28] Lipids play vital roles in biological systems as energy-storage molecules and chemical messengers in cell signaling and regulation, and are major components of the biological membranes that surround all cells and organelles.[29-31] Some of the vital functions of lipids are provided by the products of lipid degradation by phospholipid-specific hydrolases called phospholipases. Examples include diacylglycerol and phosphatidic acid from the degradation of phosphoglycerides by phospholipases C or D, and ceramide from the degradation of sphingomyelin by sphingomyelinase. Diacylcglycerol activates protein kinase

C by increasing the affinity of the enzyme for calcium(II) ion. Phosphatidic acid is a secondary

messenger in signal transduction and is a major intermediate in the synthesis of

phosphoglycerides and triacylglycerols. Ceramide acts as a signaling molecule and mediator of

cell differentiation.[29-31]  It would be reasonable to employ Ce(IV) metal ions and complexes as

lysosomal or cytoplasmic phospholipase mimics to study signal transduction pathways, as probes

to study the permeability and dynamics of lipid bilayer systems, or even as potential therapeutic

agents to reverse the build-up of phospholipids in acquired or genetic lysosomal storage disease

(phospholipidosis).
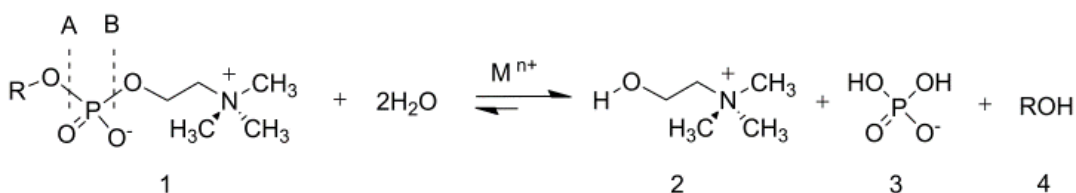


**Figure 3.1.** Metal-assisted hydrolysis of the phosphate ester bonds of a phospholipid **(1)** releases inorganic choline **(2)**, phosphate **(3)**, and ROH **(4)**. ROH = diacylglycerol for phosphatidylcholine and ceramide for sphingomyelin.

A general scheme for metal-assisted phospholipid hydrolysis is shown in Figure 3.1. At

the present, the goal of our research is to identify a pH dependent, small molecule, hydrolytic

agent by screening ligands capable of tuning the hydrolytic ability of Ce(IV) as a function of pH.

Similar to natural phospholipid-specific acidic hydrolases, which are responsible for the

degradation of phospholipids in the lysosome, this Ce(IV) complex would provide enhance

levels of phosphate ester bond cleavage of lipids at the acidic pH of the lysosome (~ 4.8) and

substantially reduce activity at cytosolic pH (~ 7.2). This pH dependent property is inherent in

acidic hydrolases and protects the cell from damage in the event of leakage of these enzymes

from the lysosome into the cytoplasm. We have previously shown that Ce(IV)-enhanced

hydrolysis of the phosphate ester bonds of the naturally occurring phosphoglyceride

phosphatidylcholine (PC) and the sphingolipid sphingomyelin (SM) at ~ pH 4.8 and pH 7.2 to give rise to the hydrolysis products inorganic phosphate and choline at 37 °C.[6-7]   Ce(IV) metal ion provided preferential hydrolytic cleavage (~ 2-fold more inorganic phosphate) at pH 4.8 compared to pH 7.2 for both lipids.[6-7]  These results served as a great foundation for our search for an "acidic hydrolase"-like hydrolytic agent.  The limitations of Ce(IV) in aqueous solutions, formation of insoluble Ce(IV) hydroxo clusters, and our requirement for greater pH dependency (higher pH 4.8 to 7.2 hydrolysis yield ratio) would all be addressed by using different ligands to tune reactivity.  In this work, our lipid models are liposomes of either L-α-phosphatidylcholine (PC) or sphingomyelin (SM).  Colorimetric assays were used to monitor the products of hydrolytic cleavage of the phosphate ester bonds of the lipids.  PC and SM were chosen for this study because they are major membrane phospholipids, making up approximately 50 % of the membrane bilayers of eukaryotic cells.[32]

## 3.3. Experimental

### 3.3.1. Materials and instruments

De-ionized, distilled water was used in the preparation of all reagents. All chemicals were of the highest purity and utilized without further purification.  L-α-phosphatidylcholine from egg chicken (catalog number 840051P) and sphingomyelin from brain porcine (catalog number 860062P) were obtained from Avanti Polar Lipids.  The metal salt $Ce(NH_4)_2(NO_3)_6$ was purchased from Aldrich. The ligands and buffers, piperazine, 2-amino-2-(hydroxymethyl)-1,3-propanediol (TRIS), 1,10-phenanthroline, and 1,3-diamino-2-hydroxypropane-N,N,N′,N′-tetraacetic acid (HPTA) were also obtained from Aldrich.  The ligands and buffers, 4-(2-hydroxyethyl)piperazine-1-ethanesulfonic acid (HEPES),  1,3-bis[tris(hydroxymethyl)methylamino]propane (BTP or bis-tris propane), 2-(4-

imidazolyl)ethylamine dihydrochloride (histamine), and 4-morpholineethanesulfonic acid (MES), and DMSO were purchased from Sigma. EDTA was purchased from Fisher Scientific. The NMR regents deuterium oxide 99 % D ($D_2O$), deuteroxide (30 wt. % in $D_2O$, 99 % D), DMSO-$d_6$, and deuterium chloride were acquired from Aldrich. *Tert*-butanol anhydrous $\geq 99.5$ % was obtained from Sigma. Malachite Green Phosphate Assay Kits (catalog number POMG-25H) were from BioAssay Systems. Amplex® Red Sphingomyelinase Assay Kits (catalog number A12220) were acquired from Invitrogen. Choline chloride standards were acquired from Aldrich. IR spectra were recorded on a Perkin Elmer Spectrum 100 FT-IR spectrometer coupled with an attenuated total reflection (ATR) sampling accessory. NMR spectra were recorded on a Bruker Advance 400 MHz NMR spectrometer. Colorimetric assays were conducted using a UV-1601 Shimadzu spectrophotometer.

### 3.3.2. Preparation of lipid vesicles

Either egg chicken phosphatidylcholine or porcine brain sphingomyelin was added to a round bottom flask and dissolved in 1 mL of chloroform. The chloroform was concentrated to dryness *in vacuo* overnight. To the dried phospholipid was added pre-heated water (55 °C for sphingomyelin and 65 °C for phosphatidylcholine) to a final concentration of 120 mM (used in 2 mM lipid hydrolysis reactions) or 2.06 mM (used in 35 µM lipid hydrolysis reactions). The solution was sonicated for 20 min at 55 °C for sphingomyelin and 65 °C for phosphatidylcholine, which are above the gel-to-fluid transition temperatures ($T_m$) of the lipids. The $T_m$ for sphingomyelin is 30 – 45 °C, and $T_m$ values for phosphatidylcholine are 41 °C (16:0 PC) and 55 °C (18:0 PC).[33-34]

### 3.3.3. Lipid hydrolysis reactions

Both 2 mM and 35 µM lipid hydrolysis reactions were performed.  The 2 mM reactions typically consisted of 10 mM $Ce(NH_4)_2(NO_3)_6$, 20 mM ligand or buffer (piperazine or  HEPES), and 2 mM sphingomyelin or phosphatidylcholine.  The 35 µM lipid hydrolysis reactions typically consisted of 1.75 mM $Ce(NH_4)_2(NO_3)_6$, 3.5 mM bis-tris propane (BTP) or buffer (piperazine or HEPES), and 35 µM sphingomyelin or phosphatidylcholine.  The ligands tris, BTP, and histamine were prepared as 200 mM aqueous stock solutions for 2 mM lipid hydrolysis.  HPTA was acquired as a 50 mM stock solution at pH 7 and EDTA was utilized as a 200 mM stock solution at pH 8.  Phenanthroline was employed as a 200 mM stock and prepared in DMSO (10 % v/v in the final reaction).  Thereafter, the metal complexes were prepared by adding a 100 mM aqueous solution of $Ce(NH_4)_2(NO_3)_6$ to 200 mM of ligand.  In subsequent experiments, 35 mM BTP and 10 mM MES buffer (or volume equivalent of water) were added to a 17.5 mM aqueous solution of $Ce(NH_4)_2(NO_3)_6$.  Corresponding lipid hydrolysis reactions in the absence of ligand were prepared by replacing the ligand with volume and concentration equivalents of piperazine or HEPES buffer solutions.  $Ce(NH_4)_2(NO_3)_6$ in buffer solutions and complexes were pre-mixed and allowed to equilibrate for 1 h at room temperature. Thereafter, the addition of 0 – 0.5 µL of concentrated and/or dilute HCl and 50 % NaOH (w/v) was added to achieve 2 sets of metal solutions, ~ pH 4.8 and ~ pH 7.2.  Reactions with a 1000 µL final volume were initiated by the addition of the pre-mixed and pH adjusted $Ce(NH_4)_2(NO_3)_6$  aqueous solutions to lipid solutions.  The lipid hydrolysis reactions were allowed to react at 37 °C or 60 °C for 0 h (placed in 4 °C fridge) and 20 h. In control reactions, the aqueous solution of $Ce(NH_4)_2(NO_3)_6$  was replaced by equivalent volumes of $ddH_2O$.  Averaged reaction pH values were calculated from pre- and post-reaction pH measurements.

The $Ce(NH_4)_2(NO_3)_6$ titration consisted of 35 µM phosphatidylcholine, 1.5 mM piperazine buffer, 0 mM – 10.0 mM $Ce(NH_4)_2(NO_3)_6$, and was reacted at 37 °C and ~ pH 4.8 for 20 h.  The time course experiments consisted of 35 µM phosphatidylcholine, buffer and/or BTP, 1.75 mM $Ce(NH_4)_2(NO_3)_6$, and were reacted at 37 °C and  ~ pH 4.8 (3.5 mM piperazine, or 3.5 mM BTP and 1 mM MES buffer) or ~ pH 7.2 (3.5 HEPES or 3.5 mM bis-tris propane) for 2, 4, 5, 11, 13, 15, 17, 20, and 30 h time intervals.  The lipid hydrolysis reactions with the synthesized BTP derivative contained 1.75 mM $Ce(NH_4)_2(NO_3)_6$ and 3.5 mM 1,3-bis-[tris-(hydroxymethyl)-methyl-amino]-2-propanol and were reacted at ~ pH 4.8 (1 mM MES buffer) or ~ pH 7.2 (1 mM MOPS buffer) for 20 h at 37 °C.  The experiment monitoring phosphate production as a function of Ce(IV):BTP ratios involved 35 µM of phosphatidylcholine reacted at ~ pH 4.8 (1 mM piperazine) or  ~ pH 7.2 (1 mM HEPES) for 20 h in the presence of 1.75 mM Ce(IV) and varied concentrations of  BTP (0.19 mM – 3.5 mM).  Averaged reaction pH values were calculated from recorded pre- and post- reaction pH measurements.

### 3.3.4. Colorimetric detection of free inorganic phosphate

A malachite green/molybdate-based colorimetric assay kit was used to detect inorganic phosphate released upon metal-assisted phosphate ester bond hydrolysis of lipids.[35]  The 2 mM lipid hydrolysis reactions were diluted by a factor of 15 for the reactions reacted at 37 °C or by 30 for the reactions reacted at 60 °C with $ddH_2O$ to a total volume of 300 µL.  Subsequently, 200 µL of the malachite green/molybdate reagent was added to the diluted reactions to a final volume of 500 µL.  Conversely, a 500 µL final volume resulted from the addition of 100 µL of the malachite green/molybdate reagent to 400 µL of the 35 µM lipid hydrolysis reaction.  The reactions were incubated for 30 min at room temperature.  A UV-1601 Shimadzu spectrophotometer was utilized to detect colorimetric inorganic phosphate product at 620 nm

against a ddH$_2$O blank. The t = 0 h reactions were treated the same as the corresponding t = 20 h reactions. Absorbance corrections from background levels of free inorganic phosphate were achieved by the subtraction of the observed absorbance at t = 0 h from the t = 20 h absorbance. The same calculations were performed for the parallel, negative no metal control reactions (Supporting information, Figures 3.S10 –S12). The absorbance difference of the negative control reactions was then subtracted from the absorbance difference of the corresponding lipid hydrolysis reactions in the presence of metal. Linear titration curves were then constructed using solutions of inorganic phosphate standards (0 – 11 μM or 0 – 35 μM), and Ce(IV) metal ion and complexes at concentrations that were the same as those used in the corresponding lipid hydrolysis reactions (Figures 3.S1 and S3 – S8 in Supporting Information).

### 3.3.5. Colorimetric detection of choline

An Amplex® Red Sphingomyelinase Assay Kit was used to detect free choline released upon metal-assisted lipid hydrolysis.[36] The assay was performed by using reagent from the kit to make a reaction cocktail: 2,850 μL of 1 X tris Buffer, 40 μL of Amplex® Red, 30 μL of horseradish peroxidase, 30 μL of choline oxidase, and 60 μL of ddH$_2$O. The lipid hydrolysis reactions were diluted 12.5 fold to a total volume of 1000 μL with ddH$_2$O. Then, a total of 40 μL of the diluted lipid hydrolysis reaction was reacted with 80 μL of the reaction cocktail, and incubated for 55 min at 37 °C. Thereafter, the lipid hydrolysis reactions (80 μL) were diluted to a total volume of 500 μL with ddH$_2$O. Free choline was quantitated with a UV-1601 Shimadzu spectrophotometer against a ddH$_2$O blank. The t = 0 h reactions were treated the same as the corresponding t = 20 h reactions. Absorbance corrections were achieved by the subtraction of the observed absorbance of t = 0 h from the t = 20 h reactions. The same calculations were performed for the parallel, negative control reactions (Supporting information, Figures 3.S10).

The absorbance difference of the negative control reactions was then subtracted from the corresponding lipid hydrolysis reactions in the presence of metal. Linear titration curves were plotted by using the diluted solutions of choline chloride standards (0 – 70 μM) with Ce(IV) metal ion and complexes at concentrations that were the same as those used in the corresponding lipid hydrolysis reactions (Figure 3.S2 in Supporting Information).

### 3.3.6. Synthesis of [Ce(BTP)$_2$(NO$_3$)$_4$]·2H$_2$O

The metal complex is a known compound and was synthesized by a published method.[3] Purification was achieved by recrystallization from an acetone-water mixture. The desired product was obtained as a yellow solid in 55.9 % yield (2.1154 g). $^1$H-NMR (400 MHz, DMSO-d$_6$, 25 °C, ppm): δ = 1.99 (bs, 2H); 3.03 (bs, 4H); 3.32 (s, 2H); 3.56 (bs, 12H); 5.30 (s, 6H); 8.28 (bs, 3H). $^{13}$C-NMR (100 MHz, D$_2$O, 25 °C, ppm) 22.70; 37.94; 56.97; 64.87. Anal. Calcd. for C$_{22}$H$_{56}$N$_8$O$_{26}$Ce (988.83 g mol$^{-1}$): C 26.72; H 5.71; N 11.33. Found C 25.35; H 5.70; N 11.48. FT-IR (ATR, cm$^{-1}$): 3343 (b, w), 3109 (b, w), 2884 (b, w), 1589 (w), 1320 (s), 1079 (s), 1019 (s), 823 (m). $^1$H-NMR, IR, and $^{13}$C-NMR spectra are located in Supporting Information as Figures 3.S16, 3.S17, and 3.S21, respectively.

### 3.3.7. Synthesis of dihydrochloride salt of 1,3-bis-[tris-(hydroxymethyl)-methyl-amino]-2-propanol and pK$_a$ determination

This known compound was synthesized by a published method.[37] The crude product was recrystallized from an ethanol-water mixture to yield the desired product as a white solid (35.3 % yield, 9.4700 g). $^1$H-NMR (400 MHz, DMSO-d$_6$, 25 °C, ppm): δ = 3.11 (m, 2H); 3.25 (m, 2H); 3.59 (s, 12H); 4.25 (bs, 1H); 5.37 (bs, 6H); 6.04 (d, 1H); 7.83 (t, 2H); 8.68 (t, 2H). $^{13}$C-NMR (100 MHz, D$_2$O, 25 °C, ppm) 45.44; 57.49; 63.46; 66.15. MS (ESI) m/z 299.2 [M + H]$^+$ (calcd

$C_{11}H_{26}N_2O_7$ for 298.3). ^{1}H and ^{13}C NMR spectra are located in Supporting Information as Figures 3.S18 and 3.S19, respectively.

To determine pKa values, a 50 mL solution of 2.5 mM 1,3-bis-[tris-(hydroxymethyl)-methyl-amino]-2-propanol in 0.1 M NaCl was titrated with degassed, standardized NaOH solution (0.05 M) at rt using a TitroLine alpha plus titrator (Schott). The pH was monitored up to 12 and followed as a function of added NaOH (mL). KaleidaGraph (v. 4.0) was used to obtain the approximate first derivative of $\Delta$NaOH (mL)/$\Delta$pH versus pH, and the $pK_a$ values were indicated by the maxima of the first-derivative plot

### 3.3.8. ^{1}H-NMR spectroscopy

Ce(IV)-induced changes in the chemical shifts of bis-tris propane were recorded in $D_2O$ at room temperature. *Tert*-butanol was used as an internal standard. The pD values were adjusted to 2.3, 5.1 – 5.2, 7.6 – 7.7, and 9.6 with NaOD and DCl in $D_2O$. The equation pD = pH + 0.4 was used to convert pH to pD values.

## 3.4. Results and Discussion

### 3.4.1. The effects of various ligands on the hydrolysis of PC by Ce(IV)

In an earlier experiment, we utilized twelve metal ion salts in an effort to hydrolytically cleave the phosphate ester bonds of L-$\alpha$- phosphatidylcholine (PC) at lysosomal pH (pH 4.8) vs. cytosolic pH (pH 7.2).[1] These results established the superiority of Ce(IV) - assisted hydrolysis over the eleven other metal ion salts tested, and led us to examine various ligands to tune hydrolysis of PC. Our goal is to design a Ce(IV)-based phospholipase mimic by creating a

hydrolytic agent with enhance levels of activity at lysosomal pH (4.8), and reduce or no levels of

activity at near-neutral pH (~ 7.2).
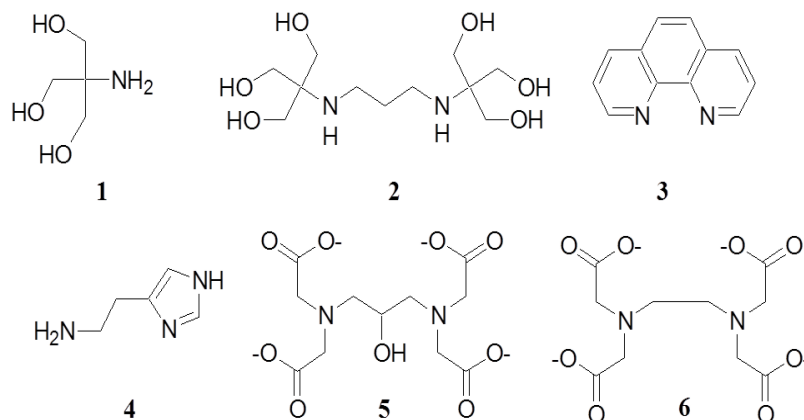


**Figure 3.2.** Ligands used to tune Ce(IV)-assisted hydrolysis of the phosphate ester bonds of phosphatidylcholine at lysosomal (pH ~ 4.8) and cytosolic (pH ~ 7.2) pH values and 60 °C. The ligands are: (**1**) tris(hydroxymethyl)aminomethane (Tris), (**2**) 1,3-bis-[tris(hydroxymethyl)methylamino]propane (BTP), (**3**) 1,10 phenanthroline, (**4**) histamine (**5**) 1,3-diamino-2-hydroxypropane-N,N,N',N'-tetraacetate (HPTA), and (**6**) ethylenediaminetetraacetate (EDTA). Reactions of Ce(IV) salt in the absence of ligands, piperazine and HEPES (4-(2-hydroxyethyl)-1-piperazineethanesulfonic acid) were used as buffers for the ~ pH 4.8 and ~ pH 7.2 reactions, respectively.

Six prospective ligands (Figure 3.2), including polyamino carboxylates and alcohols, an

amino acid derivative, and a nitrogen heterocyclic organic compound, were tested against

buffered Ce(IV) solutions in the absence of ligand for hydrolysis of the phosphate ester bonds in

lipid vesicles of PC. To tune hydrolysis as a function of pH, two mol equivalents of ligand were

added to aqueous solutions of Ce(IV). HPTA (5, Figure 3.2) is capable of binding to two

equivalents of Ce(IV), and thus, 0.5 mol equivalents were added to Ce(IV).[9]

**Table 3.1.** The correlation between the $pK_a$ values of various ligands and the pH 4.8 to pH 7.2 phosphate ratios produced by Ce(IV) complexes at 37 °C and 20 h

| Ligand[a] | $pK_a$[b] | pH 4.8 : pH 7.2 ratios |
|---|---|---|
| **1** | $pK_a = 8.3$ | 1.0 |
| **2** | $pK_{a1} = 6.8$[c] <br> $pK_{a2} = 9.1$[c] | 2.6 |
| **3** | $pK_a = 4.8$ | 0.8 |
| **4** | $pK_{a1} = 6.1$ <br> $pK_{a2} = 9.8$ | 1.2 |
| **5** | $pK_{a1} = 1.47$ (-COOH)[d] <br> $pK_{a2} = 2.62$ (-COOH)[d] <br> $pK_{a3} = 7.04$ (-NH)[d] <br> $pK_{a4} = 9.49$ (-NH)[d] | --- |
| **6** | $pK_{a1} = 2.00$ (-COOH) <br> $pK_{a2} = 2.67$ (-COOH) <br> $pK_{a3} = 6.16$ (-NH) <br> $pK_{a4} = 10.26$ (-NH) | --- |
| No Ligand | ---------- | 1.4 |
| [a] Ligands from Figure 3.2 <br> [b] Ref. 38 (unless noted) <br> [c] Ref. 3 <br> [d] Ref. 39 | | |

In Figure 3.2, histamine (**4**) and phenanthroline (**3**) were chosen based on their $pK_a$ values (Table 3.1) and ability to form stable 6- and 5- membered rings, respectively. The polycarboxylate ligands (**5** and **6**, Figure 3.2) were selected based on the previous reports that their Ce(IV) complexes promote efficient DNA cleavage.[9-10, 12] In addition, we hypothesized that the two polycarboxylate ligands EDTA and HPTA would coordinate more strongly to Ce(IV) metal ion at pH 7.2 compared to pH 4.8. Therefore, the carboxylates of the ligand would reduce the Lewis acidity of Ce(IV) at near-neutral pH that would lead to reduced hydrolysis. When pH is decreased (~ pH 4.8), Ce(IV) will have lower affinity to the carboxylate groups;

Ce(IV) Lewis acidity would then increase, which would lead to increase hydrolysis yields. The amino alcohol ligands bis-tris propane (BTP, **2**, Figure 3.2) and tris (**1**, Figure 3.2), were chosen based on Maldonado and Yatsimirsky's study of the active metal hydroxo species in aqueous solution of pre-synthesized Ce(IV) complexes and hydrolytic activity of the complexes toward an activated synthetic phosphodiester-containing substrate (BNPP).[3] Their results showed more hydrolytic cleavage of BNPP at mildly acidic pH compared to near-neutral pH by the presynthesized complex of BTP and Ce(IV).[3]

The production of inorganic phosphate by Ce(IV)-assisted hydrolysis of PC was measured using a commercially available malachite green/molybdate based colorimetric assay kit. The malachite green phosphomolybdate blue-green complex, which was monitored using a UV-visible spectrophotometer at 620 nm, was formed by the electrostatic binding of inorganic phosphate and molybdenum(VI) salt to the malachite green dye.[35]
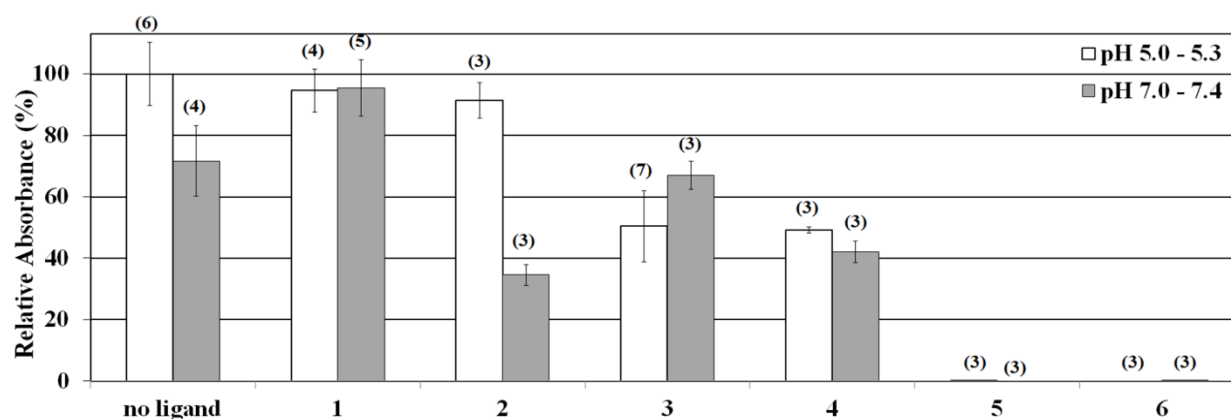


**Figure 3.3.** Percent relative absorbance at 620 nm plotted as a function of pH. A total of 2 mM PC was reacted at 60 °C for 20 h in the presence of 10 mM $Ce(NH_4)_2(NO_3)_6$ and 20 mM ligand (**1-6**, Figure 3.2) at ~ pH 4.8 or at ~ pH 7.2. For the reactions in the absence of ligand, 20 mM piperazine or HEPES buffers were used for the ~ pH 4.8 or ~ pH 7.2 reactions, respectively. The number of trials **(n)** appears in parenthesis. Error bars represent standard deviation.

The results of this experiment are shown in Figure 3.3 where the relative absorbances at 620 nm reflect relative hydrolysis levels. The corresponding pH 4.8 to 7.2 hydrolysis ratios from

Figure 3.3 and ligands' $pK_a$ values are shown in Table 3.1. A correlation between reduced hydrolysis by Ce(IV) and complex formation by some of these ligands was anticipated. The polycarboxylate ligands either completely suppressed or produced extremely low hydrolysis yields at both pH values. Phenanthroline generated slightly more hydrolysis at ~ pH 7.2 compared to ~ pH 4.8. Histamine produced slightly more hydrolysis at ~ pH 4.8 than ~ pH 7.2, and tris produced considerable and comparable hydrolysis yields at both pH values. BTP produced 2.6 fold more hydrolysis at ~ pH 4.8 compared to ~ pH 7.2 and presented a great improvement compared to the 1.4 fold pH 4.8 to pH 7.2 hydrolysis enhancements by the Ce(IV) reactions in the absence of ligand.

Heterogeneous gels of Ce(IV) hydroxide formed immediately upon the addition of $Ce(NH_4)_2(NO_3)_6$ to buffer solutions without ligand. More precipitation was observed in the ~ pH 7.2 reactions compared to the ~ pH 4.8 reaction mixtures, and Ce(IV)-assisted hydrolysis in the absence of ligand was slightly more at ~ pH 4.8 than ~ pH 7.2. Previous studies attributed the decreased hydrolysis to the increased formation of Ce(IV) hydroxo clusters as the pH was raised from ~ pH 4.8 to ~ pH 7.2.[3, 6-7] Thus, the formation of Ce(IV) hydroxo clusters with lowered net positive charge and reduced Lewis acidity are more prevalent in solutions at near-neutral pH compared to mildly acidic conditions, which leads to less efficient substrate binding to and substrate activation by Ce(IV).[6-7] Hydrolysis reactions in the presence of ligand contained less precipitation of Ce(IV) hydroxo clusters in aqueous solutions compared to reactions in the absence of ligand. The screening of the six ligands to tune Ce(IV)-assisted hydrolysis clearly shows the pH sensitivity of the metal ion center toward the hydrolysis of PC. Corresponding to $pK_a$ values of the ligands (Table 3.1), Ce(IV) metal ion hydrolysis levels (Figure 3.3) at ~ pH 4.8 are ranked as the following: tris ($pK_a$ 8.3)[38] ≈ BTP ($pK_{a1}$ 6.8)[3] > phenanthroline ($pK_a$ 4.8)[38] ≈

histamine ($pK_{a1}$ 6.1)[38] > HPTA ($pK_{a1}$ 1.47)[39] ≈ EDTA ($pK_{a1}$ 2.0)[38]. Thus, acidic ligands tend to suppress the hydrolytic activity of Ce(IV) the most. Hydrolysis levels by Ce(IV), which is correlated to Lewis acidity, is significantly reduced by the carboxylate groups of EDTA and HPTA. Both ligands have four carboxylates with $pK_a$ values less than ~ 3. Histamine and phenanthroline, less basic compared to BTP, suppressed hydrolysis at both pH values and produced pH 4.8 to 7.2 hydrolysis ratios of 1.2 and 0.8, respectively (Table 3.1). At both pH values (~ 4.8 and ~ 7.2), the coordination of the bidentate ligands histamine and phenanthroline to Ce(IV) should form 6 - and 5-membered chelate rings, respectively. Thus, reduced Lewis acidity of Ce(IV) and complex formation must occur at both pH values. There was no observed difference in the amount of precipitation formed between the ~ pH 4.8 and ~ pH 7.2 reaction mixtures of both Ce(IV) complexes based on tris and BTP. BTP and tris are similar in structure, but the ligands modulated Ce(IV)-assisted hydrolysis of PC differently. Ce(IV) coordinated to tris, a primary amine with a $pK_a$ of 8.3, provided enhance and similar levels of phosphate ester bond cleavage (ratio of 1.0, Table 3.1) at both pH values. The amine of tris would have a positive charge and ligand coordination would be relatively low at pH 4.8 and 7.2. In comparison to Ce(IV)-mediated hydrolysis in the absence of ligand, tris modulated less metal hydroxo precipitate at both pH values and higher levels of hydrolysis by Ce(IV) at pH 7.2. This later observation confirms that Ce(IV)-assisted hydrolysis of PC is influenced and mediated by tris, perhaps by the ligand's hydroxyl groups. In contrast, BTP has two amines with $pK_a$ values of 6.8 and 9.1 and the Ce(IV) complex provided enhance and suppress levels of phosphate ester bond cleavage (ratio of 2.6, Table 3.1) at ~ pH 4.8 and ~ pH 7.2, respectively. Clearly, this Ce(IV) complex hydrolytic activity is strongly pH driven by the $pK_a$ values of the donor atoms of BTP. BTP was the only ligand that passed this screening and was studied further.

With the goal of developing a synthetic Ce(IV)-based acidic phospholipase mimic with superior and suppressed activity at ~ pH 4.8 and ~ pH 7.2, respectively, two mol equivalents of BTP were added to aqueous solutions of $Ce(NH_4)_2(NO_3)_6$ (Ce(IV)-BTP). The reaction of 2 mM PC at core body temperature, 37 °C, for 20 h was monitored and quantitated by the malachite green/molybdate-based colorimetric assay to detect inorganic phosphate (3, Figure 3.1) at 620 nm and by an Amplex Red-based assay to detect choline (2, Figure 3.1) at 570 nm. In the ~ pH 4.8 reactions, $14 \pm 1$ % of choline and $6 \pm 2$ % of inorganic phosphate were produced, and the ~ pH 7.2 reactions presented substantially suppressed hydrolysis yields of less than 1 % of choline and inorganic phosphate (Supporting Information, Figure 3.S9). In a previous study, Ce(IV)-assisted hydrolysis in the absence of ligand produced moderate levels of hydrolysis, $20 \pm 2$ % of choline and $11 \pm 2$ % of phosphate from PC at ~ pH 7.2.[6] In the present study, Ce(IV)-BTP assisted hydrolysis of PC at ~ pH 4.8 demonstrated a reduction in activity by comparison to the previous study of Ce(IV)-assisted hydrolysis in the absence of ligand, which provided ~ 3 fold more choline and inorganic phosphate at ~ pH 4.8 from 2 mM PC.[6] Although yields are lower, the pH 4.8 to 7.2 hydrolysis ratios are higher because of BTP suppression of the metal's Lewis acidity at the higher pH. The evidence for this occurrence will be discussed further in this paper.

It is important to highlight the display of more choline (~ 2-fold more) than inorganic phosphate produced from the lipid vesicles of PC by both Ce(IV)-BTP and Ce(IV) in the absence of ligand at ~ pH 4.8, and by Ce(IV) in the absence of ligand at ~ pH 7.2. The production of phosphate requires the hydrolysis of both phosphate ester bonds (Bond A and B, Figure 3.1), while the hydrolysis of one phosphate ester bond (Bond B, Figure, 3.1) results in the production of choline. Alternatively, the choline could be generated by subsequent hydrolysis of the

product phosphocholine after the initial hydrolysis of the phosphate ester bond on the glycerol side of the phosphorous atom (Bond A, Figure 3.1). Evidently, the initial or most frequent hydrolysis event by the Ce(IV) metal ion and complex occurs at the phosphate ester bond on the choline side of the phosphorous atom of PC.

### 3.4.2. Optimization of the catalytic efficiency of Ce(IV)
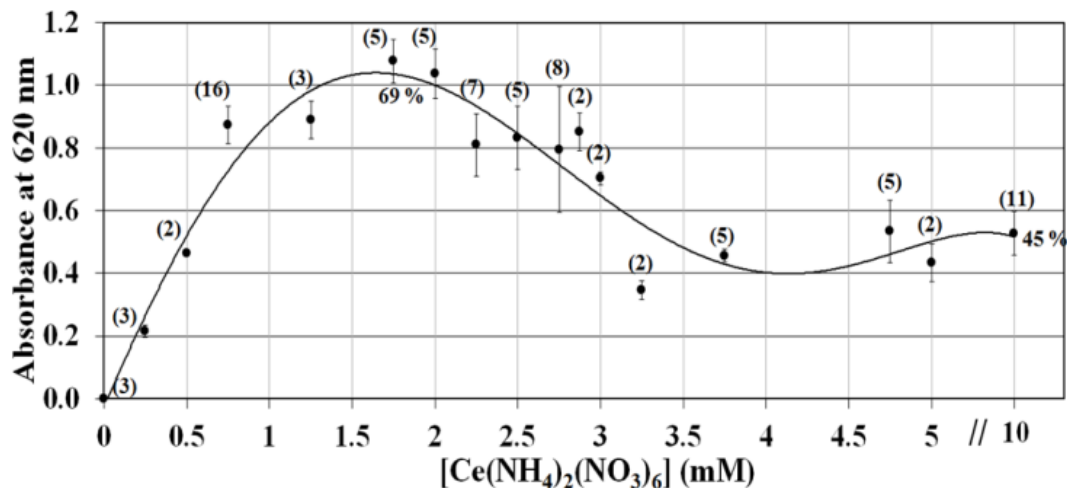


**Figure 3.4.** Absorbance at 620 nm plotted as a function of Ce(IV) concentration for malachite green-treated hydrolysis reactions containing PC. A total of 35 µM of PC was reacted at 37 °C for 20 h in the presence of 0.0 mM – 10.0 mM Ce(NH$_4$)$_2$(NO$_3$)$_6$ at pH ~ 4.8 (1.5 mM piperazine buffer). Linear titration curves generated from inorganic phosphate standards treated with malachite green displayed 69 % and 45 % inorganic phosphate yields for the 1.75 mM and 10 mM Ce(NH$_4$)$_2$(NO$_3$)$_6$ reactions, respectively. The number of trials **(n)** appears in parenthesis. Error bars represent standard deviation.

A Ce(IV) concentration profile was conducted (Figure 3.4) to maximize phosphate ester bond hydrolysis of the substrate PC at core body temperature (37 °C). A total of 35 µM of PC was reacted at 37 °C for 20 h in the presence of 0 – 10 mM Ce(IV) at pH ~ 4.8 (no ligand). The release of phosphate was followed spectrophotometrically at 620 nm with the malachite green/molybdate colorimetric assay. A linear progression (slope of 1.08) of phosphate production was first observed at Ce(IV) concentrations ranging from 0.00 to 0.75 mM (metal:PC ratios from 0 – 21). A maximum at 1.75 mM Ce(IV) was then observed (metal: substrate ratio of

50). Then, phosphate production began to decrease and then leveled off at concentrations 3.25 mM and greater (metal:PC ratios $\geq$ 93). Averaged yields of inorganic phosphate production, determined using inorganic phosphate standards, provided 69 % and 45 % inorganic phosphate for 1.75 mM and 10 mM cerium(IV)-assisted hydrolysis of 35 µM PC, respectively.

A metal to lipid ratio of 5 to 1 provided 17 % phosphate hydrolysis for 2 mM PC reacted for 20 h at 37 °C and ~ pH 4.8.[6] This information and the present Ce(IV) titration (Figure 3.4) led us to the realization that high (above ~ 90) and low (below ~ 20) metal to lipid ratios are not optimal for phosphate ester bond hydrolysis of lipid vesicles of PC. For optimal phosphate ester bond hydrolysis and enhance levels of phosphate production from 35 µM PC by Ce(IV), a metal to lipid ratio around 50 is needed. Multiple explanations for these observations can be offered. The first is that product inhibition may occur at low Ce(IV) to lipid ratios in which levels of phosphate production were less ideal. Thus, phosphate anion ($PO_4^{3-}$) would bind to and reduce the Lewis acidity of the Ce(IV) metal ion, and prevent binding of the metal to the unhydrolyzed substrate. An explanation for reduced phosphate levels as Ce(IV) concentration increases above 3 mM, is due to the formation of less active polymeric clusters of Ce(IV) hydroxo species at higher metal ion concentrations.[3, 5]

### 3.4.3. Mechanism of Ce(IV)-assisted hydrolysis of PC

In a previous study, Ce(IV) enhanced the hydrolysis of the phosphate ester bonds of lipid vesicles of SM and PC at lysosomal pH (~ pH 4.8) vs. cytosolic pH (~ pH 7.2).[6-7] Due to the strong Lewis acidity of Ce(IV), the metal ion has strong electron withdrawing ability toward substrate activation and was by far the most superior non-enzymatic catalyst toward the cleavage of phospholipids and other macromolecules (peptides and nucleic acid) compared to other metal

ions.[6-9, 22] However, Ce(IV) is known to form complicated polynuclear hydroxo clusters in aqueous solutions. For this reason, there have been limited studies on the hydrolytic active species of Ce(IV) toward the hydrolysis of substrates in aqueous solution because of precipitation of this metal ion as Ce(IV) hydroxo clusters at pH values greater than 4.[16] Thus, in acidic homogeneous aqueous solutions of 10 mM Ce(IV), polynuclear species $Ce_2(OH)_3^{5+}$, $Ce_2(OH)_4^{4+}$, and $Ce_6(OH)_{12}^{12+}$ were determined.[5] Toward lower Ce(IV) concentrations (less than 1 mM), $Ce(OH)_2^{2+}$ predominates in the acidic aqueous solutions.[5] Komiyama et al. discovered that one of these polynuclear species, $Ce_2(OH)_4^{4+}$, is the catalytic active species for the hydrolysis of cAMP and a dinucleoside monophosphate in homogeneous solutions of 1 mM Ce(IV) at a pH less than 2.5.[4] However, in the same solution, the mononuclear species $Ce(OH)_2^{2+}$ predominates but is less involved in the hydrolysis reaction.[4] The group proposed that the two Ce(IV) metal ions in the catalytic active species, $Ce_2(OH)_4^{4+}$, are bridged together by two hydroxyls and each metal ion binds to one of the two free oxygen atoms of the phosphorus atom of the substrate.[4] Maldonado and Yatsimirsky proposed the monocationic binuclear $Ce_2(OH)_7^+$ as the catalytic active species for the hydrolysis of BNPP in homogeneous solutions of Ce(IV) (~ 0.1 mM) in imidazole buffer (pH 6 -8).[3]

Previously published NMR and FT-Raman spectra showed that lanthanide metal ions preferentially bind to the free oxygen atoms of the phosphorus atom in the polar head group, phosphocholine, which lies parallel to the surface of PC bilayers.[40-42] Additionally, it has been shown that Ce(IV)-assisted hydrolysis of PC and SM releases more choline than inorganic phosphate at ~ pH 4.8.[6-7] Based on the works of Komiyama, and Maldonado and Yatsimirsky, a binuclear hydroxo complex is thought to be involved in Ce(IV)-assisted phospholipids hydrolysis in this study.
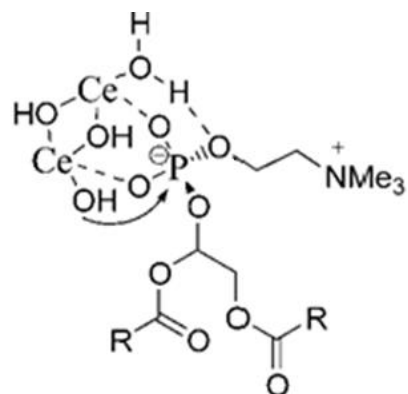
**Figure 3.5.** General mechanism for metal-assisted hydrolysis of a single PC molecule by a binuclear Ce(IV) hydroxo complex.

The general mechanism of the hydrolysis of a single molecule PC by a binuclear Ce(IV) hydroxo species is proposed in Figure 3.5 and was based on the mechanisms of phosphate ester bond hydrolysis of DNA by Ce(IV) and PC-preferring metallo-phosphodiesterases.[4, 43-44] The first step in the enhanced PC hydrolysis entails the cationic binuclear Ce(IV) hydroxo species functioning as a Lewis acid and forming a complex with PC, by the coordination of both Ce(IV) metal ions to one of the free oxygen atoms of the polar head group of the substrate. This step activates the phosphorus atom toward nucleophilic attack. The second step (Figure 3.5) involves the nucleophilic attack of the activated phosphorus center of PC, from an attack by one of the free hydroxyls coordinated to one of the Ce(IV) metal ions. In this step the cationic binuclear Ce(IV) metal center is responsible for electrostatic stabilization of the negatively charged pentacoordinate transition state which collapses to provide two products, choline and phosphatidate. It is possible that, in preparation for nucleophilic attack of the phosphorus center, water bound to Ce(IV) binds to an oxygen atom of the phosphate ester bond toward the choline side, so to assist in the release of choline and act as an acid catalyst. Further hydrolysis of phosphatidate by Ce(IV) would then provide the products, inorganic phosphate and

diacylglycerol. Similar to metallo-hydrolases, the Ce(IV) hydroxo species has a synergistic role in phospholipid hydrolysis which are substrate activation, water activation, and stabilization of the transition state.[44]

### 3.4.4. Acidic phospholipase activity of Ce(IV)-BTP

After the optimization of our reaction conditions and hydrolytic system centered around Ce(IV) metal ion, two mole equivalents of BTP were added to 1.75 mM $Ce(NH_4)_2(NO_3)_6$, reacted with 35 µM PC at 37 °C, and compared to corresponding reactions in the absence of ligand. As stated, a Ce(IV)-based acidic phospholipase mimic should display enhance levels of activity at lysosomal pH (4.8) and reduce levels of cleavage at near-neutral pH (~ 7.2).
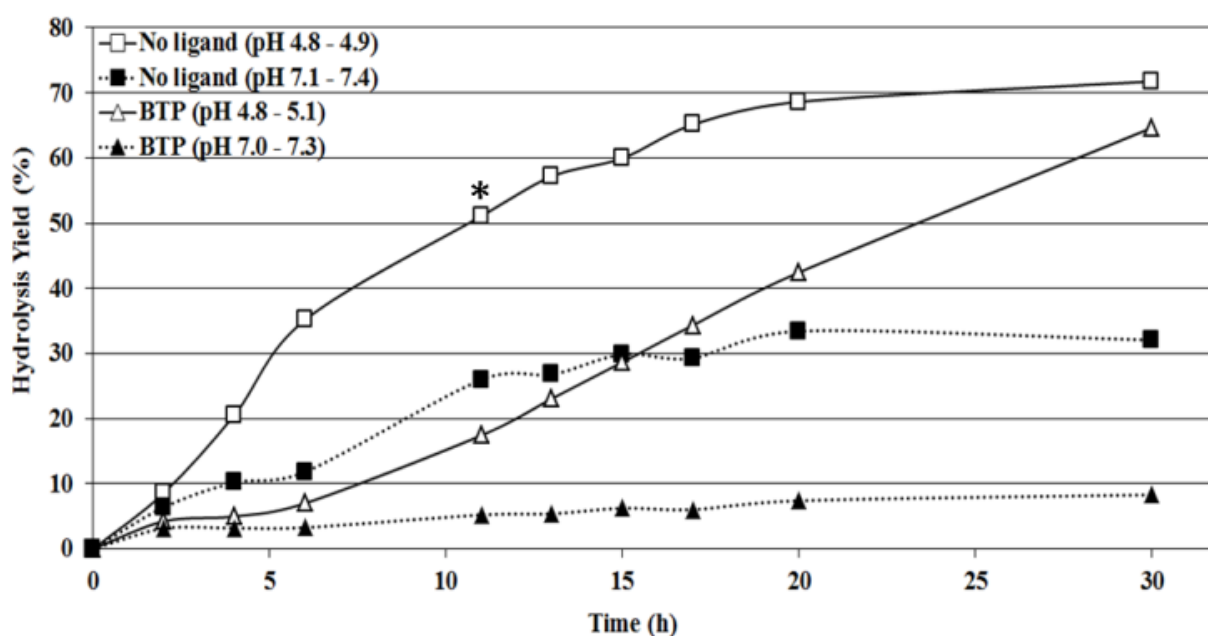


**Figure 3.6.** Averaged hydrolysis yields plotted as a function of time for malachite green detection of free inorganic phosphate. A total of 35 µM PC was reacted at 37 °C in the presence of 1.75 mM $Ce(NH_4)_2(NO_3)_6$ in the absence of ligand at ~ pH 4.8 (—□—) and ~ pH 7.2 (···■···) in 3.5 mM piperazine and HEPES buffer, respectively. The same reaction procedures were followed for 1.75 mM $Ce(NH_4)_2(NO_3)_6$ in the presence of 3.5 mM BTP at ~ pH 4.8 (—△—) (in 1 mM MES buffer) and ~ pH 7.2 (···▲···). For all data points except one (* 7 % error), experimental error is within 5 %. The numbers of trials range from 2 – 8.

The malachite green/molybdate-based colorimetric assay was used to detect and quantitate the yields of free inorganic phosphate release by Ce(IV)-assisted hydrolysis of PC at various reaction times (Figure 3.6). Ce(IV)-mediated hydrolysis at pH ~ 4.8 in the absence of ligand provided 2.3 fold faster phosphate ester bond hydrolysis, and presented an apparent pseudo first-order rate constant of $6.1 \times 10^{-2} \text{ h}^{-1}$ and half-life of 11.4 h (Supporting Information, Figure 3.S15) compared to Ce(IV)-BTP under the same reaction condition. It is important to note, Ce(IV)-BTP-assisted hydrolysis of PC leveled off after reaching an ~ 70 % hydrolysis yield of phosphate product (not shown), similar to the maximal level of hydrolysis by Ce(IV) in the absence of ligand, after the 30 h time point at 37 °C (Figure 3.6). This observation is consistent with cleavage of only the phospholipids distributed on the external leaflet of the PC lipid vesicle since small unilamellar vesicles formed by sonication typically have 68 % of the phospholipid distributed in the external monolayer.[45] The endoliposomal phospholipids are not exposed to the metal ion because of impermeability of Ce(IV) across the lipid bilayer.[27-28] Therefore, the Ce(IV) metal ion and complex are inaccessible to bind and cleave the phosphate ester bonds of the endoliposomal phospholipids.
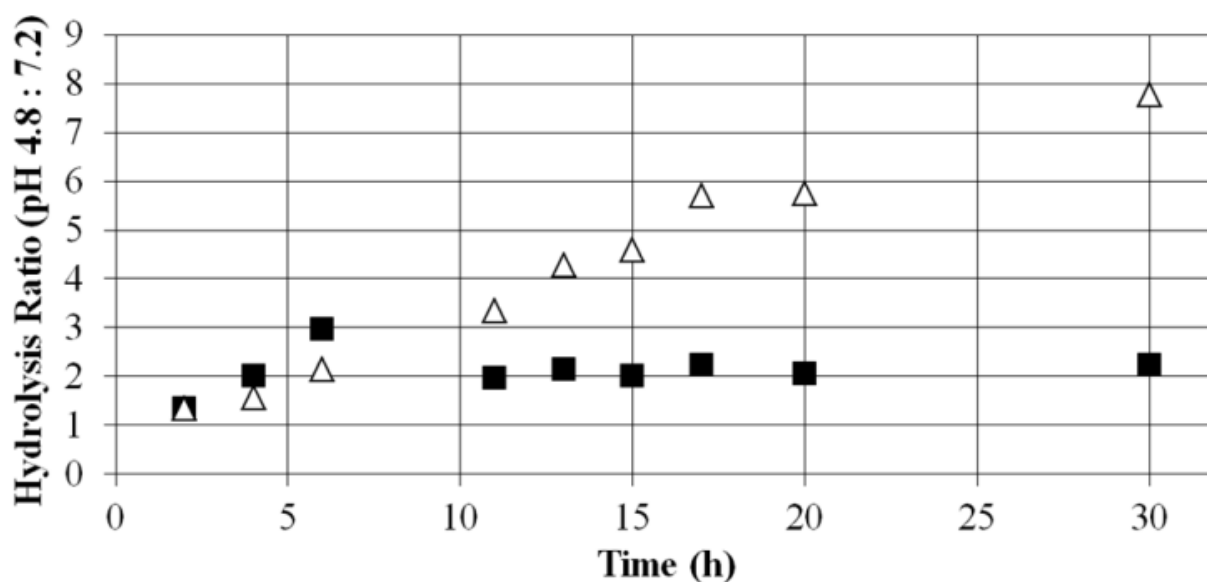
**Figure 3.7**. Ratio of pH ~ 4.8 to pH ~ 7.2 averaged hydrolysis yields from Figure 3.6. A total of 35 µM PC was treated with 1.75 mM $Ce(NH_4)_2(NO_3)_6$ in the absence of ligand (■) and in the presence of 3.5 mM bis-tris propane (BTP) (Δ).

At ~ pH 7.2, the BTP ligand suppressed Ce(IV) hydrolytic activity and prevented hydrolysis yields from reaching above 10 % during the entire 30 h time course. Figure 3.7 shows the ratio of averaged hydrolysis yields throughout the time course. Ce(IV)-BTP provided a linear increase in the ~ pH 4.8 to ~ pH 7.2 ratios, and mediated 7.8 more phosphate ester cleavage at ~ pH 4.8 compared to ~ pH 7.2 after a 30 h reaction at 37 °C. However, the Ce(IV)-mediated hydrolysis in the absence of controlling ligand presented a relatively constant and the average ratio of 2.1 ± 0.4 during the entire time course.

Our two systems, Ce(IV)-mediated hydrolysis with BTP and in the absence ligand, provided greater hydrolysis at mildly acidic pH compared to near-neutral pH. This may arise due to the nature of Ce(IV) hydroxo formation. In aqueous solution, Ce(IV) hydroxo clusters result from rigorous hydrolysis of the metal cation, and the extent of hydrolysis is sensitive to the

concentration of the metal ion and the pH environment.[3, 5] At near-neutral pH, the reduced phosphate ester bond hydrolysis is due to increase metal cation hydrolysis and leads to the formation of less active Ce(IV) hydroxo clusters. These clusters can eventually result in the formation of insoluble $CeO_2$.[3] However, BTP provided no observable precipitation of Ce(IV) (1.75 mM) metal ion at near-neutral pH as seen for Ce(IV) in the absence of ligand. The BTP provided greater pH sensitivity in the PC hydrolysis compared to hydrolysis by Ce(IV) in the absence of ligand. Maldonado and Yatsimirsky determined that the active Ce(IV) hydroxo species in aqueous solution and hydrolytic activity of a presynthesized Ce(IV) and BTP complex ($[Ce(BTP)_2(NO_3)_4]\cdot 2H_2O$) were highly pH dependent.[3] Potentiometric titrations of the pre-synthesized complex indicated that the species $Ce_4(OH)_{15}^+$, $Ce_4(OH)_{14}^{2+}$, and $Ce_4(OH)_{13}^{3+}$ predominate in aqueous solution at pH values greater than ~ 7, between ~ 5 – 7, and less than ~ 5, respectively.[3] Most importantly, hydrolytic activity on the activated synthetic phosphodiester BNPP increased due to the higher charge of the Ce(IV) hydroxo species as a result of decreasing the pH environment from 9 to 5. The extent of substrate activation and the Lewis acidity of the metal ion lessen going from higher to lower positive charge on the Ce(IV) hydroxo species. Thus, the higher charged species binds to the oxygen atoms of phosphate and enhances the electrophilicity of the phosphorous atom of PC more efficiently compared to the lower charged species. The pH sensitivity and pH dependence on the hydrolytic activity of Ce(IV)-BTP could also be correlated to the $pK_a$ values of the donor atoms of BTP. ^{1}H-NMR studies on chemical shift changes as a function pD were performed to confirm this interpretation and to understand complex formation between Ce(IV) and BTP.

^{1}H-NMR spectroscopy studies of Ce(IV)-induced chemical shift changes on BTP as a function of pD were performed. The experiment was done to better understand the pH

sensitivity and dependence provided by the polyamino alcohol ligand BTP to the hydrolytic

activity centered around the Ce(IV) metal ion.  A known complex of the formula

$[Ce(BTP)_2(NO_3)_4] \cdot 2H_2O$ was synthesized according to a published procedure by the addition of

two equivalents of BTP to one equivalent $Ce(NH_4)_2(NO_3)_6$ in an acetonitrile-water mixture.  The

synthesized complex was tested for  hydrolysis of PC at 37 °C for 20 h at mildly acidic pH but

was not explored further because of suppressed hydrolysis (~ 4 fold less) compared to the

Ce(IV)-BTP complex formed *in situ*.  A more resolved NMR spectrum was obtained from the

synthesized complex compared to the *in situ* formed complex.

**Table 3.2.** Ce(IV)-induced chemical shift changes in the methylene protons of bis-tris propane at various pD values

Chemical shift changes ($\delta$complex – $\delta$BTP) in ppm

| $pD^a$ | $CH_2CH_2$ | $NHCH_2$ | $CH_2OH$ | BTP form | $n^b$ |
|---|---|---|---|---|---|
| 2.3 | - 0.003 | - 0.004 | - 0.002 | $BTPH_2^{2+}$ | 2 |
| 5.1-5.2 | - 0.003 | - 0.004 | - 0.003 | $BTPH_2^{2+}$ | 2 |
| 7.6-7.7 | + 0.023 | + 0.018 | + 0.007 | $BTPH^+$ | 2 |
| 9.6 | + 0.035 | + 0.051 | + 0.017 | BTP | 1 |

Complex is a pre-synthesized complex with a recorded formula of $[Ce(BTP)_2(NO_3)_4] \cdot 2H_2O$. NMR spectra are shown in Figure 3.S13 and 3.S14.
$^a$pD = pH + 0.41
$^b$n = number of trials

Table 3.2 shows the chemical shift changes ($\delta_{complex}$ – $\delta_{BTP}$) between the methylene

protons positioned β to nitrogen ($CH_2CH_2$), α to nitrogen ($NH_2CH_2$), and α to alcohol ($CH_2OH$)

of complex and BTP at varied pDs.  The results displayed small upfield shifts of the BTP signals

by Ce(IV) on all methylene protons at pD 2.3 and 5.1 - 5.2. Based on the $pK_a$s of BTP ($pK_{a1}$ of

6.8 and $pK_{a2}$ of 9.1)[1] the doubly protonated form of the ligand $BTPH_2^{2+}$would dominate. At pD

7.6 – 7.7 and 9.6 where $BTPH^+$ and BTP would dominate respectively, larger Ce(IV)-induced

downfield shifts are displayed for all methylene protons. Upon increasing the pD from 7.6 - 7.7

to 9.6, the Ce(IV)-induced downfield shifts of the methylene protons positioned α to nitrogen

($NH_2CH_2$) are increased $\sim$ 3-fold, whereas a $\sim$ 2-fold increase is seen for the protons positioned

α to alcohol ($CH_2OH$). Additionally, there are $\sim$ 2-fold for pD 7.7 and $\sim$ 3-fold for pD 9.6 larger

Ce(IV)-induced downfield shifts for the protons positioned α to nitrogen ($NH_2CH_2$) compared to

protons positioned α to alcohol ($CH_2OH$).

At pD 5.1 – 5.2 and lower, there is no display of complexation between Ce(IV) metal ion

and BTP. The NMR studies show successful and distinctive Ce(IV) coordination when one or

both amines of BTP are neutral. The amines seem to direct Ce(IV) complexation to the –OH

groups of BTP, and there is more Ce(IV) coordination to the neutral form compared to the

monoprotonated ($BTPH^+$) form of the ligand. Evidently, the acidic phospholipase-type activity

of the Ce(IV)-BTP is strongly facilitated by the $pK_a$ values of the donor atoms of BTP and shows

a correlation between mediated hydrolysis of PC and the reaction pH environment. Thus, at

near-neutral pH, BTP is coordinated to Ce(IV) and mediated hydrolysis of PC is suppressed. At

mildly acidic pH, BTP is likely to be weakly associated with Ce(IV) and mediated hydrolysis of

PC is more efficient. Even though NMR studies suggest that there is no Ce(IV) metal ion

coordination to BTP in the synthesized complex at mildly acidic pH, our time course studies

(Figure 3.6) of metal-assisted hydrolysis of PC by the *in situ* formed complex suggest otherwise.

The relatively slower phosphate ester bond hydrolysis by Ce(IV)-BTP compared to Ce(IV) metal

ion in the absence of ligand at mildly acidic pH advocates that the Ce(IV) metal ion is interacting

with BTP. However, the influence of BTP on the activity of Ce(IV) metal ion is more potent at near-neutral pH compared to mildly acidic pH because of the available nitrogen atom lone pair at the higher pH value.
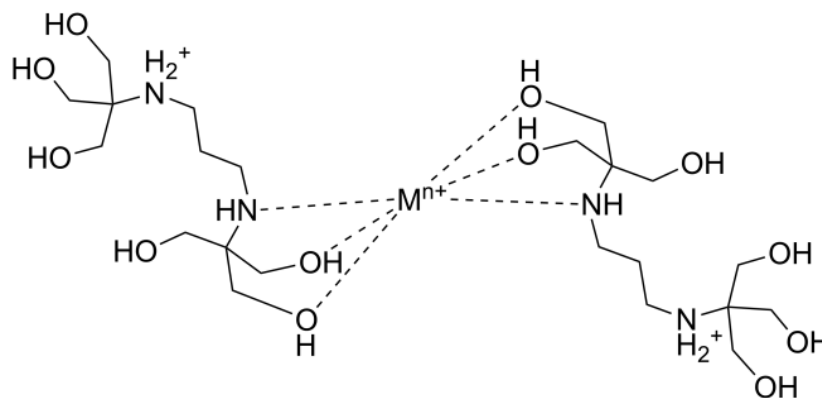


**Figure 3.8.** Proposed structure of 1:2 Ce(IV) to BTP complex at near-neutral pH. $M^{n+}$ = cationic polynuclear Ce(IV) hydroxo species.

A crystal structure illustrated the tris moiety of the ligand bis-tris coordinated to lanthanum(III) ion (2:1 ligand to metal ratio) by two oxygen and one nitrogen atoms, and with one free oxygen atom remaining.[46] Thus, it is reasonable to speculate that there is one deprotonated amine from each ligand bound to the Ce(IV) metal ion, and each ligand provides a tridentate complex (N atom and two OH groups from the tris moiety) and five-membered chelate rings formed between the amine and the metal ion (Figure 3.8).[46-47] In addition, $^1$H-NMR of [Ce(BTP)$_2$(NO$_3$)$_4$]·2H$_2$O in DMSO-d$_6$ (Supporting Information, Figure 3.S16) showed three protons (broad peak with a chemical shift of 8.26) associated with the two secondary amines of BTP. Ce(IV) is a chemically labile metal. The chemical shifts of BTP in the presence of Ce(IV) represent averaged values of the free and bound nitrogen and oxygen donor atoms in the NMR spectrum (Figure 3.S16). When BTP ligand was added to the NMR sample, new peaks corresponding to free BTP did not emerge in the new spectrum (not shown).

### 3.4.5. PC vs. SM hydrolysis by Ce(IV)
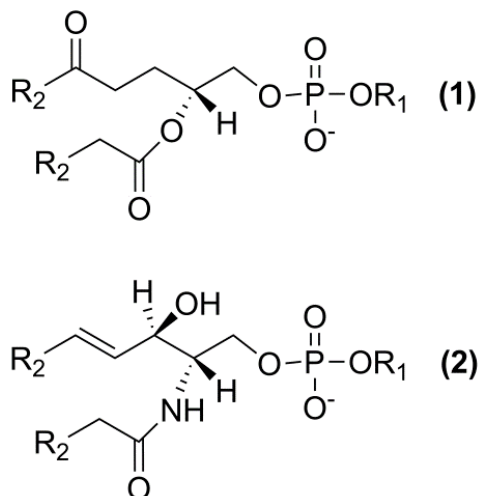


**Figure 3.9.** Phospholipids, phosphatidylcholine (**1**) and sphingomyelin (**2**). **R₁** represents the choline head group and **R₂** represents long chain fatty acid hydrocarbons of variable lengths.

In the membrane bilayer of eukaryotic cells populates 50 % of two phospholipids, PC and the sphingolipid sphingomyelin (SM).[32] PC and SM (Figure 3.9) contain the same phosphocholine polar head group, but different backbones. Significant structural and dynamic properties arise due to the distinct backbones between these two major lipids. These differences were explored in a previous study focusing on Ce(IV)-assisted hydrolysis of the phosphate ester bonds of SM and PC.[6] The results showed relatively low hydrolysis yields of $5 \pm 1$ % and $1 \pm 0.5$ % of inorganic phosphate from 2 mM SM by 10 mM of Ce(IV) at ~ pH 4.8 and ~ pH 7.2, respectively. The phosphate yield at pH 4.8 was 3.4 fold less compared to the yields of PC under the same conditions.[6] In the present study, phosphate ester bond hydrolysis of PC by Ce(IV) was optimized; thus, a comparison study of the Ce(IV) hydrolytic system on SM was examined further. Thus, two mole equivalents of BTP were added to 1.75 mM $Ce(NH_4)_2(NO_3)_6$ and reacted with 35 µM SM at 37 °C and compared to the corresponding reaction in the absence of ligand. The malachite green/molybdate-based colorimetric assay was used to detect and

quantitate the average amounts of free phosphate released by Ce(IV)-assisted hydrolysis of SM

after 20 h and 40 h reaction times.

Inorganic phosphate production from 35 µM SM, 37 °C
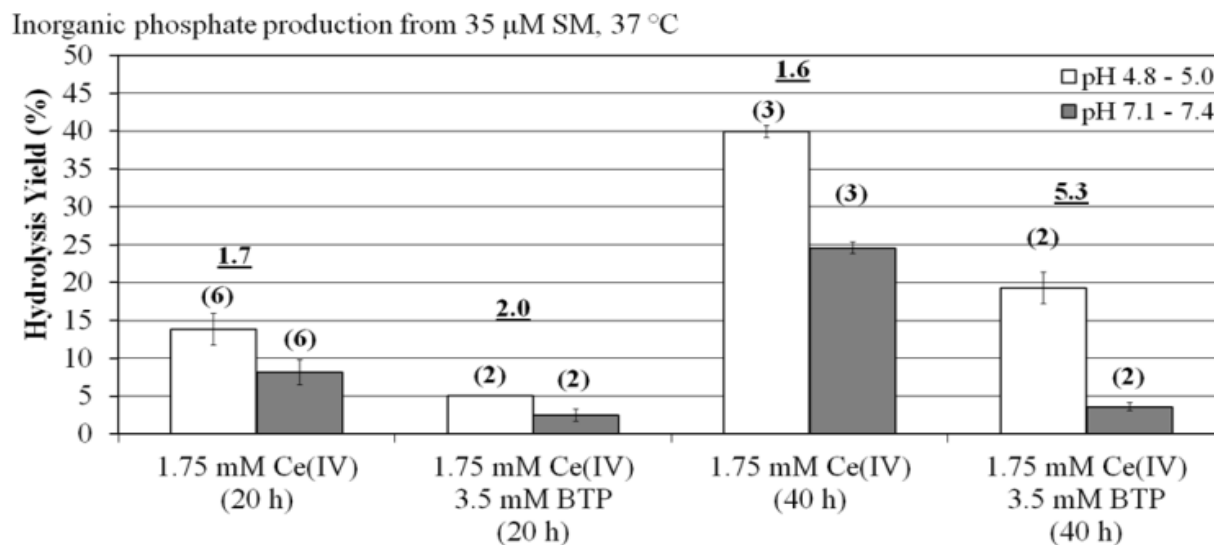


**Figure 3.10.** Averaged hydrolysis yields of SM plotted as a function of pH for malachite green detection of free inorganic phosphate. A total of 35 µM SM was reacted at 37 °C for 20 h or 40 h in the presence of 1.75 mM Ce(NH$_4$)$_2$(NO$_3$)$_6$ at ~ pH 4.8 and ~ pH 7.2 in 3.5 mM piperazine and HEPES buffer, respectively. The same reaction procedures were followed for 1.75 mM Ce(NH$_4$)$_2$(NO$_3$)$_6$ in the presence of 3.5 mM bis-tris propane at ~ pH 4.8 (in 1 mM MES buffer) and ~ pH 7.2. The number of trials **(n)** appears in parenthesis. Error bars represent standard deviation. **n** = pH 4.8 to pH 7.2 hydrolysis yield ratios.

Ce(IV)-assisted hydrolysis in the absence of ligand produced 14 ± 2 % at ~ pH 4.8 and 8

± 2 % at ~ pH 7.2 phosphate (pH 4.8 to pH 7.2 hydrolysis ratio of 1.7) from SM after 20 h at 37

°C (Figure 3.10). Whereas, Ce(IV)-BTP mediated ~ 3 fold less phosphate ester bond hydrolysis

at both pH values and provided a pH 4.8 to pH 7.2 hydrolysis ratio of 2.0 compared to the former

under the same reaction conditions. Similar to previous studies, hydrolysis of PC by Ce(IV)

yielded significantly more phosphate compared to corresponding SM reactions.[6] An example is

the ~ 5 fold reduction of phosphate production from SM compared to PC, which presented 69 %

phosphate after 20 h at 37 °C and pH 4.8, by Ce(IV) in the absence of ligand. Hydrolysis yields

of SM increased considerably by doubling the reaction time to 40 h (Figure 3.10), however,

yields are still lower compared to PC hydrolysis at the 20 h reaction time (Figure 3.6). The pH sensitivity of Ce(IV)-assisted hydrolysis in the presence of BTP is more robust at the 40 h compared to the 20 h reaction time, and the pH 4.8 to pH 7.2 hydrolysis ratio of 5.6 is comparable to the 5.7 ratio in PC hydrolysis for 20 h (Figure 3.7).

Significant structural and dynamic properties arise due to the distinct backbones between PC and SM. These differences result in lipid vesicles of PC displaying higher susceptibility toward Ce(IV)-assisted hydrolysis compared to lipid vesicles of SM. PC and SM contain different backbones, glycerol and sphingosine, respectively. The interfacial region of SM consists of an amide linkage and a free hydroxyl atom that participate in extensive networks of intra- and intermolecular hydrogen bonds.[48] In contrast, PC bilayers have a less extensive hydrogen bonding network. The two ester carbonyls in the interfacial region of PC only act as hydrogen bond acceptors toward water molecules.[32, 48] An explanation to why Ce(IV)-assisted hydrolysis of lipid vesicles of SM is less compared to lipid vesicles of PC can be explained by the reduced fluidity and suppressed lateral diffusion rates afforded by the extensive hydrogen bond network of SM molecules. This reduces the probability of an interaction between Ce(IV) metal ion and the phosphate oxygens in lipid vesicles comprised of SM.[6, 32]

### 3.4.6. The study of a bis-tris propane derivative, an attempt to improve PC hydrolysis at lysosomal pH by a dicerium complex

In an earlier experiment, the acidic hydrolytic agent, an 1:2 Ce(IV) to BTP complex, mediated enhance levels of Ce(IV)-assisted hydrolysis (42 % inorganic phosphate production after 20 h at 37 °C) at lysosomal pH (~ 4.8) and suppressed levels of hydrolysis (7 % inorganic phosphate production after 20 h at 37 °C) at near-neutral pH (~ 7.2) (Figure 3.6). This is a

significant improvement compared to Ce(IV) metal ion in the absence of ligand that presented a

lower pH 4.8 to pH 7.2 hydrolysis yield ratio of 2 and a higher hydrolysis yield of 33 % at pH

7.2. Even though superior hydrolysis ratios were obtained, BTP reduced Ce(IV)-assisted

phosphate ester bond hydrolysis of PC from 69 % to 42 % and provided a 2 fold slower

hydrolysis rate compared to hydrolysis by the metal ion in the absence of ligand after 20 h at pH

4.8 and 37 °C. Thus, to optimize phosphate ester bond cleavage by Ce(IV) complexes at pH 4.8,

we attempted to enhance substrate activation by synthesizing a BTP derivative capable of

forming bimetallic complexes with the metal ion. Our aim was to create an acidic hydrolytic

agent that displays higher levels of activity at lysosomal pH (4.8), while still displaying reduced

levels of cleavage at near-neutral pH (~ 7.2).
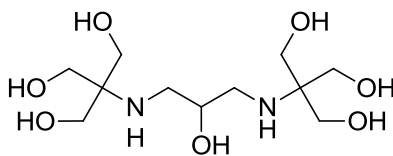


**7**

**Figure 3.11.** The structure of 1,3-bis-[tris-(hydroxymethyl)-methyl-amino]-2-propanol (BTP-OH) (**7**).

The BTP derivative the dihydrochloride salt of 1,3-bis-[tris-(hydroxymethyl)-methyl-

amino]-2-propanol (BTP-OH, **7**, Figure 3.11) contains an extra hydroxyl group located on the

central methylene atom. The new ligand was synthesized by a previously published procedure,[37]

via the addition of two equivalents of tris(hydroxymethyl)-aminomethane (tris) to one equivalent

of epichlorohydrin. This amino alcohol ligand was selected because of the observation of

double-stranded hydrolysis of plasmid DNA by a binuclear 2:1 metal to ligand complex between

Ce(IV) and HPTA (**5**, Figure 3.2) compared to only single-stranded DNA hydrolysis by an

analogous mononuclear complex (1:1 Ce(IV) to EDTA; **6**, Figure 3.2).[9-10] The investigators that

conducted this work suggested that the formation of a binuclear metal center enhanced the Lewis acidity of the hydrolytic agent which provided stronger substrate activation.[9-10]

Thus, with the goal of developing a more effective acidic hydrolytic agent based on a binuclear Ce(IV) metal center, one mol equivalent of BTP-OH was added to two equivalents of Ce(IV) (1.75 mM) in aqueous solution. Reaction with 35 µM PC at core body temperature (37 °C) for 20 h was monitored and quantitated by a malachite green/molybdate-based colorimetric assay to detect inorganic phosphate at 620 nm. The homogeneous reaction mixtures produced 8 ± 0.7 % and 2 ± 0.5 % (averaged of three trials) yields of inorganic phosphate at ~ pH 4.8 and ~ pH 7.2, respectively. Even though this ligand mediated a pH 4.8 to pH 7.2 phosphate production ratio of 4, BTP-OH considerably suppressed Ce(IV)-assisted hydrolysis (~ 4 – 5 fold less) compared to the former Ce(IV)-BTP complex at both pH values.

Previous results demonstrated that the pH dependency of lipid hydrolysis by the Ce(IV)-BTP complex was strongly facilitated by the $pK_a$ values of the donor atoms of the ligand. At mildly acidic pH, the doubly protonated form of BTP dominates in aqueous solution and the Lewis acidity of Ce(IV) is less influenced by the ligand. However, at near-neutral pH the monoprotonated form dominates, Ce(IV) is bound more tightly to the ligand, and Lewis acidity is reduced. BTP provided enhance levels of Ce(IV)-assisted PC hydrolysis ( 42 % inorganic phosphate after 20 h and 65 % hydrolysis after 30 h) at lysosomal pH (~ 4.8). This was possible because the ligand has a low effect on the electrophilicity of the metal ion at mildly acidic pH. More importantly, BTP provided pH 4.8 to 7.2 hydrolysis ratios of ~ 6 and ~ 8 after 20 h and 30 h reactions at 37 °C (Figure 3.6). In comparison to BTP, the BTP-OH provided a lower pH 4.8 to 7.2 hydrolysis ratio of ~ 4 and hydrolysis yield of 8 % at pH 4.8 after 20 h at 37 °C.

To better understand the effects of the extra hydroxyl group on the ligand (BTP-OH), a pH titration (Supporting Information, Figure 3.S20) was performed which presented $pK_{a1}$ of 6.3 $\pm$ 0.06 and $pK_{a2}$ of 8.1 $\pm$ 0.00. The pH titration demonstrated BTP-OH as a more acidic ligand compared to BTP ($pK_{a1}$ of 6.8 and $pK_{a2}$ of 9.1).[3] Our earlier experiment (Figure 3.3) indicated that more acidic ligands, especially polycarboxylate ligands, tend to suppress the hydrolytic activity of Ce(IV) in lipid hydrolysis. The more acidic ligand, BTP-OH, is capable of forming a stronger complex with Ce(IV) at mildly acidic conditions compared to BTP which displayed relatively no, or weak, coordination to the metal ion at ~ pH 4.8 (Table 3.2). Additionally, introduction of the hydroxyl group may enable the ligand to form additional five-membered chelate rings which would increase the binding constant of the ligand for Ce(IV). The close interaction with the metal ion could reduce the $pK_a$ values of the BTP-OH amino groups. There is further suppression of PC hydrolysis by Ce(IV) when the pH is increased to ~ 7.2 in the presence of BTP-OH. Thus, it may be reasonable to speculate that two ligand species exist in aqueous solution, the monoprotonated and unprotonated forms of BTP-OH at ~ pH 4.8 and ~ pH 7.2, respectively.

### 3.4.7. Optimization of the acidic hydrolytic agent by increasing the Ce(IV) to BTP ratio
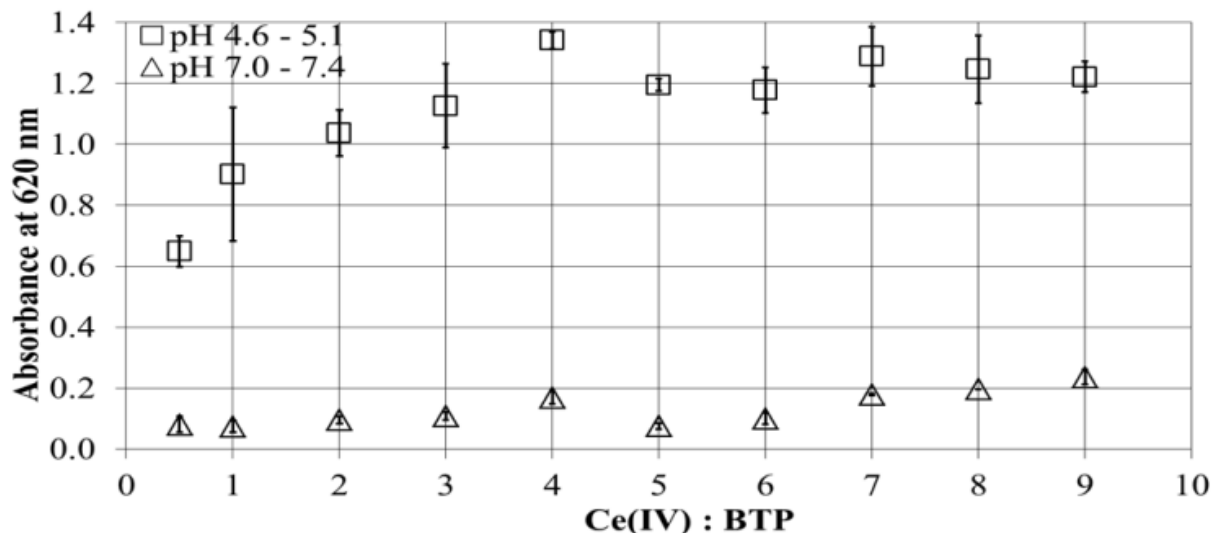


**Figure 3.12.** Absorbance at 620 nm plotted as a function of Ce(IV) to BTP ratios (Ce(IV):BTP) for malachite green-treated hydrolysis reactions containing PC. A total of 35 µM of PC was reacted at 37 °C for 20 h in the presence of 1.75 mM $Ce(NH_4)_2(NO_3)_6$ and $0.19 - 3.5$ mM BTP at pH ~ 4.8 (1 mM piperazine buffer) or pH ~ 7.2 (1 mM HEPES). Three or more trials were performed for each reaction. Error bars represent standard deviation.

To further enhance phosphate ester bond hydrolysis by Ce(IV) at core body temperature (37 °C), phosphate ester bond hydrolysis of PC was followed as a function of Ce(IV) to BTP ratio (0.5 – 9). In this experiment, a total of 35 µM of PC was reacted at ~ pH 4.8 and ~ pH 7.2 for 20 h in the presence of 1.75 mM Ce(IV) and varied concentrations of BTP (0.19 mM – 3.5 mM) (Figure 3.12). The release of phosphate was followed spectrophotometrically at 620 nm with the malachite green/molybdate-based colorimetric assay. A slight linear progression (slope of 0.172 and $R^2$ of 0.935) of phosphate production was first observed as a function of Ce(IV) to BTP ratios of 0.5 – 4.0 at ~ pH 4.8 (Figure 3.12). There was a slight maximum at Ce(IV) to BTP ratio of 4, and thereafter, phosphate production leveled off for the ~ pH 4.8 reactions. At ~ pH 7.2, phosphate production remained relatively constant at Ce(IV) to BTP ratios between 0.5 – 4.0, and thereafter, a linear increase of phosphate production with a slope of 0.042 ($R^2$ of 0.960)

was observed. Ce(IV) to BTP ratios of 4 and 5 were studied further due to the highest enhanced hydrolysis of PC at ~ pH 4.8 and highest pH 4.8 to pH 7.2 phosphate production ratio, respectively.

Averaged yields of inorganic phosphate production, determined using linear titration curves and standards of inorganic phosphate (Supporting Information, Figures 3.S6 and 3.S7), provided a 54.2 ± 0.9 % inorganic phosphate yield for the 5:1 Ce(IV) to BTP ratio and a 66.7 ± 1.3 % inorganic phosphate yield for the 4:1 Ce(IV) to BTP ratio at ~ pH 4.8 (37 °C and 20h). Additionally, the 5:1 and 4:1 Ce(IV) to BTP ratios displayed 9.6 (5.7 ± 1.1 % phosphate at pH 7.2) and 5.7 (11.6 ± 1.3 % phosphate at pH 7.2)  pH 4.8 to pH 7.2 phosphate production ratios, respectively. This is a great improvement compared to the 1:2 Ce(IV)-BTP complex and Ce(IV) in the absence of ligand, which provided  42 % (pH 4.8 to pH 7.2 ratio of 5.7) and 69 % (pH 4.8 to pH 7.2 ratio of 2.1) inorganic phosphate yield  under  the same reaction conditions at ~ pH 4.8, respectively.

In summary, this experiment showed a correlation between suppressed hydrolytic activity by Ce(IV) and higher ligand concentration at ~ pH 4.8.  The utilization of less BTP was advantageous and provided more phosphate ester bond hydrolysis at pH 4.8 (67 % by 4:1 Ce(IV) to BTP) and a higher pH 4.8 to pH 7.2 hydrolysis ratio (9.6 by 5:1 Ce(IV) to BTP) compared to 1:2 Ce(IV) to BTP ratio.  Additionally, the 4:1 Ce(IV) to BTP hydrolysis yield of  67 % is almost equivalent to Ce(IV)-assisted hydrolysis in the absence of ligand which produced 69 % inorganic phosphate after a 20 h reaction at ~ pH 4.8 (Figure 3.6).  Suppressed hydrolytic activity of Ce(IV) at pH 7.2 is still manifested at the higher Ce(IV) to BTP ratios.  Thus, the utilization of less BTP improved phosphate ester bond hydrolysis considerably at mildly acidic conditions, and

most importantly, was still capable of mediating acidic phospholipase-type activity by reducing Ce(IV) hydrolysis when pH was increased to near-neutral levels.

## 3.5. Conclusions

Our research began with the search for a potential small molecule, Ce(IV)-acidic phospholipase mimic, which displayed enhance levels of hydrolytic activity at lysosomal pH (~ 4.8) and reduce levels of cleavage at near-neutral pH (~ 7.2). Thereafter, our goal was to optimized our Ce(IV) hydrolytic system based on BTP. We found that inorganic phosphate production from liposomes of naturally occurring phospholipids (35 µM) was increased considerably by lowering the concentration of Ce(IV) from 10 mM to 1.75 mM and by increasing the Ce(IV) to BTP ratios.

Inorganic phosphate production, 37 °C, 20 h, ~ pH 4.8



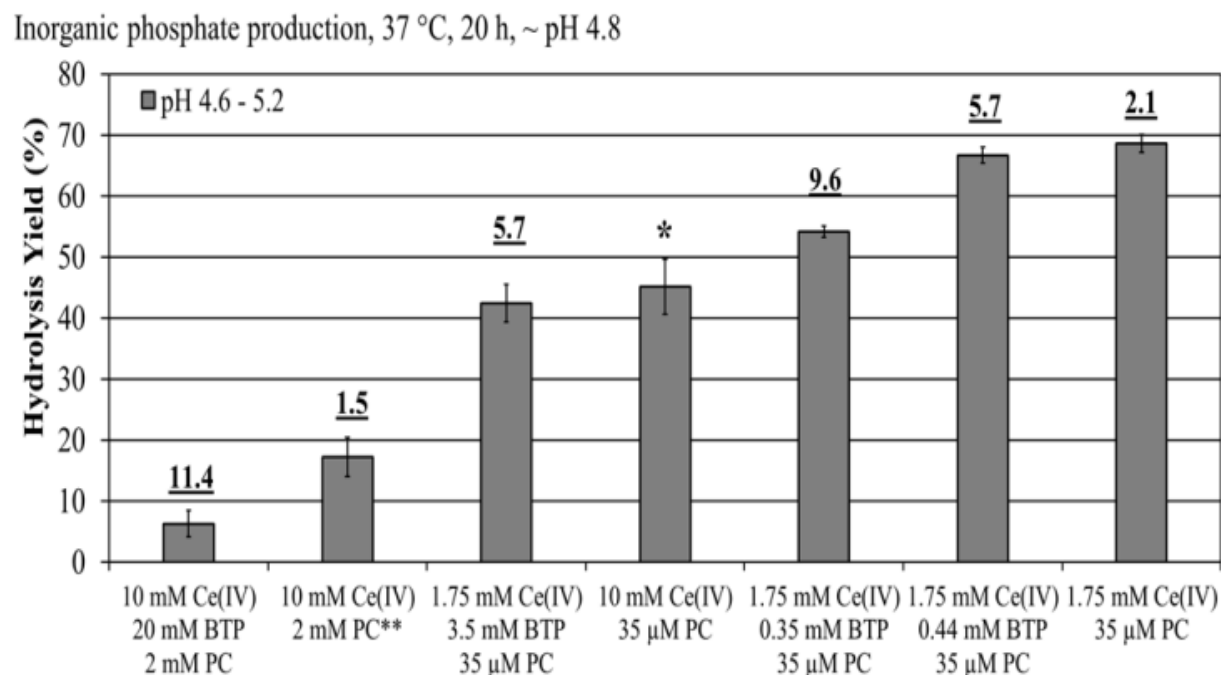**Figure 3.13.** A summary of averaged hydrolysis yields of inorganic phosphate from PC (2 mM or 35 µM) plotted as Ce(IV) metal ion or complex concentrations at ~ pH 4.8 and 20 h. **n** = averaged pH 4.8 to pH 7.2 phosphate hydrolysis yield ratios. * No inorganic phosphate hydrolysis yield at ~ pH 7.2 was determined. ** Data from ref. 6. Three or more trials were performed for each set of hydrolysis reactions.

Figure 3.13 shows combined data for PC hydrolysis by Ce(IV) at reaction ~ pH 4.8 and a time of 20 h.  An amplification of the PC hydrolysis by Ce(IV) was observed at lower metal concentrations (hydrolysis of 35 μM phospholipid by 1.75 mM Ce(IV)) compared to higher concentrations (hydrolysis of 35 μM phospholipid by 10 mM Ce(IV)). We attributed the reduced product yields to the formation of less reactive metal hydroxo clusters at the higher Ce(IV) concentrations.  Phosphate ester bond hydrolysis was also optimized by increasing the catalyst-to-substrate ratios from 5 to 50.

Polycarboxylate ligands coordinated to Ce(IV) were shown to be great mediators for nucleic acid hydrolysis.[9-10, 12]  Conversely, these strong coordinating, and acidic ligands were detrimental to Ce(IV)-assisted phospholipid hydrolysis.  Ce(IV)-BTP as an effective Ce(IV)-based acidic hydrolytic agent was demonstrated.  The amino alcohol ligand provided enhance levels of Ce(IV)-assisted PC hydrolysis ( 42 %, 54 %, and 67 % inorganic phosphate at 1:2, 5:1, and 4:1 Ce(IV):BTP ratios) at lysosomal pH (~ 4.8) and 20h at 37 °C (Figure 3.13).  This was possible because the ligand does not reduce the electrophilicity of the metal ion at lysosomal pH.  In addition, for an adequate Ce(IV) acidic phospholipase mimic, the activity should switch from on to off when going from a lysosomal pH ( ~ 4.8) to cytoplasm pH (~ 7.2) environments.  Remarkably, BTP was able to significantly reduce phosphate production from PC by interacting with Ce(IV) after increasing the pH from ~ 4.8 to ~ 7.2.  This effect arises due to the $pK_a$ values of the donor atoms of BTP.  Also, the pH increase should give rise to less active Ce(IV)-hydroxo species of lower net charge at ~ pH 7.2 compared to the more active and highly charged species formed under  mildly acidic conditions.[3]  As a result, BTP (5:1 Ce(IV) to BTP) increased the  ~ pH 4.8 to 7.2  phosphate ester bond hydrolysis ratio from 2.1 to 9.6 compared to the same concentration of Ce(IV) in the absence of ligand.  The former occurs by BTP reducing Ce(IV)

metal ion hydrolytic activity to mediate only 6 % phosphate ester bond hydrolysis at ~ pH 7.2 after 20 h at 37 °C. Overall, our research has shown that the hydrolytic activity and speciation of Ce(IV) metal ion can be controlled and tuned as a function of pH by the application of the ligand BTP to the metal catalytic center. Natural hydrolases commonly have two or more metals ions in their active site, and acidic hydrolases located in the lysosome have optimal activity at lysosomal pH and relatively no activity at cytoplasm pH. Therefore, our acidic hydrolytic agent, Ce(IV) complexes based on BTP provided our group a great foundation in our search for a synthetic, small molecule, metal-based acidic phospholipase mimic.

## 3.6. References

(1) Bonomi, R.; Scrimin, P.; Mancin, F., Phosphate diesters cleavage mediated by Ce(IV) complexes self-assembled on gold nanoparticles. *Org Biomol Chem* **2010,** *8*, 2622-2626.

(2) Grant, K. B.; Kassai, M., Major advances in the hydrolysis of peptides and proteins by metal ions and complexes. *Curr Org Chem* **2006,** *10*, 1035-1049.

(3) Maldonado, A. L.; Yatsimirsky, A. K., Kinetics of phosphodiester cleavage by differently generated cerium(IV) hydroxo species in neutral solutions. *Org Biomol Chem* **2005,** *3*, 2859-2867.

(4) Komiyama, M.; Takeda, N.; Shigekawa, H., Hydrolysis of DNA and RNA by lanthanide ions: mechanistic studies leading to new applications. *Chem Commun* **1999**, 1443-1451.

(5) Baes, F. C.; Mesmer, R. E., *The Hydrolysis of Cations*. John Wiley & Sons, Inc.: New York, 1976; p 129-145.

(6) Cepeda, S. S.; Williams, D. E.; Grant, K. B., Evaluating metal ion salts as acid hydrolase mimics: metal-assisted hydrolysis of phospholipids at lysosomal pH. *Biometals* **2012,** *25*, 1207-1219.

(7)  Kassai, M.; Teopipithaporn, R.; Grant, K. B., Hydrolysis of phosphatidylcholine by cerium(IV) releases significant amounts of choline and inorganic phosphate at lysosomal pH. *J Inorg Biochem* **2011,** *105*, 215-223.

(8)  Takarada, T.; Yashiro, M.; Komiyama, M., Catalytic hydrolysis of peptides by cerium(IV). *Chem-Eur J* **2000,** *6*, 3906-3913.

(9)  Branum, M. E.; Que, L., Double-strand DNA hydrolysis by dilanthanide complexes. *J Biol Inorg Chem* **1999,** *4*, 593-600.

(10)  Branum, M. E.; Tipton, A. K.; Zhu, S. R.; Que, L., Double-strand hydrolysis of plasmid DNA by dicerium complexes at 37 °C. *J Am Chem Soc* **2001,** *123*, 1898-1904.

(11)  Katada, H.; Seino, H.; Mizobe, Y.; Sumaoka, J.; Komiyama, M., Crystal structure of Ce(IV)/dipicolinate complex as catalyst for DNA hydrolysis. *J Biol Inorg Chem* **2008,** *13*, 249-255.

(12)  Kitamura, Y.; Komiyama, M., Preferential hydrolysis of gap and bulge sites in DNA by Ce(IV)/EDTA complex. *Nucleic Acids Res* **2002,** *30*.

(13)  Sirish, M.; Franklin, S. J., Hydrolytically active Eu(III) and Ce(IV) EF-hand peptides. *J Inorg Biochem* **2002,** *91*, 253-258.

(14)  Cullis, P. M.; Snip, E., Stereochemical course of cerium(IV)-catalyzed hydrolysis of cyclic nucleotides. *J Am Chem Soc* **1999,** *121*, 6125-6130.

(15)  Sumaoka, J.; Miyama, S.; Komiyama, M., Enormous Acceleration by Cerium(Iv) for the Hydrolysis of Nucleoside 3',5'-Cyclic Monophosphates at Ph 7. *J Chem Soc Chem Comm* **1994**, 1755-1756.

(16) Bracken, K.; Moss, R. A.; Ragunathan, K. G., Remarkably rapid cleavage of a model phosphodiester by complexed ceric ions in aqueous micellar solutions. *J Am Chem Soc* **1997,** *119*, 9323-9324.

(17) Matsumiya, H.; Nakamura, H.; Hiraide, M., Phosphoester hydrolysis by cerium(IV)-thiacalix[4]arene complexes and its application to immunoassay. *Anal Bioanal Chem* **2009,** *394*, 1471-1476.

(18) Moss, R. A.; Morales-Rojas, H., Loci of ceric cation mediated hydrolyses of dimethyl phosphate and methyl methylphosphonate. *Org Lett* **1999,** *1*, 1791-1793.

(19) Yan, J. M.; Atsumi, M.; Yuan, D. Q.; Fujita, K., (Ethylenediaminetetraacetic acid)cerium(IV) [Ce-IV(EDTA)] complexes with dual hydrophobic binding sites as highly efficient catalysts for the hydrolysis of phosphodiesters. *Helv Chim Acta* **2002,** *85*, 1496-1504.

(20) Zhao, M.; Zhao, C.; Jiang, X. Q.; Ji, L. N.; Mao, Z. W., Rapid hydrolysis of phosphate ester promoted by Ce(IV) conjugating with a beta-cyclodextrin monomer and dimer. *Dalton T* **2012,** *41*, 4469-4476.

(21) Moss, R. A.; Morales-Rojas, H.; Vijayaraghavan, S.; Tian, J. Z., Metal-cation-mediated hydrolysis of phosphonoformate diesters: Chemoselectivity and catalysis. *J Am Chem Soc* **2004,** *126*, 10923-10936.

(22) Zhu, B.; Xue, D. P.; Wang, K., Lanthanide ions promote the hydrolysis of 2,3-bisphosphoglycerate. *Biometals* **2004,** *17*, 423-433.

(23) Burgess, M., *Metal Ions in Solution*. John Wiley & Sons: New York, 1978.

(24) Kajimura, A.; Sumaoka, J.; Komiyama, M., DNA hydrolysis by cerium(IV)-saccharide complexes. *Carbohyd Res* **1998,** *309*, 345-351.
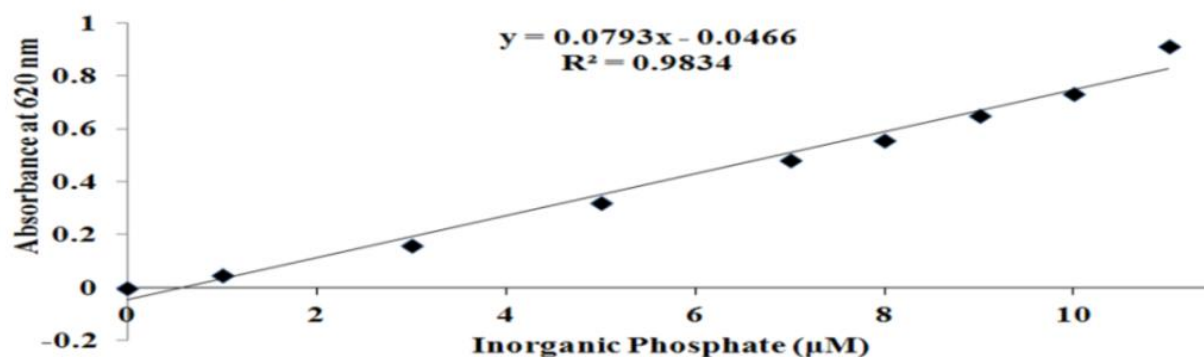
(25)  Matsumura, K.; Komiyama, M., Hydrolysis of Phosphatidylinositol by Rare-Earth-Metal Ion as a Phospholipase-C Mimic. *J Inorg Biochem* **1994,** *55*, 153-156.

(26)  Liu, H. X.; Hu, J.; Liu, X. T.; Li, R. C.; Wang, K., Effects of lanthanide ions on hydrolysis of phosphatidylinositol in human erythrocyte membranes. *Chinese Sci Bull* **2001,** *46*, 401-403.

(27)  Scrimin, P.; Caruso, S.; Paggiarin, N.; Tecilla, P., Ln(III)-catalyzed cleavage of phosphate-functionalized synthetic lipids: Real time monitoring of vesicle decapsulation. *Langmuir* **2000,** *16*, 203-209.

(28)  Moss, R. A.; Park, B. D.; Scrimin, P.; Ghirlanda, G., Lanthanide Cleavage of Phosphodiester Liposomes. *J Chem Soc Chem Comm* **1995**, 1627-1628.

(29)  Stryer, L., *Biochemistry*. fourth ed.; W. H. Freeman and Company: New York, 1995; p 344 - 691.

(30)  Dennis, A. E. R., G. S.; Billah, M. M.; Hannun, A. Y., Role of phospholipases in generating lipid messengers in signal transduction. *FASEB J* **1991,** *5*, 2068-2077.

(31)  Hannun, A. Y. B., M. R., Functions of sphingolipids and sphingolipid breakdown products in cellular regulation. *Science* **1989,** *243*, 500-507.

(32)  Niemela, P.; Hyvonen, M. T.; Vattulainen, I., Structure and dynamics of sphingomyelin bilayer: Insight gained through systematic comparison to phosphatidylcholine. *Biophys J* **2004,** *87*, 2976-2989.

(33)  Bar, L. K.; Barenholz, Y.; Thompson, T. E., Effect of sphingomyelin composition on the phase structure of phosphatidylcholine-sphingomyelin bilayers. *Biochem* **1997,** *36*, 2507-2516.

(34)  Marsh, D., *Handbook of Lipid Bilayers*. 2nd ed.; CRC Press: Boca Raton, 2013; p 548 - 549.

(35) Cogan, E. B.; Birrell, G. B.; Griffith, O. H., A Robotics-Based Automated Assay for Inorganic and Organic Phosphates. *Anal Biochem* **1999,** *271*, 29-35.

(36) He, X.; Chen, F.; McGovern, M. M.; Schuchman, E. H., A fluorescence-based, high-throughput sphingomyelin assay for the analysis of Niemann-Pick disease and other disorders of sphingomyelin metabolism. *Anal Biochem* **2002,** *306*, 115-123.

(37) Pierce, J. S.; Lunsford, C. D., Tris(hydroxymethyl)-aminomethane derivatives. IV. Substituted 4-(hydroxymethyl)oxazolidines; ester and amide interchange. *J. Am. Chem. Soc.* **1951,** *73*, 2596-8.

(38) *Handbook of Biochemistry and Molecular Biology*. 4th ed.; CRC Press: Boca Raton, 2010.

(39) Powell, J. E.; Ling, D. R.; Tse, P. K., Complexes of rare-earth elements with 1,3-diamino-2-hydroxypropane-N,N,N',N'-tetraacetic acid. *Inorg Chem* **1986,** *25*, 585-6.

(40) Hauser, H.; Phillips, M. C.; Levine, B. A.; Williams, R. J. P., Ion binding to phospholipids. Interaction of calcium and lanthanide ions with phosphatidylcholine (lecithin). *Eur J Biochem* **1975,** *58*, 133-44.

(41) Hauser, H.; Phillips, M. C.; Levine, B. A.; Williams, R. J. P., Conformation of the lecithin polar group in charged vesicles. *Nature* **1976,** *261*, 390-4.

(42) Petersheim, M.; Halladay, H. N.; Blodnieks, J., Tb3+ and Ca2+ binding to phosphatidylcholine. A study comparing data from optical, NMR, and infrared spectroscopies. *Biophys J* **1989,** *56*, 551-7.

(43) Liao, R. Z.; Yu, J. G.; Himo, F., Reaction Mechanism of the Trinuclear Zinc Enzyme Phospholipase C: A Density Functional Theory Study. *J Phys Chem B* **2010,** *114*, 2533-2540.

(44) Weston, J., Mode of action of bi- and trinuclear zinc hydrolases and their synthetic analogues. *Chem Rev* **2005,** *105*, 2151-2174.

(45)  Kensil, C. R.; Dennis, E. A., Alkaline hydrolysis of phospholipids in model membranes and the dependence on their state of aggregation. *Biochem* **1981,** *20*, 6079-85.

(46)  Oh, S. J.; Choi, Y.-S.; Hwangbo, S.; Bae, S. C.; Ku, J. K.; Park, J. W., Structure and phosphodiesterase activity of Bis-Tris coordinated lanthanide(III) complexes. *Chem Commun* **1998**, 2189-2190.

(47)  Gomez-Tagle, P.; Yatsimirsky, A. K., Phosphodiester Hydrolysis by Lanthanide Complexes of Bis-Tris Propane. *Inorg Chem* **2001,** *40*, 3786-3796.

(48)  Ramstedt, B.; Slotte, J. P., Membrane properties of sphingomyelins. *Febs Lett* **2002,** *531*, 33-37.

## 3.7. Supporting Information



**A) 0.7 mM Ce(NH$_4$)$_2$(NO$_3$)$_6$, 1.4 mM Bis-tris propane at pH 4.8**

$y = 0.0793x - 0.0466$
$R^2 = 0.9834$

*Absorbance at 620 nm* vs *Inorganic Phosphate (µM)*

**B) 0.7 mM Ce(NH$_4$)$_2$(NO$_3$)$_6$, 1.4 mM Bis-tris propane at pH 7.2**

$y = 0.0781x - 0.0459$
$R^2 = 0.988$

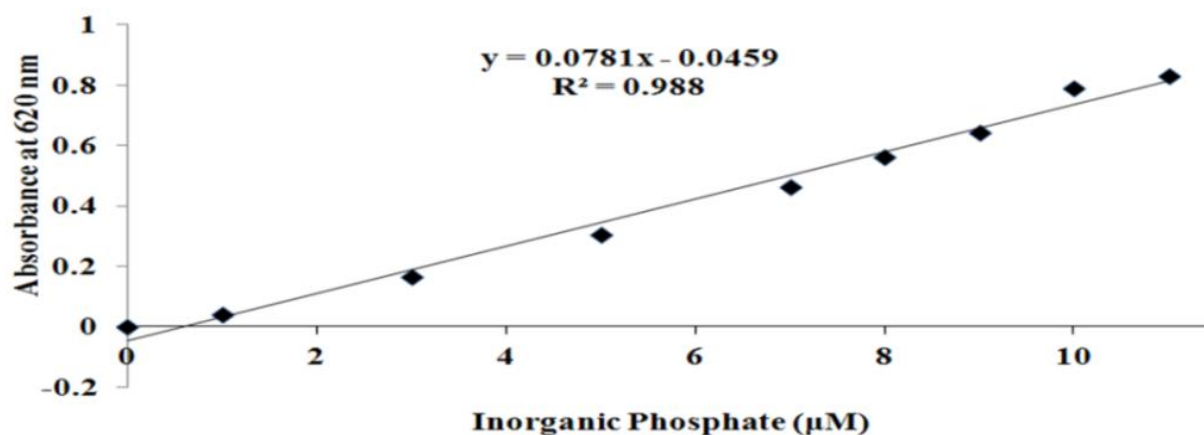*Absorbance at 620 nm* vs *Inorganic Phosphate (µM)*

**Figure 3.S1.** Representative standard curves used for the determination of free inorganic phosphate from phosphatidylcholine hydrolysis reactions. The inorganic phosphate standard solutions (300 µL) contained 0.7 mM Ce(NH$_4$)$_2$(NO$_3$)$_6$ and 1.4 mM bis-tris propane at pH 4.8 (**A**) or pH 7.2 (**B**), and 0 to 11 µM inorganic phosphate before the addition of 200 µL of malachite green/molybdate reagent. The standard solutions were treated the same as the corresponding lipid hydrolysis reactions with assay. Inorganic phosphate was detected at 620 nm with a UV-vis spectrophotometer. The concentration of the products was determined from the slope of the linear titration curve, and the percent hydrolysis yields were calculated from the formula: (actual concentration of product / 2000 µM theoretical concentration of product) * 100.
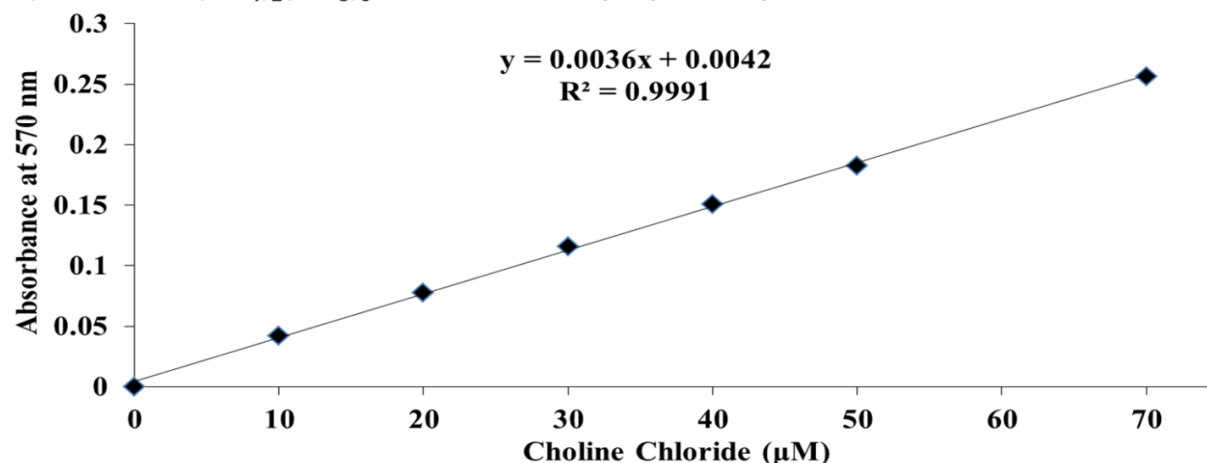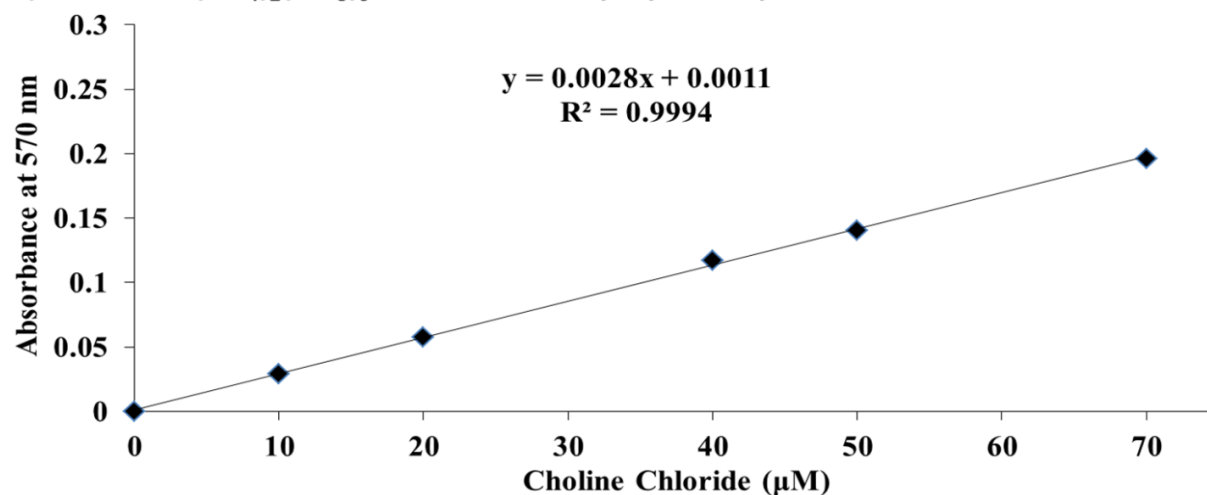
**A) 0.8 mM Ce(NH$_4$)$_2$(NO$_3$)$_6$, 1.6 mM Bis-tris propane at pH 4.8**

$$y = 0.0036x + 0.0042$$
$$R^2 = 0.9991$$

Absorbance at 570 nm vs. Choline Chloride (µM)

**B) 0.8 mM Ce(NH$_4$)$_2$(NO$_3$)$_6$, 1.6 mM Bis-tris propane at pH 7.2**

$$y = 0.0028x + 0.0011$$
$$R^2 = 0.9994$$

Absorbance at 570 nm vs. Choline Chloride (µM)

**Figure 3.S2.** Representative standard curves used for the determination of choline from phosphatidylcholine hydrolysis reactions. The choline standard solutions (40 µL) contained 0.8 mM Ce(NH$_4$)$_2$(NO$_3$)$_6$ and 1.6 mM bis-tris propane at pH 4.8 **(A)** and 7.2 **(B)**. The standard solutions were treated the same as the corresponding lipid hydrolysis reactions with assay. Choline was detected at 570 nm with a UV-vis spectrophotometer. The concentration of the products was determined from the slope of the linear titration curve, and the percent hydrolysis yields were calculated from the formula: (actual concentration of product / 2000 µM theoretical concentration of product) * 100.
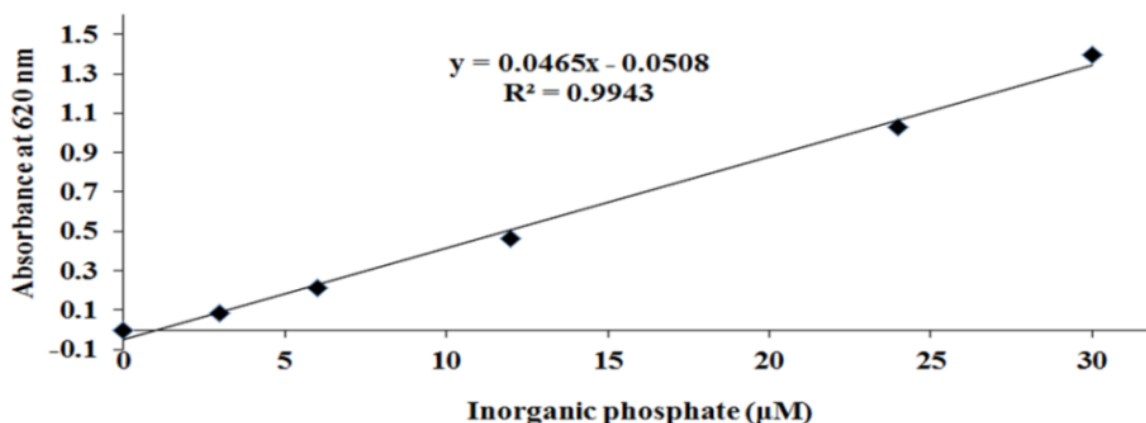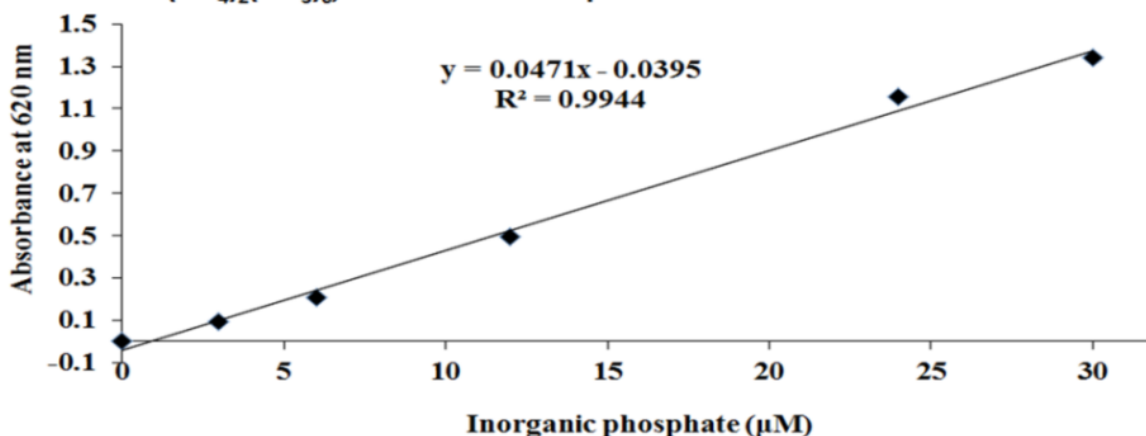
**Figure 3.S3.** Representative standard curves used for the determination of free inorganic phosphate from lipid hydrolysis reactions. The inorganic phosphate standard solutions (400 μL) contained 1.75 mM $Ce(NH_4)_2(NO_3)_6$, $0 - 35$ μM inorganic phosphate, and 3.5 mM piperazine buffer at pH 4.8 (**A**) or 3.5 mM HEPES at pH 7.2 (**B**). The standard solutions were treated the same as the corresponding lipid hydrolysis reactions by the addition of 100 μL malachite green/molybdate reagent. Inorganic phosphate was detected at 620 nm with a UV-vis spectrophotometer. The concentration of the products was determined from the slope of the linear titration curve, and the percent hydrolysis yields were calculated from the formula: (actual concentration of product / 35 μM theoretical concentration of product) * 100.

**A) 1.75 mM Ce(NH$_4$)$_2$(NO$_3$)$_6$, 3.5 mM BTP, 1 mM MES at pH 4.8**



y = 0.0465x - 0.0417
R² = 0.9925

Absorbance at 620 nm

Inorganic phosphate (μM)

**B) 1.75 mM Ce(NH$_4$)$_2$(NO$_3$)$_6$, 3.5 mM BTP at 7.2**



y = 0.0494x - 0.0466
R² = 0.9972

Absorbance at 620 nm

Inorganic phosphate (μM)

**Figure 3.S4.** Representative standard curves used for the determination of free inorganic phosphate from lipid hydrolysis reactions.  The inorganic phosphate standard solutions (400 μL) contained 1.75 mM Ce(NH$_4$)$_2$(NO$_3$)$_6$, 0 – 35 μM inorganic phosphate, and 3.5 mM bis-tris propane and 1 mM MES buffer at pH 4.8 **(A)** or 3.5 mM bis-tris propane at  pH 7.2 **(D)**. The standard solutions were treated the same as the corresponding lipid hydrolysis reactions by the addition of 100 μL malachite green/molybdate reagent.  Inorganic phosphate was detected at 620 nm with a UV-vis spectrophotometer.  The concentration of the products was determined from the slope of the linear titration curve, and the percent hydrolysis yields were calculated from the formula: (actual concentration of product / 35 μM theoretical concentration of product) * 100.
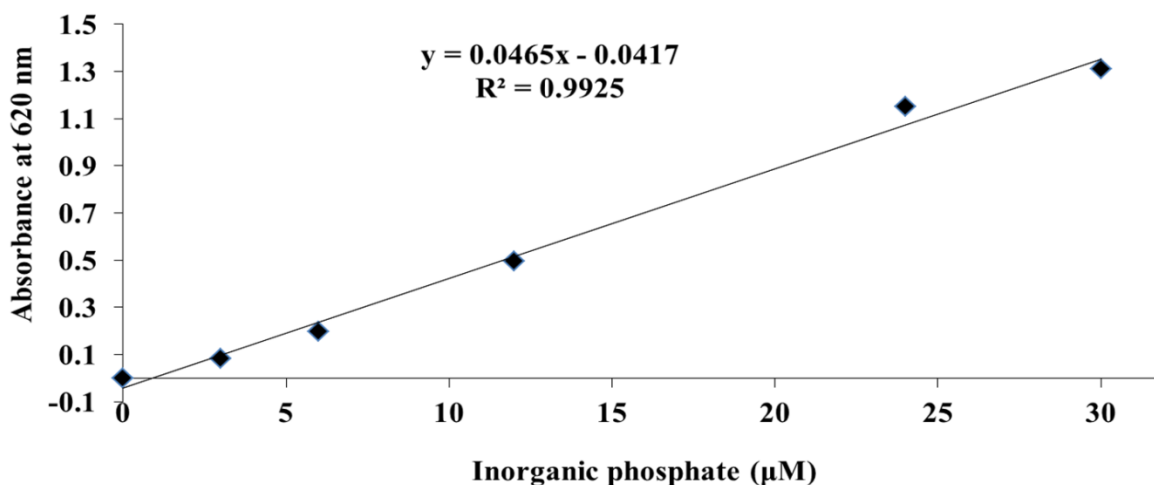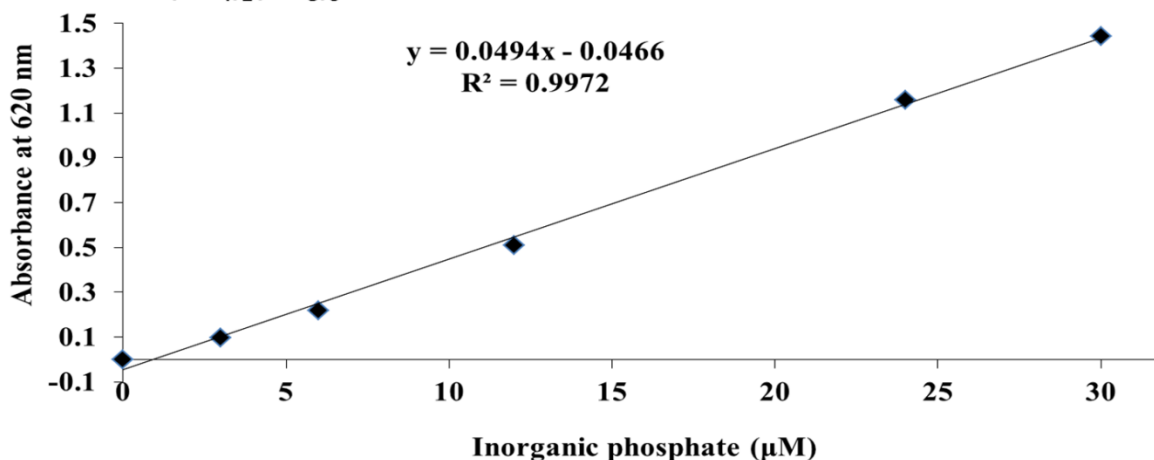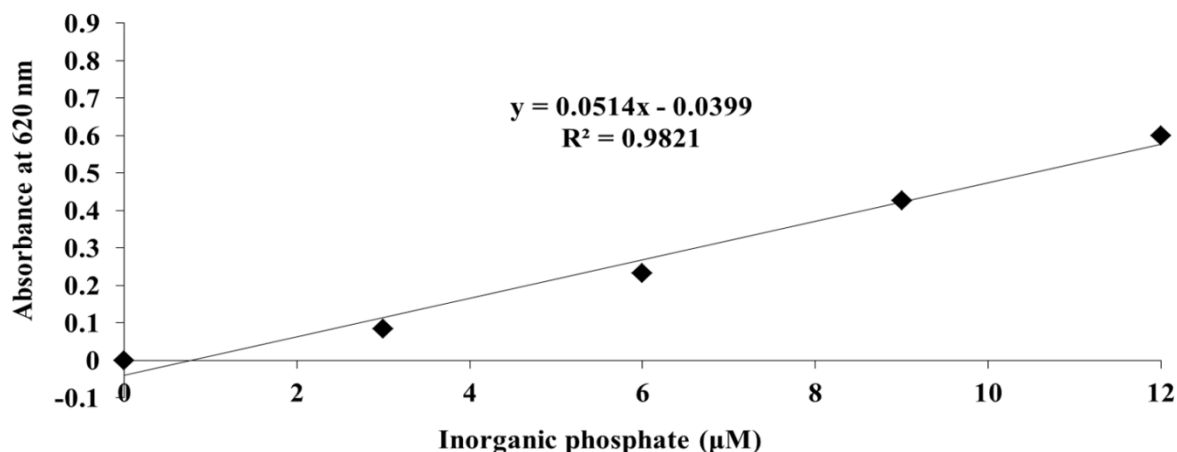
**A) 1.75 mM Ce(NH$_4$)$_2$(NO$_3$)$_6$, 0.875 mM BTP-OH, 1 mM MES at pH 4.8**



$y = 0.0514x - 0.0399$
$R^2 = 0.9821$

Absorbance at 620 nm

Inorganic phosphate (µM)

**B) 1.75 mM Ce(NH$_4$)$_2$(NO$_3$)$_6$, 0.875 mM BTP-OH, 1 mM MOPS at pH 7.2**



$y = 0.0549x - 0.0032$
$R^2 = 0.9972$

Absorbance at 620 nm

Inorganic phosphate (µM)

**Figure 3.S5.** Representative standard curves used for the determination of free inorganic phosphate from lipid hydrolysis reactions. The inorganic phosphate standard solutions (400 µL) contained 1.75 mM Ce(NH$_4$)$_2$(NO$_3$)$_6$, 0 – 12 µM inorganic phosphate, 0.875 mM bis-tris propane derivative (BTP-OH), and either 1 mM MES buffer at pH 4.8 **(A)** or 1 mM MOPS buffer at pH 7.2 **(B)**. The standard solutions were treated the same as the corresponding lipid hydrolysis reactions by the addition of 100 µL malachite green/molybdate reagent. Inorganic phosphate was detected at 620 nm with a UV-vis spectrophotometer. The concentration of the products was determined from the slope of the linear titration curve, and the percent hydrolysis yields were calculated from the formula: (actual concentration of product / 35 µM theoretical concentration of product) * 100.

**A) 1.75 mM Ce(NH₄)₂(NO₃)₆, 0.44 mM BTP, 1 mM piperazine at pH 4.8**



$y = 0.0604x - 0.035$
$R^2 = 0.9786$

**B) 1.75 mM Ce(NH₄)₂(NO₃)₆, 0.44 mM BTP, 1 mM HEPES at pH 7.2**



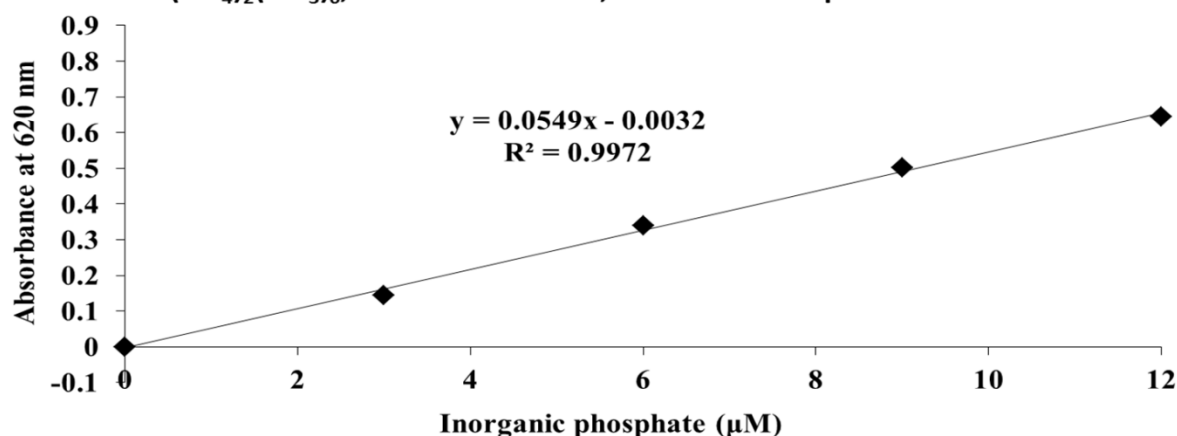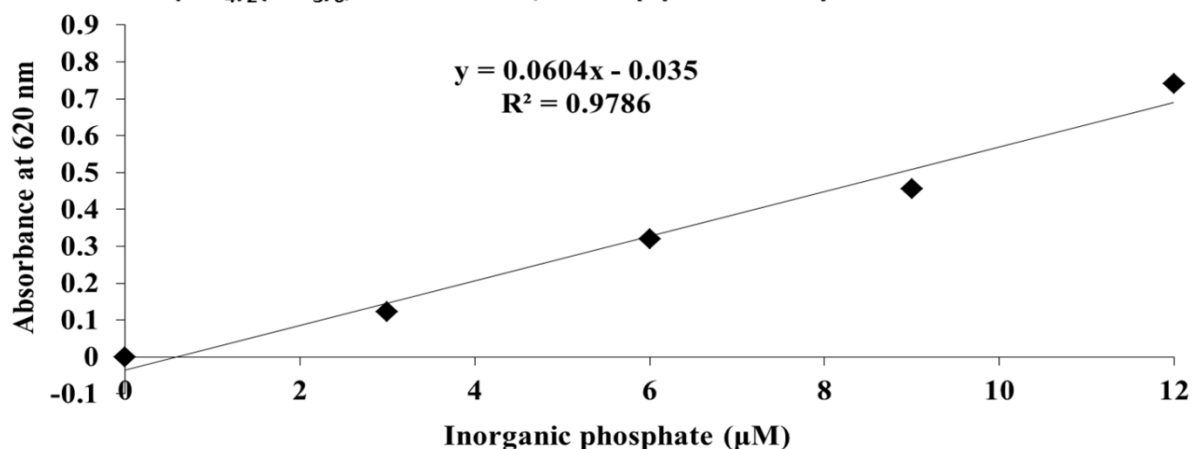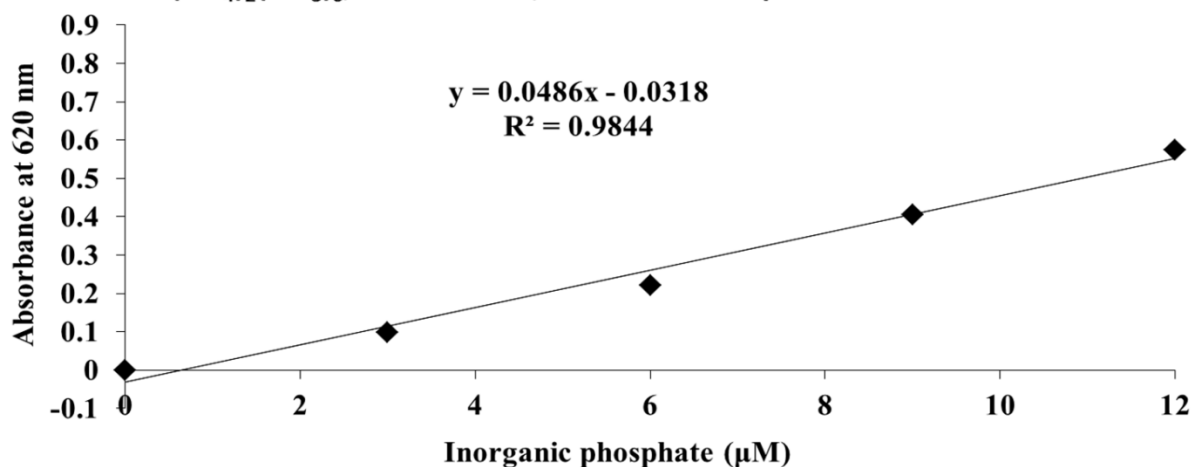$y = 0.0486x - 0.0318$
$R^2 = 0.9844$

**Figure 3.S6.** Representative standard curves used for the determination of free inorganic phosphate from lipid hydrolysis reactions.  The inorganic phosphate standard solutions (400 µL) contained 1.75 mM $Ce(NH_4)_2(NO_3)_6$, 0 – 15 µM inorganic phosphate, 0.44 mM bis-tris propane, and either 1 mM piperazine buffer at pH 4.8 (**A**) or 1 mM HEPES buffer at pH 7.2 (**B**).  The standard solutions were treated the same as the corresponding lipid hydrolysis reactions by the addition of 100 µL malachite green/molybdate reagent.  Inorganic phosphate was detected at 620 nm with a UV-vis spectrophotometer.  The concentration of the products was determined from the slope of the linear titration curve, and the percent hydrolysis yields were calculated from the formula: (actual concentration of product / 35 µM theoretical concentration of product) * 100.

**A) 1.75 mM Ce(NH₄)₂(NO₃)₆, 0.35 mM BTP, 1 mM piperazine at pH 4.8**

$$y = 0.0639x - 0.0323$$
$$R^2 = 0.9903$$

Absorbance at 620 nm

Inorganic phosphate (µM)

**B) 1.75 mM Ce(NH₄)₂(NO₃)₆, 0.35 mM, 1 mM HEPES at pH 7.2**

$$y = 0.0506x - 0.0369$$
$$R^2 = 0.9849$$
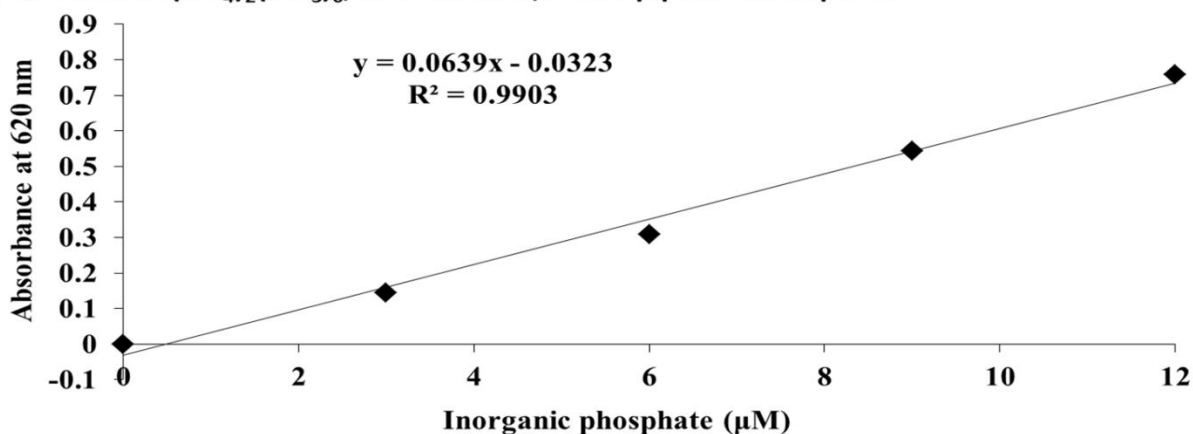
Absorbance at 620 nm

Inorganic phosphate (µM)

**Figure 3.S7.** Representative standard curves used for the determination of free inorganic phosphate from lipid hydrolysis reactions. The inorganic phosphate standard solutions (400 µL) contained 1.75 mM Ce(NH$_4$)$_2$(NO$_3$)$_6$, 0 – 15 µM inorganic phosphate, 0.35 mM bis-tris propane, and either 1 mM piperazine buffer at pH 4.8 (**A**) or 1 mM HEPES buffer pH 7.2 (**B**). The standard solutions were treated the same as the corresponding lipid hydrolysis reactions by the addition of 100 µL malachite green/molybdate reagent. Inorganic phosphate was detected at 620 nm with an UV-vis spectrophotometer. The concentration of the products was determined from the slope of the linear titration curve, and the percent hydrolysis yields were calculated from the formula: (actual concentration of product / 35 µM theoretical concentration of product) * 100.

**2.5 mM Ce(NH₄)₂(NO₃)₆, 5.0 mM piperazine at pH 4.8**

$$y = 0.0496x - 0.0667$$
$$R^2 = 0.9929$$

Absorbance at 620 nm
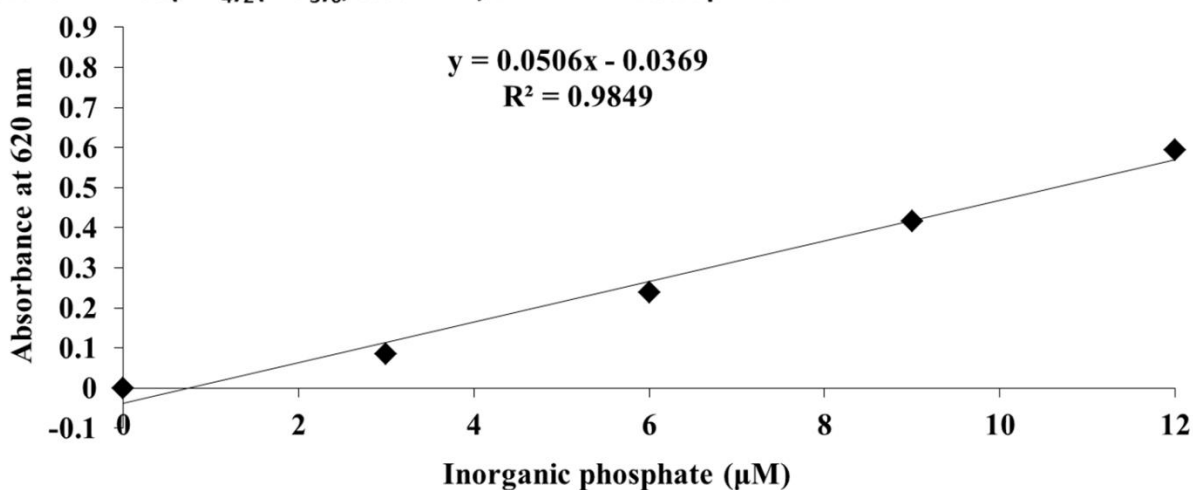
Inorganic phosphate (μM)

**Figure 3.S8.** Representative standard curve used for the determination of free inorganic phosphate from lipid hydrolysis reactions. The inorganic phosphate standard solutions (400 μL) contained 2.5 mM $Ce(NH_4)_2(NO_3)_6$, 0 – 35 μM inorganic phosphate, and 5.0 mM piperazine buffer at pH 4.8. The standard solutions were treated the same as the corresponding lipid hydrolysis reactions by the addition of 100 μL malachite green/molybdate reagent. Inorganic phosphate was detected at 620 nm with a UV-vis spectrophotometer. The concentration of the products was determined from the slope of the linear titration curve, and the percent hydrolysis yields were calculated from the formula: (actual concentration of product / 35 μM theoretical concentration of product) * 100.
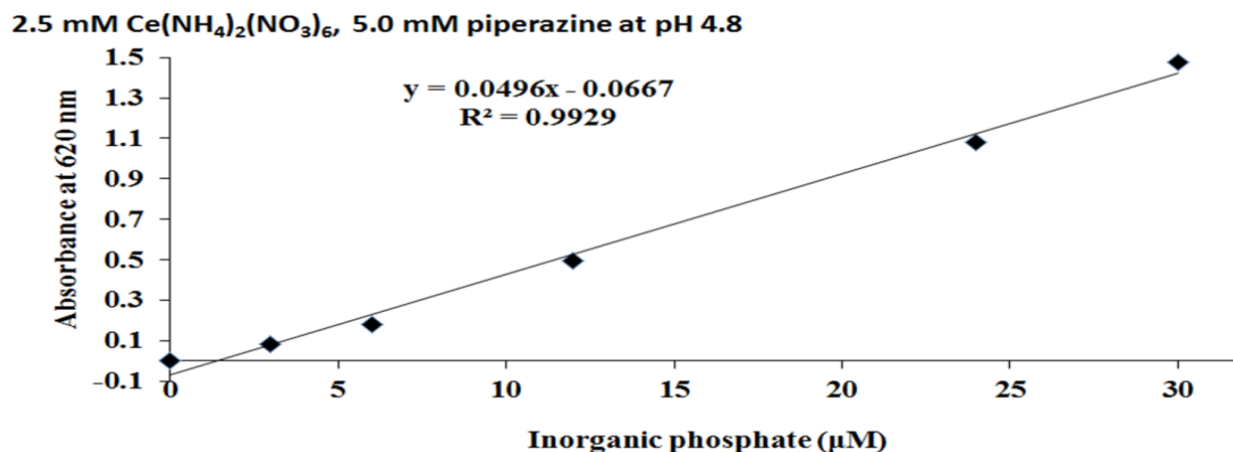
Hydrolysis Yield (%)

□ pH 4.9 - 5.2
■ pH 7.0 - 7.3

**Figure 3.S9.** Averaged hydrolysis yields plotted as a function of pH for **(A)** Malachite green detection of free inorganic phosphate and **(B)** Amplex® Red detection of free choline. A total of 2 mM PC was reacted at 37 °C for 20 h in the presence of 10 mM $Ce(NH_4)_2(NO_3)_6$ and 20 mM BTP at pH ~ 4.8 or pH ~ 7.2. The number of trials **(n)** appears in parenthesis. Error bars represent standard deviation.

A) 2 mM PC at 37 °C, total phosphate and choline
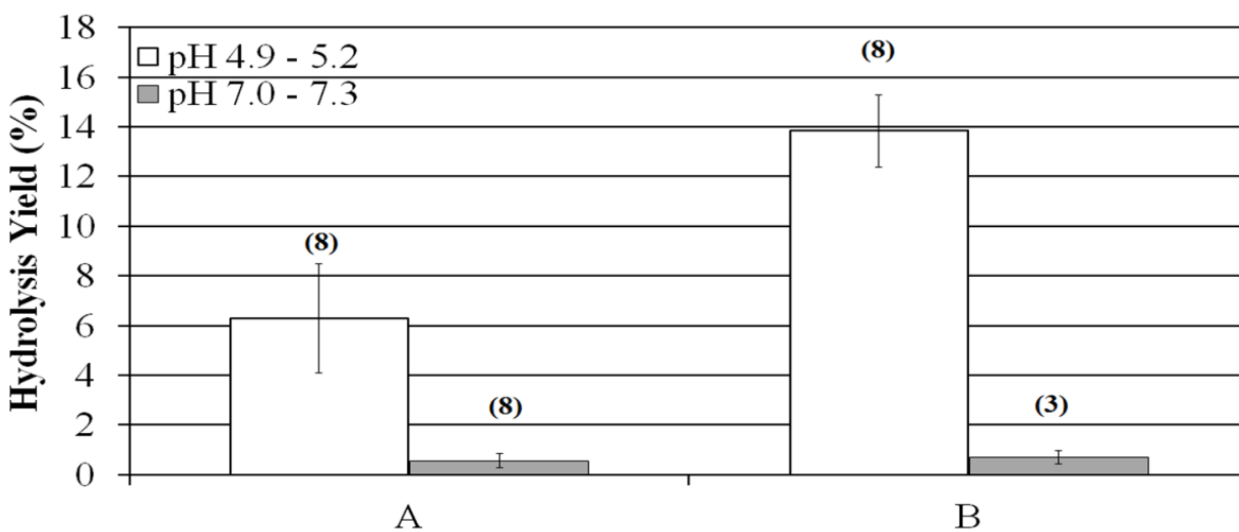


B) 35 µM PC at 37 °C, total phosphate



**Figure 3.S10.** Averaged hydrolysis yields plotted as a function of pH for malachite green detection of free inorganic phosphate and/or Amplex ® Red detection of free choline for parallel no metal controls. A total of 2 mM phosphatidylcholine (PC) was reacted at 37 °C for 20 h in the absence of 10 mM $Ce(NH_4)_2(NO_3)_6$ and in the presence of 20 mM BTP at pH 4.8 or pH 7.2 **(A)**. A total of 35 µM phosphatidylcholine was reacted at 37 °C for 20 h in the absence of 1.75 mM $Ce(NH_4)_2(NO_3)_6$ and in the presence of either 3.5 mM piperazine at pH 4.8, 3.5 mM HEPES at pH 7.2, 3.5 mM BTP (in 1 mM MES buffer) at pH 4.8, or 3.5 mM BTP at pH 7.2 **(B)**.

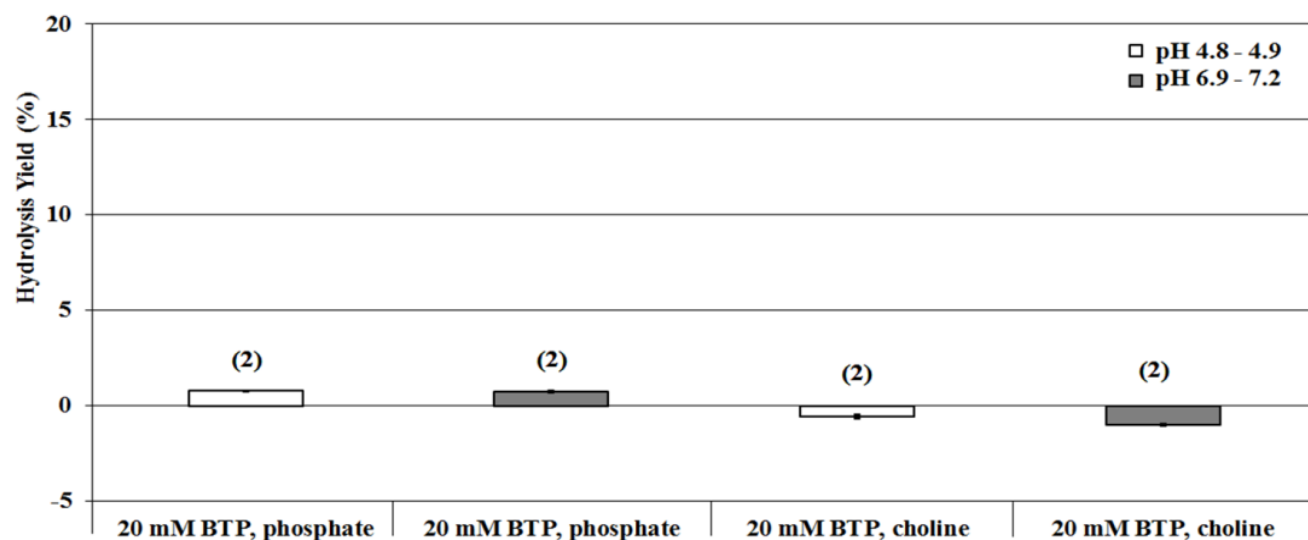A) 35 µM SM at 37 °C, total phosphate, 20 h



B) 35 µM SM at 37 °C, total phosphate, 40 h
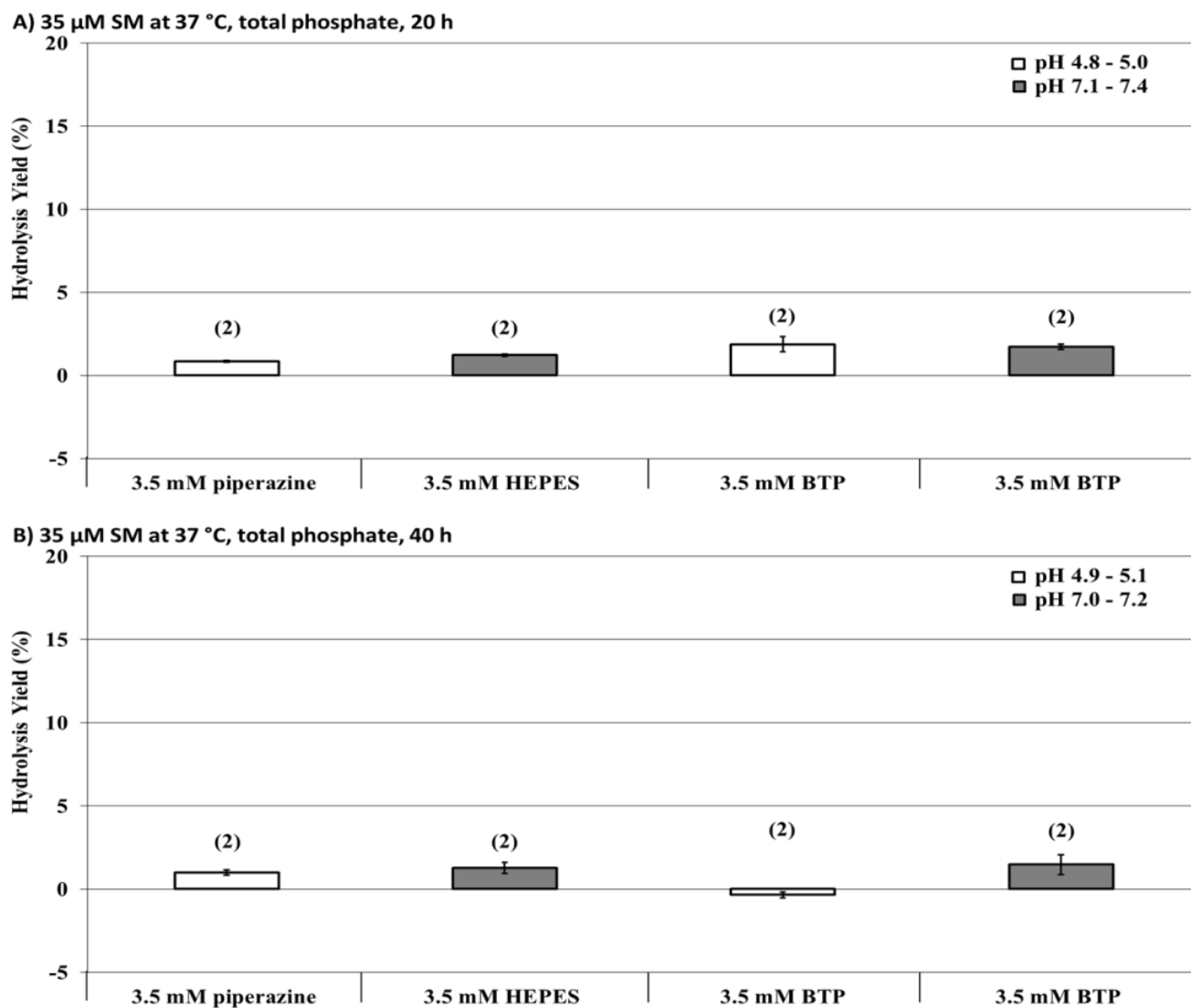


**Figure 3.S11.** Averaged hydrolysis yields plotted as a function of pH for malachite green detection of free inorganic phosphate for parallel no metal controls. A total of 35 µM sphingomyelin (SM) was reacted at 37 °C for 20 h **(A)** or 40 h **(B)** in the absence of 1.75 mM $Ce(NH_4)_2(NO_3)_6$ and in the presence of either 3.5 mM piperazine at pH 4.8, 3.5 mM HEPES at pH 7.2, 3.5 mM BTP (in 1 mM MES buffer) at pH 4.8, or 3.5 mM BTP at pH 7.2.
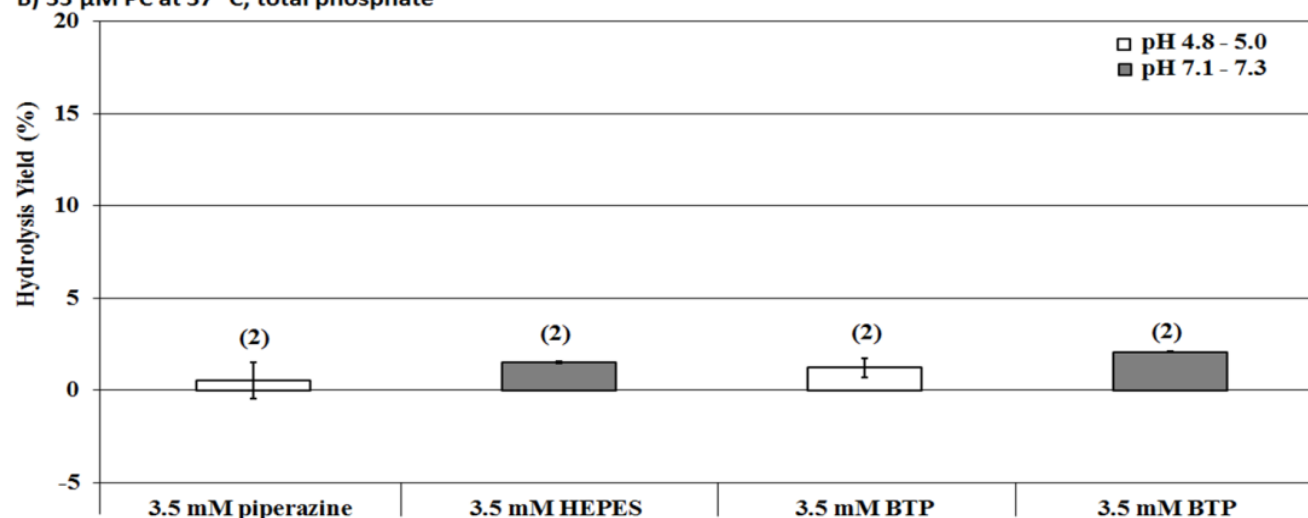
**35 μM PC at 37 °C, total phosphate**
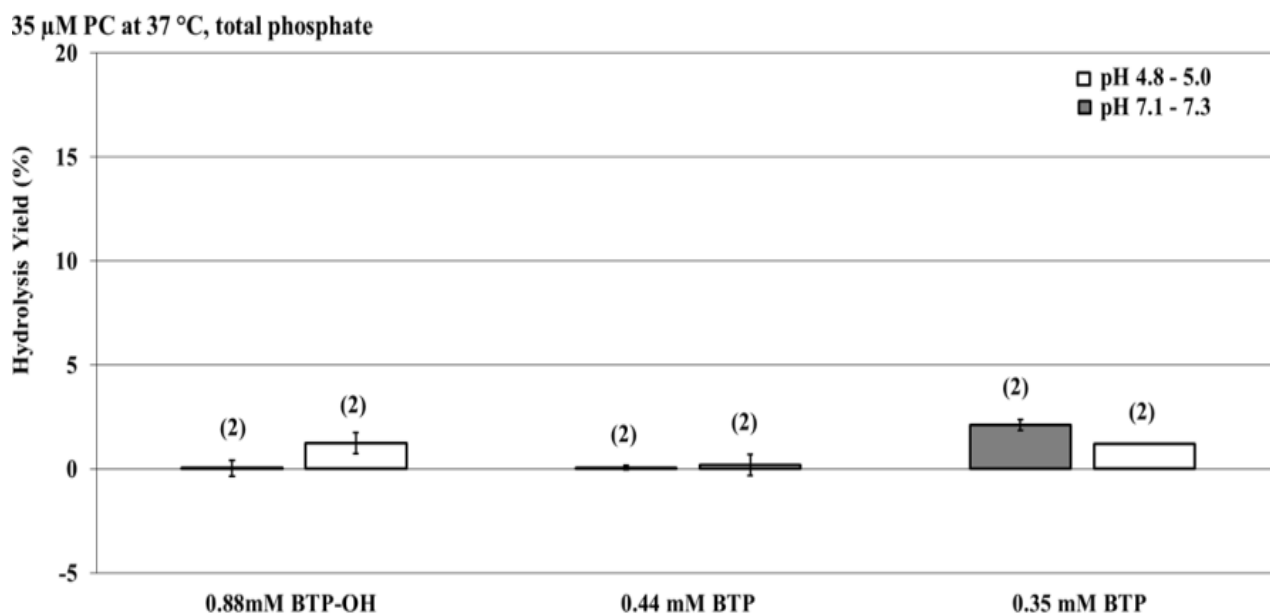


**Figure 3.S12.** Averaged hydrolysis yields plotted as a function of pH for malachite green detection of free inorganic phosphate for parallel no metal controls. A total of 35 μM phosphatidylcholine (PC) was reacted at 37 °C for 20 h in the absence of 1.75 mM $Ce(NH_4)_2(NO_3)_6$ and in the presence of 0.88 mM mM bis-tris propane derivative (BTP-OH), 0.35 mM BTP, and 0.44 mM BTP at pH 4.8 (1 mM piperazine or MES buffer) or pH 7.2 (1 mM HEPES or MOPS buffer). The number of trials **(n)** appears in parenthesis. Error bars represent standard deviation.

**A) BTP, pD 2.3**

**B) [Ce(BTP)$_2$(NO$_3$)$_4$]·2H$_2$O, pD 2.3**



**C) BTP, pD 5.1**

**D) [Ce(BTP)$_2$(NO$_3$)$_4$]·2H$_2$O, pD 5.1**
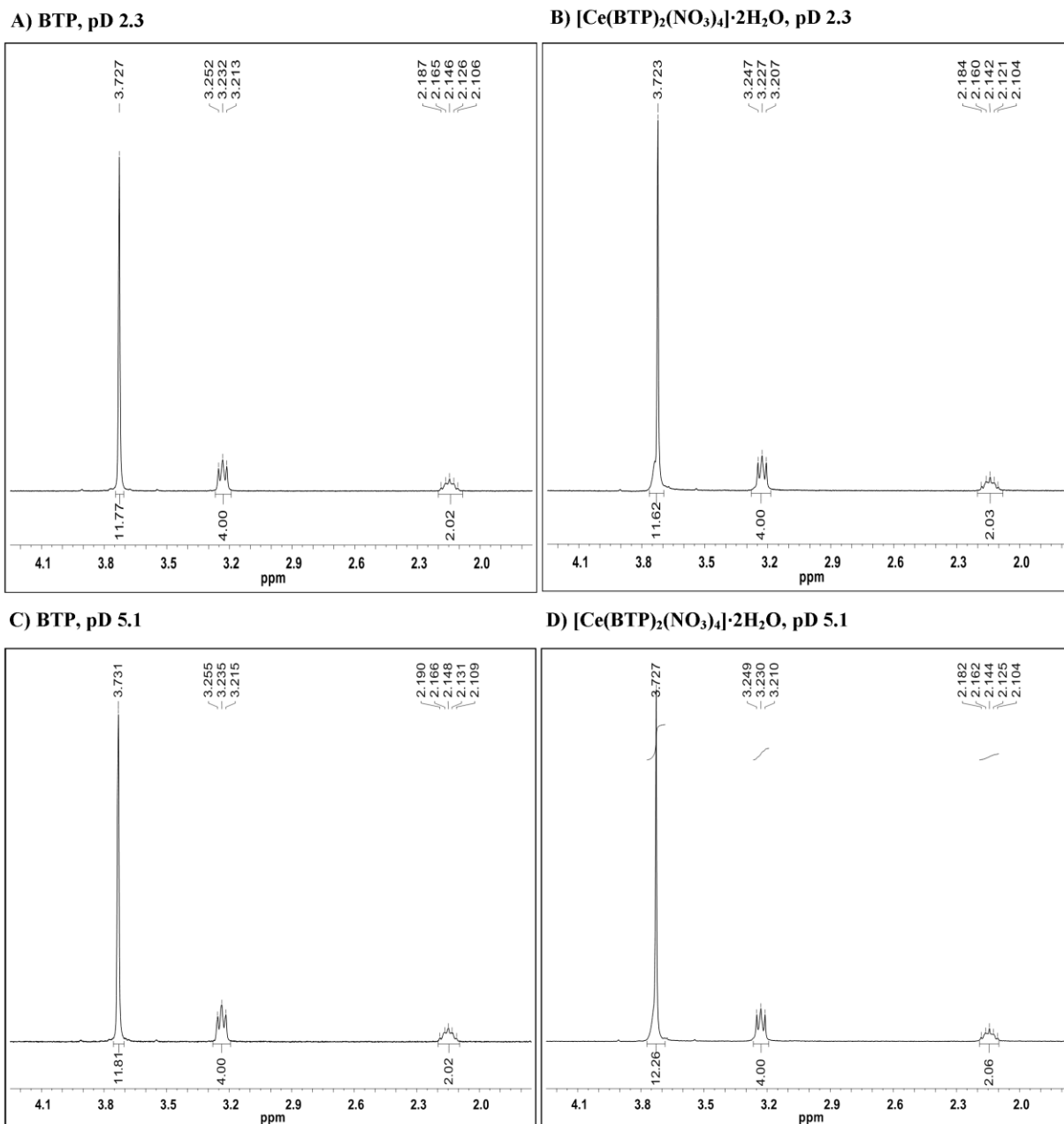


**Figure 3.S13.** $^1$H- NMR spectra of [Ce(BTP)$_2$(NO$_3$)$_4$]·2H$_2$O and BTP in D$_2$O at pD values 2.3 (**A** and **B**) and 5.1 (**C** and **D**). The pD values were adjusted with NaOD and DCl in D$_2$O. Each NMR sample contained 0.1 v/v % of *tert*-butanol as an internal standard. The spectra were recorded on a Bruker Advance 400 MHz NMR spectrometer at 25 °C.

**A) BTP, pD 7.7**

**B) [Ce(BTP)₂(NO₃)₄]·2H₂O, pD 7.7**

**C) BTP, pD 9.6**

**D) [Ce(BTP)₂(NO₃)₄]·2H₂O, pD 9.6**

**Figure 3.S14.** $^1$H- NMR spectra of [Ce(BTP)₂(NO₃)₄]·2H₂O and BTP in D₂O at pD values 7.7 **(A** and **B)** and 9.6 **(C** and **D)**. The pD values were adjusted with NaOD and DCl in D₂O. Each NMR sample contained 0.1 v/v % of *tert*-butanol as an internal standard. The spectra were recorded on a Bruker Advance 400 MHz NMR spectrometer at 25 °C.

A) 1.75 mM Ce(NH$_4$)$_2$(NO$_3$)$_6$ and 3.5 mM piperazine buffer at pH 4.8

$y = -0.0605x + 3.5423$
$R^2 = 0.9905$
$t_{1/2} = 11.4$ h

Time (h)

B) 1.75 mM Ce(NH$_4$)$_2$(NO$_3$)$_6$ + 3.5 mM bis-tris propane, and 1 mM MES buffer at pH 4.8

$y = -0.0266x + 3.6007$
$R^2 = 0.9513$
$t_{1/2} = 26.1$ h

Time (h)

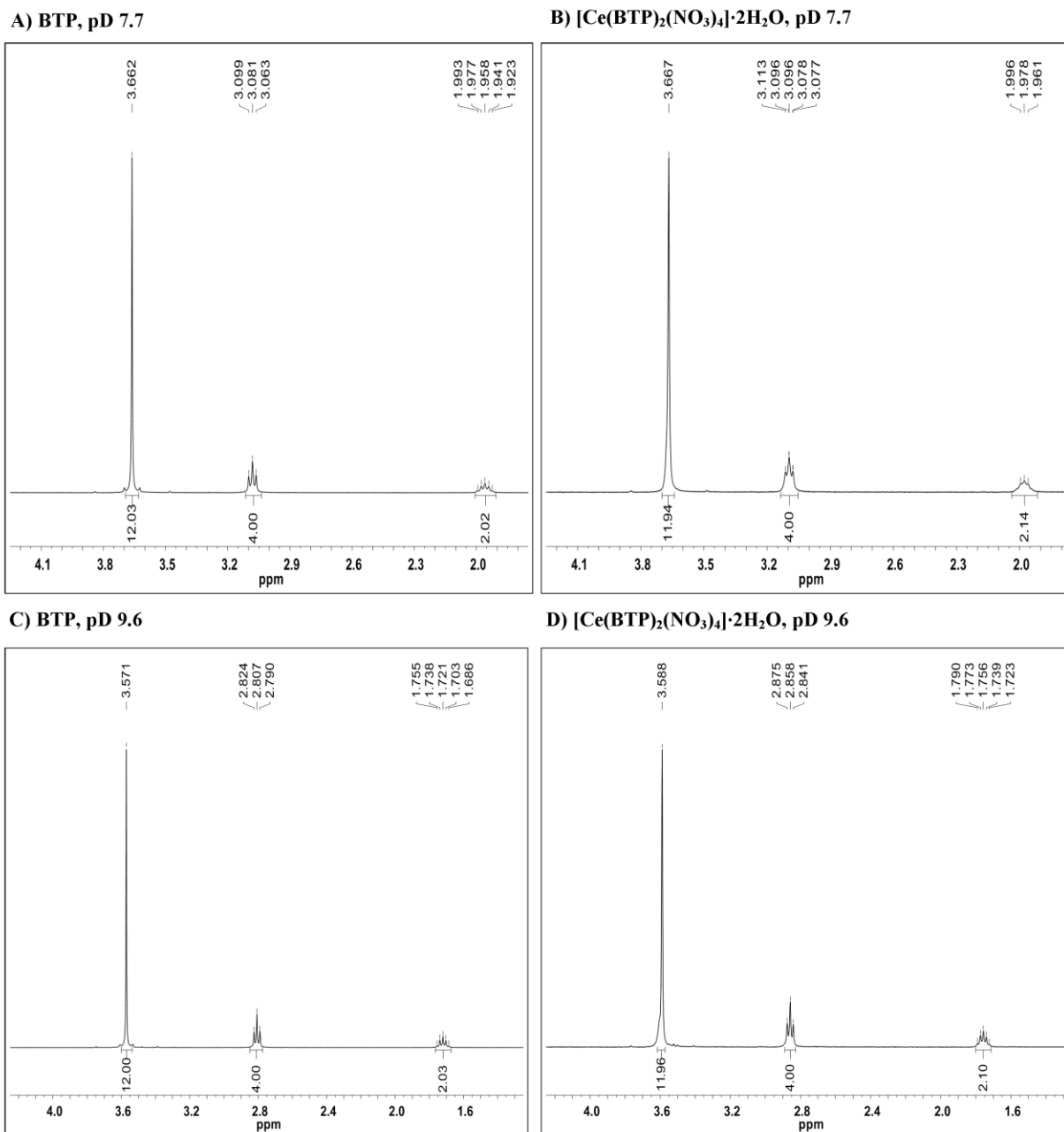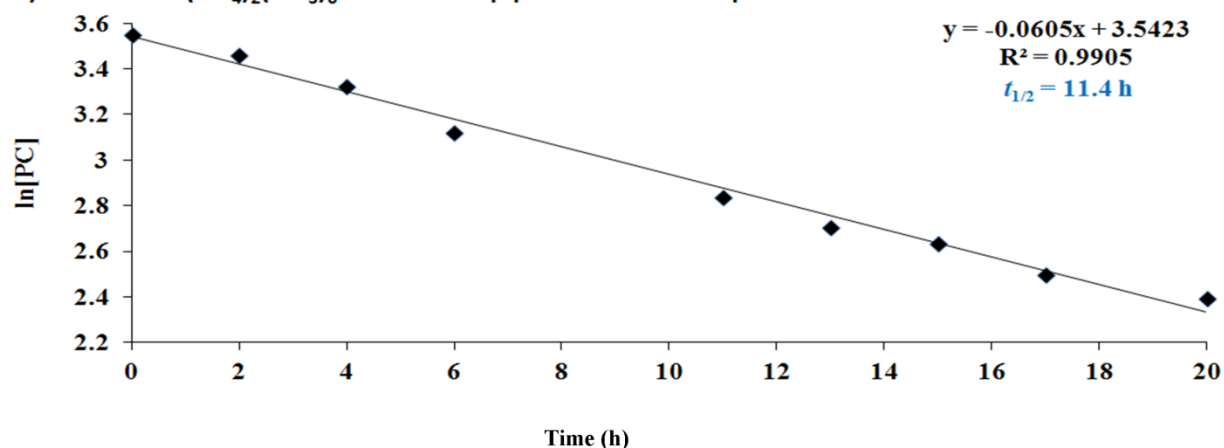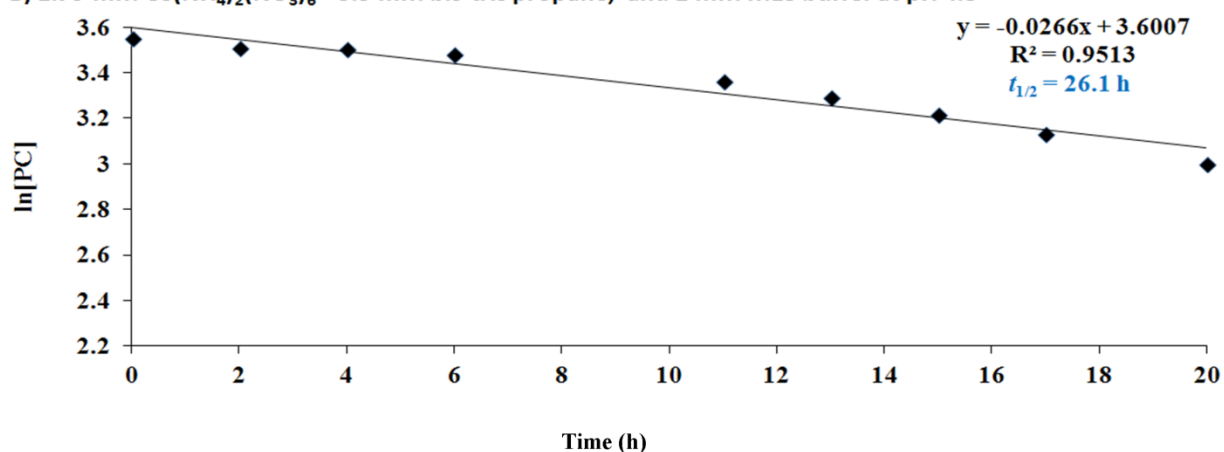**Figure 3.S15.** Time course for the degradation of PC at pH 4.8 and 37 °C by 1.75 mM Ce(NH$_4$)$_2$(NO$_3$)$_6$ in 3.5 mM piperazine buffer **(A)** or with 3.5 mM BTP in 1 mM MES buffer **(B)**. The ln[PC] is plotted as a function of time for malachite green/molybdate assay detection of phosphate. [PC] is equal to [PC$_\infty$ - PC$_t$] where PC$_\infty$ is the theoretical concentration of PC (35 µM), and PC$_t$ is the concentration of PC at times 2 h, 4 h, 6 h, 11 h, 13 h, 15 h, 17 h, and 20 h. The solid line is a linear curve fitted that provided the pseudo-first order rate constants 6.1 x 10$^{-2}$ h$^{-1}$ and 2.7 x 10$^{-2}$ h$^{-1}$ for **(A)** and **(B)**, respectively. The 30 h time point was omitted because of a deviation from linearity. PC = phosphatidylcholine.
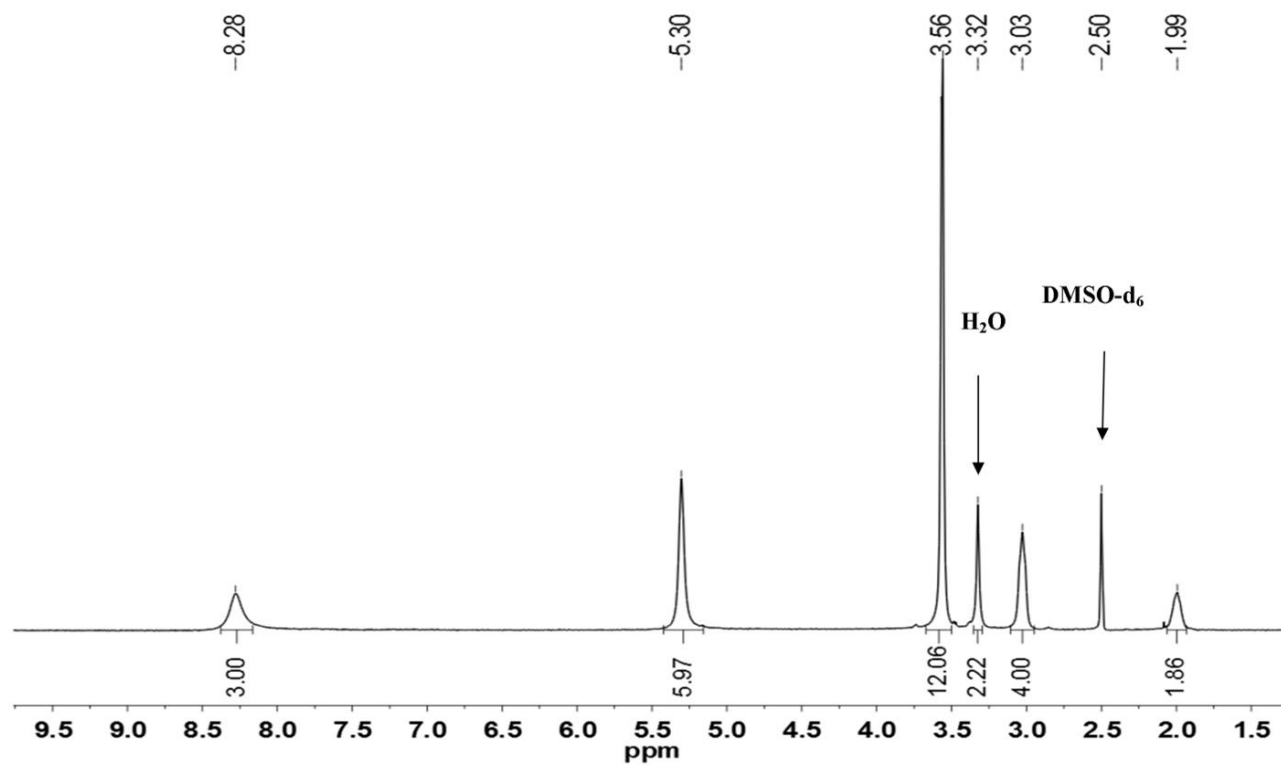
**Figure 3.S16.** The $^1$H-NMR spectrum of $[Ce(BTP)_2(NO_3)_4]\cdot 2H_2O$ was recorded on a Bruker Advance 400 MHz NMR spectrometer at 25 °C in DMSO-$d_6$.
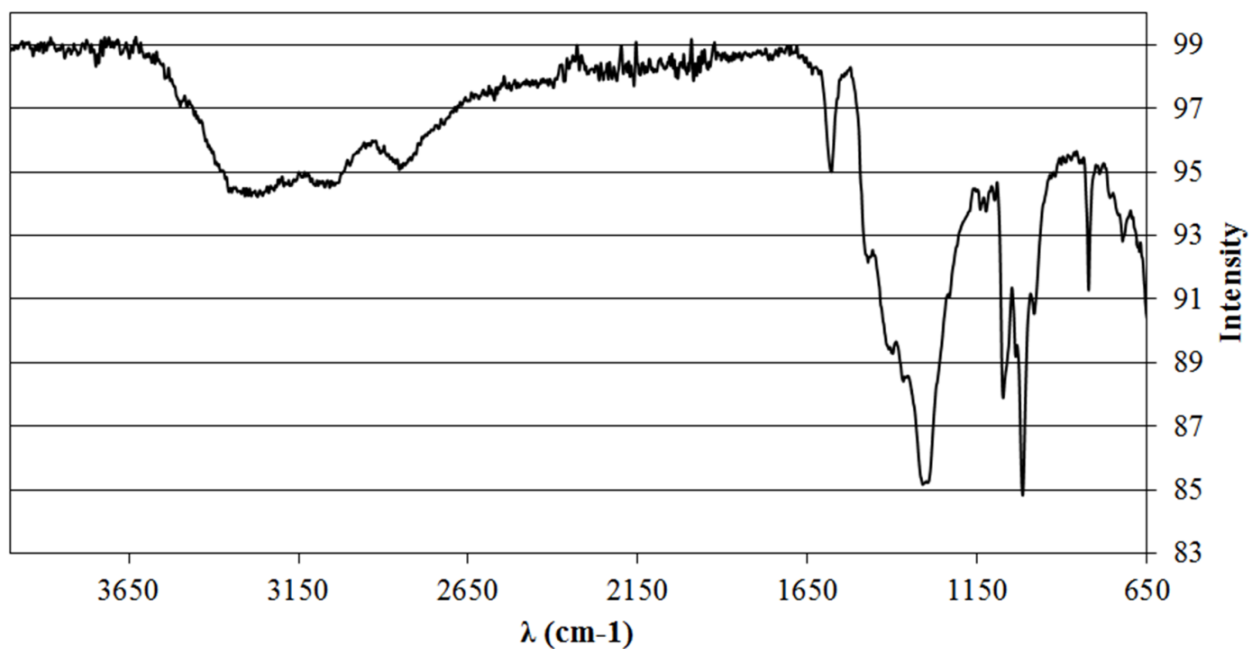
**Figure 3.S17.** IR spectrum of $[Ce(BTP)_2(NO_3)_4] \cdot 2H_2O$ was recorded on a Perkin Elmer Spectrum 100 FT-IR spectrometer coupled with an attenuated total reflection (ATR) sampling accessory. FT-IR (ATR, cm$^{-1}$)): 3343 (b, w), 3109 (b, w), 2884 (b, w), 1589 (w), 1320 (s), 1079 (s), 1019 (s), 823 (m).
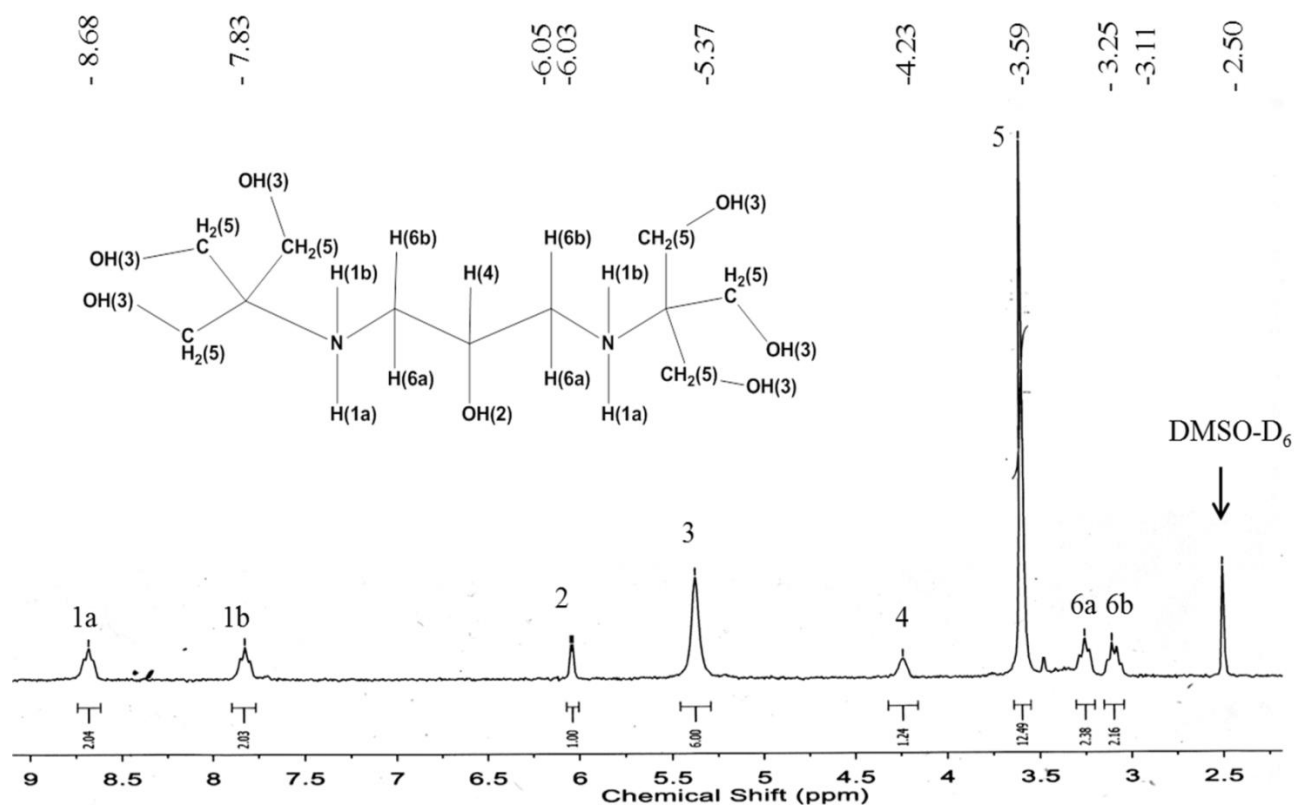
**Figure 3.S18.** The $^1$H-NMR (400 MHz) of the dihydrochloride salt of 1,3-bis-[tris-(hydroxymethyl)-methyl-amino]-2-propanol was recorded on a Bruker Advance 400 MHz NMR spectrometer at 25 °C in DMSO-d$_6$ . $^1$H-NMR (400 MHz, DMSO-d$_6$, 25 °C, ppm): δ = 3.11 (m, 2H); 3.25 (m, 2H); 3.59 (s, 12H); 4.25 (bs, 1H); 5.37 (sb, 6H); 6.04 (d, 1H); 7.83 (t, 2H); 8.68 (t, 2H).
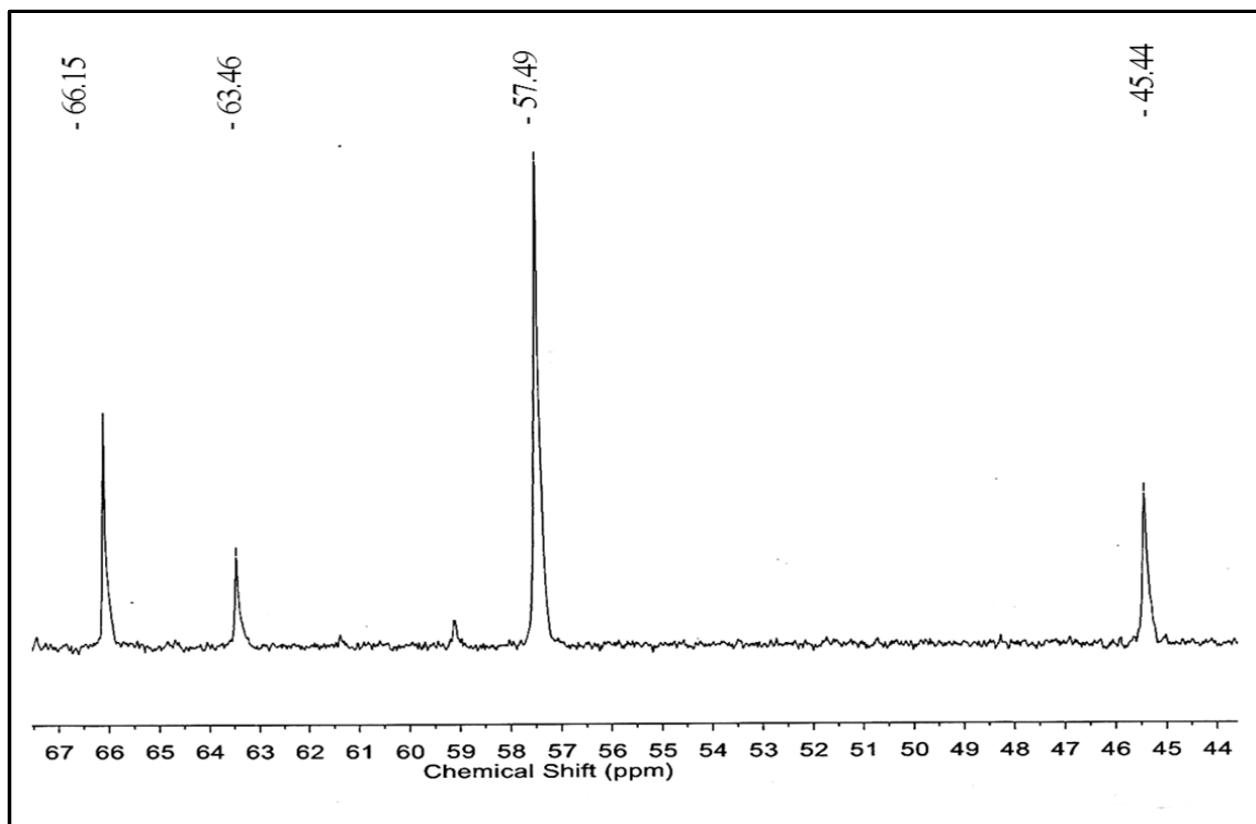
**Figure 3.S19.** The $^{13}$C-NMR (100 MHz) of the dihydrochloride salt of 1,3-bis-[tris-(hydroxymethyl)-methyl-amino]-2-propanol (Figure 3.10), was recorded on a Bruker Advance 400 MHz NMR spectrometer at 25 °C in $D_2O$. $^{13}$C-NMR (100 MHz, $D_2O$, 25 °C, ppm) 45.44; 57.49; 63.46; 66.15.
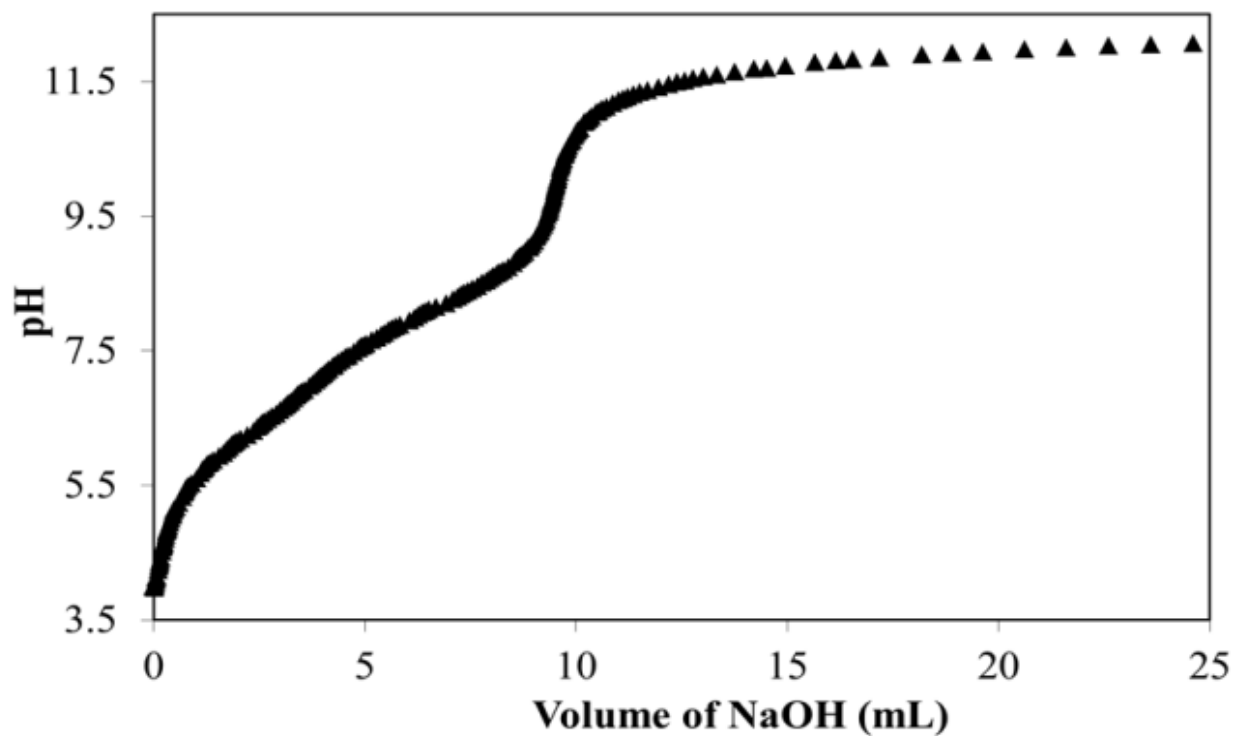
**Figure 3.S20.** Titration curve of 2.5 mM bis tris propane derivative (BTP-OH) in 0.1 M NaCl by standardized 0.05 M NaOH at 22 °C. The $pK_a$ values of 6.3 ± 0.06 ($pK_{a1}$) and 8.1 ± 0.00 ($pK_{a2}$) were determined from three trials.  KaleidaGraph (v. 4.0) was used to obtain the approximate first derivative of $\Delta$NaOH (mL)/$\Delta$pH versus pH, and the $pK_a$ values were indicated by the maxima of the first-derivative plot
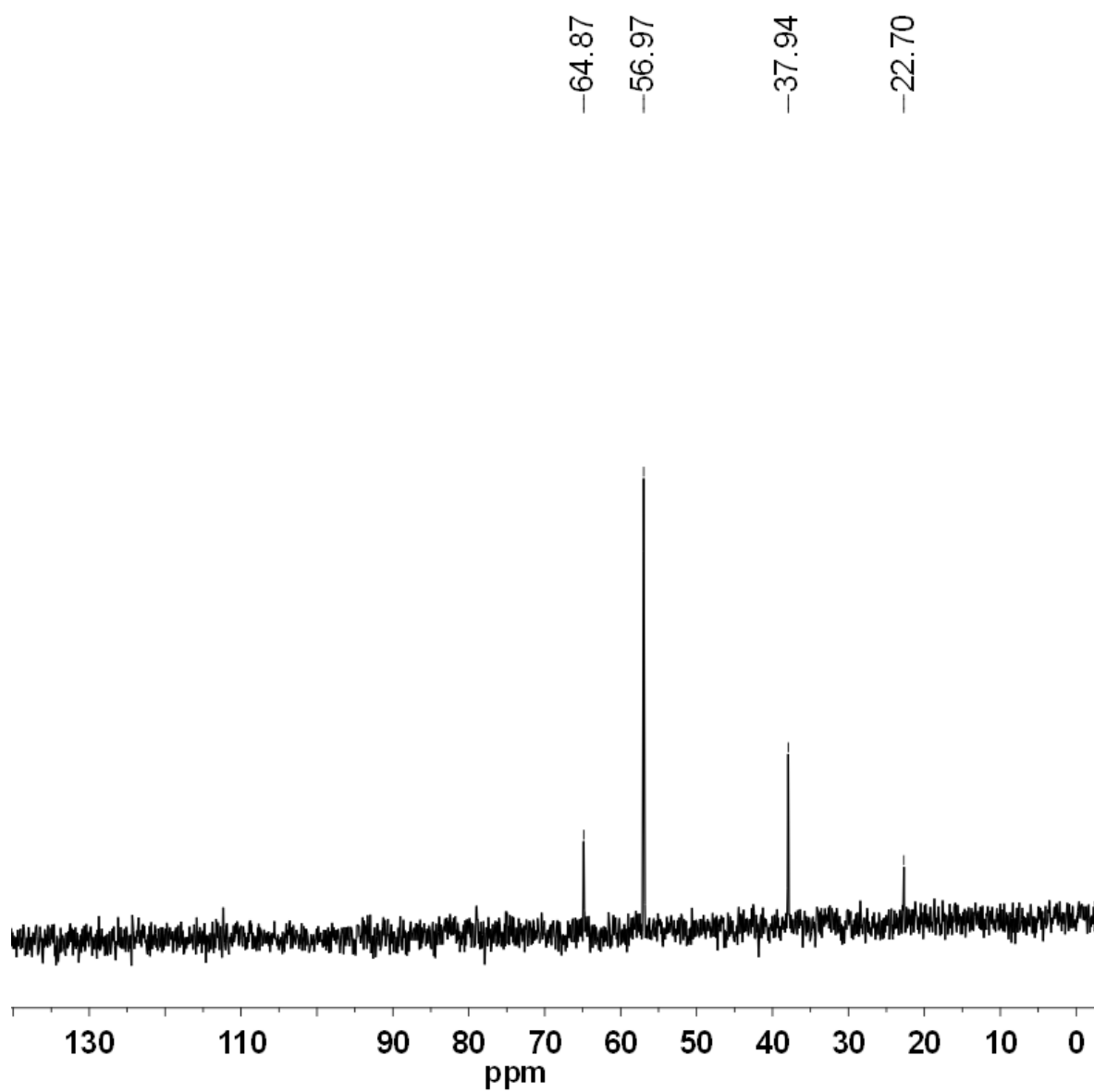
**Figure 3.S21.** The $^{13}$C-NMR (100 MHz) spectrum of [Ce(BTP)$_2$(NO$_3$)$_4$]·2H$_2$O was recorded on a Bruker Advance 400 MHz NMR spectrometer at 25 °C in D$_2$O . $^{13}$C-NMR (100 MHz, D$_2$O, 25 °C, ppm) 22.70; 37.94; 56.97; 64.87.

<div align="center">

**CHAPTER 4.**

**A REMARKABLE DNA PHOTOCLEAVING AGENT: A PHOTO-ACTIVATED**

**TRINUCLEAR CU(II) COMPLEX BASED ON HEXAAZATRIPHENYLENE**

</div>

(Dr. Antonio Lorente from the University of Alcalá performed the synthesis and characterization of the Cu(II) complex, and wrote the experimental section that pertained to the organic synthesis. The rest of the work was contributed by the author of the dissertation.)

## 4.1. Abstract

This paper describes the synthesis of a trinuclear Cu(II) complex based on 1,4,5,8,9,12-hexaazatriphenylene-hexacarboxylic acid and its interactions with double-helical DNA. Micromolar concentrations of the Cu(II) complex were able to produce at neutral pH and 37 °C double-stranded and single-stranded DNA photocleavage (350 nm).  After 50 min of irradiation, 1 μM of the complex reacted with 38 μM bp pUC19 plasmid to produce nicked and linear plasmid forms in 84 % and 14 % yields, respectively.  Scavenger and colorimetric assay experiments suggested the formation of Cu(I), superoxide anion radicals, hydrogen peroxide, and hydroxyl radicals in the photocleavage reactions.  Thermal denaturation and UV-vis absorption studies suggested that the Cu(II) complex binds to double-stranded DNA in a non-intercalative fashion.

## 4.2. Introduction

There is great interest in the design and synthesis of transition-metal complexes that bind to and cleave nucleic acids.



**Figure 4.1.** Structures of polyazaaromatic chelating ligands.

Particularly, the study of metal-complexes based on polyazaaromatic chelating ligands (Figure 4.1), such as dipyrido[3,2-d:2′,3′-f]quinoxaline (DPQ), 1,10-phenanthroline, and 1,4,5,8,9,12-hexaazatriphenylene (HAT), have played a major role in bioinorganic photochemical research.[1-19] These planar heterocyclic ligands have π-acceptor propert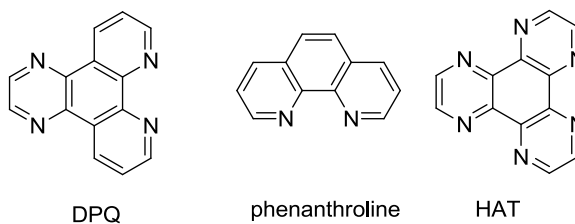ies and the potential to intercalate between DNA base pairs.[15] These types of photocleavage agents have potential applications and benefits in the areas of molecular biology, photodynamic therapy, and DNA photofootprinting.

Photocleavage by metal complexes can either target the deoxyribose or nucleobases of DNA.[2] There are a number of mechanisms that can account for photo-assisted DNA cleavage: (a) DNA base oxidation by singlet oxygen, (b) electron transfer from DNA bases to the excited state photosensitizer, (c) adduct formation between DNA bases and photosensitizer, and (d) hydrogen abstraction from deoxyribose by excited state photosensitizer and/or hydroxyl radical.[2] An example is the ruthenium complex $Ru(HAT)_3^{2+}$ photo-assisted electron transfer reaction from nucleobases to the excited metal complex ($^3$MLCT), performed single-stranded cleavage of plasmid DNA and also formed photo-adducts with guanine residues of oligonucleotides.[6,10] However, the lesser oxidation potential of the $^3$MLCT state of $Ru(phen)_3^{2+}$ provided less sufficient plasmid cleavage compared to the $Ru(HAT)_3^{2+}$, and photosensitized singlet oxygen was responsible for DNA base oxidation.[6,17,18] Another example is $Cu(DPQ)_2^{2+}$, was shown to convert supercoiled plasmid DNA into its nicked form under red light irradiation by the photosensitized generation of hydroxyl radicals.[19] Dhar et al. suggested a photo-induced process involving Cu(II)/Cu(I) redox cycle to generate the highly cytotoxic hydroxyl radicals from molecular oxygen for the cleavage of plasmid by the Cu(II) complex.[19]

Copper is an essential trace element in living organisms and is utilized by numerous enzymes for its redox activity. Copper(II) ions are closely associated with cellular DNA and

have a role in the regulation of gene expression.[20-22] *In vitro*, the metal has been shown to bind to the negatively charged oxygen of the phosphate backbone and form complexes with guanine and cytosine bases of DNA.[23] High cellular copper levels have been linked to cancer and tumor growth in humans through angiogenesis (the formation of new blood cells), and the proliferation and migration of endothelial cells.[24,25] In consideration of copper's biologically roles, copper-based DNA photonuclease agents are advantageous compared to complexes based on other metals.

Herein we report the study of an efficient photocleavage agent, a trinuclear Cu(II) complex based on a HAT derivative (**4**, Figure 4.2). The rationale behind the design of **4**, copper(II) has been utilized in photo-assisted DNA cleavage for the generation of highly cytotoxic reactive oxygen species, such as hydroxyl radicals and copper(I) peroxide, by the metal's Cu(II)/Cu(I) redox cycle.[15,19,26-28] Additionally, metal complexes of π-deficient HAT can provide photo-induced electron transfer reactions by abstracting electrons from DNA nucleobases.[10] We found that the Cu(II) complex is likely to non-intercalatively bind to DNA at low r values (r = [chromophore]/[DNA]) and gives rise to efficient double-stranded and single-stranded cleavage of pUC19 DNA in the presence of near-UV light (350 nm, 22 °C, and pH 7.0). Colorimetric assay and scavenger experiments pointed to Cu(I), and to hydrogen peroxide, superoxide, and hydroxyl radicals as the reactive oxygen species, generated in the photocleavage reactions.

## 4.3. Experimental

### 4.3.1. Materials and methods

Distilled, deionized water (ddH$_2$O) was utilized for the preparation of all buffers and aqueous solutions. Sodium phosphate dibasic salt, sodium phosphate monobasic salt, and EDTA

were acquired from Fisher Scientific.  Calf thymus DNA was obtained from Invitrogen (10

mg/mL).  PUC19 plasmid DNA was cloned from either XL-1 blue *E. coli* competent cells

(Strategene) or DH5-α competent cells according to a standard laboratory procedure.[29]  The

plasmid DNA was purified with a QIAGEN Plasmid Maxi Kit.  Sodium azide ≥ 99 %,

bathocuproinedisulfonic acid disodium salt hydrate, copper(II) chloride dihydrate ≥ 99 %,

sodium benzoate 99 %, and ethidium bromide 99 %, DMSO, catalase from bovine liver, and

superoxide dismutase from bovine erythrocytes were acquired from Sigma-Aldrich.

UV-visible analysis was recorded with a UV-2401PC Shimadzu spectrophotometer.

DNA thermal denaturation studies were performed using a Cary 300 Bio UV-visible

spectrophotometer fitted with a Cary temperature controller.  Photocleavage reactions were

performed in an aerobically ventilated Rayonet Photochemical Reactor fitted with ten RPR-3500

Å lamps (The Southern New England Ultraviolet Company).

### *4.3.2. Preparation of Cu(II) complex based on hexaazatriphenylenehexacarboxylate (4)*

The synthesis of sodium hexaazatriphenylenehexacarboxylate was performed by a

previously reported procedure.[30]  To a solution of sodium hexaazatriphenylenehexacarboxylate

(214 mg, 0.339 mmol) in water (70 mL), copper nitrate trihydrate (246 mg, 1.02 mmol) was

added.  After that, a dark precipitate was observed, which disappeared upon addition of

ethylenediamine (106 mg, 1.752 mmol). The reaction mixture was stirred at room temperature

for 96 h and then the solvent was evaporated under reduced pressure. The resulting residue was

treated with absolute ethanol (40 mL) and centrifuged. The solid thus obtained was washed with

ethanol (3x 10 mL), affording 448 mg (96% yield) of pure product. MP > 300 ºC. IR(KBr):

3310, 3218, 2360, 2341, 1610, 1383, 1043 $cm^{-1}$. ESI-TOF MS 697.66 $[(M+H+Na)^{2+}$, M =

$C_{24}H_{24}Cu_3N_{18}Na_6O_{30}$. Anal. Calcd. for $C_{24}H_{24}Cu_3N_{18}Na_6O_{30}\cdot H_2O$: C, 20.72; H, 1.88; N, 18.12. Found: C, 20.69; H, 2.02; N, 18.60.

### 4.3.3. Photocleavage of supercoiled plasmid DNA

In concentration titration experiments (40 µL total volume), 0.10, 0.25, 0.50, and 2 µM **4** were equilibrated with 38 µM bp pUC19 plasmid DNA and 10 mM sodium phosphate buffer pH 7.0. The reactions were irradiated for 50 min at 350 nm and 22 °C.

In time course experiments, a 40 µL total volume containing 10 mM sodium phosphate buffer and 38 µM bp of pUC19 plasmid DNA was irradiated in the presence and absence of 2 µM **4** at 350 nm and 22 °C for 0 min, 10 min, 20 min, 30 min, and 50 min. A parallel control reaction containing 10 mM sodium phosphate pH 7.0, 38 µM bp of pUC19, and 2 µM of Cu(II) complex was kept in the dark for 50 min.

After irradiation, 3 µL of electrophoresis loading buffer (15.0 % (w/v) Ficoll, 0.025 % (w/v) bromophenol blue) was transferred to each 40 µL reaction. A total of 20 µL of the cleavage reactions was loaded onto a 1.5 % nondenaturing agarose gel stained with ethidium bromide (0.5 µg/mL, final concentration) and electrophoresed at 160 V using 1 X TAE running buffer in an OWL A1 large gel system (Thermo Scientific). Gels were visualized on a transilluminator set at 302 nm and photographed. For the time course, concentration profile, radical scavenger, and $D_2O$ experiments, the gels were quantitated with Image Quant v. 5.0 software. The data obtained for supercoiled DNA were multiplied by a correction factor of 1.22 to account for the decreased binding affinity of ethidium bromide to supercoiled vs. nicked and linear plasmid forms.[31] Photocleavage yields were then calculated according to the following formula:

percent photocleavage = [(linear, nicked, or supercoiled DNA) / (linear + nicked + supercoiled DNA)] X 100.

### 4.3.4. Colorimetric detection of copper(I)

Reactions were prepared in a final volume of 600 μL in 10 mM sodium phosphate buffer pH 7.0, and contained 10 μM **4**, 10 μM **4** and 38 μM bp calf thymus DNA, 30 μM CuCl₂, 30 μM CuCl₂ and 38 μM bp calf thymus DNA, or 38 μM bp calf thymus DNA. As a positive control, 30 μM CuCl₂ and 30 μM *L*-ascorbic acid were utilized. The samples were irradiated at 350 nm for 30 min, while a set of parallel reactions was kept in the dark. Thereafter, bathocuproinedisulfonic acid disodium salt hydrate (42 μM final concentration) was added to each reaction and equilibrated in the dark for 30 min at 22 °C. The formation of Cu(I)-bathocuproine complex was then monitored by a UV-Vis spectrophotometer at 480 nm (scanned from 800 nm – 200 nm).

### 4.3.5. Chemically induced changes in DNA photocleavage

Reactions (40 μL total volume) containing 10 mM sodium phosphate buffer pH 7.0, 38 μM bp pUC19 plasmid DNA, 2 μM **4** (or 1 μM if noted) were irradiated at 350 nm for 30 min in the presence of either 100 U superoxide dismutase, 100 U catalase, 100 mM sodium benzoate, 100 mM sodium azide, 79 % v/v D₂O (1 μM **4**), 2 % v/v DMSO (1 μM **4**), or 100 mM EDTA. Reaction products were then resolved on a 1.5 % nondenaturing agarose gel and quantitated as described in section 4.3.2. The average % change in DNA photocleavage in the presence of radical scavengers, D₂O, and EDTA was calculated using the following formula:

percent photocleavage change (%) = [(% total of linear and nicked DNA$_{without\ reagent}$ - % total of linear and nicked DNA$_{with\ reagent}$)/(% total of linear and nicked DNA$_{without\ reagent}$)] X 100.

### *4.3.6. Thermal denaturation experiments*

Solutions (1.8 mL) in 10 mM sodium phosphate buffer pH 7.0 contained 19 μM bp DNA in the presence or absence of either 1 μM **4** or 3 μM CuCl$_2$.  The solutions (1.5 mL) were transferred to a 1.5 mL Starna quartz cuvette (1 cm) and allowed to equilibrate for 15 min at 22 °C.  The absorbance was then monitored at 260 nm as the temperature was increased from 25 °C to 100 °C at a rate of 0.5 °C min$^{-1}$.  KaleidaGraph (v. 4.0) was used to obtain the approximate first derivative of $\Delta A_{260}/\Delta T$ versus temperature.  The melting temperature ($T_m$) value was then indicated by the maximum of the first-derivative plot.

## 4.4. Results and Discussion

### *4.4.1. Synthesis of the Cu(II) Complex based on hexaazatriphenylenehexacarboxylate*
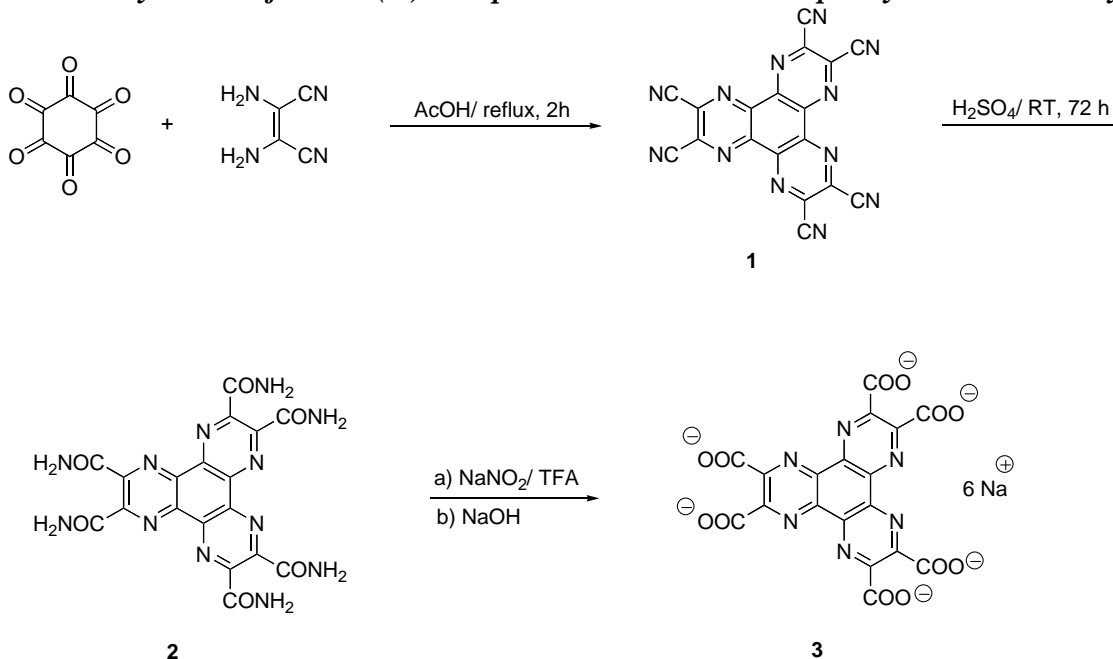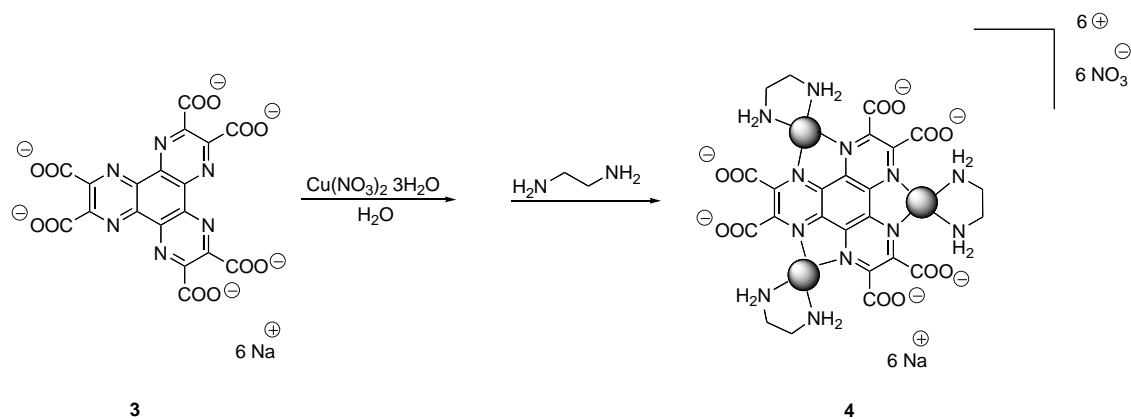
**Figure 4.2.** Scheme of the synthesis of hexaazatriphenylenehexacarboxylate **(3)** and Cu(II) complex **(4)**.

Synthesis of sodium hexaazatriphenylenehexacarboxylate (**3**) was performed by a previously reported procedure and is depicted in Figure 4.2.[30] Copper(II) complex **(4)** was then prepared by the addition of copper nitrate trihydrate (three equivalents) to an aqueous solution of sodium hexaazatriphenylenehexacarboxylate (**3**) at room temperature, and followed by further addition of five equiv of ethylenediamine.

### 4.4.2. Photocleavage of supercoiled plasmid DNA
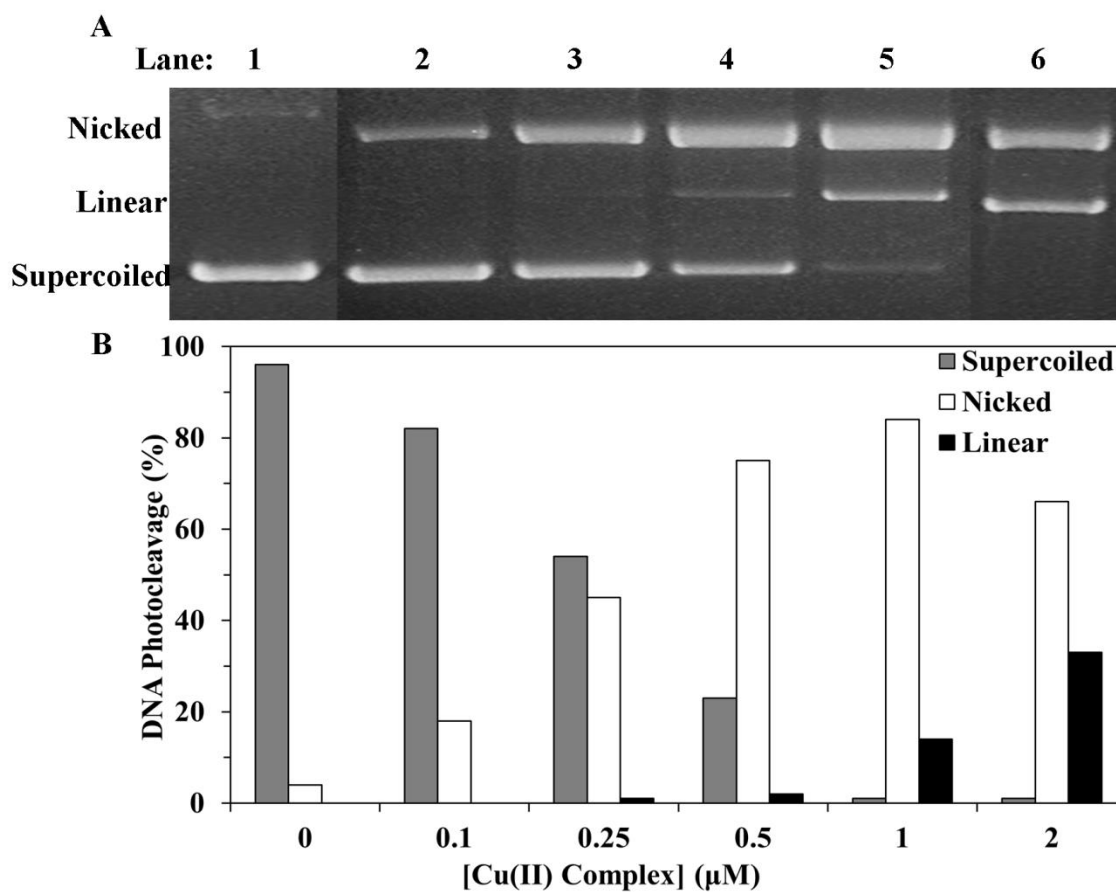


**Figure 4.3.** Photograph of 1.5 % nondenaturing agarose gel **(A)** and histogram **(B)** showing cleavage of 38 µM bp pUC19 DNA by 0, 0.1, 0.25, 0.5, 1, and 2 µM **4** irradiated at 350 nm for 50 min (22 °C and pH 7.0).
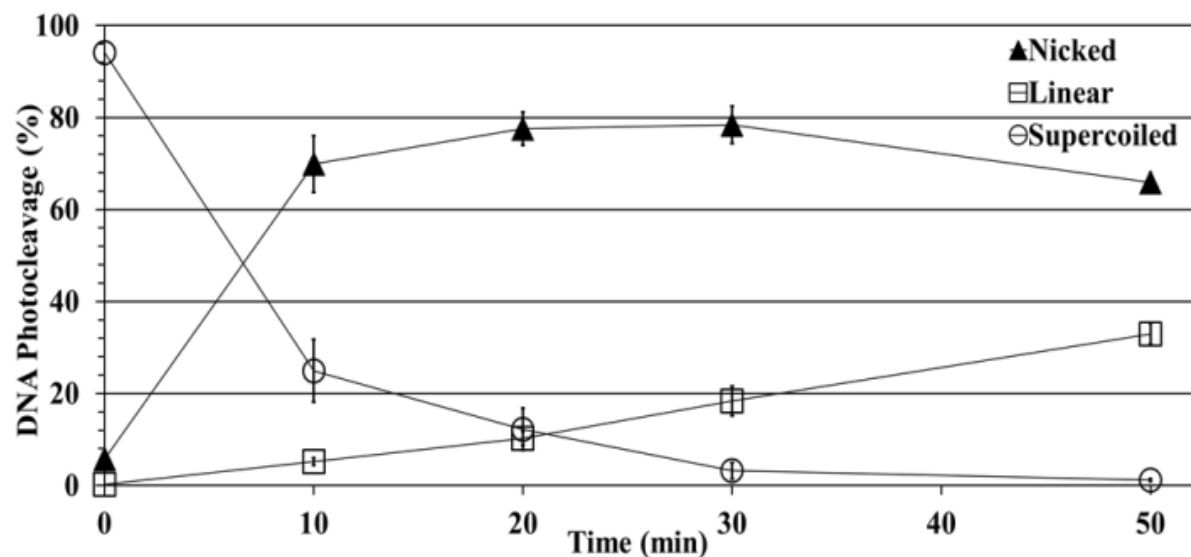
**Figure 4.4.** Photocleavage of 38 μM bp pUC19 plasmid DNA by 2 μM **4** irradiated at 350 nm for 0, 10, 20, 30, and 50 min (22 °C and pH 7.0). Data are averaged over three trials and error bars represent standard deviation. The corresponding time course gel is shown in Figure 4.S1.

To detect for single- or double-stranded DNA breaks, a preliminary concentration profile of **4** was conducted. Each individual reaction consisted of 38 μM bp pUC19 plasmid DNA in 10 mM sodium phosphate buffer pH 7.0 and 0 μM – 2 μM of **4**. The samples were irradiated for 50 min at 350 nm and 22 °C in an aerobically ventilated Rayonet Photochemical Reactor containing ten RPR-3500 Å lamps. After, the DNA photocleavage products were resolved on a 1.5 % nondenaturing agarose gel. The results of the profile displayed concentration dependent DNA photocleavage as the concentration of **4** was increased (Figure 4.3). After 50 min of irradiation, almost all of supercoiled plasmid DNA was converted into nicked and linear DNA products in the presence of 1 μM (84 % nicked and 14 % linear) and 2 μM (66 % nicked and 33 % linear) of **4**.

DNA photocleavage as a function of time was studied next. Each individual reaction contained 10 mM sodium phosphate buffer pH 7.0, 38 μM bp pUC19 plasmid DNA, and 2 μM of **4**. Parallel negative control reactions were performed with 38 μM pUC19 plasmid DNA and 10 mM sodium phosphate pH 7.0. The reactions were conducted as described above, except that

individual reactions were removed at 0 min, 10 min, 20 min, 30 min, and 50 min irradiation intervals. Time-dependent DNA photocleavage by **4** was observed (Figure 4.4). Nicked DNA production reached a plateau between 20 and 30 min, and thereafter, decreased from 78 % to 66 % at the 50 min irradiation time. The decreased in nicked DNA production is accompanied with an increase in linear DNA products (33 % linear after 50 min irradiation). The linear DNA photocleavage product is clearly shown after just 10 min (5 % linear product) of irradiation at 350 nm. A plot of linear DNA production as a function of time gives a straight line with a slope of 0.630. No DNA photocleavage products were present when DNA was irradiated in the absence of **4** (50 min at 350 nm) and parallel dark controls with 2 μM of **4** (50 min, no *hv*) (Supporting information, Figure 4.S1).

### 4.4.3. Colorimetric Detection of Copper(I)

Our next goal was to obtain experimental evidence that would substantiate a photo-induced process involving Cu(II)/Cu(I) redox cycle to cleave the plasmid DNA. The photoreduction of Cu(II) to Cu(I) could participate in a Fenton-type reaction to generate DNA damaging reactive oxygen species free hydroxyl radicals[19,32] or a Cu(I)-peroxide complex[26-28]. We utilized a colorimetric assay based on bathocuproinedisulfonic acid disodium salt hydrate (BCS) which forms a 2:1, orange colored complex with Cu(I) ($\lambda_{max}$ = 480 nm; ε = 13 500 $M^{-1}$ $cm^{-1}$).[26,33] Individual reactions consisted of 10 mM sodium phosphate buffer pH 7.0 in the presence of either 10 μM **4**, 10 μM **4** and 38 μM bp calf thymus (CT) DNA, 30 μM $CuCl_2$, 30 μM $CuCl_2$ and 38 μM bp CT DNA, or 38 μM bp CT DNA. Controls containing either 30 μM $CuCl_2$, or 30 μM $CuCl_2$ and 30 μM L-ascorbic acid were run in parallel. Reactions carried out in the dark were used as negative controls. After 30 min of irradiation at 350 nm, BCS (42 μM

final concentration) was added.  The reactions were then equilibrated in the dark for 30 min and

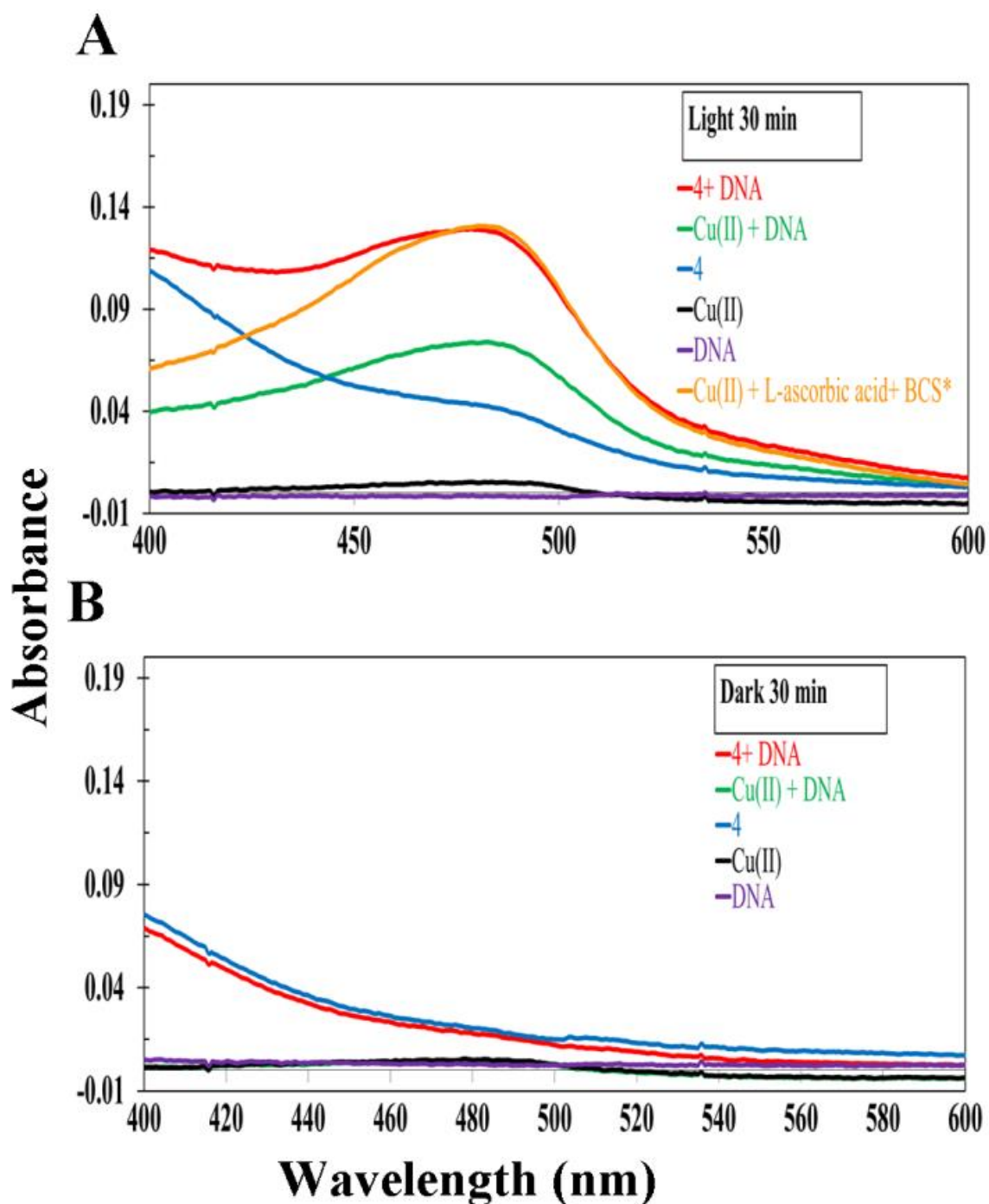analyzed by UV-visible spectrophotometry.



**Figure 4.5.** UV-visible spectra of Cu(I)-BCS complex formation in 10 mM sodium phosphate buffer pH 7.0 (22 °C).  Reactions were either irradiated at 350 nm or treated with *L*-ascorbic acid* **(A)** or kept in the dark **(B)** for 30 min.  BCS (42 µM final concentration) was added and equilibrated for 30 min prior to UV-visible analysis. Cu(II) = $CuCl_2$.

As expected, the addition of BCS to CuCl$_2$ and the reducing agent L-ascorbic acid produced a bright orange signature 480 nm absorption band corresponding to the Cu(I)-BCS complex.[26,33] No Cu(I) was detected in any of the dark DNA reactions (Figure 4.5, **B**) or reactions where BCS was omitted (Supporting information, Figure 4.S6). The reactions irradiated in the presence of **4** and DNA, CuCl$_2$ and DNA, and the **4** displayed a Cu(I)-BCS absorption (Figure 4.5, A). Out of the three mentioned, irradiation of DNA in the presence of **4** produced the most Cu(I), with a BCS spectrum similar in appearance to the positive control Cu(II) and L-ascorbic acid. Lower levels of Cu(I)-BCS absorption were observed for CuCl$_2$ in the presence of DNA and followed by **4** in the absence of DNA.

The BCS data collectively indicate that DNA and **4** are independently capable of sensitizing the one electron photoreduction of Cu(II) to Cu(I). These observations are consistent with one-electron transfer reactions in which DNA and **4** both act as electron donors upon irradiation with 350 nm of light. The photocleavage agent **4** is a less effective electron donor compared to DNA under these experimental conditions. The latter result is contrary to 419 nm sensitized photoreduction in which reduction of Cu(II) was assigned entirely to the pyridine bound copper(II) complex. The opposing trend can be explained by the fact that the 350 nm Rayonet lamps overlap with DNA absorption, whereas the 419 nm lamps do not. Rongoni et al. reported the photoreduction of Cu(II) to Cu(I) in the presence of DNA when irradiated with 310 nm light.[34] Thus, the photoreduction of the Cu(II) is facilitated by a one-electron transfer from DNA to produce Cu(I) and a DNA radical. Thereafter, the reaction of Cu(I) and O$_2$ would be expected to generate DNA cleaving reactive oxygen species, such as a Cu(I)-peroxide complex or freely diffusible hydroxyl radicals.[27,28,33,35,36] Interestingly compared to **4**, only minimal levels of DNA photocleavage were produced upon irradiation of 30 µM CuCl$_2$ at 350 nm for 30 min

(Supporting information, Figure 4.S5). Therefore, the high DNA photocleavage yields (Figure 4.3 and 4.4) and higher levels of Cu(I) production (**A**, Figure 4.5) by **4** compared to $CuCl_2$ show that the ligand hexaazatriphenylenehexacarboxylate plays a major role in DNA photocleavage, perhaps by bringing more Cu(I) in close proximity to DNA. This would enable the reactive oxygen species produced by Cu(I) to react with DNA before being quenched by solvent, and would therefore enhance DNA cleavage efficiency.[33]

### 4.4.4. Chemically induced changes in DNA photocleavage

**Table 4.1.** Average % change of DNA photocleavage by scavengers, $D_2O$, and EDTA

| Scavengers/chelator | Species targeted | Photocleavage change (%)[a] |
|---|---|---|
| EDTA (100 mM) | Cu(II) | - 90 ± 2 |
| Sodium azide (100 mM) | $^1O_2$ | - 89 ± 2 |
| DMSO (2 % v/v) | •OH | - 71 ± 7 |
| Catalase (100 U) | $H_2O_2$ | - 69 ± 3 |
| Sodium benzoate (100 mM) | •OH | - 58 ± 8 |
| SOD (100 U) | $O_2^{•-}$ | - 39 ± 2 |
| $D_2O$ (79 % v/v) | $^1O_2$ | - 5 ± 1 |

Photographs are located in Supporting Information. Figures 4.S2 and 4.S3.
[a]Average percent change data were averaged over three trials and error is reported as standard deviation

To further investigate the mechanism underlying DNA photocleavage by **4**, we examined chemically induced changes in DNA photocleavage. Individual reactions consisted of 38 μM bp of CT DNA, 2 μM **4**, and 10 mM sodium phosphate buffer pH 7.0. Reaction were preequilibrated with either the singlet oxygen ($^1O_2$) scavenger sodium azide, the hydroxyl radical (•OH) scavengers sodium benzoate and 2 % v/v DMSO, the hydrogen peroxide ($H_2O_2$) scavenger catalase, the superoxide ($O_2^{•-}$) scavenger superoxide dismutase (SOD), or the metal chelating agent EDTA (Table 4.1). From examination of average percent change in

photocleavage induced by the addition of the reagents, it is evident that sodium azide and EDTA blocked single- and double-strand break formation almost completely, followed by DMSO, catalase, and then sodium benzoate (from highest to lowest). Intermediate levels of inhibition by SOD were observed for DNA photocleavage. However, SOD produces a contributing species ($H_2O_2$) to the Cu(II)/Cu(I) redox cycling system that may lower inhibition of photocleavage by this enzyme.

Contrary to the strong inhibitory effect by the singlet oxygen scavenger sodium azide, replacing $ddH_2O$ with $D_2O$, which increases the lifetime of singlet oxygen, had relatively no effect on DNA photocleavage yields (Table 4.1). In this study sodium azide presented similar inhibition levels compared to the chelator EDTA, and other studies have shown azide anion binds to copper to form a Cu(II)-$N^{3-}$ complex at ~ pH 7 that inhibits copper-containing amine oxidases.[37,38] Thus, the involvement of singlet oxygen as a reactive oxygen species in the DNA photocleavage reaction by **4** is not supported by the $D_2O$ data shown in this present paper.

The inhibitory effects of catalase, SOD, DMSO, and of the chelating agent EDTA collectively indicate that hydrogen peroxide, superoxide and hydroxyl radicals, and metal ions participate in the DNA photocleavage reactions by **4**. Our results suggest that freely diffusible hydroxyl radicals are key contributing species in DNA cleavage by the Cu(II)/Cu(I) redox system (Figure 4.6) and not a Cu(I)-peroxide species. Hydroxyl radicals are highly cytotoxic reactive oxygen species toward DNA cleavage which involves non-selective abstraction of hydrogen atoms from the deoxyribose of DNA.[39,40]

$$Cu(I) + O_2 \longrightarrow Cu(II) + O_2^{\bullet-}$$

$$O_2^{\bullet-} + H^+ \longrightarrow HO\text{-}O^\bullet \xrightarrow{e^-} \xrightarrow{H^+} H_2O_2$$

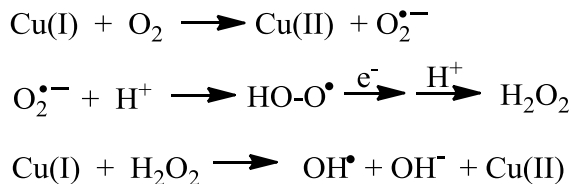$$Cu(I) + H_2O_2 \longrightarrow OH^\bullet + OH^- + Cu(II)$$

**Figure 4.6.** Proposed mechanism for the generation of hydroxyl radicals by the photo-assisted Cu(II)/Cu(I) redox cycle.

Superoxide radical and hydrogen peroxide are relatively unreactive toward DNA.[39] The

formation of the reactive oxygen species Cu(I)-peroxide follows the same steps shown in Figure

4.6, except the reaction of Cu(I) and hydrogen peroxide leads to the formation of a Cu(I)-

peroxide complex. Cooper(I)-peroxide formation in chemical- or photo-assisted Cu(II)/Cu(I)

redox cycles is typically ruled out by utilizing hydroxyl radical scavengers, such as the sodium

benzoate and DMSO reagents used in our inhibition studies, which does not affect the generation

of Cu(I)-peroxide in cleavage reactions.[19,26-28]

To account for strong DNA photocleavage inhibition in the presence of hydroxyl radical

scavengers 2 % v/v DMSO and sodium benzoate, we considered the possible interference from

trace levels of redox active iron in the reactions.

$$Fe(II) + H_2O_2 \longrightarrow OH^\bullet + OH^- + Fe(III)$$
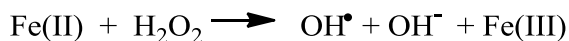
**Figure 4.7.** Mechanism of the formation of DNA damaging hydroxyl radicals by the Fenton reaction between iron metal ion and hydrogen peroxide.

Iron metal ions are known to produce hydroxyl radicals by the mechanism shown in Figure 4.7.[27]

The Fe(III) could be attracted to the carboxylates of 4, and then could assist in the production of

reactive oxygen species in close proximity to DNA by a Fe(III)/Fe(II) redox cycle. To test for

the possibility of trace metal ions in our laboratory solution contributing to photocleavage,

doubly distilled water and buffers were run through a chelex resin to remove interfering redox

metals and then tested against reactions containing unchelexed ddH$_2$O and buffer. The latter experiment showed no difference in the photocleavage reactions by **4**.

Thus, with the exclusion of photo-assisted Fenton reaction involving iron, it is conceivable that the hydroxyl radical species responsible for DNA cleavage could be contributed from a Fenton reaction catalyzed by copper shown in Figure 4.6. Therefore, it is conceivable that Cu(II) bound to hexaazatriphenylenehexacarboxylate may reduce to Cu(I), involving photo-assisted electron transfer from photo-excited DNA and HAT ligand to Cu(II). The formation of Cu(I) would catalyze the formation of superoxide radical from molecular oxygen which then dismutates to hydrogen peroxide. Thereafter, Cu(I) and hydrogen peroxide undergoes a Fenton reaction to produce diffusible hydroxyl radicals, and hydroxyl anion and Cu(II).

### 4.4.5. UV-visible absorption titration



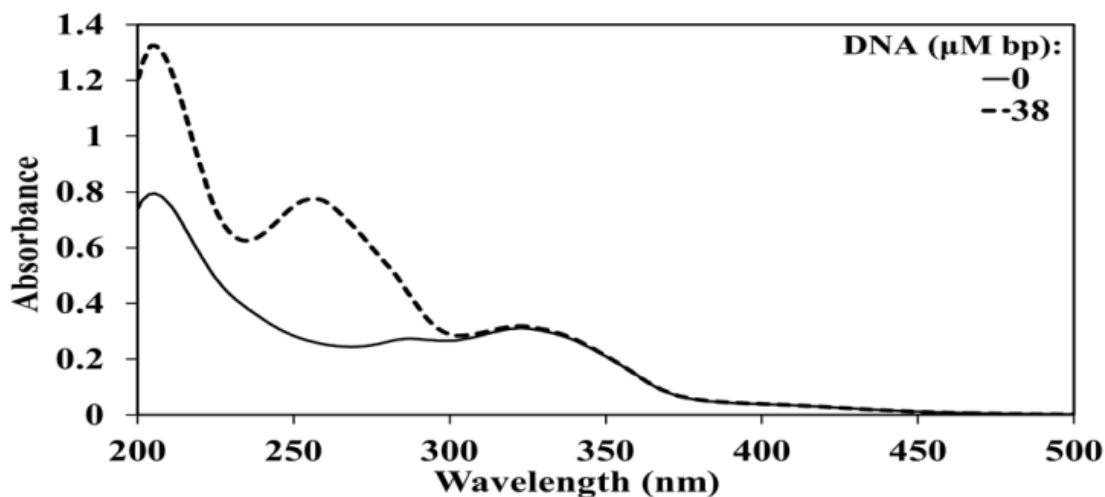**Figure 4.8.** UV-visible absorption spectra of 8 μM **4** in 10 mM sodium phosphate buffer pH 7.0 monitored in the presence and absence of 38 μM bp CT DNA. The absorption spectrum was corrected for sample dilution.

From an examination of **4**, there is a low probability of DNA intercalation involving π-π stacking interactions between the hexaazatriphenylene ring of the complex and DNA base pairs.

Intercalation would be expected to be sterically hindered by the free carboxylates and ethylenediamines bound to each Cu(II). These structural features might also inhibit DNA minor groove binding which is favored by unhindered aromatic ring systems that can make close van der Waals contacts with the walls of the groove. Major groove binding or external binding of the complex with DNA are more probable scenarios, especially if sodium cations in the reaction buffer aid in neutralizing the negatively charged carboxylates. UV-visible analysis was performed in order to screen for these binding modes (Figure 4.8). Bathochromic and hypochromic wavelength shifts are characteristics of electronic spectra of some groove binders and intercalators of DNA. Thus, UV-vis spectrophotometry was utilized to monitor the spectra of 8 μM **4** in 10 mM sodium phosphate buffer pH 7.0 as a function of CT DNA concentrations ranging from 0 μM bp – 304 μM bp (22 °C). Figure 4.9 shows the absorption spectra of 8 μM **4** in the presence and absence of 38 μM bp CT DNA. The chromophore has an absorption maximum at 324 nm. The wavelength and intensity of **4** were unchanged, even after CT DNA concentration was increased to 304 μM bp (Supporting Information Figure 4.S4). These results suggest that the Cu(II) complex may associate with DNA by external interactions.
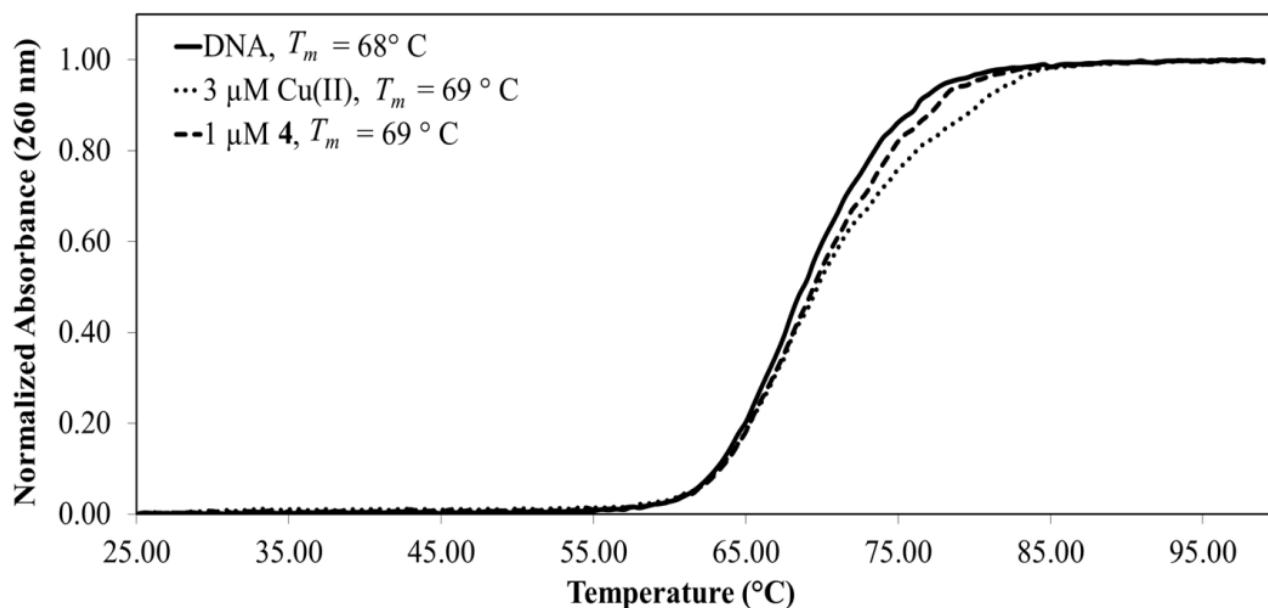
### 4.4.6. Thermal melting studies



**Figure 4.9.** Normalized thermal melting curves of 19 µM bp CT DNA in the absence and presence of 3 µM of CuCl$_2$ (Cu(II)) or 1 µM of **4** (22 °C, pH 7.0).

DNA melting temperature ($T_m$) trends can provide important information on ligand-DNA interactions.[41] Ligands that interact with DNA by intercalation or groove binding, or externally can increase the $T_m$ of DNA by stabilizing the DNA duplex.[18,26,31,41-43] Compared to intercalating ligands which often produce considerable increases in DNA melting temperature, externally bound ligands increase $T_m$ values to a lesser extent.[18] Thus to confirm the binding mode of **4** to DNA, melting temperature curves of 19 µM bp CT DNA in 10 mM sodium phosphate buffer pH 7.0 in the presence and absence of 3 µM of CuCl$_2$ or 1 µM of **4** were recorded (Figure 4.9). The addition of 1 µM **4** to 19 µM bp CT DNA, the same r value (r = [chromophores]/[DNA bp]) of 0.05 as the photocleavage reactions in Figure 4.4, increased the $T_m$ of DNA from 68 °C to 69. °C. The $T_m$ increase of DNA by 1 µM **4** is the same compared to the $T_m$ change of DNA in the presence of 3 µM of CuCl$_2$. The increase of DNA $T_m$ by CuCl$_2$ is conceivable since the

interactions of the metal ion with the negatively charged oxygen of the phosphate backbone and its ability to form complexes with guanine and cytosine bases of DNA can enhance stabilization of the DNA duplex.[23] In their study of DNA binding modes, Kelly et al. observed a small, $< 2 \, °$C, $T_m$ increase for poly[d(A-T)] DNA by ruthenium complexes based on 2,2'-bipyridyl and 2,2',2''-terpyridyl, and suggested that the complexes externally bind to DNA. Whereas in the same study, an intercalating ruthenium complex presented a 5 °C $T_m$ increase at the same r value (0.05).[18] Thus, the similar DNA $T_m$ in the presence of $CuCl_2$ and the small magnitude of the $T_m$ change by **4** suggest that the photocleavage agent binds to DNA in a non-intercalative fashion that may involve external binding.

While the precise nature of the DNA binding mode of **4** awaits confirmation by high resolution structural analysis, the UV-visible, melting temperature and photocleavage results point to the possibility of external DNA interactions. High levels of plasmid DNA photocleavage were attained using micromolar concentrations of **4** (Figure 4.3 and 4.4). When bound externally, chromophores have more access to oxygen and as a result can generate DNA damaging reactive oxygen species more efficiently compared to intercalated and groove bound chromophores.[31,44] External interactions of **4** with DNA may be favored by the negative steric interaction of the carboxylate and ethylenediamine groups of the complex with the base pairs and grooves of DNA.

## 4.5. Conclusions

In summary, here we report the synthesis of a trinuclear Cu(II) complex based on hexaazatriphenylenehexacarboxylate. Irradiation of micromolar concentrations of **4** at 350 nm provided high levels of DNA photocleavage under near-physiological conditions of temperature and pH (22 °C and pH 7.0). Although the exact mechanism of the photocleavage reaction is not

yet fully understood, at this time we believe that the formation of single-stranded and double-stranded DNA breaks may involve external binding of the chromophore to DNA. This efficiently promotes a type I photodynamic reaction mechanism in which Cu(II) is photoreduced to Cu(I), with the ligand and DNA as electron donors. We propose that Cu(I) reacts with ground state triplet oxygen to generate superoxide. Thereafter, the superoxide radicals undergo a Fenton reaction to produce diffusible, DNA damaging hydroxyl radicals. In conclusion, the utilization of copper-based photonucleases is of considerable interest because of the bioavailability of copper at the cellular level. Our future work will focus on the development of new copper photonucleases that absorbs at low-energy light (600 nm – 800 nm).

## 4.6. References

(1)  Armaroli, N., Photoactive mono- and polynuclear Cu(I)-phenanthrolines. A viable alternative to Ru(II)-polypyridines? *Chem. Soc. Rev.* **2001,** *30*, 113.

(2)  Armitage, B., Photocleavage of Nucleic Acids. *Chem. Rev.* **1998,** *98*, 1171.

(3)  Blasius, R.; Moucheron, C.; Kirsch-De Mesmaeker, A., Photoadducts of metallic compounds with nucleic acids - role played by the photoelectron transfer process and by the TAP and HAT ligands in the RuII complexes. *Eur. J. Inorg. Chem.* **2004**, 3971.

(4)  Chelucci, G.; Thummel, R. P., Chiral 2,2'-Bipyridines, 1,10-Phenanthrolines, and 2,2':6',2''-Terpyridines: Syntheses and Applications in Asymmetric Homogeneous Catalysis. *Chem. Rev.* **2002,** *102*, 3129.

(5)  Dhar, S.; Senapati, D.; Das, P. K.; Chattopadhyay, P.; Nethaji, M.; Chakravarty, A. R., Ternary Copper Complexes for Photocleavage of DNA by Red Light: Direct Evidence for Sulfur-to-Copper Charge Transfer and d-d Band Involvement. *J. Am. Chem. Soc.* **2003,** *125*, 12118.

(6)  Elias, B.; Kirsch-De Mesmaeker, A., Photo-reduction of polyazaaromatic Ru(II) complexes by biomolecules and possible applications. *Coord. Chem. Rev.* **2006,** *250*, 1627.

(7)  Goswami, T. K.; Chakravarthi, B. V. S. K.; Roy, M.; Karande, A. A.; Chakravarty, A. R., Ferrocene-Conjugated l-Tryptophan Copper(II) Complexes of Phenanthroline Bases Showing DNA Photocleavage Activity and Cytotoxicity. *Inorg. Chem.* **2011,** *50*, 8452.

(8)  Gude, L.; Fernandez, M.-J.; Grant, K. B.; Lorente, A., Syntheses and copper(ii)-dependent DNA photocleavage by acridine and anthracene 1,10-phenanthroline conjugate systems. *Org. Biomol. Chem.* **2005,** *3*, 1856.

(9)  Kirsch-De Mesmaeker, A.; Orellana, G.; Barton, J. K.; Turro, N. J., Ligand-dependent interaction of ruthenium(II) polypyridyl complexes with DNA probed by emission spectroscopy. *Photochem. Photobiol.* **1990,** *52*, 461.

(10)  Lecomte, J.-P.; Kirsch-De Mesmaeker, A.; Feeney, M. M.; Kelly, J. M., Ruthenium(II) Complexes with 1,4,5,8,9,12-Hexaazatriphenylene and 1,4,5,8-Tetraazaphenanthrene Ligands: Key Role Played by the Photoelectron Transfer in DNA Cleavage and Adduct Formation. *Inorg. Chem.* **1995,** *34*, 6481.

(11)  McMilllin, D. R.; McNett, K. M., Photoprocesses of Copper Complexes That Bind to DNA. *Chem. Rev.* **1998,** *98*, 1201.

(12)  Moucheron, C.; Kirsch-De Mesmaeker, A.; Choua, S., Photophysics of Ru(phen)$_2$(PHEHAT)$^{2+}$: A Novel "Light Switch" for DNA and Photo-oxidant for Mononucleotides. *Inorg. Chem.* **1997,** *36*, 584.

(13)  Rutherford, T. J.; Van Gijte, O.; Kirsch-De Mesmaeker, A.; Keene, F. R., Stereoisomers of Mono-, Di-, and Triruthenium(II) Complexes Containing the Bridging Ligand 1,4,5,8,9,12-

Hexaazatriphenylene and Studies of Their Photophysical Properties. *Inorg. Chem.* **1997,** *36*, 4465.

(14) Sammes, P. G.; Yahioglu, G., 1,10-Phenanthroline: a versatile ligand. *Chem. Soc. Rev.* **1994,** *23*, 327.

(15) Szacilowski, K.; Macyk, W.; Drzewiecka-Matuszek, A.; Brindell, M.; Stochel, G., Bioinorganic Photochemistry: Frontiers and Mechanisms. *Chem. Rev.* **2005,** *105*, 2647.

(16) Tossi, A. B.; Kelly, J. M., A study of some polypyridylruthenium(II) complexes as DNA binders and photocleavage reagents. *Photochem. Photobiol.* **1989,** *49*, 545.

(17) Fleisher, M. B.; Waterman, K. C.; Turro, N. J.; Barton, J. K., Light-induced cleavage of DNA by metal complexes. *Inorg. Chem.* **1986,** *25*, 3549.

(18) Kelly, J. M.; Tossi, A. B.; McConnell, D. J.; OhUigin, C., A study of the interactions of some polypyridylruthenium(II) complexes with DNA using fluorescence spectroscopy, topoisomerization and thermal denaturation. *Nucleic Acids Res.* **1985,** *13*, 6017.

(19) Dhar, S.; Senapati, D.; Reddy, P. A. N.; Das, P. K.; Chakravarty, A. R., Metal-assisted red light-induced efficient DNA cleavage by dipyridoquinoxaline-copper(ii) complex. *Chem. Commun.* **2003**, 2452.

(20) Fuerst, P.; Hamer, D., Cooperative activation of a eukaryotic transcription factor: interaction between copper(I) and yeast ACE1 protein. *Proc. Natl. Acad. Sci. U. S. A.* **1989,** *86*, 5267.

(21) Schumann, K.; Classen, H. G.; Dieter, H. H.; Konig, J.; Multhaup, G.; Rukgauer, M.; Summer, K. H.; Bernhardt, J.; Biesalski, H. K., Hohenheim consensus workshop: copper. *Eur. J. Clin. Nutr.* **2002,** *56*, 469.

(22) Thiele, D. J., Metal-regulated transcription in eukaryotes. *Nucleic Acids Res.* **1992,** *20*, 1183.

(23) Zimmer, C.; Luck, G.; Fritzsche, H.; Triebel, H., DNA-copper(II) complex and the DNA conformation. *Biopolymers* **1971,** *10*, 441.

(24) Goodman, V. L.; Brewer, G. J.; Merajver, S. D., Copper deficiency as an anti-cancer strategy. *Endocr. Relat. Cancer* **2004,** *11*, 255.

(25) Nasulewicz, A.; Mazur, A.; Opolski, A., Role of copper in tumor angiogenesis - clinical implications. *J. Trace Elem. Med. Biol.* **2004,** *18*, 1.

(26) Fernandez, M.-J.; Wilson, B.; Palacios, M.; Rodrigo, M.-M.; Grant, K. B.; Lorente, A., Copper-Activated DNA Photocleavage by a Pyridine-Linked Bis-Acridine Intercalator. *Bioconjugate Chem.* **2007,** *18*, 121.

(27) Oikawa, S.; Kawanishi, S., Distinct mechanisms of site-specific DNA damage induced by endogenous reductants in the presence of iron(III) and copper(II). *Biochim. Biophys. Acta, Gene Struct. Expression* **1998,** *1399*, 19.

(28) Yamamoto, K.; Kawanishi, S., Hydroxyl free radical is not the main active species in site-specific DNA damage induced by copper(II) ion and hydrogen peroxide. *J. Biol. Chem.* **1989,** *264*, 15435.

(29) Sambrook, J. F., F. E.; Maniatis, T. *Molecular Cloning, A Laboratory Manual*; 2nd ed.; Cold Spring Harbor Press: New York, 1989.

(30) Kanakarajan, K.; Czarnik, A. W., Synthesis and some reactions of hexaazatriphenylenehexanitrile, a hydrogen-free polyfunctional heterocycle with D3h symmetry. *J. Org. Chem.* **1986,** *51*, 5241.

(31)  Terry, C. A.; Fernandez, M.-J.; Gude, L.; Lorente, A.; Grant, K. B., Physiologically Relevant Concentrations of NaCl and KCl Increase DNA Photocleavage by an N-Substituted 9-Aminomethylanthracene Dye. *Biochemistry* **2011,** *50*, 10375.

(32)  Flowers, L.; Ohnishi, S. T.; Penning, T. M., DNA Strand Scission by Polycyclic Aromatic Hydrocarbon o-Quinones: Role of Reactive Oxygen Species, Cu(II)/Cu(I) Redox Cycling, and o-Semiquinone Anion Radicals. *Biochemistry* **1997,** *36*, 8640.

(33)  Wong, A.; Huang, C. H.; Crooke, S. T., The mechanism of deoxyribonucleic acid breakage induced by 4'-(9-acridinylamino)methanesulfon-m-anisidine and copper: role for cuprous ion and oxygen free radicals. *Biochemistry* **1984,** *23*, 2946.

(34)  Rongoni, E.; Scafati, A.; Matzeu, M.; Belli, M.; Onori, G.; Reale, A.; Balerna, A.; Bianconi, A.; Bernieri, E., UV-induced reduction of Cu(II) in DNA complex studied by Cu-K-edge XANES. *Biopolymers* **1986,** *25*, 217.

(35)  Li, Y.; Kuppusamy, P.; Zweier, J. L.; Trush, M. A., ESR evidence for the generation of reactive oxygen species from the copper-mediated oxidation of the benzene metabolite, hydroquinone: role in DNA damage. *Chem. Biol. Interact.* **1995,** *94*, 101.

(36)  Sinha, B. K.; Leinisch, F.; Bhattacharjee, S.; Mason, R. P., DNA Cleavage and Detection of DNA Radicals Formed from Hydralazine and Copper(II) by ESR and Immuno-Spin Trapping. *Chem. Res. Toxicol.* **2014,** *27*, 674.

(37)  Juda, G. A.; Shepard, E. M.; Elmore, B. O.; Dooley, D. M., A Comparative Study of the Binding and Inhibition of Four Copper-Containing Amine Oxidases by Azide: Implications for the Role of Copper during the Oxidative Half-Reaction. *Biochemistry* **2006,** *45*, 8788.

(38)  Schwartz, B.; Olgin, A. K.; Klinman, J. P., The Role of Copper in Topa Quinone

Biogenesis and Catalysis, as Probed by Azide Inhibition of a Copper Amine Oxidase from Yeast.

*Biochemistry* **2001,** *40*, 2954.

(39)  Cadet, J.; Delatour, T.; Douki, T.; Gasparutto, D.; Pouget, E.-P.; Ravanat, J.-L.; Sauvaigo,

S., Hydroxyl radicals and DNA base damage. *Mutat. Res., Fundam. Mol. Mech. Mutagen.* **1999,**

*424*, 9.

(40)  Paillous, N.; Vicendo, P., Mechanisms of photosensitized DNA cleavage. *J. Photochem.

Photobiol., B* **1993,** *20*, 203.

(41)  Wison, W. D. T., A. F.; Fernandez-Saiz, M.; Rigl, C. T. *Evaluation of Drug-Nucleic

Interactions by Thermal Melting*; Humana Press: Totowa, 1997; Vol. 90.

(42)  Wilson, B.; Fernandez, M.-J.; Lorente, A.; Grant, K. B., Synthesis and DNA interactions of

a bis-phenothiazinium photosensitizer. *Org. Biomol. Chem.* **2008,** *6*, 4026.

(43)  Wilson, B.; Gude, L.; Fernandez, M.-J.; Lorente, A.; Grant, K. B., Tunable DNA

Photocleavage by an Acridine-Imidazole Conjugate. *Inorg. Chem.* **2005,** *44*, 6159.

(44)  Akerman, B.; Tuite, E., Single- and double-strand photocleavage of DNA by YO, YOYO

and TOTO. *Nucleic Acids Res.* **1996,** *24*, 1080.

## 4.7. Supporting Information
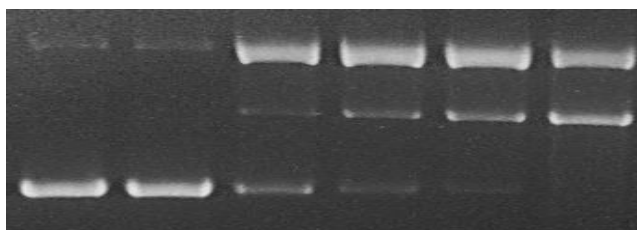
| Lane: | 1 | 2 | 3 | 4 | 5 | 6 |
|---|---|---|---|---|---|---|



| | 1 | 2 | 3 | 4 | 5 | 6 |
|---|---|---|---|---|---|---|
| Irradiation time (min) | 50 | 0 | 10 | 20 | 30 | 50 |
| **4** | – | + | + | + | + | + |
| % N | 4 | 6 | 70 | 78 | 78 | 66 |
| % L | 0 | 0 | 5 | 10 | 18 | 33 |
| % S | 96 | 94 | 25 | 12 | 3 | 1 |

**Figure 4.S1.** Photograph of 1.5 % nondenaturing agarose gel showing photocleavage of pUC19 plasmid DNA (38 µM bp).  Time course experiment in the presence and absence of  2 µM **4** irradiated at 350 nm and 22 °C for 0 min, 10 min, 20 min, 30 min, and 50 min. Only 50 minute irradiation of pUC19 plasmid DNA was performed for the reaction containing no photocleavage agent. **N** = nicked, **L** = linear, and **S** = supercoiled.  Data corresponds to time course experiment in Figure 4.4. Data are averaged over three trials.
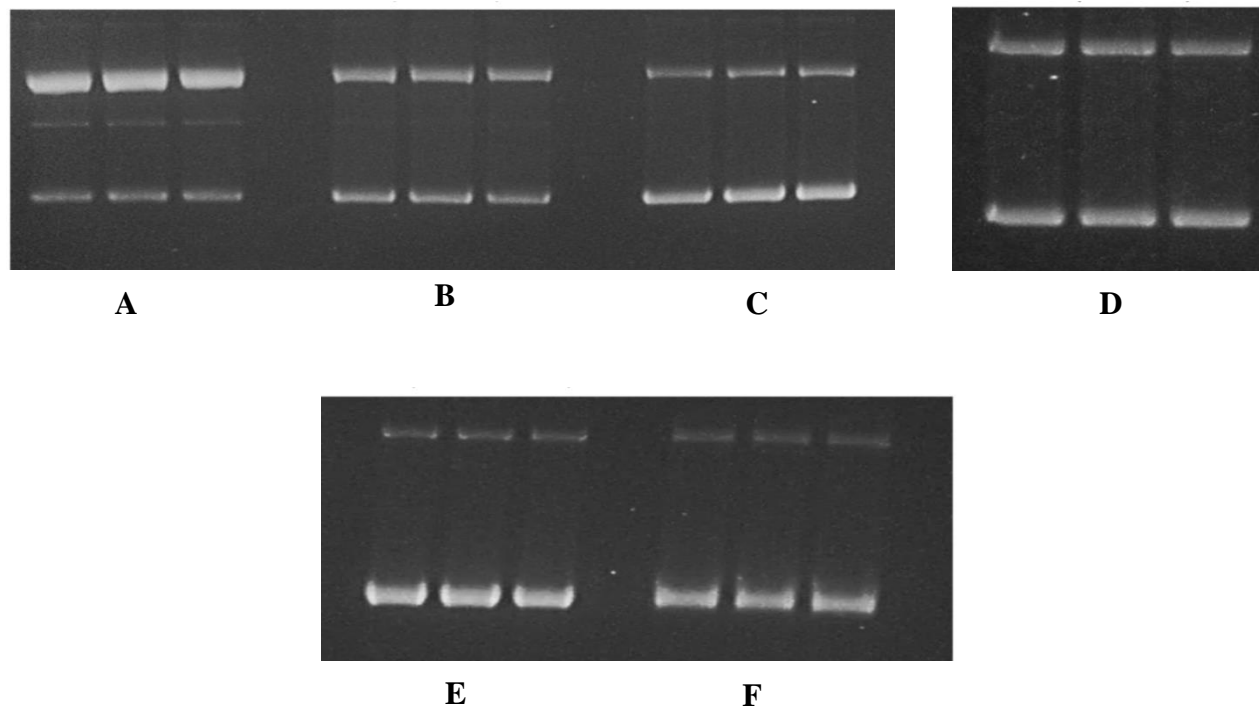
A          B          C          D
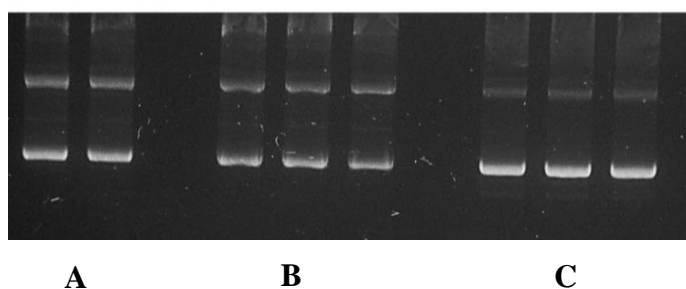
E          F

**Figure 4.S2.** Photograph of 1.5 % nondenaturing agarose gels showing photocleavage of pUC19 plasmid DNA (38 μM bp) by 2 μM **4** in sodium phosphate buffer pH 7.0 in the absence of inhibitor **(A)**, and in the presence of 100 U superoxide dismutase **(B)**, 100 U catalase **(C)**, 100 mM sodium benzoate **(D)**, 100 mM sodium azide **(E)**, and 100 mM EDTA **(F)**. Three trials were run for each reaction and acquired a 30 min irradiation time at 350 nm and 22 °C. Data corresponds to data in Table 4.1.



A          B          C

**Figure 4.S3.** Photograph of 1.5 % nondenaturing agarose gel showing photocleavage of pUC19 plasmid DNA (38 μM bp) by 1 μM **4** in sodium phosphate buffer pH 7.0 in the absence of inhibitor **(A)**, and in the presence of 79 % v/v D$_2$O **(B)** and 2 % v/v DMSO **(C)**. Three trials were run for each reaction and acquired a 30 min irradiation time at 350 nm and 22 °C. Data corresponds to data in Table 4.1.
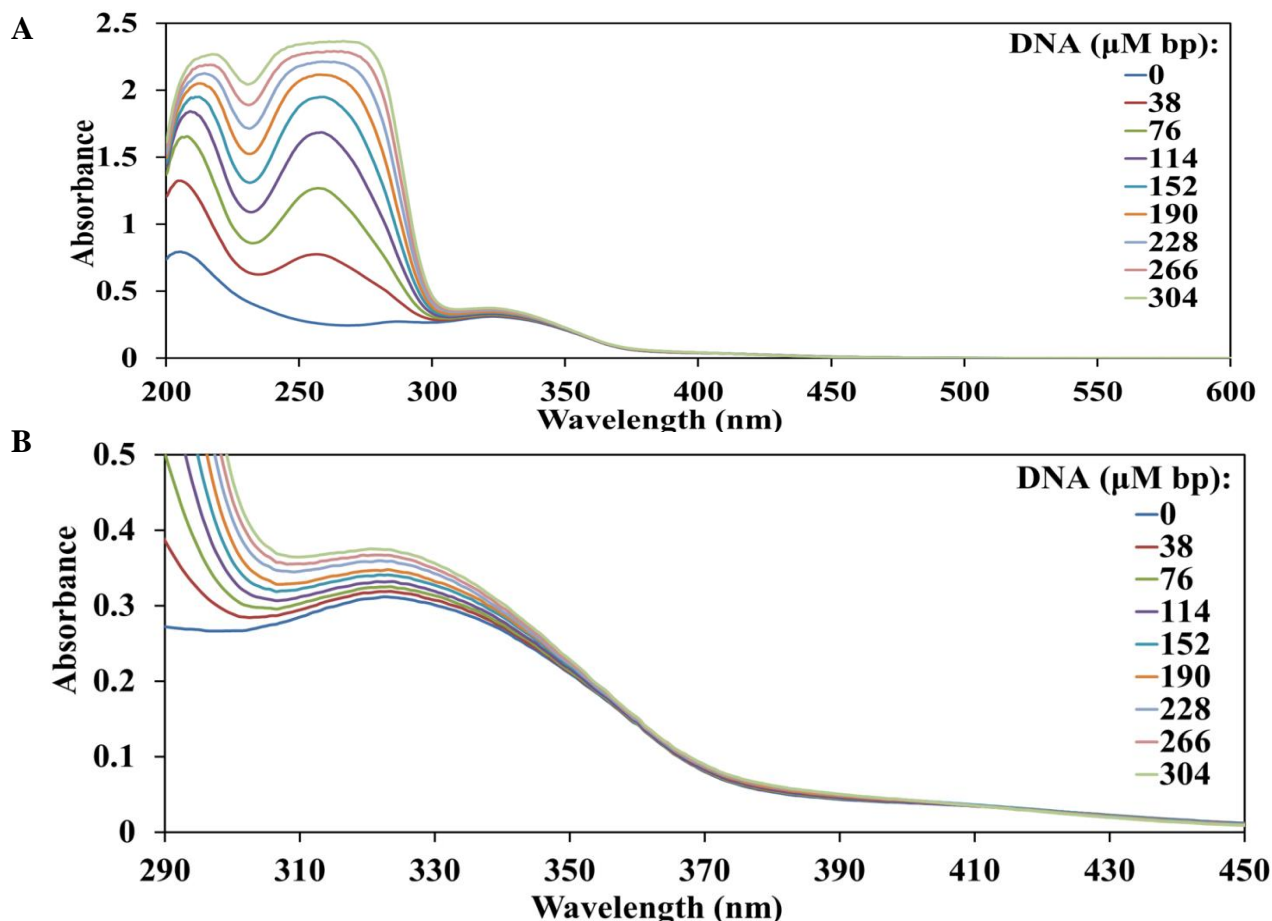
**Figure 4.S4.** UV-visible absorption spectra of 8 μM **4** in 10 mM sodium phosphate buffer pH 7.0 was monitored as a function of CT DNA concentration (0 μM bp – 304 μM bp) at 22 °C from 200 nm – 600 nm **(A)** and 290 nm – 450 nm **(B)**. The absorption spectrum has been corrected for sample dilution. Data correspond to Figure 4.8.
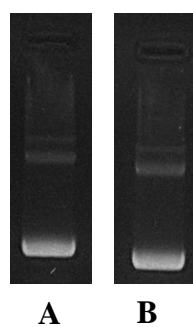


**Figure 4.S5.** Photocleavage of 38 μM bp pUC19 plasmid DNA by 30 μM CuCl$_2$ at 22 °C and pH 7.0 for 30 min in the dark **(A)** or irradiated at 350 nm **(B)**.
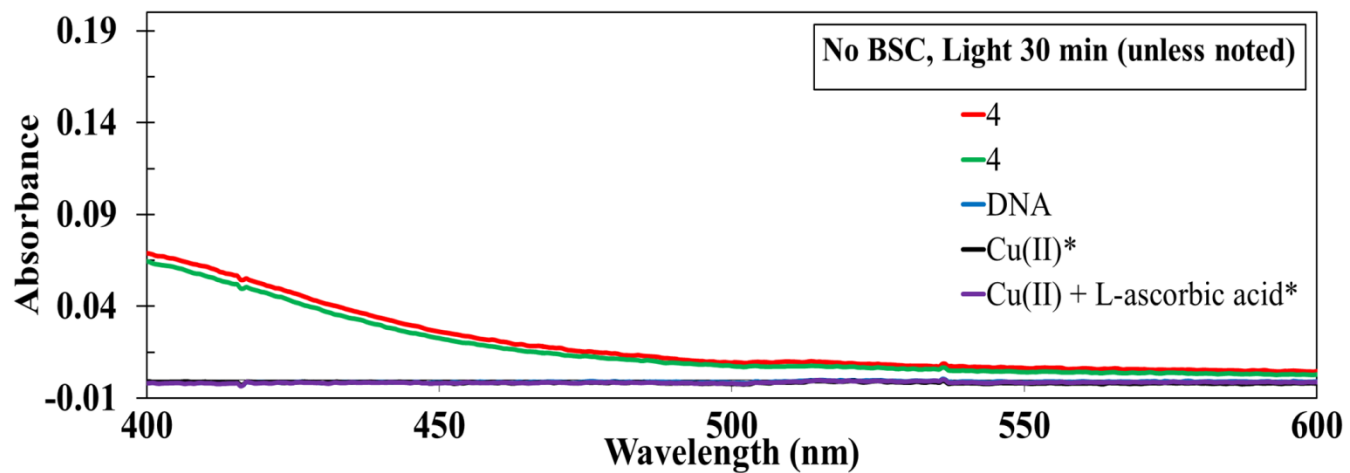
**Figure 4.S6.** UV-visible spectra of Cu(I) assay to detect Cu(I)-BCS complex formation in 10 mM sodium phosphate buffer pH 7.0 (22 °C). Reactions were either irradiated at 350 nm (* except Cu(II) + L-ascorbic acid) for 30 min. BCS was omitted in these experiments. Cu(II) = CuCl$_2$.